

A Song of Ice and a Warm Southern Ocean

The paleoceanographic evolution of the Oligocene–Miocene Southern Ocean

Frida Snilstveit Hoem



A Song of Ice and a Warm Southern Ocean

The paleoceanographic evolution of the Oligocene – Miocene Southern Ocean

**Het lied van ijs en een warme Zuidelijke Oceaan
De paleoceanografische evolutie van de Oligoceen-Mioceen Zuidelijke Oceaan**

(met een samenvatting in het Nederlands)

**En sang om is og et varmt Sørishav
Den paleoceanografiske utviklingen av Sørishavet gjennom Oligocene og Miocene**

(med et sammendrag på Norsk)

Proefschrift

ter verkrijging van de graad van doctor aan de Universiteit Utrecht
op gezag van de rector magnificus, prof.dr. H.R.B.M. Kummeling,
ingevolge het besluit van het college voor promoties in het openbaar te verdedigen
op vrijdag 7 oktober 2022 des ochtends te 10.15 uur door

Frida Snilstveit Hoem

geboren op 9 januari 1992 te Oslo, Noorwegen

Promotor:

Prof. dr. H. Brinkhuis

Copromotoren:

Dr. P.K. Bijl

Dr. F. Sangiorgi

Members of the dissertation committee:

Prof. Dr. Carlota Escutia

Department of Marine Geoscience, Instituto Andaluz de Ciencias de la Tierra, Consejo Superior de Investigaciones Científicas (CSIC) – Universidad de Granada, Armilla, Spain

Dr. Anna von der Heydt

Department of Physics, Marine and Atmospheric Research, Physical Oceanography, Utrecht University, Utrecht, the Netherlands

Prof. Dr. Douwe van Hinsbergen

Department of Earth Sciences, Mantle dynamics & theoretical geophysics, Utrecht University, Utrecht, the Netherlands

Prof. Dr. Jörg Pross

Institute of Earth Sciences, Heidelberg University, Heidelberg, Germany

Prof. Dr. Stefan Schouten

Department of Marine Biogeochemistry and Toxicology, Netherlands Institute for Sea Research, Texel and Department of Earth Sciences, Utrecht University, Utrecht, The Netherlands

Dit proefschrift werd mogelijk gemaakt met financiële steun van het Nieuw Nederlands Polair Programma van de Nederlandse Organisatie voor Wetenschappelijk Onderzoek (NWO)

Utrecht Studies in Earth Sciences 260

A Song of Ice and a Warm Southern Ocean

The paleoceanographic evolution of the Oligocene – Miocene Southern Ocean

Frida Snilstveit Hoem

Utrecht 2022

ISSN 2211-4335

ISBN 978-90-6266-628-7

USES No. 260

Author contact: f.s.hoem@uu.nl or frida.snh@gmail.com

Cover art and design by Marlo Gransworthy (@MarloWordyBird, www.wordybirdstudio.com)

Cover design by Margot Stoete and Frida Snilstveit Hoem

Copyright © 2022 F. S. Hoem. All rights reserved. No part of this publication may be reproduced in any form, by print or photo print, microfilm or any other means, without written permission by the publishers.

Printed in the Netherlands by Ipskamp printing

Contents

Chapter 1: General introduction	7
Chapter 2: Temperate Oligocene surface ocean conditions offshore of Cape Adare, Ross Sea, Antarctica <i>Hoem, F. S., Valero, L., Evangelinos, D., Escutia, C., Duncan, B., McKay, R. M., Brinkhuis, H., Sangiorgi, F., and Bijl, P. K.: Climate of the Past, 17, 1423-1442, 2021.</i>	19
Chapter 3: Late Eocene – early Miocene evolution of the southern Australian subtropical front: a marine palynological approach <i>Hoem, F. S., Sauermilch, I., Hou, S., Brinkhuis, H., Sangiorgi, F., and Bijl, P. K.: Journal of Micropalaeontology, 40, 175-193, 2021.</i>	45
Chapter 4: Strength and variability of the Oligocene Southern Ocean surface temperature gradient <i>Hoem, F., Sauermilch, I., Aleksinski, A., Huber, M., Peterse, F., Sangiorgi, F., and Bijl, P.K.: Nature Communications Earth and Environment, in review.</i>	69
Chapter 5: Late Cenozoic Sea Surface Temperature evolution of the South Atlantic Ocean <i>Hoem, F. S., K., López-Quirós, A., van de Lagemaat, S., Etourneau, J., Brinkhuis, H., Peterse, F., Sangiorgi, F., and Bijl, P. K.: To be submitted</i>	89
Chapter 6: Late Cenozoic oceanographic evolution of the South Atlantic Ocean <i>Hoem, F. S., van den Broek, K., López-Quirós, A., van de Lagemaat, S., Bohaty, S., Brinkhuis, H., Sangiorgi, F., and Bijl, P. K.: In prep Journal of Micropaleontology</i>	113
References	129
Samenvatting in het Nederlands	146
Sammendrag på Norsk	147
Acknowledgments	148
Curriculum Vitae	151
Publications	152

Chapter 1

General introduction

1 Motivation

Since the beginning of the industrial era, anthropogenic greenhouse gas emissions have raised primarily due to burning of fossil fuels. The concentration of carbon dioxide (CO₂) in the atmosphere increased from 278 part per million (ppm) to a yearly average of 416 ppm in 2021 (Mauna Loa Observatory, Hawaii). High greenhouse gas concentrations have increased the insulating capacity of Earth's atmosphere (greenhouse effect) by trapping reflected/outgoing heat from the Earth's surface and causing the global mean temperature to rise by >1°C and counting (IPCC, 2021). The ocean has absorbed about 30% excess CO₂ and ~90% excess heat from anthropogenic warming (Von Schuckmann et al., 2020), whereby the Southern Ocean is warming the most (60-90%; Sallée, 2018; Auger et al., 2021) and is absorbing about 1/3 of the surplus (anthropogenic-derived) CO₂ emissions via the southern upwelling cell (Terhaar et al., 2021).

The Southern Ocean forms an important node for the global ocean/atmosphere circulation system and is a major sink for carbon from atmosphere to ocean. The mixing of all three northern-sourced waters (Indian, Pacific, and Atlantic) means that the Southern Ocean is vital in the exchange of nutrients, salt, and heat between all of the world's oceans (Sarmiento et al., 2004). With no continental barriers (i.e. that Drake Passage and Tasmanian Gateway are open), the Southern Ocean hosts the strongest surface ocean current on Earth, the Antarctic Circumpolar Current (ACC). The east flowing westerly wind-driven ACC, strongly constrained by landforms and bathymetric features, has a steep latitudinal surface temperature gradient and a set of strong, complex frontal systems (Figure 1). Ongoing climate warming is expected to result in the intensification, and poleward shift of the southern westerly winds (SWW) (Toggweiler, 2009), leading to strengthening of the ACC (Wu et al., 2021) and, in turn, also to increasing upwelling of warmer circumpolar deep water onto Antarctica's continental shelves (Schmidtko et al., 2014). These warmer waters penetrating under the Antarctic ice shelves facilitate subsurface melting of the ice shelves that add to the surface melting due to a warmer atmosphere. Subsurface melting of ice shelves will cause loss of buttressing, destabilizing grounded ice upstream (Pritchard et al., 2012). The Antarctic ice sheets (AIS), Earth's largest land ice reservoir, equivalent to 57.9 meters of mean global sea level rise (DeConto et al., 2021), is in vast areas marine terminating and/or grounded below sea level and thus sensitive to warm ocean waters (Fretwell et al., 2013). However, since these important roles have only recently been discovered, long term Southern Ocean dynamics have not yet been appropriately represented in numerical models used for future sea level rise projections (Rintoul et al., 2018). Improved knowledge of not only its modern dynamics, but notably also the past evolution of this important driver and mitigator of global climate is now urgently needed.

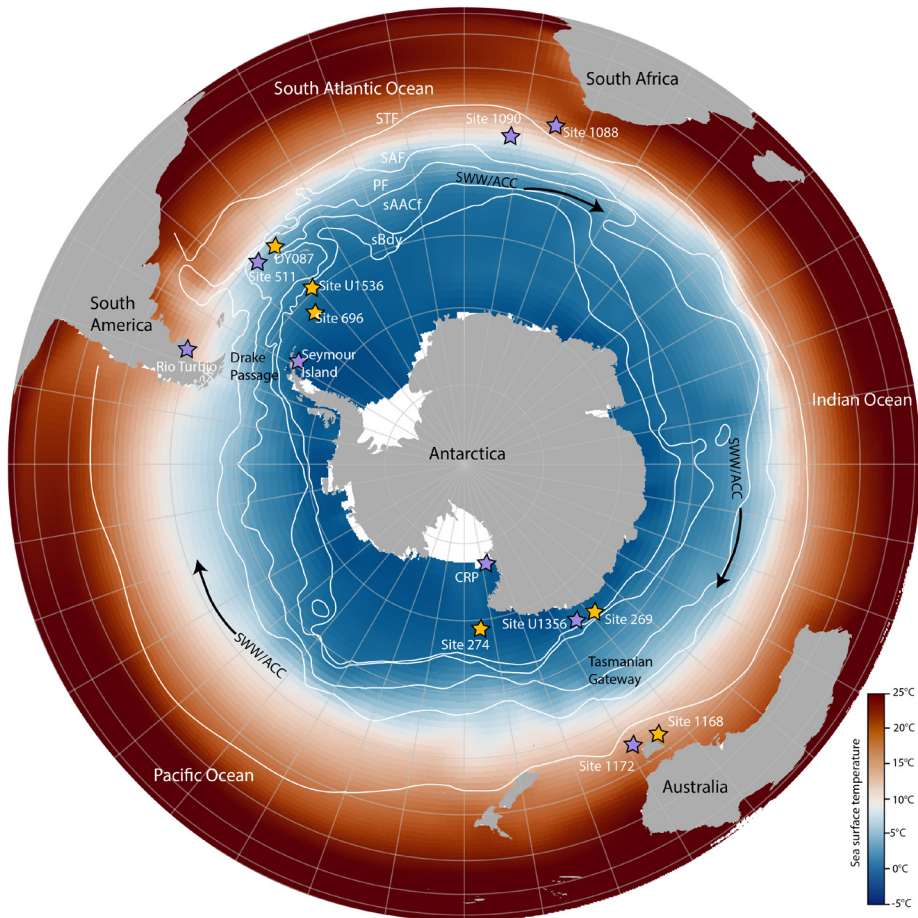


Figure 1. Present day map of the Southern Ocean showing the location of the marine sediment drill sites (DSDP/ODP/IODP) included in this thesis. Yellow stars show the from which we generate new paleoceanographic data. Purple stars show the main drill sites with exciting data we compare our new data to. The colors show average January SSTs from 1971-2000 (Reynolds et al., 2002). The white lines represent the smoothed, simplified position of circumpolar fronts interpreted by Orsi et al. (1995). From north to south: Subtropical Front (STF), Subantarctic Front (SAF), Polar Front (PF), Southern ACC Front (sACCf) and Southern Boundary (sBdy) Front (e.g., Orsi et al., 1995). The black arrows indicate the path of the southern westerly wind belt (SWW; Lamy et al., 2010), which drives the Antarctic Circumpolar Current (ACC).

2 The geologic past informs our future

The response of the AIS to atmospheric and Southern Ocean warming remains a key uncertainty in predicting sea level rise during and beyond this century (IPCC, 2021, Rintoul et al., 2018). Understanding how Southern Ocean dynamics previously responded to high atmospheric CO₂ concentrations, warmer climates and changing oceanographic and atmospheric circulation in the geologic past can aid the understanding and improve sea level projections. In order to reconstruct

e.g., past ice volumes, CO₂, climate and general oceanic conditions we have to rely on indirect inferences, so called environmental proxy records. Such proxies are measurable variables in the geological archive that provide information about past ocean or climate conditions. For example, water mass properties (e.g., temperature, nutrients, freshwater input, productivity, sea-ice presence, current strength) may be preserved in sediments in the form of varying microfossil assemblages, variable amounts of organic matter, and changing chemical, elemental, and isotopic composition of e.g., calcareous and siliceous shells, and various other sedimentary components. Thus, marine sedimentary records from the open ocean together provide a long archive of past climatic, oceanographic and environmental conditions. Through ocean drilling, most commonly carried out by the Integrated Ocean Drilling Program (IODP) and its predecessors (ODP/DSDP), kilometers of sediments, penetrating 100s meters below the sea floor have been retrieved (drill cores), which have recorded Earth's climate of the past ~170 Million years (Becker et al., 2019).

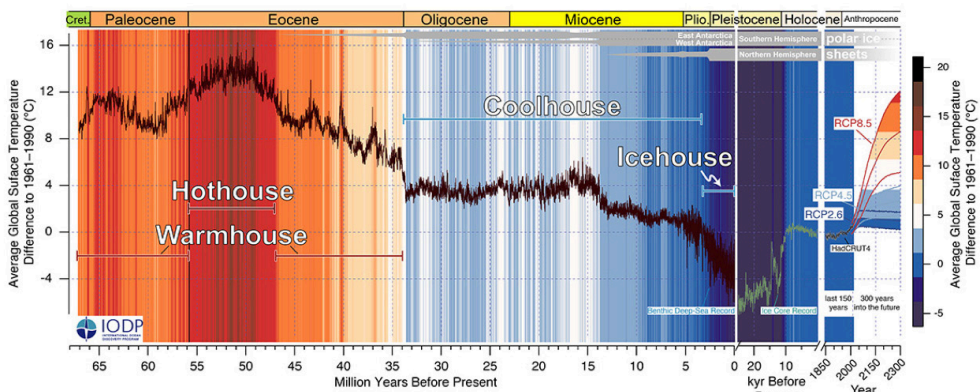


Figure 2. Trends in past and future global mean temperature with respect to present day derived from Cenozoic Global Reference benthic foraminifer carbon and oxygen Isotope Dataset (CENOGRID), from ocean drilling core sites spanning the past 66 million years by Westerhold et al. (2020). Cenozoic climate curve overlain on hot/cold colour bands, indicating hothouse, warmhouse, coolhouse and icehouse climate states. Future projections for global temperature for three Respective Concentration Pathways (RCP) scenarios (IPCC, 2013). The thickness of the grey bars at the top of the plot indicates the ice sheets volume.

The oxygen isotopic composition of calcareous shells of benthic foraminifera ($\delta^{18}\text{O}$), which reflects changes in continental ice volume and/or deep-sea temperature, has been a pivotal instrument for paleoclimatologists in reconstructing the climate evolution of the Cenozoic era (65-0 million years (Ma)) (Figure 2; Zachos et al., 2008; Westerhold et al., 2020). During the Early Cenozoic era, the Earth underwent one of the most fundamental global climate changes known in geological history, from hot and warm-house conditions (~56-34 Ma) to coolhouse/icehouse conditions (<34 Ma). The latter, marking the Eocene-Oligocene Transition (EOT), is characterized by a stepwise, large increase (~1-1.5 ‰) in benthic foraminifera $\delta^{18}\text{O}$ records, indicates a drop in ocean temperature, and the onset of large continental Antarctic ice sheets (AIS) (DeConto and Pollard, 2003; Coxall et al., 2005). After the EOT, throughout the Oligocene and Miocene, AIS experienced multiple cycles of advance and retreat, as indicated in proxy records by large and rapid changes in global sea level, up to 40 m amplitude variations (Kominz et al., 2008; Miller et al., 2020) and strong (up to 1‰) variability in deep-sea benthic foraminiferal $\delta^{18}\text{O}$ (Pälike et al., 2006; Westerhold et

al., 2020). Near the Oligocene-Miocene boundary (OMB, 23 Ma) an ~1‰ positive excursion in benthic foraminiferal $\delta^{18}\text{O}$ values indicates large-scale AIS expansion, with the East Antarctic Ice Sheet (EAIS) estimated to have grown from 50-125% of its present-day size (Pekar and DeConto, 2006). Following this cooling step, the subsequent Miocene Climatic Optimum (MCO, ~17-14 Ma) represents an unusual warm phase during which the EAIS partly melted (Foster et al., 2012; Levy et al., 2016; Sangiorgi et al., 2018). At ~14 Ma, another major climate cooling known as the Middle Miocene climate transition (MMCT, ~14 Ma) occurred, when the AIS expanded. Since the MMCT, the AIS became less variable (Holbourn et al., 2005; Lewis et al., 2008; Shevenell et al., 2008). Although benthic foraminifera $\delta^{18}\text{O}$ provides a good indication of past global climate variability, it incorporates a mixed signal of ice volume and deep sea temperatures and doesn't directly record the variability of the AIS and its sensitivity to ocean temperature. To constrain the fate of AIS in a warmer-than-present and higher-than present CO_2 world, one approach is to reconstruct oceanographic conditions close to the Antarctic margin during past analogue intervals for future climates.

The inferred decreasing atmospheric CO_2 concentration from >1000 ppm during the Eocene (56.0-33.9 Ma), to around 750 ppm or lower at the beginning of the Oligocene (DeConto and Pollard, 2003; Pearson et al., 2009; Anagnostou et al., 2016), is believed to be the main driver of the cooling and eventual onset of Antarctic (and later Northern Hemisphere) glaciation. The onset of the ACC, induced by the concomitant tectonic opening of both Southern Ocean gateways (Figure 1; Tasmanian Gateway and Drake Passage) was believed to be elemental in large scale Antarctic glaciation (Kennett, 1977; Exon et al., 2004), but this simple early idea has been dismissed in recent years (Huber et al., 2004; Stickley et al., 2004; Bijl et al., 2013) although still debated by some. The Drake Passage was likely narrow and shallow during the EOT, with a weak throughflow, not strong enough to 'thermally insulate Antarctica' (Zhang et al., 2010). Thus, it is unlikely that Drake Passage played an essential role in the EOT (Goldner et al., 2014). However, throughout the Oligocene and Miocene, reorganisations of oceanic surface and deeper conditions around the Southern Ocean might explain some of the large variability seen in the Antarctic ice sheet (Kennedy et al., 2015). Uncertainties and gaps in both paleo- CO_2 reconstructions and complete records of the evolution of Southern Ocean oceanic conditions hampers accurate model simulations and complicates the full understanding of past ice-ocean-climate interactions (e.g., Gasson and Keisling, 2020).

Reconstructing post EOT Oligocene and Miocene (~34-5 Ma) oceanographic conditions, using suited proxy records in Southern Ocean marine sediments will assist resolving key questions about the consequence of varying CO_2 concentrations, ice volume and progressive tectonic opening and deepening of the Southern Ocean gateways on the evolution of the oceanography and the ocean heat transport through time towards the Antarctic ice sheet.

3 Reconstructing Oligocene-Miocene Southern Ocean paleoceanographic surface conditions.

The majority of the 'traditional' paleoceanographic and paleoclimatic proxies use elemental and isotopic composition of foraminifera ($\delta^{18}\text{O}$, $\delta^{13}\text{C}$, Δ_{47} , Mg/Ca) and biostratigraphic and environmental proxies derived from diatom, radiolarian and coccolithophorid assemblages. All these tools rely on the preservation of siliceous and calcareous organisms. Carbonate solubility in seawater drastically increases under colder temperatures (Fabry et al., 2009). Furthermore, drilling deep into the seafloor may lead to surpassing the diagenetic front of biogenic opal thereby silicates

will not be preserved (van Cappellen and Qiu, 1997). Therefore, in the Oligocene to Miocene Southern Ocean Antarctic-proximal waters are siliceous and calcareous shells prone to dissolution. Thus, in the absence of carbonaceous and siliceous sediment, we here rely on other, in this case organic proxies which preserve well at high latitudes, such as organic walled dinoflagellate cysts (dinocysts) and organic biomarker sea surface temperature reconstructions (TEX₈₆).

3.1 Marine Palynology

Palynology is the morphological analysis and study of acid-resistant organic matter, and the post processing residue, called 'palynofacies' typically includes palynodebris and palynomorph fractions. The latter includes the morphologically recognizable remains of single and multicellular organisms (e.g., from various aquatic organisms including dinoflagellates, acritarchs and prasinophytes, but also terrestrial elements of lower and higher plants, such as pollen and spores).

Dinoflagellates, together with foraminifera, diatoms, coccolithophorids and radiolarians constitute most of the modern marine plankton. Dinoflagellates are single-celled, marine and freshwater eukaryotic protists that can be autotrophic, heterotrophic or both (mixotrophic), and symbiotic. During their sexual and vegetative reproduction, some 20% of modern dinoflagellate species form a non-motile resting (dormant) cyst, which wall can be organic, siliceous, agglutinated, or calcareous. Notably the non-cellulosic, 'bioplastic' organic-walled dinoflagellate cysts (dinocysts) are widely used for chronostratigraphical and paleoenvironmental analysis (e.g., Fensome, 1993; Head, 1996). The highly resistant organic composition of their wall allows dinocysts to typically be preserved (in absence of oxidation) in high latitude sediments where siliceous (e.g., diatoms) and calcareous (e.g., foraminifers and coccoliths) organisms often undergo dissolution.

Cyst-producing dinoflagellates have very specific environmental preferences. The distribution of dinocysts in the surface sediments has been linked to varying water properties such as nutrient availability, temperature, salinity, oxygen of the bottom waters, primary productivity and sea-ice cover (Wall et al., 1977; Dale, 1996; Prebble et al., 2013; Zonneveld et al., 2013). Based on the notion that habitat affinities and feeding strategies of most modern dinoflagellates (and their cysts) can be extrapolated to the fossil record, we use 'deep-time' dinocyst assemblages to interpret paleoenvironments and paleoceanography (Brinkhuis, 1994; Sluijs et al., 2005; Bijl et al., 2013; Prebble et al., 2013; Crouch et al., 2014; Egger et al., 2018; Frieling and Sluijs, 2018; Kulhanek et al., 2019). Many Oligocene and Miocene dinocyst species and genera are either extant, or – when extinct – belong to an extant families for which some generalization on the preferred niche may be made.

Today, a pronounced latitudinal separation of dinocyst assemblages exists across the Southern Ocean (Esper and Zonneveld, 2002; Prebble et al., 2013; Marret et al., 2020; Thole et al., in prep.). The various oceanic fronts are each characterized by their own marked gradients in ocean conditions like temperature and/or salinity (e.g., Orsi et al., 1995; Olbers et al., 2004). Since the different frontal systems have a different oceanographic signature, we can track the movements of these fronts through time studying dinocyst assemblages in past sediment records. Dinocysts can also be used as biostratigraphic tool to determine the age of the sediment and have shown to be powerful biostratigraphic tool in the Southern Ocean (e.g., Brinkhuis et al., 2003a, b; Sluijs et al., 2005; Tauxe et al., 2012; Pross et al., 2012; Houben et al., 2011, 2013; Stocchi et al., 2013; Bijl et al., 2013, 2018a, 2021; Williams et al., 2017). Dinocysts are increasingly and successfully used as a tool for biostratigraphy and paleoceanographic reconstructions of the Oligocene-Miocene Southern Ocean (e.g., Brinkhuis et al., 2003; Bijl et al., 2013; Houben et al., 2013; Guerstein et al., 2014; Clowes et al., 2016; Warny et al., 2016; Bijl et al., 2018b; Sangiorgi et al., 2018).

3.2 Organic geochemistry

In order to quantitatively reconstruct sea surface temperature (SST), we applied the so-called TEX₈₆ (TetraEther indeX of 86 carbon atoms) proxy, which is based on the temperature-dependent cyclisation of isoprenoidal glycerol dialkyl glycerol tetraethers (GDGTs) produced by thaumarchaeotal membrane lipids (Schouten et al., 2002). Lipid biomarkers are essentially molecular fossils of lipids produced by several groups of Archaea and Bacteria (e.g., Schouten et al., 2013). The use of TEX₈₆ as a proxy for SST relies upon the assumption that isoprenoidal GDGTs in marine sediments are principally derived from membrane lipids of marine pelagic Thaumarcheota (Schouten et al., 2013). We use ratios of GDGTs as proxies to detect potential overprinting factors that may bias the pelagic signature of the sedimentary GDGTs, and exclude the samples which show potential for a overprinted signal. Several calibrations exist to convert TEX₈₆ values into SSTs based on modern core-top datasets (e.g., Kim et al., 2010; Tierney and Tingley, 2015).

3.3 Selected study sites

The remote and rough nature of Southern Ocean with its treathening icebergs makes ocean drilling a challenging and expensive feat. Furthermore shelf sediments are typically discontinuous or reworked due to erosion by the advances and retreats of the Antarctic ice sheet across the shelf. The Antarctic proximal drilling is further limited by the large winter sea ice extent. Therefore we study the available, often non-continuous, Southern Ocean sedimentary archives drilled and curated by IODP and its predecessor using advancement of new techniques to best possible reconstruct the past Southern Ocean conditions. In this PhD thesis I quantitatively analyzed the remains of organic walled dinoflagellate cysts (dinocysts), and TEX₈₆ on sediments from drill cores (DSDP/ODP/IODP Sites 269, 274, 696, 1168 and U1536 and piston cores DY087; yellow stars, Figure 1) spanning the Late Eocene to Miocene (37-5 Ma) (Figure 3). The selected records are strategically located from Antarctic proximal to Antarctic distal to record changes in latitudinal temperature and environmental gradients. The variability or similarity in records at high or low latitudinal position in the Southern Ocean can record the changes in ocean circulation and migrations of frontal systems.

4 The enigmatic Oligocene conditions: warm ice-proximal SSTs

Oligocene-Miocene dinocyst and TEX₈₆ records from the Antarctic margin, offshore Wilkes Land, Site U1536 (Bijl et al., 2018b; Hartman et al., 2018; Sangiorgi et al., 2018; Figure 3) show warm ocean temperatures (SST = 10-21°C) and a striking lack of cold water and sea ice affiliated dinocysts and temperate SSTs. This means that – quite unexpectedly – relatively *warm* conditions prevailed close to the Antarctic ice sheets at that time. Although global climate was generally warmer than today, the coexistence of an ice sheet (albeit mostly reduced compared to present-day) and warm ocean temperatures requires a different oceanographic configuration from that of today. A warmer Oligocene Southern Ocean could be the result of generally high atmospheric *p*CO₂ concentrations (300-700 ppm; <https://www.paleo-co2.org>), but higher atmospheric CO₂ levels would also be associated with reduced ice volume (Gasson et al., 2014). Furthermore, model simulations show ice sheet growth increases poleward heat transport (Knorr and Lohmann, 2014), but at the same time induces local cooling at the Antarctic margin (Goldner et al., 2014). The mystery of warm high latitude SSTs proximal to the Antarctic ice sheets needs to be unraveled.

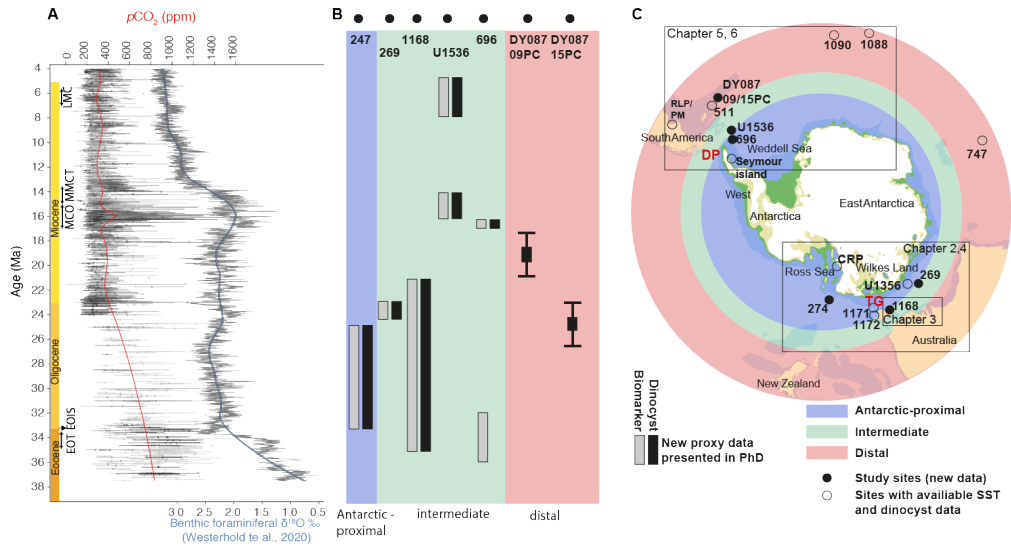


Figure 3. A. Late Eocene-Miocene paleo-CO₂ estimates from <https://www.paleo-co2.org> (Hoenisch, 2021; black-gray dots with error bars with red line showing the LOESS smoothed curve, span = 0.1). Benthic foraminiferal δ¹⁸O, smoothed by a locally weighted function over 20 kyr (thin black curve; CENOGRID; Westerhold et al., 2020) with thick blue line showing the LOESS smoothed curve (span = 0.1). B. Stratigraphic range of sediment material analyzed in this PhD thesis. C. The paleogeographical position of sedimentary records used in this thesis. Paleogeographic map is made in Gplates (35 Ma) (<http://www.gplates.org>), based on the global geodynamic rotation model from Müller, et al. (2018).

One alternative hypothesis is that marine ice sheet terminations were restricted to the southernmost parts of the Antarctic margin, facilitated by a higher-than-modern Antarctic paleo-topography (Wilson et al., 2013), while elsewhere the ice sheets were mostly terrestrial (e.g., Bijl et al., 2018b; Sangiorgi et al., 2018), limiting the Antarctic glacial cooling effect on proximal SSTs (Singh et al., 2016). Immediately after the Eocene-Oligocene transition, ~32.8 million years ago, a continental scale ice sheet reached the coast of Antarctica (Stocchi et al., 2013; Galeotti et al., 2016). However, throughout the Oligocene and into the early Miocene, Antarctic ice sheets retreated and advanced as indicated by the documented rapid sea level variations, ranging up to 40 m in amplitude (Kominz et al., 2008; Gallagher et al., 2013). We do note that these oscillations are still subject to debate (McKay et al., 2016; De Vleeschouwer et al., 2017). The limited sea ice expansion and reduced formation of Antarctic bottom waters have been linked to a weaker oceanic frontal system, which allowed the intrusion of warmer water masses from lower latitudes to penetrate closer to the Antarctic margin (Levy et al., 2016; Hartman et al., 2018; Salabarnada et al., 2018; Sangiorgi et al., 2018).

Another hypothesis, viz considering a more restricted width of critical Southern Ocean gateways (Tasmanian Gateway and Drake Passage) may also have been at play in ocean heat redistribution according to e.g., Hill et al. (2013). Closed ocean gateways, which can reduce meridional temperature gradients by enhancing ocean poleward heat transport or by increasing local radiative heating through albedo feedbacks or enhanced atmospheric moisture transport (England et al., 2017) may thereby have sustained warm SSTs while simultaneously maintaining terrestrial ice sheets.

4.1 Tectonic configurations of Southern Ocean gateways

It is widely acknowledged that the opening of Southern Ocean gateways (Tasmanian Gateway and Drake Passage) must have transformed Southern Ocean surface circulation and redistribution of heat (Huber et al., 2004; Bijl et al., 2013; Sijp et al., 2014; 2016). The Tasmanian Gateway tectonic evolution is by now relatively well constrained; early southern opening of the Tasmanian Gateway started around 49-50 Ma (Huber et al., 2004, Stickley et al., 2004; Bijl et al., 2013) with a change of the tectonic course of Australia from the northeast to the north and opened to deep oceanic circulation between 35.5 and 33.5 Ma, and further widened between 33 and 30 Ma (Stickley et al., 2004). However, the timing and nature of opening, widening, and deepening of the Drake Passage is still much debated, ranging from between 50 Ma and 6 Ma (Barker et al., 2007; Livermore et al., 2007; Eagles and Jokat, 2014; Maldonado et al., 2014). A deep-water throughflow through Drake Passage has been suggested from 41 Myrs onwards (Scher and Martin, 2006). Meanwhile, sedimentation rates and erosion of deep-sea sediments in the South Pacific (Lyle et al., 2007; Barker and Thomas et al., 2004) suggests that circumpolar ocean circulation was weak until at least the Late Oligocene (~26 Ma; Hill et al., 2013). Just like the paleoceanographic reconstructions from the South Pacific recording the changes related to Tasmanian Gateway opening and deepening, has South Atlantic and South Indian Ocean sedimentary records the potential to reconstruct the profound effect of Drake Passage opening on the oceanographic conditions.

Focus of the thesis

Considering the above, it has become clear that the Oligocene-Miocene (~34-5 Ma) was likely characterized by globally relatively warm temperatures, rather high and variable CO₂ levels (300-750 ppm) and strongly fluctuating Antarctic ice volumes. And indeed, as such, this time interval may provide valuable past analogues for future climates, considering the projected atmospheric CO₂ concentrations for the end of this century and beyond (IPCC, 2021) (Figure 2). Yet, fundamental questions remain about the past Southern Ocean structure and its role in the (in)stability of Antarctic ice-sheets from this critical deep time slice. In the Oligocene, surprisingly warm sea surface temperatures (SST) appear to have prevailed on the Antarctic Margin (Site U1356), in the vicinity of the Antarctic ice sheet (Bijl et al., 2018b; Hartman et al., 2018). Central to this thesis is therefore the question how representative Site U1356 is for Antarctic coastal conditions since this warmth has not been put into context of the oceanographic conditions of the rest of the Southern Ocean.

With my collaborators, in this thesis, I provide this context by reconstructing the latitudinal SST gradients, variability and position of ocean frontal systems and oceanic environmental conditions of Tasmanian Gateway and Drake Passage regions of the Southern Ocean from the Late Eocene until Late Miocene (37-5 Ma) using new TEX₈₆-based SSTs and dinocyst assemblage data. This thesis first describes the paleoceanographic conditions around the Tasmanian Gateway, at the boundary between the Indian and Pacific Oceans (Chapter 2-4). Then we move to the opposite side of Antarctica to describe the oceanographic context of the South Atlantic, east of the Drake Passage (Chapter 5-6).

In **Chapter 2** we show that temperate (TEX₈₆ SST: 10-17°C) and relatively oligotrophic surface ocean conditions prevailed offshore the Ross Sea continental margin (DSDP Site 274), during the Oligocene (33.7-24.4 Ma). This extends the warm surface ocean conditions recorded offshore

Wilkes Land (IODP Site U1356) towards the Ross Sea, implying that the Southern Ocean oceanography was indeed fundamentally different from modern conditions. Next, we study how such warm Oligocene high latitude SSTs are reflected in lower latitude records from the Australian-Antarctic basins along the Australian Margin. However, in order to do so we must first establish the depositional- and surface environmental conditions offshore southern Australia. In **Chapter 3** we present Late Eocene to Early Miocene (37-20 Ma) palynomorph assemblages (dinocysts, acritarchs, pollen and spores) from the western Tasmanian continental slope (ODP Site 1168), compared with new interpretations of seismic data to record the depositional and palaeoceanographic history in the context of the opening and deepening Tasmanian Gateway between Australia and Antarctica. Locally at Site 1168 we found a transition from abundant pollen and spores from land, high nutrient dinocysts and extant neritic (shallow sea) dinocysts in the Late Eocene to more abundant modern open ocean dinocyst groups through the Oligocene-Early Miocene. The new seismic interpretations showed that Upper Eocene sediments filled up a sedimentary (micro)basin enclosed by two basement highs with winnowing and reworking in the top, while the Oligocene and Miocene sediments showed evidence of bottom current activity. Together these results confirm the subsidence of the Tasmanian continental margin during the Oligocene (Stickley et al., 2004; Brinkhuis et al., 2003). The absence of major shifts in dinocyst assemblages contrasts with other records in the region and suggests stable surface oceanographic conditions during the Oligocene. This reflects the continued influence of the proto-Leeuwin Current along the southern Australian coast as Australia continued to drift northward. The relatively “warm” dinocyst assemblages at ODP Site 1168, compared with the cold assemblages at Antarctic Integrated Ocean Drilling Program (IODP) Site U1356, testify to the establishment of a pronounced latitudinal temperature gradient in the Oligocene Southern Ocean. In **Chapter 4** we present the Late Eocene-Early Miocene (TEX₈₆-based) SST gradient evolution in the Australian-Antarctic basin in more detail. The results show an increase in the SST gradient across the Southern Ocean starting at ~26 Ma, when Antarctic-proximal SSTs cooled. This is in contrast to a synchronous decrease in global benthic foraminiferal $\delta^{18}\text{O}$ indicating ice mass loss/deep sea warming. Considering the potential drivers of such cooling through comparing our results to climate and ocean models (Kennedy-Asser et al., 2019; Sauermilch et al., 2021), we conclude that the Late Oligocene Antarctic-proximal SST cooling is not primarily driven by changes in $p\text{CO}_2$ and ice sheet configuration (Hill et al., 2013; Gasson et al., 2014; Knorr and Lohmann, 2014; England et al., 2017), but by paleogeographic configurations.

Now that we have established a better understanding of paleoceanographic evolution in the Australian-Antarctic basin, we move over to the opposite side of the Southern Ocean in **Chapter 5** where we present new (ODP Site 696 and IODP Site U1536) SST records from the South Atlantic, which we combine with existing data into an overall South Atlantic compilation. We record two time intervals of prominent climate transitions; the Late Eocene-Early Oligocene and the Middle-Late Miocene. Across the Eocene-Oligocene transition our results show a weak latitudinal temperature gradient across the South Atlantic which we ascribe to a persistent Subpolar gyre circulation, connecting all sites, and an absence of a strong throughflow through Drake Passage. Surprisingly, southern South Atlantic SSTs at the earliest Oligocene glaciation were similar to those of the warm Miocene Climatic Optimum (MCO). Apparently, the Oligocene Antarctic ice sheet could coexist with warm ice-proximal surface ocean conditions, while the Miocene Antarctic ice sheet could be strongly reduced in spite of a relatively cold ice-proximal South Atlantic Ocean. Southern South Atlantic SSTs cooled to ~5°C at the onset of the Middle Miocene Climate Transition (MMCT), making it the coldest oceanic region around Antarctica and the likely location for deep water formation. The Late Miocene glacial expansion and northward migration of frontal systems

cooled the rest of the Southern Ocean, while the already cooled southern South Atlantic remained cold. Finally, in **Chapter 6** we present new Late Eocene-Late Miocene dinocyst assemblage data from the southwestern South Atlantic marine sediment drill cores (IODP Site U1536, ODP Site 696 and piston cores from Maurice Ewing Bank). We compare our data to available dinocyst and SST records (Chapter 5) from the South Atlantic to reconstruct the oceanographic and frontal system evolution. The South Atlantic dinocyst assemblages indicate persistent circulation of the subpolar gyre throughout the EOT, consistent with the SST reconstructions from Chapter 5. The disappearance of Antarctic endemic and typical cold-water indicative dinocysts North of Drake Passage by the mid-Oligocene (between 32 and 26 Ma) suggests breakdown of the dominant gyral circulation and strengthening of frontal systems, separating the warm subtropics from the polar Antarctic margin. From the MCO (16 Ma) to the MMCT (14 Ma) oligotrophic, warmer water indicative dinocysts are replaced by protoperidinioid dinocysts indicative of cold, sea-ice-influenced Antarctic-proximal surface water conditions, while TEX_{86} SSTs drop from 14°C to 7-5°C (Chapter 5). This is consistent with the drop in atmospheric $p\text{CO}_2$ (below 300 ppm; Badger et al., 2013) and increase in benthic foraminifera $\delta^{18}\text{O}$, indicating global cooling conditions and/or increasing ice volume. Although many gaps in the record of oceanographic change in the late Cenozoic Southern Atlantic persists, our compilation shows for the first time the stepwise breakdown of the large South Atlantic subpolar gyre into the modern-like oceanographic regime with strong frontal systems and latitudinal gradients.

Integration and outlook

By quantifying Oligocene to Miocene oceanic conditions from critical locations around Antarctica we provide new insights for an improved mechanistic understanding of Southern Ocean paleoceanographic evolution. This involves new reconstructions of Southern Ocean circulation and frontal system migrations during past warm Oligocene and Miocene climates, which shows us how the southern polar ocean operates under warmer-than-present-day conditions. The information on Southern Ocean sea surface temperature and ecology/environment provided in this thesis can be used as fundamental boundary condition to improve model simulations and to test the fitness of models simulating past oceanographic conditions.

Having successfully revisited studied and archived marine sedimentary records (some as old as 50 years), we have shown that these potentially overlooked records still holds valuable information when using new and improved proxy methods, and is a clear demonstration of the value of curation of sedimentary archives and data. Furthermore, the conducted studies can provide information to guide targeted future drilling projects. Ultimately geographic coverage of sedimentary archives is the main limiting factor for further understanding in order to fully constrain the role of a warm Southern Oceans on Antarctic ice sheet melt.

Chapter 2

Temperate Oligocene surface ocean conditions offshore of Cape Adare, Ross Sea, Antarctica

Frida S. Hoem¹, Luis Valero², Dimitris Evangelinos³, Carlota Escutia³, Bella Duncan⁴, Robert M. McKay⁴, Henk Brinkhuis^{1,5}, Francesca Sangiorgi¹, and Peter K. Bijl¹

1. Department of Earth Sciences, Utrecht University, Utrecht, the Netherlands

2. Department of Earth Sciences, University of Geneva, Geneva, Switzerland

3. Department of Marine Geoscience, Instituto Andaluz de Ciencias de la Tierra, Consejo Superior de Investigaciones

Científicas (CSIC)–Universidad de Granada, Armilla, Spain

4. Antarctic Research Centre, Victoria University of Wellington, Wellington, New Zealand

5. Royal Netherlands Institute for Sea Research (NIOZ), Texel, the Netherlands

Published in *Climate of the Past*, 1423–1442, 2021: <https://doi.org/10.5194/cp-17-1423-2021>

Abstract

Antarctic continental ice masses fluctuated considerably during the Oligocene ‘coolhouse’, at elevated atmospheric CO₂ concentrations of ~600–800 ppm. To assess the role of the ocean in the Oligocene ice sheet variability, reconstruction of past ocean conditions in the proximity of the Antarctic margin is needed. While relatively warm ocean conditions have been reconstructed for the Oligocene offshore of Wilkes Land, the geographical extent of that warmth is unknown. In this study, we reconstruct past surface ocean conditions from glaciomarine sediments recovered from Deep Sea Drilling Project (DSDP) Site 274 offshore of the Ross Sea continental margin. This site, located offshore of Cape Adare is ideally situated to characterize Oligocene regional surface ocean conditions, as it is situated between the colder, higher-latitude Ross Sea continental shelf and the warm-temperate Wilkes Land margin in the Oligocene. We first improve the age model of DSDP Site 274 using integrated bio- and magnetostratigraphy. Subsequently, we analyse organic walled dinoflagellate cyst assemblages and lipid biomarkers (TEX₈₆, TetraEther index of 86 carbon atoms) to reconstruct surface palaeoceanographic conditions during the Oligocene (33.7–24.4 Ma). Both TEX₈₆-based sea surface temperature (SST) and microplankton results show temperate (10–17°C±5.2°C) surface ocean conditions at Site 274 throughout the Oligocene. Oceanographic conditions between the offshore Wilkes Land margin and Cape Adare became increasingly similar towards the late Oligocene (26.5–24.4 Ma); this is inferred to be the consequence of the widening of the Tasmanian Gateway, which resulted in more interconnected ocean basins and frontal systems. Maintaining marine terminations of terrestrial ice sheets in a proto-Ross Sea with offshore SSTs that are as warm as those suggested by our data requires a strong ice flux fed by intensive precipitation in the Antarctic hinterland during colder orbital states but with extensive surface melt of terrestrial ice during warmer orbital states.

1 Introduction

The Southern Ocean plays a crucial role in global ocean circulation, stability of the Antarctic ice sheet and the carbon cycle. At present, strong temperature gradients isolate Antarctica from the influence of warmer surface water from lower-latitude regions. Despite its crucial role, little is currently known about the evolution of the Southern Ocean. Southern Ocean surface conditions cooled during the mid-Eocene (<49 Ma; Bijl et al., 2009, 2013), which culminated in the initiation of Antarctic continental-scale glaciation at the Eocene-Oligocene transition (EOT ~33.7 Ma; Zachos et al., 1994; Coxall et al., 2005; Bohaty et al., 2012). The overall higher bedrock elevation and larger subaerial area of Antarctica during the Oligocene (33.9-23.0 Ma; Gradstein et al., 2012; Wilson et al., 2013; Paxman et al., 2019) allowed for the occupation of large terrestrial ice caps. Antarctic ice-proximal records suggest that these ice sheets extended onto the coast, forming ice margins with marine terminations (Escutia et al., 2011; Scher et al., 2011; Galeotti et al., 2016). Apparently, Southern Ocean temperatures at the earliest Oligocene oxygen isotope step (EOIS) cooled enough to sustain the marine-terminating ice sheets. Following the EOIS, deep-sea $\delta^{18}\text{O}$ gradually rebounded (Zachos et al., 2008), suggesting long-term loss of Antarctic ice and/or gradual deep-sea warming. Indeed, the Oligocene remained a relatively warm time interval globally (O'Brien et al., 2020). However, on orbital timescales, Oligocene Antarctic ice volume underwent major fluctuations in size (e.g. Pälike et al., 2006; Galeotti et al., 2016; McKay et al., 2016; Liebrand et al., 2017; Levy et al., 2019), and the role Southern Ocean sea surface temperature (SST) conditions played in these fluctuations still remains poorly understood, mostly due to the sparse geographic coverage of reconstructions of Oligocene SSTs.

Warm-temperate Oligocene SSTs (13-25°C) and frontal system reconstructions at the Wilkes Land margin were derived from organic walled dinoflagellate cyst (dinocyst) assemblages at Deep Sea Drilling Project (DSDP) Site 269 (Evangelinos et al., 2020) and Integrated Ocean Drilling Program (IODP) Site U1356 (Bijl et al., 2018b). These were corroborated with quantitative SSTs based on organic biomarkers (TEX₈₆, TetraEther index of 86 carbon atoms; Hartman et al., 2018) and with sedimentological and lithological interpretations (Salabarnada et al., 2018; Evangelinos et al., 2020). Data seem to indicate a southward displacement of the (proto-) Southern Ocean fronts, perhaps favoured by the still constricted, narrow Tasmanian Gateway (Scher et al., 2015), and consequent southward deflection of warm ocean currents (Figure 1b). The relative absence of iceberg rafted debris in most of the Oligocene sedimentary record of IODP Site U1356 (Escutia et al., 2011; Salabarnada et al., 2018; Passchier et al., 2019) suggests that the East Antarctic Ice Sheet (EAIS) in the Wilkes Land sector may have been predominately land based, indicating limited ice sheet-ocean interaction in this sector of the EAIS. Sedimentary records recovered from cores located near the Transantarctic Mountain outlet glaciers, such as DSDP Site 270 (Kulhanek et al., 2019), CIROS-1 (Cenozoic Investigations of the Ross Sea-1; Barrett, 1989) and Cape Roberts Project (CRP; Naish et al., 2001; Prebble et al., 2006; Houben et al., 2013) have provided important insights into widespread advances of both the East and West Antarctic ice sheets, terminating into the western Ross Sea. TEX₈₆-based SST records indicate lower temperatures (6-14°C) in the Ross Sea during the Oligocene (Levy et al., 2016; Duncan, 2017) than offshore of the Wilkes Land margin (Hartman et al., 2018), suggesting a large (~7°C), much larger than present, (sub-) surface ocean temperature difference between the two sectors. However, it remains unknown if the warm conditions offshore of the Wilkes Land margin were unique or if similar temperatures existed close to the Ross Sea continental shelf in the Oligocene.

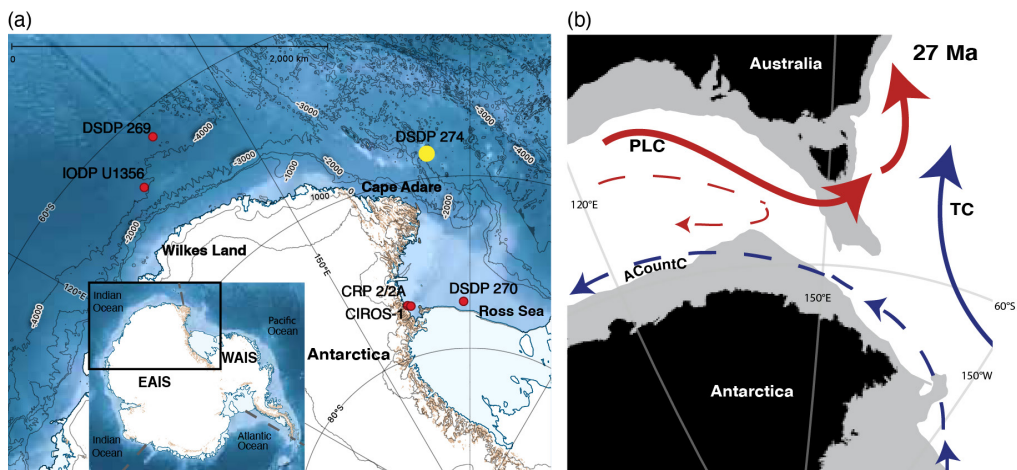


Figure 1. (a) Ross Sea to Wilkes Land margin bathymetry with present-day locations of DSDP/IODP/CRP drill sites included in this study (red dots). The new data generated for this study comes from DSDP Site 274, marked by yellow dot. The base map is from Quantarctica GIS package, Norwegian Polar Institute. The insert shows the Antarctic continent and the surrounding oceans (divided by gray dotted lines) to give a broader regional context to the study area. (b) A synthesis of paleoceanographic settings at 27 Ma. The paleogeographic position is generated with G-plates (<http://www.gplates.org>), based on the global plates geodynamic motion model from Müller et al. (2018). Light grey indicates the continental lithosphere. The inferred ocean currents are drawn after reconstructions by Stickley et al. (2004). TC = Tasman current, PLC = Proto-Leeuwin Current and ACountC = Antarctic Counter Current. Blue arrows indicate cooler ocean currents and red indicate warmer ocean currents. Relative current strength is indicated by arrow size.

To this end, we investigated sediments recovered during DSDP Leg 28 at Site 274, located on the offshore continental rise in the Ross Sea, ~250 km northwest of Cape Adare (Hayes et al., 1975), which is at an intermediate location between the aforementioned sites in the Ross Sea and offshore of Wilkes Land (Figure 1). DSDP Leg 28 retrieved valuable sedimentary records from the continental shelf and rise regions of the Ross Sea, but poor age control has long hampered their use in reconstructing past ocean conditions. Moreover, the archives were devoid of calcareous foraminifers, denying the use of their wall geochemistry, which is typically utilised for the reconstruction of ocean conditions. Studies based on dinocysts have, however, allowed both age control and palaeoceanographic interpretations as, for example, the result of the established connection between dinocyst assemblage composition and surfacewater conditions of the present-day Southern Ocean (Prebble et al., 2013; Zonneveld et al., 2013; Marret et al., 2020). Recent dinocyst records from the Ross Sea region, notably CRP (Clowes et al., 2016) and DSDP Site 270 (Kulhanek et al., 2019), and from Wilkes Land, IODP Site U1356 (Sangiorgi et al., 2018; Bijl et al., 2018a, b) and DSDP Site 269 (Evangelinos et al., 2020), have provided new biostratigraphic constraints. We used these constraints, alongside new biostratigraphic and magnetostratigraphic analyses, to improve the age model of DSDP Site 274. We then interpret palaeoceanographic conditions with dinocyst assemblages and generate quantitative SST reconstructions with lipid biomarkers (TEX₈₆). By comparing these results with available reconstructions from the Ross Sea and Wilkes Land in selected time slices, we evaluate how surface oceanographic conditions changed and latitudinal heat transport developed through the Oligocene.

2 Material

2.1 Site description

DSDP Site 274 (68°59.810 S; 173°25.640 E; 3326 m water depth; Figure 1a), is located on the lower continental rise in the northwestern Ross Sea, about 250 km north-northeast of Cape Adare (Hayes et al., 1975). Sediments were collected using punch-core rotary drilling on the Glomar Challenger in February 1973 (Hayes et al., 1975). Currently, the region is seasonally covered by sea ice (Fetterer et al., 2020), and the present-day mean annual SST is $\sim -1^{\circ}\text{C}$ (Locarnini et al., 2018). The site is in the vicinity of the southern upwelling margin of the Antarctic Divergence and is currently located in the path of a major outflow for Antarctic Bottom Water, spilling out over the western Ross Sea continental shelf where it is deflected westward (Orsi and Wiederwohl, 2009). The location of DSDP Site 274 is ideal for studying the offshore Oligocene oceanic properties in the Ross Sea (Figure 1b), which we compare to documented Antarctic ice sheet and ocean conditions from proximal Ross Sea records (Figure 1a).

2.2 Lithology and depositional settings

Drilling at DSDP Site 274 penetrated 421 mbsf (metres below the sea floor) and recovered a total of 43 cores containing 275.5 m of sediment. We focus our study on the interval between 174.2 and 408.5 mbsf (cores 19-43; Figure 2a). Sediment within this interval is mainly composed of (i) diatomrich detrital silty clay with varying abundances of diatoms, from trace amounts to up to 80% (diatom ooze) (174.2-328 mbsf), and (ii) silty claystones and interbedded chert layers (328-408.5 mbsf). Scattered iceberg-rafted debris (IRD; pebbles and granules) has been documented between 152 and 323 mbsf. Below 323 mbsf, chert layers compromised core recovery, and at 415 mbsf, the basalt basement was reached (Hayes et al., 1975). The sediment cores are rather homogenous and lack strong sedimentary structures. The strong biscuiting and fracturing of lithified sediment testify to drilling disturbance due to the rough nature of rotary drilling and may have obscured depositional sedimentary structures. Downslope transport of sediment from the Ross Sea continental shelf to the site potentially complicates the reconstruction of local pelagic-derived ocean conditions. The lithology and the seismic patterns (Hayes et al., 1975) suggest that sediment in the Oligocene was transported and deposited within the Adare Basin through a combination of downslope gravity currents and subsequent reworking by bottom currents (Hayes et al., 1975).

3 Methods

3.1 Age model

The shipboard age model (Hayes et al., 1975), based on a few biostratigraphic (diatom, radiolarian and calcareous nannofossils) age tie points, initially dated the DSDP Site 274 sedimentary record overlying the basalt to Late Eocene-Quaternary. More recently, Cande et al. (2000) dated the ocean crust underneath DSDP Site 274, using palaeomagnetic data, to chron 13, ~ 33.5 Ma, which is 200 kyr younger than the EOT and 5-7 Myr younger than it was dated during the expedition (Hayes et al., 1975). Granot et al. (2010) formulated seismic stratigraphic units and correlated these units with the Ross Sea continental shelf. The lowermost regional unconformity (328 mbsf) above the basement (Hayes et al., 1975) corresponds to a Ross Sea unconformity (RSU) found in the Northern Basin, RSU6, and estimated to be of Early Oligocene age (34-26.5 Ma; De Santis et al., 1995; Granot et al., 2010; Kulhanek et al., 2019). The major unconformity at 180.5 mbsf, between

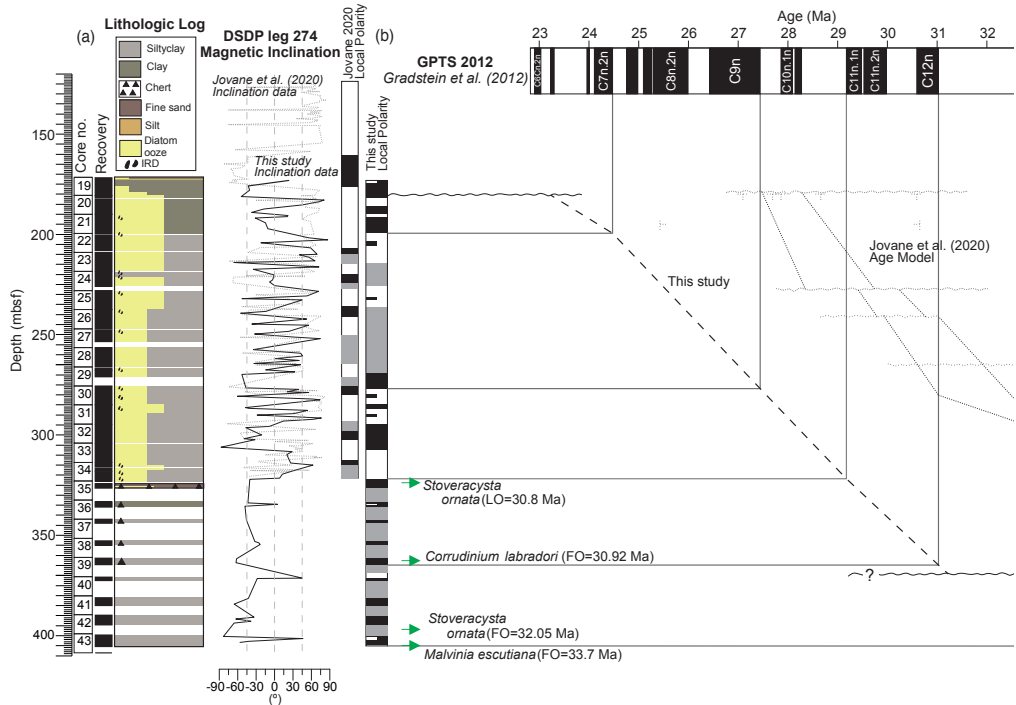


Figure 2. (a) Core numbers, core recovery and lithological description of the cores based on the initial DSDP reports (Hayes et al., 1975). (b) Magnetic correlation for Site 274 with comparison to Jovane et al. (2020) (dotted lines). Inclination values define local magnetic polarity zones. Magnetostratigraphic correlation is firstly guided by new dinocyst constraints, biostratigraphic markers from shipboard report and subsequently by correlation between local polarity zones and the GTS2012 timescale (Gradstein et al., 2012). Low intensity, shifting directions, and low recovery precludes magnetozone identification for some intervals. Characteristic orthoplots showing demagnetization steps is included in Supplementary Figure S1. Arrows indicate age (Ma) biostratigraphic tie points according to the age model described in Table 2. Extrapolations has been made between the age tie points (stippled lines) with sedimentation rates indicated in between. HO = Highest occurrence, LO = Last occurrence, FO = First occurrence.

cores 19 and 20 (Hayes et al., 1975), is tied to seismic reflectors RSU4 and RSU4a (Granot et al., 2010), which are aged to the mid-Miocene, ~15.8-14.6 Ma and ~17/16.9 Ma respectively (Pérez et al., 2021). To further improve the age model, we generated new age tie points based on dinocyst biostratigraphy and magnetostratigraphy to better constrain the age of the sedimentary record (cores 43-17). Dinocyst biostratigraphy follows Bijl et al. (2018a), who reassessed dinocyst species first and last occurrence datums calibrated against the GTS 2012 international geological timescale (Gradstein et al., 2012). Magnetic reversals on the sediment samples were identified through stepwise demagnetisation experiments performed using the 2G magnetometer with an inline alternating fields (AF) demagnetiser attached to an automatic sample handler in Fort Hoofddijk (Utrecht University) and the 2G-SRM750 Superconducting Rock Magnetometer housed at the Paleomagnetic Laboratory of Barcelona (CCiTUB-CSIC). As core orientation is not reconstructed, magnetic declinations are discarded and only magnetic inclinations are used to determine polarities.

Recently, Jovane et al. (2020) carried out a palaeomagnetic study at the DSDP Site 274, focusing on magnetic properties and magnetic mineralogy characterisation; by means of a review of the available biostratigraphic constraints, they also propose a new age model. Here, we compare their age model with ours and discuss the differences.

3.2 Organic geochemistry

To reconstruct sea (sub-) surface temperature (SST), we applied the TEX₈₆ (TetraEther indeX of 86 carbon atoms) proxy (Schouten et al., 2002), which is based on the temperature-dependent cyclisation of isoprenoidal glycerol dialkyl glycerol tetraethers (GDGTs) produced by thaumarchaeotal membrane lipids. GDGTs were extracted from powdered and freeze-dried sediments using an accelerated solvent extractor. Lipid extracts were then separated into an apolar, ketone and polar fraction by Al₂O₃ column chromatography using hexane: dichloromethane methanol (DMC; 9: 1, v: v), hexane: DCM (1: 1) and DCM: MeOH (1: 1) as respective eluents. A total of 99 ng of a synthetic C46 (mass-to-charge ratio, m/z = 744) GDGT standard was added to the polar fraction, which was subsequently dissolved in hexane: isopropanol (99: 1, v/v) to a concentration of ~3 mg ml⁻¹ and filtered over a 0.45 µm polytetrafluoroethylene filter. The dissolved polar fractions were injected and analysed by high-performance liquid chromatography-mass spectrometry (HPLC-MS), using double-column separation (Hopmans et al., 2016). GDGT peaks in the HPLC chromatograms were integrated using ChemStation software.

3.2.1 TEX₈₆ calibrations

Several calibrations exist to convert TEX₈₆ values into SSTs based on modern core-top datasets (Kim et al., 2010). We follow the discussion by Hartman et al. (2018) and use the linear calibration by Kim et al. (2010) to calculate the TEX₈₆ result into SST, which include the high-latitude core-top values. As we present peak areas of individual GDGTs in the Supplement (Table S2), other calibrations can be plotted as well.

3.2.2 TEX₈₆ overprints and bias

We use ratios of GDGTs as proxies to detect potential overprinting factors that may bias the pelagic signature of the sedimentary GDGTs. The relative contribution of terrestrial GDGT input has been reconstructed using the branched and isoprenoid tetraether (BIT) index (Hopmans et al., 2004). Samples with BIT index values >0.4 may be biased by soil and river-derived GDGTs (Bijl et al., 2013). However, we do note that the validity of this proxy for soil organic matter input is called into question now that it has become clear that branched GDGTs may also be produced in the marine realm (Peterse et al., 2009; Sinninghe Damsté, 2016) and in terrestrial ecosystems that contain crenarchaeol (Pearson et al., 2004). The methane index (Zhang et al., 2011) flags overprint by sedimentary methanogenic activity, the GDGT-2/GDGT-3 ratio (Taylor et al., 2013) signals overprint by archaeal communities dwelling deeper into the water column, and the GDGT-0/Crenarchaeol ratio (Blaga et al., 2009; Sinninghe Damsté et al., 2009; Taylor et al., 2013) flags overprint by in situ production of isoprenoidal GDGTs in lakes and rivers as well as contribution from Euryarchaeota. The ring index (Zhang et al., 2016) can detect deviations from a pelagic character in the GDGT “assemblage”. Samples which had overprinting values in these biasing indices were marked as unreliable. High-latitude TEX₈₆-SST reconstructions are believed to be skewed towards summer temperatures (Schouten et al., 2013; Ho et al., 2014), but studies around Antarctica have found that archaea appear most abundantly in winter and early spring, with maximum abundances in the subsurface at around 100 m (e.g. Church et al., 2003; Kalanetra et al.,

2009; Massana et al., 1998). However, there is a general agreement that TEX₈₆ captures the relative SST trend (Richey and Tierney, 2016) remarkably well despite these uncertainties, and this will be our main focus when interpreting the results.

3.3 Palynology

3.3.1 Palynological processing and taxonomy

A total of 50 samples, 2 per core (Core 43-17), were processed for palynology using previously published palynological processing and analytical procedures of the Laboratory of Palaeobotany and Palynology (e.g. Bijl et al., 2018a). Freeze-dried or oven-dried sediment was crushed and weighed (on average 10 g, SD of <1 g). A tablet of a known amount of *Lycopodium clavatum* spores (a marker grain) was added prior to palynological processing to allow for quantification of the absolute number of dinocysts per sample. In order to digest carbonates and silicates, the sediment underwent the following: treatment in 30% HCl overnight to remove calcium carbonate; treatment in 38% HF overnight to digest silicates; addition of 30% HCl to remove fluoride gels; and, finally, centrifugation and decantation. Organic residues were isolated between 250 and 10 µm sieve meshes, with the help of an ultrasonic bath to break down and clear out agglutinated organic particles. Residues were mounted on glass slides using glycerine jelly. Palynomorphs were counted using a Leica DM2500 LED transmitted light optical microscope. While the main focus was on dinocysts, terrestrial palynomorphs, acritarchs and prasinophyte algae (unicellular planktonic autotrophs) were quantified as well, and the presence and relative abundance of other organic remains were noted. Dinocyst taxonomy follows Williams et al. (2017), Clowes et al. (2016) and informal species as presented in Bijl et al. (2018a). Specimens were identified to a species level when possible. A minimum of 200 identifiable dinocysts were counted per slide at 400x magnification, while the remainder of the slide was scanned at 200x magnification to identify rare taxa not observed during the regular count. Samples with counts of <50 in situ specimens were discarded for qualitative assessment. All slides are logged in the collection of the Laboratory of Palaeobotany and Palynology, Utrecht University.

3.3.2 Dinocyst palaeoecological affinity

The present-day surface sediment distribution of dinocysts depends mostly on surface-water temperature but also on nutrient availability, salinity, primary productivity and sea ice cover (Dale, 1996; Prebble et al., 2013; Zonneveld et al., 2013). We assume that habitat affinities and trophic levels of modern dinoflagellate species remained similar throughout the Oligocene and Neogene, although shifts in environmental preferences have been demonstrated for a very limited number of species, e.g. *Impagidinium pallidum* (de Schepper et al., 2011). Here, we use the modern relationship between dinocyst occurrence and properties of the overlying water to infer oceanographic conditions in the past for extant species (Bijl et al., 2013; Prebble et al., 2013). To determine the habitat affinities and trophic level of extinct dinoflagellates, we rely on previously published papers where a link to palaeoceanographic proxies for temperature, runoff and/or freshwater input, and nutrient conditions was demonstrated (Bijl et al., 2011, 2018a; Frieling and Sluijs, 2018; Egger et al., 2018). We separate the dinocyst assemblages into gonyaulacoid (G) and protoperidinioid (P) cysts. In the Southern Ocean, G-cysts generally include phototrophic temperate dinocysts, associated with warm oligotrophic open-water conditions (Prebble et al., 2013). At present, G-cysts are rare in close proximity to the Antarctic ice sheet (Prebble et al., 2013). An exception is *Impagidinium pallidum* which is currently found in low percentages in Antarctic environments in the vicinity of the polar

front (Zonneveld et al., 2013). The extant *Operculodinium* spp., *Pyxidinospis* spp., *Corrudinium* spp., *Impagidinium* spp. and *Nematosphaeropsis labyrinthus* are absent or represent a minor component of the polar assemblages. P-cysts are produced by heterotrophic dinoflagellates and are usually found in nutrient-rich environments: river outlets, upwelling areas and sea ice zones (Zonneveld et al., 2013). In the present-day Southern Ocean, where the Antarctic Divergence upwelling favours a dominance of P-cysts, species such as *Brigantedinium* spp., *Selenopemphix* spp. and, especially, *S. antarctica* are common (Prebble et al., 2013). *S. antarctica* is a species that shows an affinity with sea ice conditions (Zonneveld et al., 2013; Marret et al., 2020).

3.3.3 Reworked versus in situ dinocysts

One issue with studying sediment records in the proximity of glaciated margins is separating reworked from in situ species, which is needed for obtaining reliable biostratigraphic constraints and palaeoceanographic signals (Macphail, 2021). In turn, quantifying the history of reworked material through time may yield information about the depositional conditions on the Ross Ice Shelf. In this study, we follow the interpretations of Bijl et al. (2018a) and separated dinocyst species into an assumed reworked and an in situ group a priori (Table 1). We applied statistical analysis to test a priori assumptions (Bijl et al., 2018a) on in situ or reworked dinocyst species and to quantitatively measure co-variability between environmental variables and palynological data. Our palynological data were analysed using correspondence analysis (CA), a linear ordination method to explore the differences in assemblages between samples. The palynological data (relative abundance) were plotted in the C2 software program (Juggins, 2007) using square root transformation.

Table 1: List of palynomorphs and their abbreviated codes found in the CA-plot (Figure 5). Assumed in situ and reworked dinoflagellate cyst taxa are assigned to Protoperidinioid protoperidinioid (P-cyst) taxa and Gonyaulacoid (G-cyst) taxa. (chrons).

In situ protoperidinioid taxa	Code	In situ gonyaulacoid taxa	Code
<i>Brigantedinium pynei</i>	Br pyn	<i>Achomosphaera alcornu</i>	Ac alc
<i>Brigantedinium simplex</i>	Br sim	<i>Batiacasphaera</i> spp. pars	Ba spp
<i>Brigantedinium</i> spp. pars.	Br spp	<i>Batiacasphaera cooperi</i>	Ba coo
<i>Lejeunecysta</i> spp.pars	L spp	<i>Batiacasphaera compta</i>	Ba com
<i>Lejeunecysta acuminata</i>	L acu	<i>Batiacasphaera</i> sp. B sensu Bijl et al., 2018	Ba spB
<i>Lejeunecysta adeliensis</i>	L ade	<i>Cerebrocysta</i> spp.	Cer spp
<i>Lejeunecysta attenuata</i>	L att	<i>Cleistosphaeridium</i> sp A. sensu Bijl et al., 2018	Cl spA
<i>Lejeunecysta fallax</i>	L fal	<i>Corrudinium</i> spp. pars	Co spp
<i>Lejeunecysta katatonos</i>	L kat	<i>Corrudinium labradori</i>	Co lab
<i>Lejeunecysta rotunda</i>	L rot	<i>Gelatia inflata</i>	G inf
<i>Lejeunecysta</i> sp. A	L spA	<i>Hystrichokolpoma bullatum</i>	Hy bul
<i>Malvinia escutiana</i>	M esc	<i>Impagidinium cf aculeatum</i>	I acu
<i>Protoperidinium</i> indet.	Prot	<i>Impagidinium cantabrigiense</i>	I can
<i>Selenopemphix antarctica</i>	Se ant	<i>Impagidinium velorum</i>	I vel
<i>Selenopemphix brinkhusii</i>	Se bri	<i>Impagidinium victorium</i>	I vic
<i>Selenopemphix nephroides</i>	Se nep	<i>Impagidinium paradoxum</i>	I par
<i>Selenopemphix</i> spp. pars	Se spp	<i>Impagidinium pallidum</i>	I pal
Dinocyst sp. 1	Dino sp1	<i>Impagidinium</i> sp. A sensu Bijl et al., 2018	I spA

In situ protoperidinioid taxa	Code	In situ gonyaulacoid taxa	Code
Reworked peridinioid cysts		<i>Nematosphaeropsis labyrinthus</i>	N lab
<i>Alterbidinium distinctum</i>	Al dis	<i>Operculodinium</i> sp. A sensu Bijl et al., 2018	O spA
<i>Deflandrea</i> spp. pars	Df spp	<i>Operculodinium centrocarpum</i>	O cen
<i>Moria zachosii</i>	M zac	<i>Operculodinium eirikianum</i>	O eir
<i>Phthanoperidinium</i> spp. pars	Ph spp	<i>Operculodinium janducheni</i>	O jan
<i>Senegalinium</i> spp.	Sen spp	<i>Operculodinium piasekii</i>	O pia
<i>Spinidinium</i> spp. pars	Spd spp	<i>Operculodinium</i> spp. pars	O spp
<i>Vozzhennikovia</i> spp. pars	Voz spp	<i>Pyxidinoopsis</i> spp.	Pyx spp
Other P-cyst reworked	otr-P	<i>Spiniferites ramous</i>	Sf ram
		<i>Spiniferites bulloideus</i>	Sf bul
		<i>Spiniferites</i> spp. pars	Sf spp
		<i>Stoveracysta kakanuiensis</i>	St kak
		<i>Stoveracysta ornata</i>	St orn
		Reworked gonyaulacoid cysts	
		<i>Arachnodinium antarcticum</i>	A ant
		<i>Cerebrocysta</i> spp. pars RW	Cer RW
		<i>Corrudinium regulare</i>	Co reg
		<i>Corrudinium incompositum</i>	Co inc
Other palynomorphs		<i>Emneadocysta</i> spp. pars	Enn spp
Unidentified Dinocyst 1	Indet 1	<i>Hystrichokolpoma rigaudiae</i>	H rig
Unidentified Dinocyst 2	indet 2	<i>Hystrichosphaeridium truswelliae</i>	Hy tru
Unidentified Dinocyst 3	indet 3	<i>Impagidinium</i> spp. pars RW	I RW
Terrestrial	Terr	<i>Operculodinium</i> spp. RW	Ope RW
Pterospermella/green algae	Ptero	<i>Pentadinium laticinctum</i>	P lat
Acritarch spp.	Acrit spp	<i>Thalassiphora pelagica</i>	Th pel
Acritarch chorate/spiney spp.	Acri spiney	<i>Tuberculodinium vancampoae</i>	T van
<i>Leiosphaeridia</i>	Leios	<i>Turbiosphaera</i> spp. pars RW	Tur spp
<i>Cymatosphaera</i> spp. pars	Cym Spp	Other G-cyst reworked	otr-G

4 Results

4.1 Revised age model

Based on four new dinocyst-based first occurrence (FO) and last occurrence (LO) datums found in the DSDP Site 274 record, we provide additional age constraints for the age model upon which we correlate five new palaeomagnetic reversal results to specific magnetic chrons (based on Gradstein et al., 2012; Table 2). Palaeomagnetic results are generally of low quality (Figure 2b). We interpret this to result from both a low natural remnant magnetisation (NRM) intensity (typically between 10 and 50 A m⁻²) and the likely growth of iron sulfides during the ~50-year storage of the cores, which are probably the cause of magnetic noise as well as the partial isolation of the characteristic component in some samples (Figure S1, Table S1). Due to the low quality of results, we are cautious and are only confident in those magnetozones with at least three adjacent samples sharing similar polarity values. Cores 23 to 19 express a well-defined polarity pattern. Below, the interval encompassing cores 26-28 (269.12-214.43 mbsf; shown in grey in Figure 2b) does not show a definite pattern and,

consequently, was not considered for palaeomagnetic correlation. The lower part, cores 35-43, has a very low recovery and is prone to normal polarity directions. Magnetostratigraphic results for the upper Oligocene generally agree with those recently published by Jovane et al. (2020), as shown in Figure 2. For the lower part of the record, our biostratigraphic results provide new tie points that indicate a lower-Oligocene age, instead of the previously published upper-Eocene age (Hayes et al., 1975; Jovane et al., 2020). The presence of the marker dinocyst *Malvinia escutiana* (FO = 33.7 Ma; Houben et al., 2011, 2019) in the lowermost sediment sample (Core 43, 404.66 mbsf), directly overlying the basement, indicates an Early-Oligocene age of the lowermost sediment that was also suggested from the age of the underlying ocean crust (Cande et al., 2000). Thus, we correlated the normal magnetozone in Core 43 (400.7 mbsf) with magnetic chron C13n. A few sections above, we find the FO of *Stoveracysta ornata* (32.5 Ma) at 396.62 mbsf, the FO of *Operculodinium eirikianum* (31.56 Ma) at 352.78 mbsf, the FO of *Corrudinium labradori* (30.92 Ma) at 362.42 mbsf, and the LO of *Stoveracysta ornata* (30.8 Ma) at 323.6 mbsf. Thus, we suggest that the reversal in the lower part of Core 34 (321.2 mbsf) is correlated with the top of C11n.1n (29.18 Ma) and that the normal magnetozone found in cores 29 and 30 (277 mbsf) is correlated with chron C9n (Table 2). Core 21 (~190.8 mbsf) contains one isolated calcareous nannofossil horizon (Burns, 1975) dominated by *Chiasmolithus altus*, which marks the oldest age of 25.44 Ma (chron C8n; Gradstein et al., 2012). Cores 34-20 are included in the diatom *Pyxilla Prolungata* zone (Hayes et al., 1975), which also suggests an Early-Oligocene age (>25 Ma); however, the LO of *Pyxilla Prolungata* is thought to go on until the Oligocene-Miocene boundary (23 Ma) (Gombos, 1977). Based on these initial reported biostratigraphic observations (Hayes et al., 1975), we correlate the base of the normal magnetozone of Core 21 (199.47 mbsf) with the base of chron C7n.2n (24.4 Ma). A few biostratigraphic constraints, including middle-Miocene radiolarian species in Core 19 (Hayes et al., 1975), indicate that the latest Oligocene and Oligocene-Miocene transition is missing in a large hiatus of ~7 Myr between cores 19 and 20 (181.23 mbsf). We abstain from correlating the normal magnetozone of Core 19 to a specific chron, due to the limited biostratigraphic markers; thus, we support Jovane et al. (2020), who suggested Langhian to Burdigalian ages. Extrapolating linearly between chrono and biostratigraphic tie points (Figure 2b, Table 2), we calculate the average sedimentation rate in the Oligocene to be 2.4 cm/kyr.

Table 2. Improved age model for the Oligocene of DSDP Site 274 determined by dinocysts biostratigraphy indicators (FO denotes first occurrence, and LO denotes last occurrence) and palaeomagnetic reversals (chrons).

FO/LO	Genus, Chron	Species	Age (Ma)	Depth (mbsf)	Depth error	Event source
	Base of C7n.2n		24.474	199.47		This study
	Base of C9n		27.44	277		This study
	Top of C11n.1n		29.18	321.2		This study
LO	<i>Stoveracysta</i>	<i>ornata</i>	30.8	323.655	2.015	This study
FO	<i>Corrudinium</i>	<i>labradori</i>	30.92	362.42	1.24	This study
	Base of C12n		31.03	363.44		This study
FO	<i>Stoveracysta</i>	<i>ornata</i>	32.5	396.62	5.25	This study
	Base of C13n		33.7	400.17		This study
FO	<i>Malvinia</i>	<i>escutiana</i>	33.7	404.66	n/a	This study

4.2 Lipid biomarkers

A total of 39 of the 42 samples processed for lipid biomarkers showed no indication of overprints by biasing indices (Figure S2). The low BIT index value (<0.08 , with one exception at 361 mbsf; Figure S2) suggests low terrestrial organic material influence, relative to marine GDGT production. The normal Ring index values (Figure S3), with only two outliers, suggest normal pelagic contributions to the sedimentary GDGTs. Thus, overall, TEX_{86} values represent an in situ pelagic SST signal. Moreover, the absence of co-variance between TEX_{86} and indices for overprint suggest that the high variability in TEX_{86} also represents a pelagic signal. TEX_{86} values range from 0.44 to 0.55. Using the linear calibration of Kim et al. (2010) (Figure 4c), SSTs vary between 10 and 17°C ($\pm 5.2^\circ\text{C}$) throughout the record, with noticeable variability. Below 342 mbsf, reconstructed SSTs are relatively high and variable (10–16°C). Between 335 and 248 mbsf, SSTs are lower and display lower variability (10–13°C) at the same sample resolution as above. An increase in SST of $\sim 6^\circ\text{C}$ at 248 mbsf marks the onset of a second interval with high variability in SST.

4.3 Palynomorphs and dinocyst assemblages

A total of 43 of the 50 samples analysed contain sufficient dinocysts. All samples that were too low in dinocysts came from the top of the studied record (186.66–155.68 mbsf) and were discarded. Samples showed a varying abundance of four palynomorph groups: reworked dinocysts, in situ dinocysts, terrestrial palynomorphs, and acritarchs and prasinophytes (Figure 4a). The sediments below 352.5 mbsf are dominated by reworked dinocysts, which decrease in abundance above this depth. From 352.5 mbsf to the top of the record, in situ dinocysts constitute the most abundant palynomorph group, followed by acritarchs, which slightly increase up-core. Pollen and spores remain low throughout the entire record ($<6\%$). Furthermore, our palynological samples contain a varying amount of pyritised microfossils and amorphous organic material.

4.3.1 Dinocyst taxonomy

Identification of dinocysts on a species level was possible in most cases (Table S3). However, some dinocysts were only defined on a genus level when distinctive features were lacking. *Brigantedinium* spp. includes all round brown specimens. *Batiacasphaera* spp. includes small sub-spherical cysts with an angular, likely apical archeopyle and, if any, minute surface ornamentation. *Pyxidiniopsis* spp. has similar features to *Batiacasphaera* spp. but is typically (even) smaller, has a thicker, slightly darker wall, and is less folded with a single plate precingular archeopyle. Dinocysts with a smooth, spherical, psilate, hyaline wall and a free, angular-rounded operculum (five to six sides) generally found within the cyst are hereby informally named “Dinocyst sp. 1”. The saphopylic archeopyle of Dinocyst sp. 1 resembles that of *Brigantedinium* spp. and *Protoperidinium* spp.; thus, we consider Dinocyst sp. 1 to belong to the (heterotrophic) protoperidinioid (P) cysts.

4.3.2 Reworked dinocyst assemblages

The lowermost 60 m of the sediment record, below 352.5 mbsf, yields abundant and diverse dinocysts that are common in Eocene Southern Ocean sediments (Bijl et al., 2013; Cramwinckel et al., 2020; Crouch et al., 2020), including *Vozzhemikovia apertura*, *Deflandrea antarctica*, *Enneadocysta* spp. and *Phthanoperidinium* spp. These species are found throughout the entire record, but their relative abundance decreases up-section. We note good preservation of some of the more delicate dinocysts, which have known biostratigraphic ranges that predate the age of the ocean crust underneath DSDP Site 274; therefore, we still regard them to be reworked. However,

we cannot rule out that these typical Late-Eocene dinocysts were still present in the Early Oligocene and, therefore, in situ deposited in the record (Bijl et al., 2018a).

4.3.3 In situ dinocyst assemblages

In the lowermost 15 m of the record, below 390.4 mbsf, the (apparent) in situ assemblage (Figure 4b) is dominated by P-cyst species, Dinocyst sp. 1 and *Brigantedinium* spp., indicating high nutrient levels in open-ocean settings. Given that *Brigantedinium* spp. has a preference for open-ocean conditions, often with proximity to upwelling areas both in the modern and the ancient ocean (Zonneveld et al., 2013; Sluijs et al., 2005), we render it unlikely that it was transported from the continental shelf and reworked. *Brigantedinium* spp. and Dinocyst sp. 1 have not been reported from CRP-3 (Clowes et al., 2016) or the Eocene erratics (Levy and Harwood, 2000) from the Ross Sea area. The good preservation state of the delicate Dinocyst sp. 1 and *Brigantedinium* spp. species argues for in situ production. The extinct P-cyst species *Malvinia escutiana* occurs throughout the record: its relative abundance increases from the bottom of the record towards its peak interval from 224 mbsf to the top of the record. At about 335 mbsf, the dinocyst assemblages change significantly. Above this depth, G-cysts associated with open, possibly warmer and oligotrophic waters dominate the assemblages. This shift in the dinocyst assemblage does not coincide with any remarkable change in the lithology. Hence, we are confident that the assemblage shift is a real feature in the record and not a result of the selective preservation of P- and G-cysts. It is known that P-cysts are more sensitive than G-cysts to oxidation (e.g. Zonneveld et al., 2010), and any mechanism (bottom currents, mixing, sediment starvation) that favours sediment oxygenation would decrease the probability of finding P-cysts preserved in the record relative to G-cysts. *Batiacasphaera* spp., *Pyxidinopsis* spp. and *Cerebrocysta* spp. compose the majority of the G-cysts. *Spiniferites* spp. is relatively abundant (~10-20% of the total in situ dinocyst counts) in the interbedded chert layers below 352.5 mbsf and again, although less prominently, at 221.4 mbsf, whereas it remains low (<4%) in the rest of the record. *Operculodinium* spp. is common (10-20%) between 201 and 221 mbsf. The highest amount of *Operculodinium* spp. (27%) was found at 239.16 mbsf. *Nematosphaeropsis labyrinthus* is only registered between 361 and 352 mbsf (green line in Figure 4b). *Impagidinium* spp. remains low (<7%) in all samples. Throughout the record, dinocyst species indicative of cold water are rare. *Selenopemphix antarctica*, a major component of the modern Antarctic coastal assemblages (Zonneveld et al., 2013), is never abundant and is only present in few samples (between 390.44 and 333 mbsf, and at 302 mbsf). *I. pallidum*, a dinocyst abundant in polar areas of the modern ocean (Zonneveld et al., 2013; Marret et al., 2020) but known for its tolerance to higher temperatures in the past (de Schepper et al., 2011), has a scattered low presence throughout the record.

4.3.4 Other palynomorphs: pollen, acritarchs and prasinophyte algae

The consistently sparse pollen assemblages from DSDP Site 274 suggest a shrubby tundra landscape with low-growing Nothofagaceae and Podocarpaceae. The offshore and off path location with respect to the wind patterns from the continent may be an explanation for the low pollen numbers, and we cannot make further interpretations regarding the terrestrial ecology. The relative abundance of acritarchs and prasinophytes seems to increase up-core. Transparent chorate acritarchs are the most dominant throughout the record. *Leiosphaeridia* spp. is only sporadically present and is most common in the lowermost sediments (>390 mbsf). Prasinophyte algae *Cymatiosphaera* spp. is found throughout the record but is more abundant around 285 mbsf and above 224 mbsf

4.4 Correspondence analysis

The CA on our palynological results (Figure 3, Table S4) resulted in the first two axes explaining 46% of the total variance (31% for axis 1, and 15% for axis 2), which is high given the multidimensionality of the high dinocyst diversity. Most of the dinocysts that were assumed to be reworked a priori (purple circles in Figure 3) show negative scores on axis 2 (64%). Those taxa that do not have a negative score on axis 2 generally have low total counts or relative abundances (small circles in Figure 3). Overall, the species that we consider to be definitely in situ (see also Bijl et al., 2018a) have negative scores on axis 1, and reworked taxa tend to cluster on the positive side of axis 1. Terrestrial palynomorphs (pollen and spores) plot in the same area as the reworked dinocyst taxa. The overall separation of reworked and in situ taxa on the first CA axis gives us confidence that our a priori assumption of in situ and reworked is correct (Table 1).

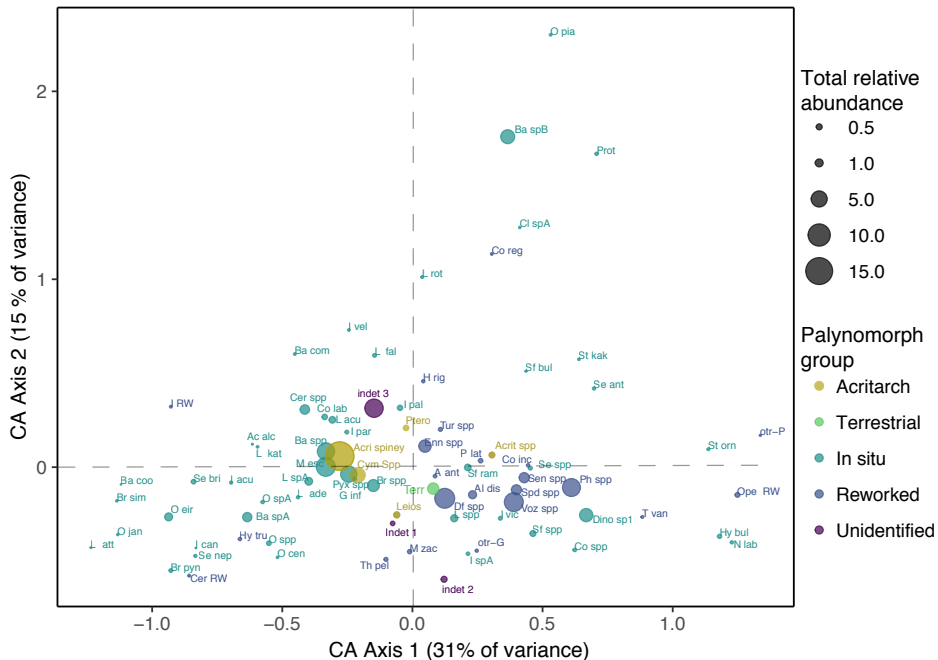


Figure 3. Correspondence analysis (CA) of the dinocyst assemblage data from DSDP Site 274. The size of the points indicates the total relative abundance of the specific species. The abbreviations of the dinocysts species can be found in Table 1. The data were plotted in the C2 software program (Juggins, 2007). The analysis scores are provided in Table S4.

5 Discussion

5.1 Updated age model

The age model for DSDP Site 274 is updated with four additional biostratigraphic datums and five magnetostratigraphic datums. Specifically, age constraints in the bottom (early Oligocene, 33.7 Ma, 404.66 mbsf) and top (late Oligocene, 24.4 Ma, 181.23 mbsf) of the studied interval (408.5-174.2 mbsf) have been improved. However, the few existing age constraints for the middle part (mid-Oligocene, 307.1-199.5 mbsf) do not allow a significant improvement of the existing age model for

this interval (Figure 2b, Table 2). Jovane et al. (2020) presented an update of the biostratigraphic constraints of Site 274 and, afterwards, guided their magnetostratigraphic correlation with these constraints. Like ours, their polarity pattern alone is not sufficient to provide an independent chronology. Our obtained polarity pattern is similar to Jovane et al. (2020) for the upper part of our study, i.e. late Oligocene (Figure 2b). This is also true for the unclear polarity zone between cores 29 and 25 where Jovane et al. (2020) also found inclinations that produce a uncertain polarity pattern. Our correlation with the timescale, however, differs in the lower part of the section, below 320 mbsf, where we provide new magnetostratigraphic data and biostratigraphic age constraints, and implement the most recent insights on the age of the ocean crust underlying the site (Cande et al., 2000). This results in younger ages for the lower part of the section, which are propagated upwards, altogether indicating younger ages for DSDP Site 274 compared with the study of Jovane et al. (2020) and the initial report. We acknowledge that although our new constraints have improved the age model, large uncertainties remain due to moderate recovery, reworked material, weak NRM intensities (Table S1) and the limited occurrence of age-diagnostic microfossils. This means that between tie points, sedimentation rates may vary and hiatuses could be present. Therefore, we plot the data in the depth domain and indicate the age tie points next to the depth scale (Figs. 2, 4). Notwithstanding these age model uncertainties, the proxy data that we present provide a rare glimpse into early- to middle Oligocene surface-water conditions.

5.2 Palaeotemperature and palaeoenvironment in the Oligocene at DSDP Site 274

Combined, the temperature, in situ and reworked palynomorph results provide integrated palaeoceanographic configurations offshore of the Ross Sea margin during the Oligocene (33.7-24.4 Ma) (Figure 4). Furthermore, we combine our reconstruction with those available around the East Antarctic margin from the western Ross Sea and Wilkes Land to obtain a regional perspective.

5.2.1 Surface oceanographic conditions

Both dinocyst assemblages and TEX_{86} -based SST results (Figure 4b, c) consistently suggest temperate surface-ocean conditions. High variability in the dinocyst- and TEX_{86} -SST reconstructions reflects highly dynamic surface-ocean conditions. Although P-cyst species are abundant in the top and bottom of the record, suggesting nutrient-rich conditions, the middle part of the record is dominated by a high abundance of G-cyst species, indicating that oligotrophic and warm conditions prevailed (Figure 4b). The dominance of G-cysts implies that upwelling (the proto-Antarctic Divergence) was greatly reduced or located far away from the site. Above 265 mbsf, the more frequent shifts between P-cyst-dominated and G-cyst-dominated assemblages reflects strongly varying oceanographic conditions, perhaps as a result of shifting frontal system locations or dynamics (as offshore of Wilkes Land; Salabarnada et al., 2018; Bijl et al., 2018b; Hartman et al., 2018). The scarce presence of typical sea-ice-affiliated dinocysts suggests that sea ice was absent or that the sea ice seasonal coverage was strongly reduced (Bijl et al., 2018b) compared with the present day (Fetterer et al., 2020). The dinocyst assemblages mostly contain known marine species, indicative of normal ocean salinities. However, Dinocyst sp. 1 (turquoise in Figure 4b), abundant in sediments at >335 mbsf, morphologically resembles the peridinioid *Senegalinium* spp., a genus known for its high tolerance to low surface-water salinities (Sluijs and Brinkhuis, 2009). If morphology is indicative of environmental conditions, the region could have been under the influence of meltwater and/or increased precipitation during the early Oligocene. The overall abundance of reworked (Eocene) dinocysts suggests the erosion of marine sediments on the Ross Sea continental shelf and the transport thereof towards the abyssal plain by wind-driven transport

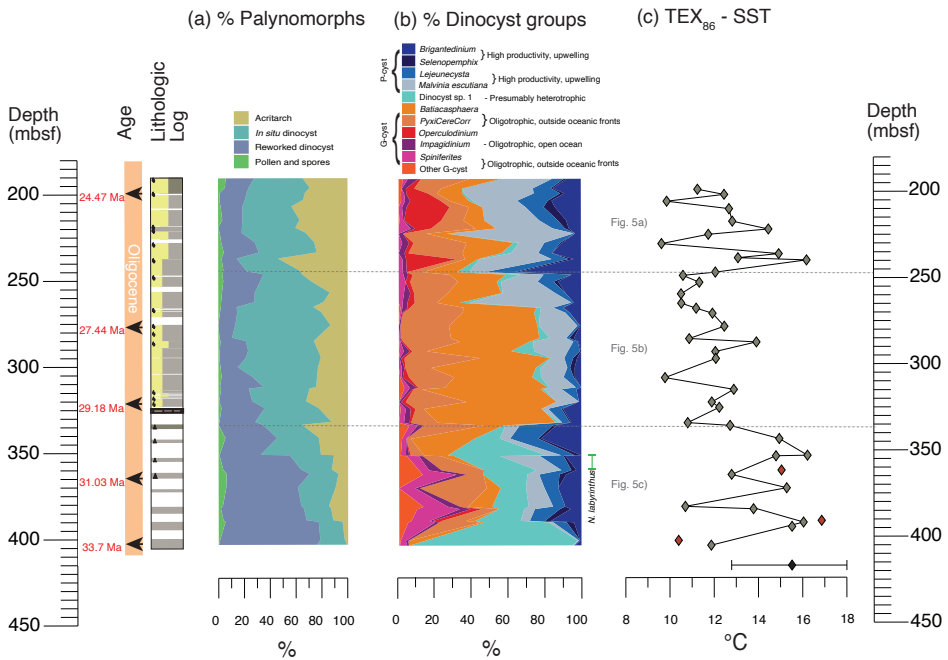


Figure 4. Lithological (the legend is the same as Figure 2), palynological and TEX_{86} -SST results from DSDP Site 274 plotted against depth. Arrows indicate age (Ma) tie points according to the age model described in Table 2. The dotted grey line indicates the time slices selected for Figure 5. (a) The cumulative relative abundance of palynomorph groups. (b) The cumulative relative abundance (%) of selected dinocyst groups recorded in the studied interval. Blue tones are P-cysts, and red-tones are G-cysts. (c) TEX_{86} -based SSTs (linear calibration; Kim et al., 2010), calibration error is $\pm 5.2^{\circ}\text{C}$, are indicated by the black bar at the bottom of the plot. The TEX_{86} outliers are marked in red.

of surface water or through density-driven bottom water flow cascading down the continental slope. In general, the Oligocene dinocyst assemblages found at DSDP Site 274 are similar to present-day dinocyst assemblages living between the subantarctic and subtropical front, where temperatures range from 0 to 15°C (Prebble et al., 2013). This is in line with the high TEX_{86} SSTs (10 – 17°C) and indicates much warmer surface waters with lower nutrient levels than today, although the site is currently located in an area with average SSTs $\sim -1^{\circ}\text{C}$ (Locarnini et al., 2018).

5.2.2 Oligocene oceanography and climate evolution at DSDP Site 274 in a regional context

The generally warm SSTs throughout the Oligocene suggest that the recorded high productivity at the site was probably not the result of cold upwelled waters. However, in the early Oligocene (404.66–335.34 mbsf), the relatively abundant P-cysts do indicate high-nutrient and, possibly, low-salinity surface-water conditions (Figure 4b). Instead of upwelling, we suggest that strong surface-water mixing stimulated ocean primary productivity at the site, perhaps with additional nutrient sources through melting from the Ross Sea continental margin. Rifting of the western Ross Sea shelf since 60 Ma (Huerta and Harry, 2007) has created thick Eocene sedimentary successions on the Ross Sea shelf. Glacial isostatic adjustments as a response to the Antarctic ice sheet buildup

(~48-34 Ma) caused reorganisation of shelf sedimentation (Stocchi et al., 2013), notably increases in sedimentation rates due to the accumulation space created by higher sea level and bedrock subsidence in some regions and erosion due to bedrock uplift at others. Strata drilled at DSDP Site 270 on the Ross Sea continental shelf indicate periods of early-Oligocene glaciomarine deposition derived from local ice caps nucleated on elevated highs prior to tectonic subsidence in that region (De Santis 1999; Kulhanek et al., 2019). Turbid meltwater derived from the margins of these marine terminating ice caps and from glaciomarine/fluvial systems at the margins of outlet glacier along the Transantarctic Mountain front (Fielding et al., 2000) would also allow for transport via a suspended sediment load or downslope processes towards the continental rise at DSDP Site 274, similar to the Wilkes Land continental rise (Bijl et al., 2018b; Salabarnada et al., 2018). The high abundance of reworked Late-Eocene dinocysts testifies to the influence of continental shelf-derived surface water towards the site, which brings nutrients and promotes productivity (increase in P-cysts). This high amount of reworked dinocysts could further argue for a reworked TEX₈₆-SST signal. However, the nearshore character of the Eocene reworking (abundant pro deltaic, marginal-marine peridinioid cysts) would have increased the branched, soil-derived GDGTs. This sharply contradicts the low (<0.08) BIT values (Figure S2). After ~29 Ma (335 mbsf), the relatively high TEX₈₆-based SSTs (10-17°C) and abundant offshore, temperate dinocyst species *Operculodinium* spp., *Spiniferites* spp. and *Nematosphaeropsis labyrinthus* (Figure 5b, c) indicate a long period of temperate conditions at DSDP Site 274. The co-varying trend between dinocyst species and the SSTs indicates that SST has a strong influence on the biotic response. For the first time, *Malvinia escutiana* is found in mid Oligocene sediment (<265 mbsf); this extends the LO of this species relative to previous reports (Bijl et al., 2018a). Its high abundance suggests that conditions were favourable for this species and makes it unlikely that its occurrence in the mid-Oligocene represents a reworked signal. The CA plot (Figure 3) shows that *Malvinia escutiana* co-varies with oligotrophic and temperate dinocyst groups as well as with acritarchs. This suggests that *Malvinia* favours open-water and low-nutrient conditions. A conundrum in our data is the increase in G-cyst groups, *Batiacasphaera* spp., *Pyxidinopsis* spp. and *Cerebrocysta* spp., in the mid-Oligocene and the decrease in P-cyst abundances synchronous with declining SST starting at ~29 Ma (335.3 mbsf). At present, these G-cysts are associated with more northerly subantarctic and subtropical front zone regions (Prebble et al., 2013) with temperate ocean conditions. Although temperate dinocyst and lipid biomarker signals are generally consistent in the record, an increase in G-cyst assemblages affiliated with warm conditions corresponds to a decrease in SST between ~29 and 26.8 Ma (335.3-252.2 mbsf). Here, we argue that decreasing nutrient levels cause P-cyst to be replaced by G-cysts. Throughout the record, variability in nutrient conditions rather than temperature seems to be the driving factor in dinocyst distribution. Abundance of transparent chorate acritarchs at DSDP Site 274 generally follows warmer SSTs, similarly to what was found in the record of Site U1356 offshore of Wilkes Land (Bijl et al., 2018b). The CA analysis showed little covariance between acritarchs and reworked cysts, suggesting that the acritarchs are in situ. At ~26.5 Ma (239.2 mbsf), the acritarchs peak is synchronous with a peak in temperate dinocyst species (*Operculodinium* spp.). Acritarchs as well as *Operculodinium* spp., a pioneer species, are known to be opportunist (e.g. Dale, 1996). Previous studies on Antarctic proximal records, from the CIROS-1 core (Hannah, 1997) and DSDP Site 270 (Kulhanek et al., 2019), have associated the presence of acritarchs (*Leiosphaeridia* spp.) and prasinophytes (*Cymatiosphaera* spp.) with episodes of sea ice melting. We did not find abundant *Leiosphaeridia* spp. Thus, we interpret that the meltwater influence was reduced at DSDP Site 274, compared with sites on the Ross Sea continental shelf that were more proximal to the glaciated margin.

5.3 Regional perspective

We compare our Oligocene palaeoceanographic reconstructions from DSDP Site 274 with records from off the Wilkes Land margin (Site U1356; Hartman et al., 2018; Salabarnada et al., 2018; Bijl et al., 2018a, b; Sangiorgi et al., 2018) and the Ross Sea (Houben et al., 2013; Clowes et al., 2016; Kulhanek et al., 2019; Duncan, 2017) (Figure 5). For this comparison, published TEX_{86} data from the Wilkes Land margin (Hartman et al., 2018) and the Ross Sea (Duncan, 2017) were converted to SSTs using the linear calibration of Kim et al. (2010) (calibration error of $\pm 5.2^\circ\text{C}$).

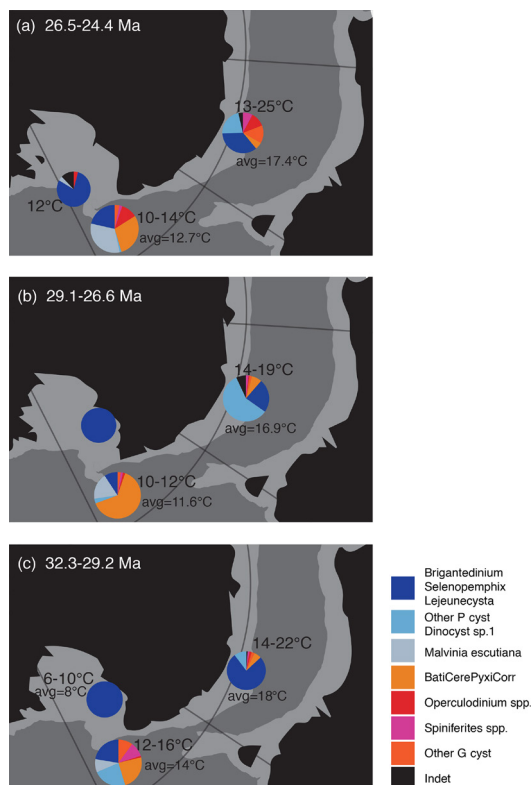


Figure 5. Synthesis of sea surface temperature and dinocysts assemblage changes between the early (c), mid (b) and late Oligocene (a) in the Ross Sea (CRP, DSDP Site 270), offshore Cape Adare (This study, DSDP Site 274) and Wilkes Land margin (Site U1356). The pie charts visualize the dinocyst assemblage composition at respective sites (see legend). Dinocyst assemblage data from the Wilkes Land margin, U1356, comes from Bijl et al. (2018a, b) for all panels (a-c). Dinocyst assemblage data from the Ross Sea is gathered from DSDP Site 270 (Kulhanek et al., 2019) for panel a) and from CRP (Houben et al., 2013; Clowes et al., 2016) for panel (b) and (c). The TEX_{86} -SST data from Wilkes Land, U1356 comes from Hartman et al. (2018), 35 TEX_{86} -data points were used; 7 in (a), 9 in (b) and 19 in (c). In the Ross Sea there is a lack of TEX_{86} -SST data from the mid Oligocene, but Duncan (2017) presented unpublished TEX_{86} -data from CIROS- (12 TEX_{86} -data points), here displayed in panel (c), and from DSDP Site 270, where only one data point matched our mid-early Oligocene time slice in panel (a). All TEX_{86} data have been converted to the SST using linear calibration of Kim et al. (2010) (calibration error: $\pm 5.2^\circ\text{C}$). The paleogeographic position is generated with G-plates (<http://www.gplates.org>), based on the global plates geodynamic motion model from Müller et al. (2018).

Early Oligocene (32.3–29.2 Ma, 391–335 mbsf)

DSDP Site 274 TEX_{86} -SST results suggest a slightly lower average offshore temperature in the Ross Sea ($\sim 4^{\circ}\text{C}$) than at Wilkes Land (Site U1356) but higher temperatures ($\sim 6^{\circ}\text{C}$) than at the ice-proximal Ross Sea site (CIROS-1; Figure 5c). This observation is consistent with the position of DSDP Site 274, which was at higher palaeolatitudes compared with Site U1356 but at lower latitudes and offshore of the ice proximal sites within the Ross Sea. Indeed, evidence from the CRP cores in the Ross Sea showed that continental-scale ice sheets first expanded towards the Ross Sea around 32.8 Ma (Galeotti et al., 2016). Prior to 31 Ma (350 mbsf), the SST record from DSDP Site 274 shows some of its highest temperatures, while SSTs at Site U1356 decrease. One important consideration is whether these sites in the Ross Sea and Wilkes Land can be compared in the context of belonging to a latitudinal transect, given that they are separated by an evolving Tasmanian Gateway, which is a conduit that separates the eastern Indian and southwestern Pacific oceans. Although a deep-water connection in the Tasmanian Gateway was established in the Oligocene, the passageway was still restricted (Stickley et al., 2004; Bijl et al., 2013). Studies of the palaeobathymetry and sedimentary mechanisms in the Southern Ocean through the Cenozoic (e.g. Scher et al., 2015; Hochmuth et al., 2020) show the Tasmanian Gateway as well as the Pacific sector of the Southern Ocean deepen between 34 and 27 Ma, allowing easier throughflow and exchange between the different ocean sectors. The limited covariability of the Adare Basin and Wilkes Land margin, as well as different SSTs might signal a disconnect between the two sites, perhaps due to a still restricted Tasmanian Gateway. While synchronous SST variability and changes therein between the sectors after 31 Ma suggest a connection between the ocean basins, which is in line with other studies (Scher et al., 2015), a SST difference between both sectors remains. The abundance of low-nutrient/temperate-affiliated dinocyst taxa (G-cyst) is higher at DSDP Site 274 than at the Wilkes Land margin and within the Ross Sea continental shelf, implying that nutrient input was lower at the offshore Ross Sea location than at more proximal sites, with a higher degree of meltwater input.

Latest early Oligocene to earliest late Oligocene: “mid-Oligocene” (29.1–26.6 Ma, 333–239 mbsf)

In the “mid-Oligocene”, the disparity with respect to absolute SST average values between DSDP Site 274, the Ross Sea and the Wilkes Land margin is the strongest. Both the Wilkes Land margin and the Ross Sea have a high P-cyst content (Figure 5b). Palynomorphs from Ross Sea shelf deposits from the Oligocene, dominated by *Lejeunecysta* spp. and brackish water prasinophyte *Cymatiosphaera* (CRP: Prebble et al., 2006; Clowes et al., 2016), suggest meltwater input in the Ross Sea region through this time interval (Prebble et al., 2006). In contrast, our dinocyst assemblages suggest pelagic, low-nutrient, marine conditions, while the low numbers of terrestrial palynomorphs point to limited freshwater or meltwater input at DSDP Site 274. Similar to the Wilkes Land margin SST record, DSDP Site 274 SSTs decrease towards the Late Oligocene.

Late Oligocene (26.5 to ~ 24.4 Ma, 239–192.7 mbsf)

The average TEX_{86} -based SST results (Figure 5a) for IODP Site U1356 and DSDP Site 274 show large ($>6^{\circ}\text{C}$) temperature variability (Hartman et al., 2018). At DSDP Site 274, we can exclude the known non-thermal biases as the cause of the strong variability (Figure S2); therefore, we also note stronger SST variability in the late Oligocene. It is noteworthy that we see a temperature peak at DSDP Site 274 at the beginning of this interval at 26.5 Ma (239 mbsf) which is similar to what was reconstructed at the Wilkes Land margin (Hartman et al., 2018). This temperature peak coincides with a rapid decrease in the $\delta^{18}\text{O}$ isotope records that may be linked to the deglaciation of large parts of the Antarctic ice sheet following a large transient glaciation centred on ~ 26.8 Ma (Pälike et

al., 2006). The increase in the abundance of *Operculodinium* spp. at all three sites (DSDP sites 270 and 274, and IODP Site U1356) is a testament to the temperate conditions and/or lower nutrient availability at the time.

The DSDP Site 274 sediment record is virtually barren of palynomorphs <192.7 mbsf (~24.4 Ma), 11.7 m below the hiatus (181 mbsf) in the record, with the sediments above estimated to be of middle-Miocene age (Hayes et al., 1975). As our SST reconstructions exclude continuous sea ice cover as a possible explanation, we interpret that oxic degradation consumed palynomorphs at the sea floor. Three reasons for increased oxygen delivery at the sea floor are proposed. The first explanation is that strengthening of the Antarctic Circumpolar Current (ACC) increased deep ventilation. This is unlikely given that the ocean frontal systems would have moved progressively northward while the Tasmanian Gateway widened, which would also have displaced the ACC flow northwards, away from the site. The second explanation is that winnowing ocean bottom currents and decreased sedimentation rates could have caused the oxic conditions that we propose and were the reason behind the disappearance of dinocysts. However, winnowing would not have only eroded palynomorphs and would have resulted in the coarsening of sediments, which we do not see. The lithology of the 192.7-181 mbsf interval, where dinocyst are barren, is diatom-rich silty-clay. Decreased sedimentation rates would have prolonged the oxygen exposure time of palynomorphs once at the sea floor. Although our age model has limitations, a decrease in sedimentation rates (to 1.8 cm/kyr) is observed above 192.7 mbsf. The final explanation is that bottom water formation on the Ross Sea continental margin delivered increased oxygen-rich bottom waters to the site. Heightened obliquity sensitivity has been interpreted to be associated with enhanced oceanic-influence mass balance controls on marine-terminating ice sheets, with limited sea ice extent (Levy et al., 2019). Levy et al. (2019) interpreted a prominent increase in the sensitivity of benthic oxygen isotope variations to obliquity forcing (termed “obliquity sensitivity”) between 24.5 and 24 Ma, synchronous with the first occurrence of ice-proximal glaciomarine sediments at DSDP Site 270, disconformities in CRP-2/2A and a large turnover in Southern Ocean phytoplankton. The major expansion of the ice sheet close to the Oligocene-Miocene boundary in the Ross Sea (Levy et al., 2019; Kulhanek et al., 2019; Evangelinos et al., 2021) argues in favour of Ross Sea bottom water strengthening, leading to the slowdown of the sedimentation rates above 192.7 mbsf and the formation of the >7 Myr duration hiatus at ~181 mbsf.

5.4 Implications for ice-proximal conditions, hydrology and ice sheets: a hypothesis

Warm and generally oligotrophic conditions relatively proximal to the Antarctic margin during the Oligocene imply that the Southern Ocean oceanography was fundamentally different from modern conditions (e.g. Deppeler and Davidson, 2017). Although our data suggest that ocean conditions were colder inshore than further offshore, they remain warm considering their proximity to marine-terminating outlet glaciers and ice caps in the Ross Sea area (De Santis et al., 1999; Galeotti et al., 2016; Levy et al., 2019; Kulhanek et al., 2019; Evangelinos et al., 2021). Levy et al. (2019) provided a model for ice-proximal to ice-distal oceanographic conditions in the Ross Sea during the Oligocene. In that model, Transantarctic Mountain outlet glaciers draining the EAIS, or local marine-terminating ice caps in the Ross Sea, were particularly affected by the wind-driven southward advection of warmer subsurface waters onto the Ross Sea shelf, similar to how Circumpolar Deep Water is being transported onto some regions of the continental shelf today (e.g. Wouters et al., 2015; Shen et al., 2018). The subsurface waters in that conceptual model were indicated as being warmer than the overlying low-salinity surface waters derived from glacial melts during glacial maxima, but this stratification is broken down during interglacials. The sample

resolution of our dataset is too low to capture the full amplitude of orbital variability. However, as each 2 cm sample represents 800 years, the variability that we see in our record could be the result of strong environmental variability on orbital timescales. Hence, the high variability in our data supports the interpretation of Levy et al. (2019), with temperate surface waters at DSDP Site 274 on the continental rise of the Ross Sea margin suggesting a well-mixed water column, as it would be difficult to envisage intermediate waters warmer than the surface waters. In this scenario, colder stratified surface water due to (sea ice) melting would be largely restricted to the coastal Ross Sea sites of DSDP Site 270, CRP and CIROS-1. Temperate surface waters offshore of the Ross Sea shelf would provide a source of heat that limits the advance of marine terminating glacial systems into the Ross Sea and Wilkes Land continental shelves.

Pollen assemblages and high SSTs at DSDP Site 274, supported by terrestrial palynomorphs found at CRP-2 (Askin and Raine, 2000), suggest that the climate was warm enough to allow atmospheric melt to be the dominant control on the ice mass balance and a potential driver of deglaciation during warm orbital configurations. In addition, the warm ocean could have promoted an intensification of the hydrological cycle and consequent moisture delivery to the Antarctic hinterland, similar to what has been hypothesised for the Miocene Climatic Optimum (Feakins et al., 2012). Enhanced intense precipitation in the Antarctic hinterland would favour ice accumulation during cold orbital states to sustain a marine termination for the predominately terrestrial ice sheets. In an Early- to mid-Oligocene climate that was warmer than present, precipitation and glaciation on the hinterlands could be further promoted by high elevation and a larger Antarctic landmass size (Paxman et al., 2019). Indeed, general circulation models (GCMs) for the ice-free Eocene do suggest enhanced precipitation delivery to the Antarctic continent (e.g. Huber and Caballero, 2011; Baatsen et al., 2018). If part of the source of that precipitation was the warm Southern Ocean proximal to the ice sheet, Rayleigh distillation would be reduced, leading to relatively enriched Oligocene ice sheet $\delta^{18}\text{O}$ compared with that of today and, therefore, relatively depleted sea water $\delta^{18}\text{O}$. The calculation of ice volumes from benthic foraminiferal oxygen isotope records (e.g. Lear et al., 2000; Bohaty et al., 2012; Liebrand et al., 2017) does consider a variety of values for the isotopic composition of the Oligocene Antarctic ice sheet. We argue that the warm oceanographic conditions, invoking strong precipitation and, possibly, a more local source of precipitation than today (Speelman et al., 2010) would explain how $\delta^{18}\text{O}$ of Antarctic ice was on the less depleted end of previous assumptions. This increases the calculated Antarctic ice mass that was installed during the EOIS (Bohaty et al., 2012) as well as the Antarctic ice volume that fluctuated over strong Oligocene orbital cycles (Liebrand et al., 2017). In the future, this idea could be further tested through higher-resolution reconstructions, δD reconstructions on plant matter, and isotope-enabled palaeoceanographic and ice sheet modelling studies. In any case, future isotope-enabled ice sheet modelling should factor in warm Southern Ocean conditions for realistic estimates of Antarctic ice volume. This may imply an even higher sensitivity of Antarctic ice sheets to orbitally forced climate variability than previously assumed, and it assigns a large role to mass balance controlled by surface melt and oceanography in ice sheet stability during past warm climates, through both hydrological and basal and surface melt processes.

6 Conclusions

We show that temperate (TEX_{86} SST: $10\text{-}17^\circ\text{C} \pm 5.2^\circ\text{C}$) and relatively oligotrophic surface ocean conditions prevailed off the Ross Sea margin during the Oligocene (33.7-24.4 Ma). This agrees with the warm SSTs recorded offshore of Wilkes Land and also demonstrates that warm surface waters influenced the East Antarctic Ice Sheet margin in both the Ross Sea and Wilkes Land during the Oligocene. The warm surface ocean temperatures at DSDP Site 274 and colder SST on the Ross Sea continental shelf with evidence of temporary marine termination of ice caps and glaciers demonstrate a strong inshore to offshore temperature gradient in the Ross Sea. We posit that the warm surface ocean conditions near the continental shelf break during the Oligocene may have promoted increased heat delivery and precipitation transport towards the Antarctic hinterlands that lead to highly dynamic terrestrial ice sheet volumes in the warmer climate state of the Oligocene. During cold orbital phases, enhanced precipitation may have sustained high ice flux and the advance of terrestrial ice sheets and ice caps into shallow marine settings. During warm orbital configurations of the Oligocene, the heat delivery may have resulted in widespread surface melt and retreat of the terrestrial ice sheets into the hinterland.

Acknowledgements

This work used Deep Sea Drilling Project archived samples and data provided and curated by the International Ocean Discovery Program and its predecessors. We thank the Paleomagnetic Laboratory CCiTUB-ICTJA CSIC for support with the palaeomagnetic analysis. We are also grateful to Natasja Welters and Giovanni Dammers for technical support at the Utrecht University GeoLab.

Financial support

This research has been supported by the NWO Polar Programme (grant no. ALW.2016.001.); the Spanish Ministry of Economy, Industry and Competitiveness (grant no. CTM2017-89711-C2-1-P/CTM2017-89711-C2-2-P), co-funded by the European Union through FEDER funds; and the Alexander S. Onassis Public Benefit Foundation PhD research grant (grant no. F ZL 016-1/2015-2016).

Supplementary Information Chapter 2

The supplementary tables and figures related to this chapter is available online, at:

<https://doi.org/10.5194/cp-17-1423-2021-supplement>

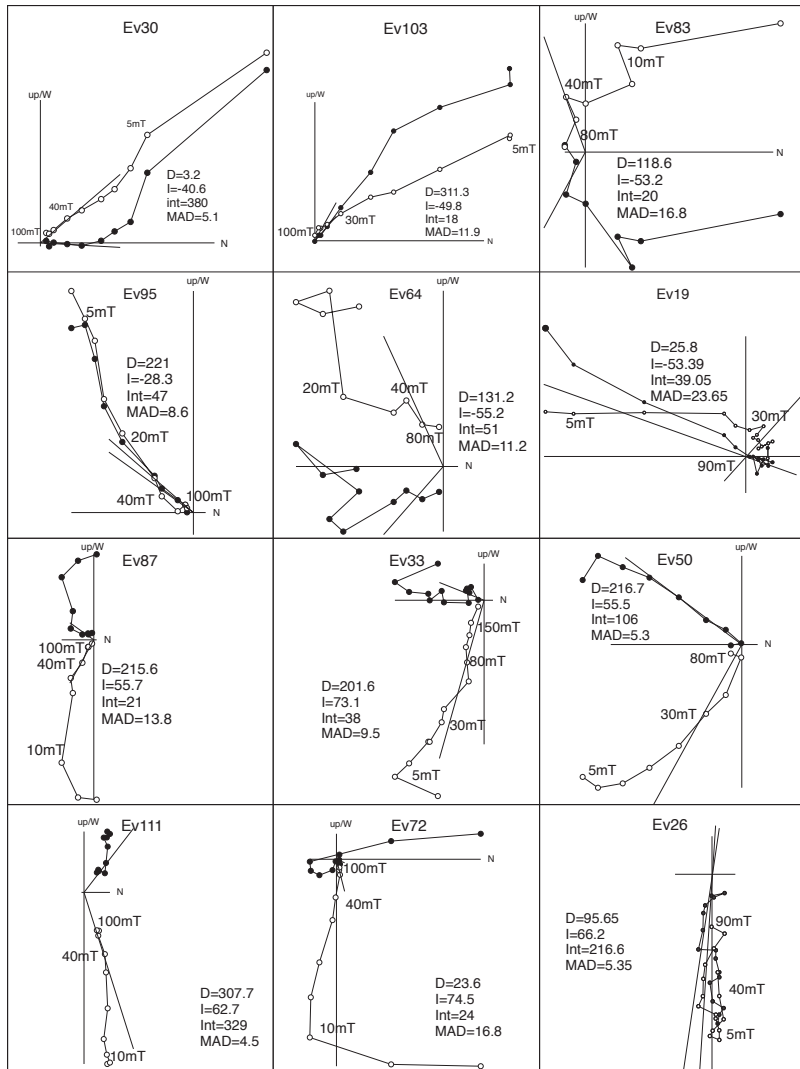


Supplementary Table S1: Table with a summary of demagnetization data results. Sample identification, Core location indicating core, section and depth (mbsf), Declination, Inclination, Sample intensity (in A/m²), MAD values and remarks including the steps used for interpretation. Resultant orthoplots are depicted in Figure S1.

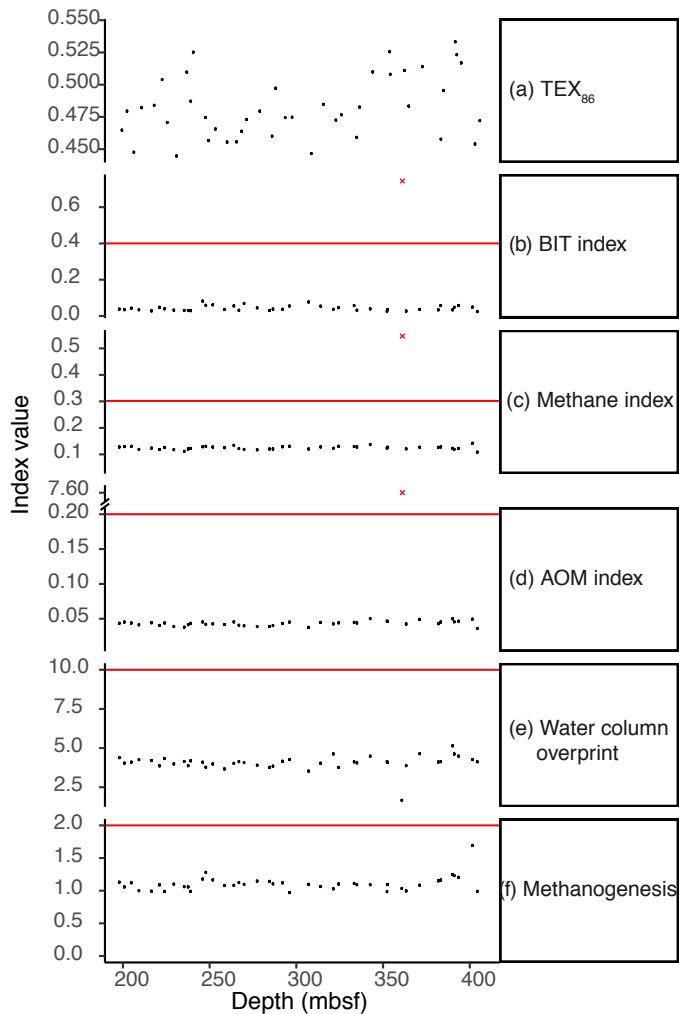
Supplementary Table S2: Concentrations of GDGTs at Site 274. All samples and corresponding depths, age of sample, GDGT peak area values, TEX₈₆ (Schouten et al., 2002) and BIT index values (Hopmans et al., 2004), Methane Index (Methzhang) values (Zhang et al., 2011), GDGT2/Crenarchaeol ratios (Weijers et al., 2011), GDGT-0/Crenarchaeol ratios (Blaga et al., 2009) and GDGT-2/GDGT-3 ratios (Taylor et al., 2013), and RING index (Sinninghe Damsté, 2016). SST calibrations from Kim et al., 2010; Kim et al., 2012. SSTK10L = linear calibration of Kim et al. (2010). Discarded samples (OUTLIER=TRUE) with outlier values are based on BIT > 0.4, GDGT2/GDGT3' > 5, 'GDGT0/cren' > 2 and 'Methzhang' > 0.3.

Supplementary Table S3: Total palynomorph assemblage counts DSDP Site 274 cores 43-21.

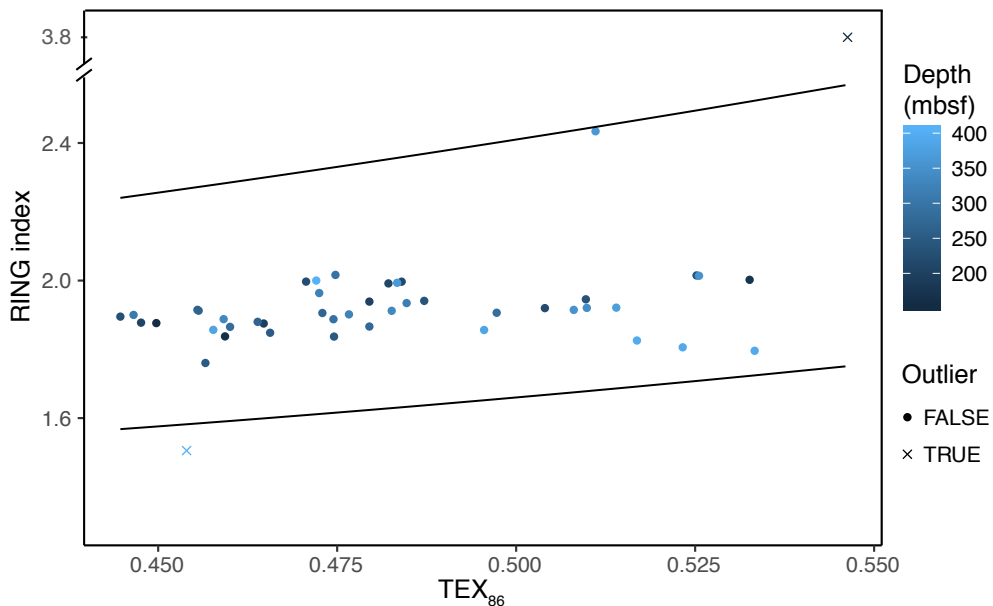
Supplementary Table S4: Correspondence analysis (CA) scores of the dinocysts assemblage data from DSDP Site 274.



Supplementary Figure S1: Orthogonal plots of representative samples. Most of the samples used for the correlation show two distinctive directions, both in normal samples and in reversed samples. Inclination values are also indicated. Open plots indicate inclinations (vertical projection). All calculated directions are available in Table S1. Samples were calculated by means of the Paldir and paleomagnetism.org (Koymans et al., 2016) programs.



Supplementary Figure S2: Relevant GDGT indices to filter out biased outliers (red crosses) in the generated GDGT data (Table S2), plotted against sample depth (mbsf). The red line marks the limit of reliable values. a) TEX_{86} (Schouten et al., 2002). b) BIT index values (Hopmans et al., 2004). c) Methane Index (Methzhang) values (Zhang et al., 2011). d) AOM index (GDGT2/Crenarchaeol ratios) (Weijers et al., 2011). e) Water column overprint values (GDGT-2/GDGT-3 ratios) (Taylor et al., 2013). f) Methanogenesis values (GDGT-0/Crenarchaeol ratios) (Blažina et al., 2009).



Supplementary Figure S3: Cross plot between the ring index and TEX₈₆ values of samples from DSDP Site 274. The lines mark the outer ranges of the ring index (Zhang et al., 2016), outside of which samples have outlying values (marked as crosses). The shade of blue indicates the sample depth (mbsf).

Chapter 3

Late Eocene-early Miocene evolution of the southern Australian subtropical front: a marine palynological approach

Frida S. Hoem¹, Isabel Sauermilch¹, Suning Hou¹, Henk Brinkhuis^{1,2}, Francesca Sangiorgi¹ and Peter K. Bijl¹

1. *Marine Palynology and Paleoceanography, Department of Earth Sciences, Utrecht University, Utrecht, The Netherlands.*

2. *Royal Netherlands Institute for Sea Research (NIOZ), Texel, The Netherlands*

Published in *Journal of Micropaleontology*, <https://doi.org/10.5194/jm-40-175-2021>

Abstract

Improvements in our capability to reconstruct ancient surface-ocean conditions based on organic-walled dinoflagellate cyst (dinocyst) assemblages from the Southern Ocean provide an opportunity to better establish past position, strength and oceanography of the subtropical front (STF). Here, we aim to reconstruct the late Eocene to early Miocene (37-20 Ma) depositional and palaeoceanographic history of the STF in the context of the evolving Tasmanian Gateway as well as the potential influence of Antarctic circumpolar flow and intense waxing and waning of ice. We approach this by combining information from seismic lines (revisiting existing data and generating new marine palynological data from Ocean Drilling Program (ODP) Hole 1168A) in the western Tasmanian continental slope. We apply improved taxonomic insights and palaeoecological models to reconstruct the sea surface palaeoenvironmental evolution. Late Eocene-early Oligocene (37-30.5 Ma) assemblages show a progressive transition from dominant terrestrial palynomorphs and inner-neritic dinocyst taxa as well as cysts produced by heterotrophic dinoflagellates to predominantly outer-neritic/oceanic autotrophic taxa. This transition reflects the progressive deepening of the western Tasmanian continental margin, an interpretation supported by our new seismic investigations. The dominance of autotrophic species like *Spiniferites* spp. and *Operculodinium* spp. reflects relatively oligotrophic conditions, like those of regions north of the modern-day STF. The increased abundance in the earliest Miocene of *Nematosphaeropsis labyrinthus*, typical for modern subantarctic zone (frontal) conditions, indicates a cooling and/or closer proximity of the STF to the site. The absence of major shifts in dinocyst assemblages contrasts with other records in the region and suggests that small changes in surface oceanographic conditions occurred during the Oligocene. Despite the relatively southerly (63-55°S) location of Site 1168, the rather stable oceanographic conditions reflect the continued influence of the proto-Leeuwin Current along the southern Australian coast as Australia continued to drift northward. The relatively “warm” dinocyst assemblages at ODP Site 1168, compared with the cold assemblages at Antarctic Integrated Ocean Drilling Program (IODP) Site U1356, testify to the establishment of a pronounced latitudinal temperature gradient in the Oligocene Southern Ocean.

1 Introduction

Late stages of continental break-up between Australia and Antarctica in the late Eocene-early Miocene led to gradual deepening and widening of the Tasmanian Gateway (Lawver et al., 1992; Cande and Stock, 2004; Whittaker et al., 2013). This process redirected Southern Ocean surface water circulation (Stickley et al., 2004a; Bijl et al., 2013; Sijp et al., 2014, 2016) and regionally redistributed ocean heat (Sijp et al., 2014, 2016) with notable consequences for Antarctic surface water temperatures (Houben et al., 2019; Sauermilch et al., 2021). While the general oceanographic consequences of the opening of the Tasmanian Gateway – the breakdown of gyres and the onset of a wind-driven, eastward-flowing current – are now broadly understood (Stickley et al., 2004a; Bijl et al., 2013; Hill et al., 2013; Sijp et al., 2014; Houben et al., 2019), the development of Southern Ocean frontal systems (Nelson and Cooke, 2001), such as the subtropical front (STF), and ultimately the evolution and strengthening of the Antarctic Circumpolar Current (ACC) as the gateway widens (Hill et al., 2013) are largely unexplained.

To a large extent, our knowledge on the development of Paleogene Southern Ocean surface circulation is built on biogeographic patterns in organic-walled dinoflagellate cyst assemblages (Wrenn and Beckman, 1982; Bijl et al., 2011) as well as supporting information from other microfossil groups (Pascher et al., 2015), both backed up by numerical model simulations (e.g. Huber et al., 2004; Sijp et al., 2014). Dinoflagellates are single-celled, predominantly marine, eukaryotic protists, which represent an important group of marine plankton. During their life cycle, ~15% of modern dinoflagellate species produce preservable organic-walled resting cysts (dinocysts), which can be found in marine sedimentary archives (e.g. Fensome, 1993; Head, 1996). Dinocysts are increasingly and successfully used as a proxy for palaeoceanographic reconstructions in the Southern Ocean (e.g. Houben et al., 2013; Prebble et al., 2013; Bijl et al., 2018; Sangiorgi et al., 2018).

In 2000, Ocean Drilling Program (ODP) Leg 189 drilled five sites around Tasmania – on the western Tasmanian margin (Site 1168), the South Tasmanian Rise (sites 1169, 1170 and 1171) and the East Tasmanian Plateau (Site 1172) – with the goal of reconstructing the timing, nature and climatic consequences of the opening of the Tasmanian Gateway (Figure 1a; Exon et al., 2001a). Site 1168 is presently located north of the STF and contains a near-continuous sediment record of late Eocene-Quaternary age. The site is in the path of the Zeehan Current, a saline, warm surface water flowing off western Tasmania that originates from the Leeuwin Current (Ridgway and Condie, 2004). Brinkhuis et al. (2003) provided a preliminary overview of the late Eocene-Quaternary dinocyst assemblage distribution and illustrated the main trends in palynomorph distribution. The study by van Simaey et al. (2005) detected the typical boreal taxon *Svalbardella* spp. in the Oligocene record of Site 1168 and showed that the species likely migrated across the Equator into the Southern Ocean in response to the inception of cold, glacial phase Oi-2b, around 27.1 Ma.

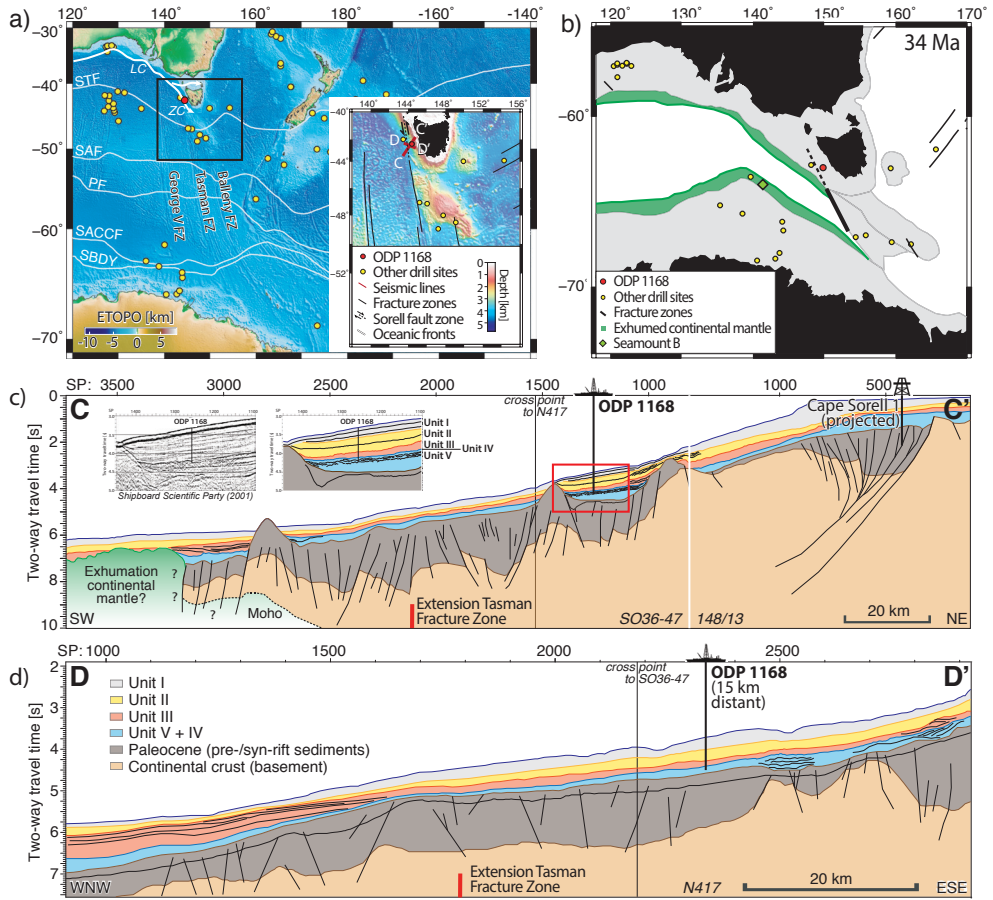


Figure 1 (a) Present-day map of the Australian sector of the Southern Ocean showing ODP Site 1168 (red dot), other drill sites mentioned in this study (yellow dots), ocean fronts (white lines; STF is the subtropical front, SAF is the subantarctic front, PF is the polar front, SACCF is the Southern Antarctic Circumpolar Current front and SBDY is the southern boundary) and southern Australian ocean currents (white arrow; LC is the Leeuwin Current and ZC is the Zeehan Current). The map uses the regional 1 min gravity-derived Earth Topography and Bathymetry map (Weatherall et al., 2015). The inset shows high-resolution shipboard bathymetry data from the study area (gaps filled with the Earth Topography and Bathymetry map) with seismic profiles presented in this study (red lines), prominent fracture zones (black lines) and the extended Sorell Fault Zone (dashed line; after Miller et al., 2002). (b) Palaeogeographic map of the Tasman region at 34 Ma (using the plate model of Whittaker et al., 2013) with the location of the interpreted exhumed continental mantle domain along the Australian-Antarctic ocean-continent transition (green region; after McCarthy et al., 2020). Panels (c) and (d) interpreted multichannel seismic reflection profiles crossing ODP Site 1168 (for the location, see panel b; for details, see the legend). (c) The inset panels show the uninterpreted (Exon et al., 2001b) and interpreted seismic section crossing ODP Site 1168 with tied lithological units. Also shown are the pre-Eocene-Oligocene transition sediment stratigraphy after Sauermilch et al. (2019a) and Hill et al. (1997), and the interpreted continental mantle exhumation following McCarthy et al. (2020). Panel (d) shows the legend of the sedimentary units (Exon et al., 2001b).

Empirical relationships between extinct species abundance and proxy data for oceanographic conditions (e.g. Wall et al., 1977; Pross and Brinkhuis, 2005; Sluijs et al., 2005; Frieling and Sluijs, 2018) have strengthened the use of dinocysts for past oceanographical reconstructions. These have been used, for example, to detect a circum-Antarctic biotic turnover across the Eocene-Oligocene transition (EOT) with the origination of a sea-ice ecosystem (Houben et al., 2013) and a shift towards upwelling-related primary productivity (Houben et al., 2019; Bijl et al., 2018) in the Southern Ocean. Meanwhile, knowledge of dinocyst ecological preferences in the modern ocean has greatly advanced in the last couple of decades (e.g. Zonneveld et al., 2013), particularly for the Southern Ocean (Prebble et al., 2013; Marret et al., 2020). These modern affinities of dinocysts have been successfully used to resolve Antarctic-proximal oceanic conditions in the Oligocene and Miocene (Sangiorgi et al., 2018; Bijl et al., 2018; building on pioneering work from studies such as Hannah et al., 2000). Moreover, recently, the tectonic history of Australian-Antarctic separation and the palaeoenvironmental consequences have been reconstructed in more detail (Whittaker et al., 2013; Williams et al., 2019; Sauermilch et al., 2019a, 2021). Together, this knowledge facilitates reinterpretation of the original shipboard reconstruction of the depositional environments at Site 1168 (Exon et al., 2001b).

Here, we revisit Site 1168 (Exon, 2001b; Brinkhuis et al., 2003; Hill and Exon, 2004) and the first results, and focus in more detail on the sediments deposited during the late Eocene-early Miocene. Integrating new interpretations of the seismo-stratigraphy, an improved integrated bio-magnetostratigraphic age model and new interpretations from high-resolution dinocyst assemblage data, we provide an updated view of the evolving depositional environment and palaeoceanographic conditions. We analyse our results in the context of those from other sites in the Australo-Antarctic Gulf (AAG) (IODP Site U1356 – Bijl et al., 2018; ODP Site 1128 and Browns Creek – Houben et al., 2019; east of Tasmania, ODP Site 1172 – Sluijs et al., 2003; in and offshore of the Ross Sea, Cape Roberts Project – Clowes et al., 2016; and Deep Sea Drilling Project, DSDP, Site 274 – Chapter 2) to build a picture of the late Eocene-early Miocene (37-20 Ma) palaeoceanographic evolution in the region of the widening Tasmanian Gateway.

2 Material

2.1 ODP Leg 189, Site 1168: site description, age model and lithology

Ocean drilling at the western Tasmanian margin ODP Site 1168 (42°38.40'S, 144°25.30'E; present-day water depth of 2463.3 m; Figure 1) reached a total depth of 883.5 m below the seafloor (mbsf) with a recovery of 98%. The drill site is located within a small, filled sedimentary basin embedded by two basement highs (~25 km length; Figure 1c). The upper Eocene-Miocene sedimentary record has a clear palaeomagnetic signal, from which magnetochrons can be defined by connecting palaeomagnetic reversals to biostratigraphic events from planktic foraminifera, dinocysts and calcareous nannofossils (Pfuhl and McCave, 2003; Sluijs et al., 2003; Stickley et al., 2004b; Pross et al., 2012; Houben et al., 2019). Here, we recalibrated all of the bio- and magnetostratigraphic datums from Stickley et al. (2004) to the Geologic Time Scale 2012 (GTS2012; Gradstein et al., 2012), using the latest information from the Nannotax and Microtax web catalogues (Young et al., 2017) (Figure 2 and Table S1 in the Supplement). The Shipboard Scientific Party (Exon et al., 2001a, b) distinguished four lithologic units in the studied interval between 876 and 340 mbsf (units II to V). Unit V consists of black organic-rich siltstones and claystone of Late Eocene age until 762 mbsf, overlain by Unit IV (748.6-762 mbsf) which consists of 13.4 m of dark-grey glauconitic, quartzose

sandstone and clayey organic-rich siltstone. Unit III (660–748.6 mbsf) is composed of olive-grey nannofossil-bearing organic clayey siltstone. Unit II (340–660 mbsf) is dominated by nannofossil chalks and claystones of varying silt content of Oligocene-early Miocene age. In general, the sediment colour becomes progressively lighter up-section, with increasing calcium carbonate and declining organic carbon content (Figure 2). Calcium carbonate (CaCO_3) is low (<15 wt%) in Unit V and highly variable (0 wt%–40 wt%) in Unit IV. CaCO_3 increases stepwise in units III and II, from ~700 to 550 mbsf (~10 wt%–40 wt%) and from 450 to ~370 mbsf (~20 wt%–50 wt%) respectively (Exon et al., 2001b). The total organic carbon (TOC) content is high, 5 wt%, at the bottom of the record and decreases until Unit IV (~750 mbsf). TOC is lower, <1 wt%, for the interval above 700 mbsf (units III–II). The average sedimentation rate is calculated as ~6 cm kyr⁻¹ for the late Eocene, declining to ~3 cm kyr⁻¹ in the Oligocene and further to ~2 cm kyr⁻¹ in the early Miocene (Exon et al., 2001b).

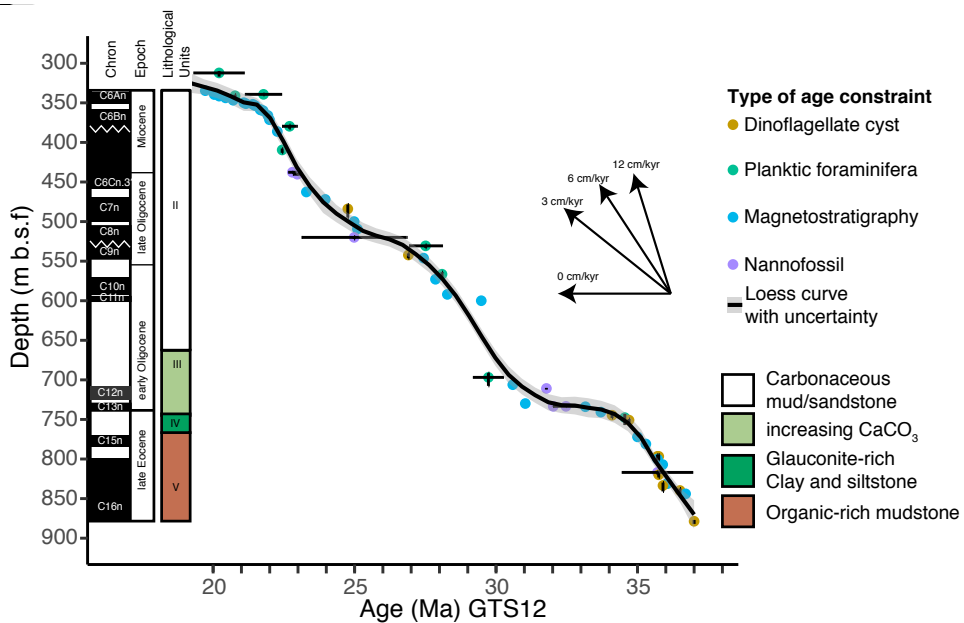


Figure 2. Age-depth model of ODP Site 1168, based on magneto- and biostratigraphy (calcareous nannofossils, planktic foraminifera, diatoms and dinocysts) after Stickley et al. (2004b), here recalibrated to GTS2012 of Gradstein et al. (2012) (Table S1 in the Supplement). A smoothed line is drawn through the age constraints using the loess smoothing method with a span of 0.1. Lithological units are indicated to the right of the palaeomagnetic chrons and the indication of epochs (Exon et al., 2001b). The arrows indicate the sedimentation rate.

2.2 Palaeolatitute and palaeobathymetry

Palaeolatitudes for the western Tasmanian margin between 37 and 20 Ma changed from 63 to 55°S (van Hinsbergen et al., 2015; Matthews et al., 2016), which is still substantially further south than its modern latitude (42.5°S). This is due to the progressive opening of the AAG since the late Eocene, which caused a northward movement of Australia (with Tasmania) (Cande and Stock, 2004). The same tectonic widening caused deepening of the Tasmanian continental flanks throughout the

Eocene-Oligocene. A recent study by Hochmuth et al. (2020) suggested deepening of the site from inner-neritic to bathyal depths from a palaeodepth of about 700 m at 29 Ma to a depth of 1500 m by 21 Ma.

3 Methods

3.1 Seismic stratigraphy

We present seismo-stratigraphic interpretations of two multichannel seismic reflection profiles crossing (line SO36-47) and closely passing (line N417) Site 1168 (Figure 1c, d). We follow the seismic interpretation of Sauermilch et al. (2019a) and Hill et al. (1997) for the sedimentary units and continental crust, and the exhumed subcontinental mantle part is our own (following the characteristics of McCarthy et al., 2020). Key reflections are linked to lithological units, largely following interpretations by Sauermilch et al. (2019a) and the Shipboard Scientific Party (Exon et al., 2001b). We used the time-depth relationship derived from downhole sonic p-wave velocities measured at Site 1168 (Exon et al., 2001b) for the core-seismic correlation. This method of velocity measurements is most accurate for seismic integration, particularly for calcareous-rich sediments (Sauermilch et al., 2019b).

ODP Site 1168 is located within an enclosed sedimentary basin, surrounded by now buried bathymetric highs (Figure 1c). Characteristic seismic features, amplitude and internal reflection patterns can be used to follow key reflections and sedimentary units across this embedded basin. However, some uncertainties remain, as the basement highs disrupt the continuity of the reflection pattern. In order to calculate the regional thickness extensions of the sedimentary units in metres, we use interval velocities from downhole sonic measurements at Site 1168. We interpreted the exhumation of subcontinental mantle material offshore of western Tasmania, along its ocean-continent transition zone (OCT; Figure 1). The interpretation of the mantle domain followed the analytical scheme of Gillard et al. (2015) and McCarthy et al. (2020), who investigated exhumed mantle domains of the offshore central southern Australian and conjugate East Antarctic margins (Seamount B, east of Adélie Rift Block) respectively.

3.2 Palynological processing and analysis

We studied 123 samples for palynological content: 84 were samples that were revisited and recounted from the previously studied palynological record by Brinkhuis et al. (2003), and 39 were additional samples processed to increase the resolution. The processing of sedimentary samples for palynological analysis followed standard procedures at the Laboratory of Palaeobotany and Palynology, Utrecht University (e.g. Brinkhuis et al., 2003; Bijl et al., 2018). Dried sediment samples were crushed and weighed (on average 10 g, standard deviation, SD, of <1 g) before they were digested with 30% cold hydrochloric acid (HCl) and 38% cold hydrofluoric acid (HF) for carbonate and silicate removal respectively. The remaining palynological residues were sieved on a 10 µm nylon mesh, using an ultrasonic bath to disintegrate agglutinated organic particles. No oxidation or alkali agents were used. The palynological residues were mounted on glass slides using glycerine jelly, sealed with nail varnish and counted (under 400× magnification) using a Leica DM2500 LED transmitted light optical microscope. When possible, at least 200 dinocyst specimens were counted (Mertens et al., 2009). Slides containing less than 50 dinocyst specimens were excluded from further analysis.

3.3 Marine palynomorph taxonomy and distribution patterns

We provide detailed counts of dinocysts and other aquatic palynomorphs (acritarchs and prasinophyte algae) (Table S2 in the Supplement). Dinocyst taxonomy as cited in Williams et al. (2017) is followed. Acritarch and prasinophyte taxonomy follows that of Hannah (1998, 2006), Prebble et al. (2006) and Hartman et al. (2018a). We also included a broad count of terrestrial palynomorphs in order to calculate the relative abundances between terrestrial and marine palynomorphs. Detailed analyses of terrestrial palynomorphs and terrestrial palaeoenvironmental evolution at Site 1168 is the focus of another paper (Amoo et al., 2021).

3.3.1 Dinocyst ecological preferences

The present-day distribution of dinocysts (Figure 3) depends mostly on surface water temperature but also on nutrient availability, salinity, water depth, bottom-water oxygen, primary productivity and sea-ice cover (e.g. Dale, 1996; Prebble et al., 2013; Zonneveld et al., 2013; Marret et al., 2020). In order to use dinocyst assemblages as palaeoceanographic proxies, we assume that the habitat affinities and trophic strategy of modern dinoflagellate species have remained similar through time; therefore, we utilise the modern relationship between dinocysts and overlying water properties as a model for the “deep-time” ecological niches (Sluijs et al., 2005; Prebble et al., 2013; Sangiorgi et al., 2018). Palaeoecological preferences of extinct species are uncertain. To tackle this problem, the ecological affinity of extinct dinocyst taxa was reconstructed across well-defined climatic transitions (Brinkhuis, 1994; Houben et al., 2013; Egger et al., 2018), using the co-occurrence of extinct species with those for which the ecological information is still available, e.g. modern species (e.g. Schreck and Matthiessen, 2013), or in comparison to other palaeoceanographic proxies for temperature, runoff/freshwater input and nutrient conditions (Bijl et al., 2011; De Schepper et al., 2011; Frieling and Sluijs, 2018).

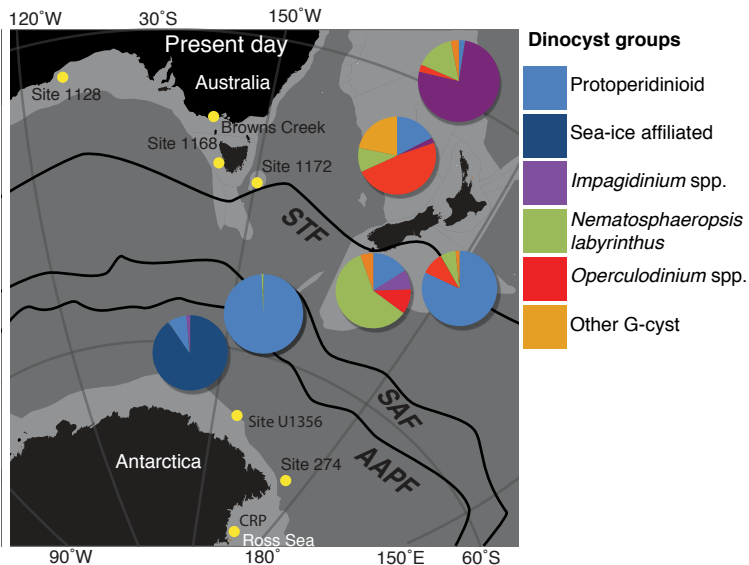


Figure 3. The present-day distribution of dinoflagellate cyst assemblages in the southwest Pacific sector of the Southern Ocean, derived from surface sample data generated by Prebble et al. (2013) and displayed in Sangiorgi et al. (2018). The black lines illustrate the location of oceanic fronts (Orsi et al., 1995), and yellow dots mark the present-day locations of the drill sites studied (ODP Site 1168) and discussed in this paper (IODP Site U1356, ODP Site 1172 and 1128, DSDP Site 269 and 274, Cape Roberts Project – CRP, and Browns Creek). STF is the subtropical front, SAF is the subantarctic front and AAPF is the Antarctic polar front. Land masses are indicated in black, and the continental lithosphere is shown in light grey in the location map generated by GPlates freeware (<http://www.gplates.org>, last access: 13 June 2016), based on the global plates geodynamic motion model from Müller et al. (2018).

In this paper, we apply this principle to divide dinocyst taxa into eco-groups (Table 1), based on the context of the Southern Ocean. We utilise the notion that protoperidinioid cysts and peridinioid dinocysts in general (e.g. *Protoperidinium* cpx., *Deflandrea* spp. and *Svalbardella* spp.) are predominantly produced by heterotrophic dinoflagellates and, thus, prefer a habitat with nutrient-rich, productive surface waters, whereas gonyaulacoid dinocysts principally reflect autotrophic/phototrophic dinoflagellates and distribute themselves mostly according to other surface water parameters (e.g. Pross and Brinkhuis, 2005; Sluijs et al., 2005). Cysts derived from heterotrophic dinoflagellates, notably the protoperidinioids, are generally more sensitive to oxic bottom conditions than autotrophic dinoflagellates, which may, to an unknown degree, represent bias in the interpretation of relative abundance data in dinocyst assemblages (Zonneveld et al., 2010). Some dinocyst taxa are known to have strong temperature preferences. Typical cold-water indicators are *Svalbardella* spp. (van Simaey et al., 2005) and *Gelatia inflata* (e.g. Egger et al., 2018), whereas *Hystrichokolpoma rigaudiae* (Louwye et al., 2008) and *Lingulodinium machaerophorum* (e.g. De Schepper et al., 2011) are taxa indicative of warm water. We also use the neritic to oceanic classification scheme of dinocyst taxa by Pross and Brinkhuis (2005) in order to deduce proximity to the shoreline. Further, we discuss the changes in surface-ocean current influence by analysing the relative abundance of Antarctic-endemic, cosmopolitan and low-latitude taxa (Sluijs et al., 2005; Bijl

et al., 2011). These papers show that surface-ocean currents derived from the waters surrounding Antarctica are dominated by Antarctic-endemic dinocysts, whereas mid-/low-latitude-derived currents such as the East Antarctic Current and proto-Leeuwin Current are sources of cosmopolitan and low-latitude taxa.

Finally, we track Southern Ocean frontal systems' movements using the environmental associations of modern dinocysts by Prebble et al. (2013) as a model. Today, a pronounced latitudinal separation of dinocyst assemblages across the Southern Ocean exists (Prebble et al., 2013) (Figure 3). Surface samples from the Antarctic margin, south of the subantarctic front (SAF), are dominated by the peridinioid cysts *Selenopemphix antarctica* with a minor abundance of *Brigantedinium* spp. (Prebble et al., 2013), whereas the dinocyst assemblage in the surface sample at Site 1168 shows abundant Gonyaulacoid cysts of the genera *Impagidinium*, *Nematosphaeropsis*, *Spiniferites* and minor occurrence of the peridinioid cyst *Brigantedinium*. The latter dominates the polar frontal zone, where mixing and upwelling of nutrient-rich waters and strong seasonality in sea-ice cover exists. *Nematosphaeropsis*, *Operculodinium* and *Impagidinium* prevail in surface waters with mean annual temperatures of 8-17°C (Prebble et al., 2013). Abundant *Nematosphaeropsis* has been described as an indicator of the region south of the STF, in the subantarctic zone (Prebble et al., 2013). The highest abundances of the cosmopolitan *Operculodinium centrocarpum* sensu Wall and Dale (1966) are found in samples north of the STF. *Impagidinium* spp. is abundant under (relatively warm) oligotrophic, oceanic, conditions (Zonneveld et al., 2013). *I. aculeatum* is most abundant south of the STF, and *I. paradoxum* is slightly more abundant north of the STF (Prebble et al., 2013). An exception is *I. pallidum*, which is abundant in both polar areas in the modern ocean (Zonneveld et al., 2013; Marret et al., 2020) but is also recorded at temperate sea surface temperatures (SSTs) during the Neogene (De Schepper et al., 2011). Therefore, we interpret the palaeoecological significance of *I. pallidum* in the past with caution (De Schepper et al., 2011), and place this species in the *Impagidinium* group. Members of the long-ranging cosmopolitan *Spiniferites* spp. appear most abundantly north of the STF. *S. ramosus* is most common, and in more shore-proximal settings, *S. mirabilis* is today most common between 30 and 40°S and with SSTs >15°C (Zonneveld et al., 2013).

Table 1. Dinocyst assemblage groups and their ecological and frontal system affinity.

Complex	Dinocyst taxa	Ecological affinity
<i>Homotryblum</i> cpx.	<i>Homotryblum</i> spp. <i>Eocladopyxis</i> spp. <i>Heteraulacacysta</i> spp. <i>Polysphaeridium</i> spp.	Inner-neritic/restricted marine-lagoonal setting (Sluijs et al., 2005; Frieling and Sluijs, 2018)
<i>Glaphyrocysta</i> cpx.	<i>Glaphyrocysta</i> spp. <i>Areoligera semicirculata</i>	Inner-neritic, high-energy settings (Stover et al., 1996; Sluijs et al., 2005)
<i>Cleistosphaeridium</i> cpx.	<i>Cleistosphaeridium</i> spp. <i>Dapsilidinium</i> spp. <i>Enneadocysta</i> spp.	Inner-neritic, relatively marginal setting (Brinkhuis, 1994)
Criboperidinioideae	<i>Apteodinium australiense</i> <i>Cooksonidium capricornum</i> <i>Cordosphaeridium cantharellus</i> <i>C. fibrospinosum</i> <i>C. minimum</i> <i>Thalassiphora pelagica</i>	Mid-shelf and neritic environments (Brinkhuis, 1994)
<i>Lingulodinium</i> cpx.	<i>L. machaerophorum</i>	Inner- to outer-neritic, warm, seasonally stratified waters, medium-high nutrients (Sluijs et al., 2005; Zonneveld et al., 2013)
<i>Pyxidinospis</i> cpx.	<i>Batiacasphaera</i> spp. <i>Cerebrocysta</i> spp. <i>Corrudinium</i> spp. <i>Pyxidinospis</i> spp.	Outer-neritic setting (Brinkhuis, 1994; Sluijs et al., 2005)
<i>Reticulatosphaera</i>	<i>R. actinocoronata</i>	Outer-neritic setting (Brinkhuis, 1994; Pross and Brinkhuis, 2005; Sluijs et al., 2005)
<i>Hystrichokolpoma</i> spp.		Outer-neritic/oceanic setting (Pross and Brinkhuis, 2005)
<i>Spiniferites</i> cpx.	<i>Spiniferites ramosus</i> <i>S. mirabilis</i> <i>Achomosphaera alcornu</i> <i>Hafniasphaera septata</i>	Cosmopolitan environment (Brinkhuis, 1994; Zonneveld et al., 2013)
<i>Operculodinium</i> spp.	<i>Operculodinium centrocarpum</i> <i>O. piaseckii</i> <i>O. janduchenei</i>	Cosmopolitan/oceanic environment Abundant north of STF (Brinkhuis, 1994; Prebble et al., 2013)
<i>Impagidinium</i> spp.	<i>Impagidinium aculeatum</i> <i>I. dispersitum</i> <i>I. maculatum</i> <i>I. sphaericum</i> <i>I. paradoxum</i> <i>I. patulum</i> <i>I. pallidum</i> *	Oligotrophic oceanic environment (Wall et al., 1977; Pross and Brinkhuis, 2005; Zonneveld et al., 2013) * Abundant in both polar areas of the modern ocean (Zonneveld et al., 2013; Marret et al., 2019) but also recorded in association with temperate SSTs in the Neogene (De Schepper et al., 2011)
<i>Nematosphaeropsis labyrinthus</i>		Oceanic/subantarctic zone (Crouch et al., 2010; Prebble et al., 2013)
<i>Gelatia inflata</i>		Cold-water setting (Brinkhuis and Biffi, 1993; Guerstein et al., 2008)
<i>Deflandrea</i> spp.	<i>Deflandrea</i> spp.	Heterotrophic, neritic to oceanic setting (Röhl et al., 2004; Sluijs et al., 2005)
Protoperidinioid cpx.	<i>Brigantedinium</i> spp. <i>Lejeunecysta</i> spp. <i>Selenopemphix</i> spp. <i>Protoperidinium</i> spp.	Nutrient-rich cold waters, related to inner-neritic environments (Harland and Pudsey, 1999; Sluijs et al., 2003; Zonneveld et al., 2013)
<i>Svalbardella</i> spp.	<i>Svalbardella cooksoniae</i>	Cold water tolerant (van Simaëys et al., 2005)

3.3.2 Acritarchs and organic remains of prasinophyte algae

Acritarchs represent “acid resistant organic walled microfossils of unknown affinity” (Evitt, 1963) and likely represent organic remains of polyphyletic origin, including prasinophyte algae. As of 2021, the latter group has received more attention, and some life cycle stages are indeed composed of preservable organic matter (Parke et al., 1978; Mudie et al., 2021). These may be single-celled and/or multicellular, colonial stages. Examples include the multicellular *Botryococcus* and *Pediastrum*, and the unicellular *Tasmanites* and *Pterospermella* spp. Although there are large uncertainties regarding the biological and ecological affinity of acritarchs and prasinophytes, they are often considered as potentially opportunistic species and often co-occur with indications of increased freshwater input and increased stratification (Mudie, 1992; Hannah, 2006; Prebble et al., 2006; De Schepper and Head, 2014). At the Antarctic margin, acritarchs such as *Leiosphaeridia* spp. have been associated with glacial retreat and freshwater discharge (Hannah, 2006; Warny et al., 2006; 2016) and are still present in modern samples (Hartman et al., 2018a). However, abundant skolochorate acritarchs in the Oligocene-Miocene at the Wilkes Land coast are associated with incursions of warm water (Bijl et al., 2018). Brinkhuis et al. (2003) also reported samples with a massive influx of small skolochorate acritarchs of unknown affinity around Tasmania at Site 1168 and Site 1172, in addition to the remains of prasinophyte algae. Prasinophyte algae, such as *Cymatiosphaera* spp. and *Tasmanites* spp., accumulate in relatively near-shore marine to brackish nutrient-rich environments (Mudie et al., 2021).

4 Results

4.1 Seismic stratigraphy

The lithological boundaries from ODP Site 1168 are tied to the crossing seismic reflection profile (Figure 1c) using the time-depth relationship from downhole sonic velocities (Exon et al., 2001a, b). The drilled lithological units V and III-I are clearly visible in the seismic lines, whereas the very thin (13.4 m) Unit IV is only detectable as a strong reflection pattern (Figure 1c). An additional key unconformity underlies the drilled sections, dated to the Palaeocene, extrapolated from industry well site Cape Sorell 1 (Boreham et al., 2002) (Figure 1c). Here, we focus on the sedimentary units V-II, deposited between the late Eocene and early Miocene.

Unit V-IV

Unit V reaches a maximum thickness of about 0.5 s TWT (two-way travel time) or ~400-500 m. In the embedded basin, the thickest part of Unit V is located towards the land. The internal reflections in the upper part of this unit are chaotic, with varying amplitudes and characteristic hummocky structures. Internal reflections and the top boundary thin out and onlap onto both basement highs, southwest and northeast (Figure 1c). However, the top boundary reflection slightly overlaps the basement high oceanward in the WNW-ESE direction (Figure 1d). As the lithological Unit IV is very thin and barely detectable in the seismic data, it is likely that this overlapping section is Unit IV. The seismic characteristics of the upper section of Unit V are significantly different on each side of the Tasmanian Fracture Zone (TFZ) and the connected basement highs. The deposition east of the TFZ, around Site 1168, shows chaotic, hummocky features and reworking. Particularly the hummocky reflections have been previously interpreted as deltaic influence (Exon et al., 2001a, b). West of the TFZ, the deposition of the late Eocene material is more homogenous and undisturbed along the upper slope (Figure 1d). Further offshore along the lower continental slope to abyssal

plain, this sedimentary unit has been slightly reworked. This structure shows onlapping reflections onto the slope and is likely part of the contourite drift system observed along the Australian and Antarctic margins that formed due to strengthening clockwise currents in the AAG (Sauermilch et al., 2019a).

Unit III

The overlying Unit III, dated to the early Oligocene, is thinner (maximum thickness ~ 0.3 s TWT in the embedded basin) with internal reflections of weaker amplitudes. Towards the landward basement high, sediment waves are observed that continue to be present and intensify in the overlying late Oligocene-early Miocene unit (Unit II; Figure 1c). Unit III becomes significantly thicker towards the foot of the continental slope with internal reflections onlapping onto the slope (Figure 1d).

Unit II

Unit II is ~ 0.5 s TWT thick and its top boundary reflection onlaps onto the peak of both basement highs (Figure 1c). A high-amplitude internal reflection within Unit II can be correlated to the Oligocene-Miocene transition (Figure 1c, insets). The upper section of Unit II (early Miocene; ~ 0.3 s TWT thick) contains high-amplitude, relatively undisturbed and parallel internal reflections. At each end of the basin, the unit's internal and top boundary truncate to a prominent unconformity, which has been correlated to the mid-late Miocene transition (Figure 1c).

Ocean-continent transition

The most oceanward (SW) section of the seismic line (Figure 1c) shows features characteristic of subcontinental mantle exhumation. A high-amplitude, continental dipping reflection is detected at ~ 10 s TWT depth, which rises up to about 9 s TWT and disappears (Figure 1c; shot points, SP, 2500-3200). This sharp rising feature is interpreted as the Moho boundary and is characteristic of regions with exhumed subcontinental mantle along the ocean-continent transition (OCT; Gillard et al., 2015; McCarthy et al., 2020). The continental basement and pre-/syn-rift sediments contain closely spaced fault structures, indicating major deformation in the region during mantle exhumation. The imaged domain of exhumed mantle in the seismic line is about 30 km wide; however, it likely continues oceanward, beyond the extension of the seismic line.

4.2 Palynological assemblages

We record a fair coupling between changes in lithology and changes in the three major palynomorph groups: dinocysts, acritarchs and terrestrial palynomorphs (Figure 4). The terrestrial palynomorphs are dominant in the upper Eocene-lower Oligocene part (units V-III) of the record, which also has the highest TOC levels. In the middle of lithological Unit III, below 700 mbsf (30.5 Ma), the high relative abundance of terrestrial palynomorphs rapidly decreases to 5%-15%, concomitant with a decrease in TOC, and remains low in the overlying nannofossil chalks and silty claystones (Unit II). In the Oligocene, from 700 to 400 mbsf (30.5-22.4 Ma), dinocysts are the most abundant palynomorph group and comprise up to 88% of all palynomorphs. In the Miocene, acritarchs dominate the assemblages, reaching up to 90% of the total palynomorph assemblage. Acritarchs reach the highest relative and absolute abundances at 540-520 mbsf and above 400 mbsf. The second peak in the lower Miocene is synchronous with increased amounts of calcium carbonate (40 wt%).

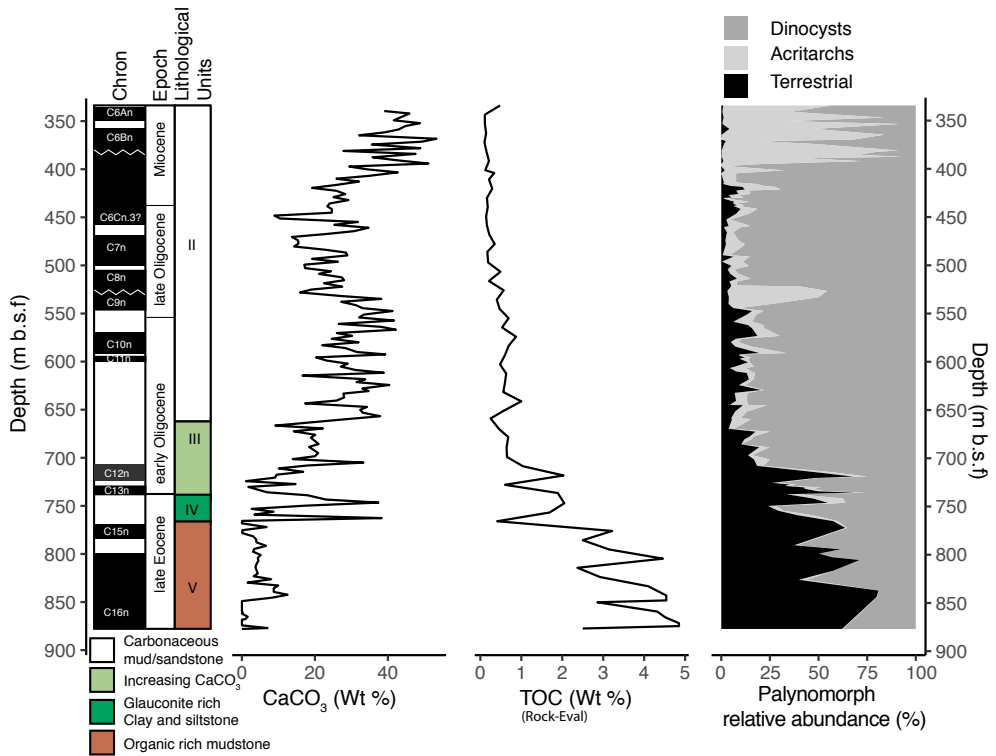


Figure 4. Stacked relative abundance of the three major palynomorph groupings (terrestrial palynomorphs, acritarchs and dinocysts), plotted against depth (mbsf), next to the magnetostratigraphic framework (Gradstein et al., 2012), lithological units, and shipboard total organic carbon (TOC, wt%) and calcium carbonate (CaCO₃, wt%) data (Exon et al., 2001b).

3

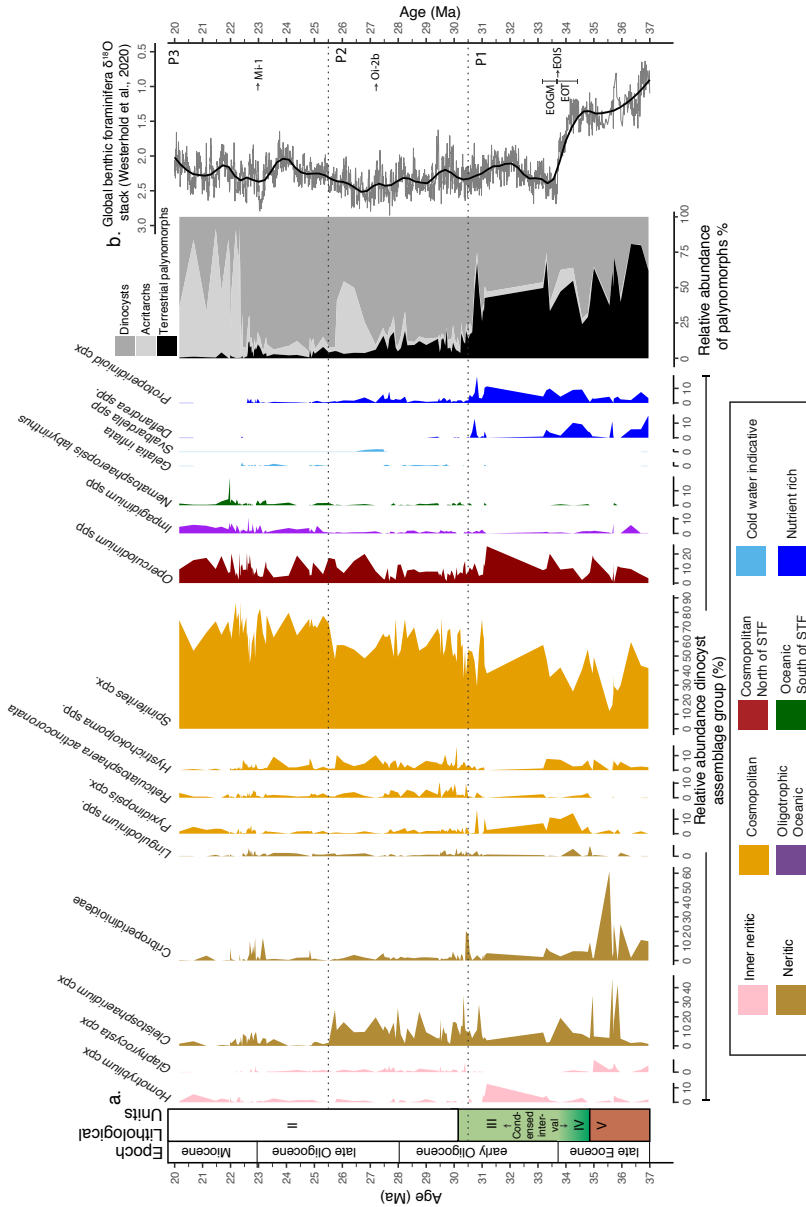


Figure 5. (a) Relative abundance (%) of selected dinocyst taxa and/or groups (Table 1), ordered from their known occurrence in inshore (left) to offshore (right) environments, with heterotrophic taxa (light and dark blue) to the right. Dinocyst taxa have been assigned to an ecological group (see legend), based on the context of this study, consistent with interpretations from Röhl et al. (2004) and Frieling and Sluijs. (2018). The relative abundance of terrestrial palynomorphs, acritarchs and dinocysts with respect to the total palynomorph counts is shown in greyscale. (b) Global benthic foraminiferal $\delta^{18}\text{O}$ stack record by Westerhold et al. (2020). The thick black line represents the loess smoothing curve with a span of 0.1. Selected isotopic events are marked, following Hutchinson et al. (2021): EOT is the Eocene-Oligocene transition, EOGM is the earliest Oligocene glacial maximum, EOIS is the earliest Oligocene oxygen isotope step, Oi-2b is the Oligocene glaciation/isotopic event 1. The stippled black lines at 30.5 and 25.5 Ma distinguish the three phases/time intervals (P1, P2 and P3) discussed in Sect. 5.1.

4.2.1 Dinocyst assemblages

From the 123 samples counted, 106 samples yield abundant and well-preserved dinocysts (Figure 5). Identification of dinocysts on a species level was possible in most cases; however, some dinocysts were only categorised on a genus level when distinctive features were lacking. The quantitative requirement of counting to a minimum of 200 dinocyst was met for most of the samples, except for those from the upper Eocene, where terrestrial palynomorphs dominate the record, and from the lower Miocene, where acritarchs dominate the palynomorph assemblages (Table S2 in the Supplement).

Dinocyst assemblages are dominated by the Gonyaulacoid (autotrophic) taxa *Spiniferites* spp. (30%-90%), with the common (5%-25%) and consistent occurrence of *Operculodinium* spp., *Cleistosphaeridium* spp. and *Hystrichokolpoma* spp. Dinocysts of the family Cribroperidinioideae were sporadically present to common (10%-40%). Other dinocysts taxa present (0%-10%) throughout were *Glaphyrocysta* cpx., *Lingulodinium* spp., *Pyxidiniopsis* cpx., *Reticulosphaera* spp., *Gelatia inflata* and the Goniodomideae of the genus *Homotryblium*. Among the heterotrophic dinocysts, *Deflandrea* spp. and the *Protoperidinioid* cpx. (including *Brigantedinium* spp., *Protoperidinium* spp., *Lejeunecysta* spp. and *Selenopemphix* spp.) were common (10%-20%) prior to 30.5 Ma (phase 1) and remained present (0%-10%) throughout the record. *Svalbardella* spp. is present in a short interval between 26.8 and 27.5 Ma (chron C9n). The dinocyst assemblages show increasingly consistent occurrences of more outer-neritic to open-oceanic and cosmopolitan taxa such as *Cleistosphaeridium*, *Hystrichokolpoma* spp., *Reticulosphaera* spp., and increasingly more abundant *Spiniferites* spp., *Operculodinium* spp., *Impagidinium* spp. and *Nematosphaeropsis labyrinthus*. At 25.5 Ma (phase 3), *Cleistosphaeridium* cpx. rapidly decreases, *Spiniferites* cpx. becomes highly dominant, and *Impagidinium* spp., with *I. paradoxum* as the most common species, becomes increasingly more abundant. A pronounced increase in the abundance of *Apteodinium australiense* (Cribroperidinioideae) occurs at the Oligocene-Miocene boundary interval (~23.1-22.9 Ma). A peak in the abundance of *Nematosphaeropsis labyrinthus* occurs around 22 Ma. Simultaneously, *Hystrichokolpoma rigaudiae* and *Lingulodinium machaerophorum* decrease to their lowest abundance in the study record. Increasing the sample resolution and the number of dinocysts counted per sample in this study led similar dinocyst assemblages being found to those presented in the initial report by Brinkhuis et al. (2003).

4.2.2 Acritarchs and other palynomorphs

Acritarch assemblages are dominated by skolochorate forms. We informally name occasionally abundant unidentified small (10 µm) skolochorate acritarchs with various spine lengths as Acritarch sp. 1 (long spines) and Acritarch sp. 2 (short spines) (Plate S1 in the Supplement). The abundance of acritarchs does not correlate to that of reworked dinocysts, which argues for in situ production. We record a large peak in Acritarch sp. 2 around 25.8-26.8 Ma. Acritarch sp. 1 (long spines) becomes the dominant (40-90% of total marine palynomorphs) palynomorph in the early Miocene part of the record (22.3-20 Ma). Smooth-walled transparent spheres are recorded as *Leiosphaeridia*. Members of *Leiosphaeridia* spp. generally appear in low abundance (<5%) from 35 Ma onwards. Transparent spheres with a perforated wall structure are informally named Acritarch sp. 3 (15-20 µm; Plate S1 in the Supplement). Acritarch sp. 3 first appears after 33.5 Ma and sporadically appears in low abundance (0%-6%) until 22.6 Ma. Prasinophyte algae *Cymatiosphaera* spp. is sporadically present in very low numbers (<3% of total marine palynomorphs) in the Oligocene. *Tasmanites* spp. is only present in very low numbers between 35 and 30.6 Ma (Table S2 in the Supplement).

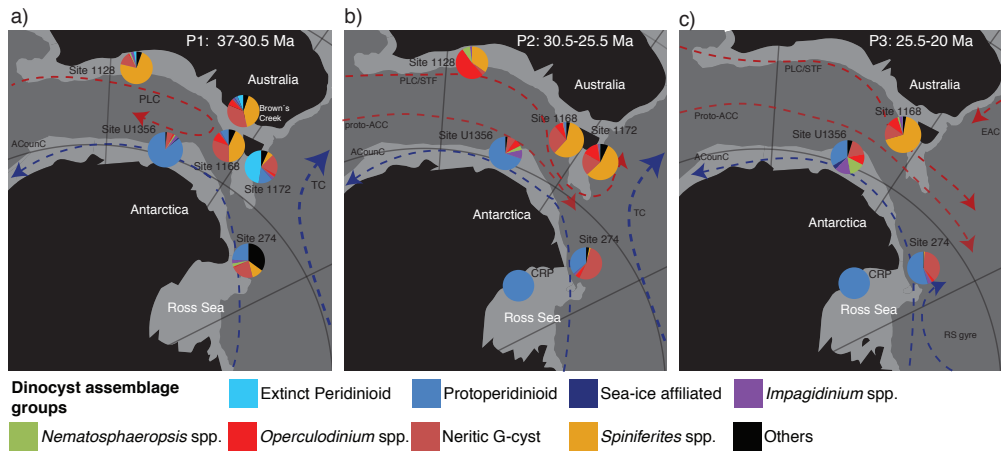


Figure 6. Dinocyst biogeographic patterns in the Tasmanian sector in three time slices in the late Eocene-early Miocene: (a) 37-30.5 Ma (31 data points), (b) 30.5-25 Ma (42 data points) and (c) 25-20 Ma (50 data points). The dinocyst assemblage of ODP Site 1168 (this study) is presented along with that from IODP Site U1356 (Bijl et al., 2018), DSDP Site 274 (Chapter 2), Cape Roberts Project (CRP) (Clowes et al., 2016), ODP Site 1172 (Sluijs et al., 2003), Site 1128 and Browns Creek (Houben et al., 2019) (Table S3 in the Supplement). The dinocyst taxa and/or ecological groups are indicated by different colours (see legend), following interpretations by Röhl et al. (2004) and Frieling and Sluijs. (2018). The “extinct peridinioid” group consists of *Phthanoperidinium* spp., *Spinidinium* spp. and *Vozzhennikovia* spp., *Deflandrea phosphoritica* and the *Wetzelielloideae* group. The blue and red stippled lines with arrows indicate flow direction, with proposed cool (blue) and warm (red) ocean currents that may have prevailed in the indicated areas during the different time intervals (e.g. Stickley et al., 2004a). EAC is the East Australian Current, PLC is the proto-Leeuwin Current, STF is the subtropical front, TC is the Tasman Current, proto-ACC is the proto-Antarctic Circumpolar Current and ACounC is the Antarctic Counter Current. The palaeogeographic position of the sites is generated with GPlates (<http://www.gplates.org>, last access: 13 June 2016), based on the global plates geodynamic motion model from Müller et al. (2018). Light grey indicates the continental shelf.

5 Discussion

5.1 Local depositional environment and palaeoenvironmental changes

Based on changes in the relative abundance of dinocyst assemblage groups, acritarchs and terrestrial palynomorphs (Figure 5), we divide the record into three phases (P1-P3) of regional palaeoenvironmental change, independent of the lithological units, and compare these to the seismic and lithological investigations at Site 1168: (1) 37-30.5 Ma – transition from mid-shelf to outer-neritic conditions; (2) 30.5-25.5 Ma – outer-neritic conditions with transport of detrital material from the shelf; and (3) 25.5-20 Ma – transition from outer-neritic to more oligotrophic, oceanic conditions and frontal system development.

5.1.1 Late Eocene-early Oligocene (P1: 37-30.5 Ma)

Dinocyst assemblages with abundant *Spiniferites* spp. suggest a shallow mid-shelf setting on the western Tasmanian continental margin at this time, although with strong input from shallow depositional settings (interpreted from the abundance of terrestrial palynomorphs and lagoonal

Homotryblium cpx.). Heterotrophic *Deflandrea* spp. and *Brigantedinium* spp. are common, and terrestrial input (30%-75% terrestrial palynomorphs) is high. The combination of these suggests high freshwater runoff from the shore, which increased the nutrient input to the site, favouring primary productivity. The observed seismic hummocky structures in the upper part of Unit V also reflect transport from shallower parts of the continental shelf.

During the rift to drift transition of Australia and Antarctica, the sedimentary environment along the western Tasmanian margin was likely strongly affected by the activity of the Sorell Fault Zone which later extended to the Tasman Fracture Zone with the onset of seafloor spreading (Figure 1a, b) (e.g. Miller et al., 2002). This tectonic feature likely acted as a bathymetric barrier for ocean circulation to reach Site 1168 (e.g. Hill and Exon, 2004; Sauermilch et al., 2019a). In addition, recently published petrological and geophysical data directly along the conjugate Antarctic margin revealed that the late rifting stage was affected by the exhumation of subcontinental mantle (Seamount B, east of Adélie Rift Block; McCarthy et al., 2020). Petrological constraints tentatively indicate that melt infiltrated into the subcontinental mantle along the OCT during its rift to drift transition. This likely led to heating of the subcontinental mantle and changing petrological characteristics, increasing the buoyancy of the region. Consequently, this could have led to uplift and/or slower thermal subsidence compared with those of “normal” (mid-ocean ridge basalt) oceanic crust (e.g. Müntener et al., 2010). Seismic data along the western Tasmanian margin indicate a similar mantle exhumation pattern (Figure 1c). As Seamount B and Site 1168 are directly conjugate, it can be assumed that the mantle uplift could also have affected the western Tasmanian margin, leading to an uplift and/or delayed thermal subsidence of the Tasmanian margin during the time of continental break-up. Organic-rich sediments indicate eutrophic, poorly ventilated bottom conditions, possibly sluggish circulation. This is in line with the palynological and seismic interpretation of a shallow and enclosed graben system.

In the glauconitic interval (Unit IV) that straddles the EOT, lithology and dinocyst assemblages become more variable, probably as a result of the progressive deepening of the continental slope. Unit IV is very thin and only visible as a strong seismic reflection. Therefore, it is difficult to distinguish between upper Unit V and Unit IV in the seismic profiles. However, the boundary reflection is clearly wavy with hummocky features (Figure 1c, insets), which could be an indicator for winnowing. The early Oligocene section overlying the glauconite layer corresponds to seismic Unit III with sediment waves along the landward basement high (Figure 1c). These indicate some bottom current activity and increased oxygen delivery, although signs of winnowing have now ceased. As a result, TOC decreases while CaCO₃ increases. The return of coastal assemblages and terrestrial palynomorphs around 31 Ma might reflect the Oi-2a glaciation event (Miller et al., 1991; Palike et al., 2006; Galeotti et al., 2016; Westerhold et al., 2020). This caused a lower sea level at these latitudes (Gallagher et al., 2020), which spurred sediment transport from the Australian continental margin. However, the overall decrease in terrestrial palynomorphs, (proto) peridinioid cysts and inner-neritic dinocysts in the glauconite layer does reflect deepening of the Tasmanian continental slope between ~35.5 and 30.5 Ma, consistent with that in nearby Site 1172 (Stickley et al., 2004b) and with final separation between Tasmania and Antarctica (Whittaker et al., 2013).

5.1.2 Oligocene transitional phase (P2: 30.5-25.5 Ma)

In this interval, the cosmopolitan dinocysts *Spiniferites* spp. become more dominant, and species indicative of coastal/lagoonal environments and terrestrial palynomorphs decrease abruptly around 30.5 Ma, indicating that the distance to shore has potentially increased, although the site is still at or close to the continental shelf. Throughout the Oligocene, occasional peaks of the neritic groups

Cleistosphaeridium cpx. and Cribroperidinioideae indicate varying influx from the inner-neritic shelf, perhaps as a result of sea level changes (Gallagher et al., 2013). The seismic profiles show wavy sediment structures in units III and II along the landward basement high. During the late Oligocene, they intensify and form more prominently in Unit II, which could indicate increasing bottom current activity.

The constant abundance of *Spiniferites* cpx., *Operculodinium* spp., *Hystrichokolpoma* spp. and *Lingulodinium machaerophorum* as well as the low abundance of the typical cold-water indicator *Gelatia inflata* indicate the relatively constant influence of warm water (Egger et al., 2018), in line with indications of subtropical to warm temperate and always above freezing Australian hinterlands (Greenwood and Wing, 1995; Holdgate et al., 2017). Although, assemblages vary somewhat from sample to sample, there is no large change in the relative proportion of the main components of the assemblage throughout this interval that would suggest a change in oceanographic conditions. The exception is the occurrence of *Svalbardella* spp. in magnetochron C9n. The study of van Simaey et al. (2005) linked the migration of *Svalbardella* spp. to the Southern Hemisphere during the second large benthic $\delta^{18}\text{O}$ excursion in the Oligocene, the Oi-2b glacial episode (Miller et al., 1991; Zachos et al., 1994; Pekar et al., 2002). The sudden occurrence of *Svalbardella* spp. indicates that Antarctic cooling and glacial expansion also affected the distal sites in the Southern Ocean.

5.1.3 Late Oligocene-early Miocene (P3: 25.5-20 Ma)

In the late Oligocene, we note a sharp decrease in the neritic dinocyst groups (mostly *Cleistosphaeridium* cpx.) as well as a further increased dominance of *Spiniferites* spp. and more abundant oceanic taxa (*Impagidinium* spp. and *Nematosphaeropsis labyrinthus*). This corroborates the continuous subsidence of the Tasmanian region (Stickley et al., 2004a), shifting depositional environments from a restricted inner-neritic basin to the deposition of carbonate ooze in a well-oxygenated open ocean along a continental slope at middle bathyal depths (Exon et al., 2001a, b; Boreham et al., 2002). The sediment wave features found in the lower part of Unit II seem to mostly disappear in the upper part of Unit II during the early Miocene, which is potentially caused by the continuous deepening of the margin.

Impagidinium paradoxum, the most abundant of the *Impagidinium* group, which starts to become more abundant at 25.5 Ma, is today most abundant in samples within 5° latitude north or south of the STF (Prebble et al., 2013) (Figure 3). *Nematosphaeropsis labyrinthus*, today most common south of the STF (Prebble et al., 2013) in the subantarctic zone, also increases in abundance from 25.5 Ma onwards, peaking in the early Miocene. This could indicate northward expansion of the frontal systems and an approaching subantarctic zone towards Site 1168 in the late Oligocene-early Miocene. The very low abundance of the warm-water-affiliated taxa *Hystrichokolpoma rigaudiae* (e.g. Louwye et al., 2008) and *Lingulodinium machaerophorum* (e.g. De Schepper et al., 2011) suggest a slight cooling in the early Miocene compared with the late Oligocene.

5.2 Tectonic and palaeoceanographic changes in the Tasmanian region

5.2.1 Seismic and lithological evidence of changing oceanographic conditions

A shallow connection between the AAG and the southwest Pacific across the southwestern South Tasmanian Rise has existed since ~49 Ma near the Antarctic continental margin (Bijl et al., 2013) and perhaps since ~38 Ma across or north of the South Tasmanian Rise (Stickley et al., 2004a). However, the proto-Leeuwin Current (PLC), which transported warm subtropical waters into the

AAG during the Eocene (Huber et al., 2004; Bijl et al., 2011; Sauermilch et al., 2019a), did not cross the Tasmanian Gateway until 35.5 Ma (Stickley et al., 2004a; Houben et al., 2019). Lithological barriers west and/or south of the Tasmanian rise, e.g. the Tasman Fracture Zone (TFZ), potentially restricted throughflow across the Tasmanian Gateway (Exon et al., 2004; Sauermilch et al., 2019a), which we here see diminished after the EOT, when graben have filled and continental margins subside.

The strongly different seismic structure of the continental slope on either side of the TFZ indicates that the TFZ and the extended Sorell Fault Zone played a significant role in the depositional evolution of the region during the Eocene and early Oligocene, and likely also affected ocean circulation flow. The South Tasman Rise and adjacent margins started to subside between 35.5 and 30.2 Ma, in conjunction with the final break-up between Australia and Antarctica (Cande and Stock, 2004; Whittaker et al., 2013; Williams et al., 2019; Mccarthy et al., 2020). This coincided with the sediment filling of embedded basins, draping the local expressions of the basement highs and leading to a depositional environment of a deepening continental slope.

Results from high-resolution ocean model simulations suggests that, during the time between 36 and 33.6 Ma, deepening of one of the gateways (Drake Passage or Tasmanian Gateway) below 300 m whilst the second gateway was already open (Sauermilch et al., 2021) could, in part, explain some of the oceanographic changes showed in available proxy records from Southern Ocean sediment drill cores (e.g. Houben et al., 2019; Westerhold et al., 2020). In the simulation (Sauermilch et al., 2021), depth changes from 300 to 600 m led to prominent surface water cooling offshore of Antarctica, whilst the subpolar gyres (Weddell and Ross gyres) weakened and shrank significantly and an eastward proto-Antarctic Circumpolar Current that was weaker than the present day current could be established. Model-data comparison suggests further gateway deepening (>600 m) occurring from 33.6 to 30 Ma, likely leading to stronger bottom-water currents passing through the Tasmanian Gateway. Between 32 and 30 Ma, the first deep-water current to pass the Tasmanian Gateway was flowing westward from the Pacific to the Indian Ocean (Scher et al., 2015), perhaps in compensation for the throughflow of the PLC. By 30.2 Ma, the Tasmanian Gateway was deep enough to fully connect the former AAG and the southern Pacific through the eastward flow of water masses originating within the AAG or southeastern Indian Ocean (Sluijs et al., 2003; Stickley et al., 2004a). Sediment waves observed in seismic data from the early until the late Oligocene (partly until the earliest Miocene) support this hypothesis. Sites around the Southern Ocean have quasi-synchronous glauconite horizons, caused by current winnowing and sediment starvation, and are often condensed, such as Unit IV and lower Unit III at Site 1168 (Houben et al., 2019; Sauermilch et al., 2019a). These are equivalent to a widespread known regional unconformity, the Marshall unconformity (Carter, 1985; Fulthorpe et al., 1996). Stickley et al. (2004a) associated the Tasmanian glauconite intervals with accelerated subsidence of the South Tasman continental blocks, while Houben et al. (2019), who recorded the late Eocene glauconite sands as a Southern Ocean-wide phenomenon, linked them to invigorated surface current intensity where progressive pre-EOT atmospheric cooling played a defining role.

5.2.2 Palynological evidence of sea surface ecological changes across the widening Southern Ocean

To provide a wider, Southern Ocean perspective to the results of ODP Site 1168 during these times of Tasmanian Gateway widening, we compare palynological data from different drill sites in the region for the same time intervals (phases 1-3) as in Sect. 5.2 (Figure 6).

Ice-proximal palynological records from the Ross Sea shelf, Cape Roberts Project (CRP) (Prebble et al., 2006; Clowes et al., 2016), are dominated by *Lejeunecysta* spp., and *Cymatiosphaera* spp. in the Oligocene with the addition of *Brigantedinium* spp. in the late Oligocene-early Miocene (Hannah et al., 2000; Prebble et al., 2006; Clowes et al., 2016). This likely indicates generally cold temperate, nutrient-rich, productive waters where seasonal sea ice melts. The more distal locations, DSDP Sites 269 and 274 and IODP Site U1356, are bathed by temperate waters (Bijl et al., 2018; Sangiorgi et al., 2018; Hartman et al., 2018b; Salabarnada et al., 2018; Evangelinos et al., 2020; Chapter 2) and represented open-ocean high-nutrient conditions of the Antarctic divergence. Our study shows that ocean waters at the Australian margin in the late Eocene-early Miocene resembled those of modern subtropical water near-shore sites north of New Zealand (Prebble et al., 2013), despite the more southerly position of Australia. This shows a strong differentiation in dinocyst assemblages at either side of the AAG starting in the late Eocene and increasing in the Oligocene (<30.5 Ma) to early Miocene, indicating that the frontal systems were evolving in place, which contrasts with the early Eocene conditions (e.g. Bijl et al., 2013) (Figure 6).

The intensified deepening and widening of the Tasmanian Gateway between ~35.5 and 30.2 Ma facilitated the throughflow of the PLC (Stickley et al., 2004a, b). After 30.2 Ma, we record that this throughflow caused profound changes in the dinocyst assemblages on the east side of the Tasmanian Gateway (ODP Site 1172; Sluijs et al., 2003), with the disappearance of the Antarctic-derived “extinct peridinioid” cysts and an increase in cosmopolitan dinocyst species, making the dinocyst assemblages strikingly similar at Site 1168 and Site 1172 for P2 (Figure 6b). However, at Site 1168, the throughflow was of little influence. Indeed, deepening of the continental slope does limit the input of coastal dinoflagellate cyst species and terrestrial palynomorphs, but it does not profoundly alter the remaining outer-neritic to oceanic dinocyst assemblage. This testifies to a continuous influence of the PLC. South Australian surface-ocean conditions remained surprisingly invariant to large-scale Antarctic glaciation, onset of circumpolar flow (Stickley et al., 2004a; Sijp et al., 2014) and appearance of Antarctic sea ice (Houben et al., 2013), despite its southerly position. Indeed, circumpolar flow through the Tasmanian Gateway was likely still slow throughout the Oligocene (Hill et al., 2013; Evangelinos et al., 2020; Sauermilch et al., 2021).

5.2.3 Environmental interpretation of acritarchs and prasinophyte algae across the Southern Ocean

The peak of Acritarch sp. 2 around 26.8-25.8 Ma (550-520 mbsf) and Acritarch sp. 1 bloom from 22.3 Ma (400 mbsf) (Figure 5) occur around the same time as a slight decrease in sedimentation rate (Figure 2) and coincide with the high carbonate (CaCO_3) content (Figure 4) (Pfuhl and Mccave, 2003). The first acritarch bloom is not observed at the other Southern Ocean sites in the vicinity of the Tasmanian Gateway but correlates with carbonate-rich and iceberg-rafted debris free interglacial sediments at IODP Site U1356 between 25 and 26 Ma (Salabarnada et al., 2018). The Site 1168 peak in acritarchs in the early Miocene is comparable and coeval to that in a carbonate-rich intervals of IODP Site U1356 (Bijl et al., 2018), where “*Cymatiosphaera*-like” acritarchs dominate the assemblages of the late Oligocene (<24.5 Ma) to mid-Miocene. Carbonate-rich intervals during the late Oligocene-early Miocene at Site U1356, along with oligotrophic, temperate dinocysts suggest a trend of increased acritarch abundance during warmer intervals. However, due to little indication of warming in the early Miocene in the dinocyst record or the benthic foraminiferal $\delta^{18}\text{O}$ record by Westerhold et al. (2020), we suggest the higher CaCO_3 at Site 1168 to reflect a transition in lithology linked to changes in environmental conditions, likely due to decreased detrital input as a consequence of decreased precipitation in the hinterland (McGowran et al., 2004). At DSDP Site

269, *Leiosphaera* spp. is the most common palynomorph in the upper Oligocene-lower Miocene (Evangelinos et al., 2020). At DSDP Site 274, acritarch assemblages (mainly skolochorate, similar to our *Acritarch* sp. 1) are relatively low (<30%) throughout the lower Oligocene but increase towards the upper Oligocene (Chapter 2). Acritarch blooms in each of the various records analysed seem to be linked to a different environmental condition. Therefore, we cannot identify a main environmental driver of acritarch blooms across the Southern Ocean during the late Oligocene-early Miocene.

6 Conclusions

We present new seismic interpretations and marine palynological association data to reconstruct the late Eocene to early Miocene palaeoceanographic conditions on the western Tasmanian continental margin. Upper Eocene sediments are embedded in a sedimentary basin enclosed by two basement highs, whereas material of EOT – earliest Oligocene age draped basement highs and show some indications of sediment reworking and winnowing. In the Oligocene to lower Miocene units, seismic features show evidence of bottom current activity. The Tasmanian Fracture Zone and the Sorell Fault Zone likely acted as a bathymetric barrier for ocean currents to reach Site 1168 during the late Eocene. Possible buoyancy-related uplift of the region through subcontinental mantle exhumation (Figure 1c) during this time may have added to the bathymetric isolation effect. Palynological data confirm these seismic interpretations of the subsidence of the Tasmanian continental margin (Stickley et al., 2004a), with a transition from abundant terrestrial palynomorphs, Protoperidinioid cysts and extant neritic dinocysts in the total palynological counts in the late Eocene to the increasing abundance of modern oceanic dinocyst groups through the Oligocene-early Miocene. The different dinocyst assemblages north and south across the widening Southern Ocean reflect the onset of modern oceanographic conditions with a pronounced latitudinal temperature gradient starting in the late Eocene, manifesting itself in the Oligocene with more established frontal systems in the Southern Ocean. We suggest a northward broadening of the STF and subantarctic zone towards Site 1168 in the early Miocene. Aside from the gradual disappearance of inner-neritic – neritic species through the Oligocene record and the introduction of oceanic species common south of the STF (subantarctic zone), there are no significant changes to the surface-ocean properties or ocean currents at the western Tasmanian marginal Site 1168 in the Oligocene.

Acknowledgements

Sediment samples were provided by the Ocean Drilling Program (ODP). We thank Natasja Welters, Mariska Hoorweg and Giovanni Dammers for technical support at the Utrecht University GeoLab. We thank Spectrum Geo Ltd and the Federal Institute for Geosciences and Natural Resources Germany for providing the seismic reflection data sets. We acknowledge IHS Markit for the provision of the IHS Kingdom software used in this research.

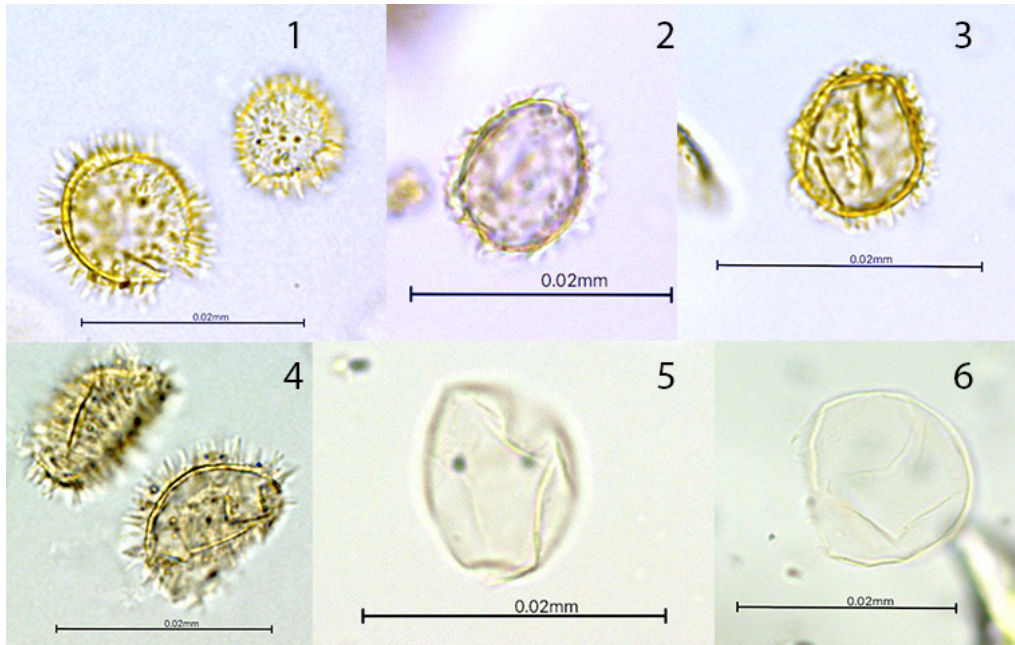
Financial support

This research has been supported by the Dutch Research council, Nederlandse Organisatie voor Wetenschappelijk Onderzoek (NWO) polar programme (grant no. ALW.2016.001), and the European Research Council, H2020 programme (grant no. OceaNice 802835).

Supplementary Information Chapter 3

The supplementary tables and figures related to this chapter is available online, at:

<https://doi.org/10.5194/jm-40-175-2021-supplement>.



Supplementary plate 1. Light Microscopy photos of informally named Acritarchs, abundantly encountered in samples from ODP Site 1168, 877–334 m b.s.f. (1) Acritarch sp. 1, 1168 038X-04w 60-62 cm, slide 2, mid focus. (2) Acritarch sp. 2, 1168-45X-1W 2–4 cm, slide 2. (3) Acritarch sp. 2 1168-56X-01W 60-62cm, slide 1. (4) Acritarch sp. 1, 1168-038x-04w 60-62 cm, slide 2. (5) Acritarch sp. 3 1168-46X-1W 61–64 cm, slide 1. (6) Acritarch sp. 3 1168-46X-1W 61–64 cm, slide 1.

Chapter 4

Strength and variability of the Oligocene Southern Ocean surface temperature gradient

Frida S. Hoem¹, Isabel Sauermilch¹, Adam K Aleksinski², Matthew Huber², Francien Peterse¹, Francesca Sangiorgi¹ and Peter K. Bijl¹

1. Department of Earth Sciences, Utrecht University, Utrecht, The Netherlands.

2. Department of Earth, Atmospheric and Planetary Sciences, Purdue University, West Lafayette, USA.

In review: Communications Earth & Environment

Abstract

Large Oligocene Antarctic ice sheets co-existed with warm Southern Ocean waters. To provide a broader Southern Ocean perspective to such warmth, we reconstruct the strength and variability of the Oligocene Australian-Antarctic latitudinal sea surface temperature (SST) gradient. Our Oligocene TEX₈₆-based SST record from offshore southern Australia shows temperate (20–29°C) conditions throughout, despite northward tectonic drift. A persistent SST gradient (~5–10°C) exists between Australia and Antarctica, which increases during glacial maxima. The SST gradient increases from ~26 Ma onwards, due to decreasing Antarctic-proximal SSTs. Meanwhile, benthic foraminiferal oxygen isotope decline indicates ice loss/deep-sea warming. These contrasting patterns are difficult to explain by greenhouse gas forcing alone. Timing of the SST cooling coincides with deepening of Drake Passage and fits well with results of ocean model experiments that demonstrate that Drake Passage opening cools the Antarctic coast. We conclude that Drake Passage deepening cooled Antarctic coastlines which enhanced thermal isolation of the Antarctic ice sheet.

1 Introduction

Southern high-latitude sea surface temperature (SST) records from the Oligocene (33.9–23.0 Ma) (Liu et al., 2009; Hartman et al., 2018; Houben et al., 2019; Chapter 2) show unexpectedly warm-temperate conditions, despite evidence for the coeval presence of large Antarctic ice sheet (Bohaty et al., 2012), which extended to the margins of the continent (Galeotti et al., 2016; Levy et al., 2019). This apparent contradiction requires reconciliation (O'Brien et al., 2020). A warm Oligocene Southern Ocean could be the result of generally high atmospheric $p\text{CO}_2$ concentrations (300–700 ppm; <https://www.paleo-co2.org> (Hoenisch, 2021)), but higher $p\text{CO}_2$ would also be associated with reduced ice volume (Gasson et al., 2014). Furthermore, since enhanced Antarctic ice volume should have cooled marginal seas (Goldner et al., 2014) the mystery of warm high latitude SSTs and greater ice volume grows. One alternative hypothesis is that marine ice sheet terminations were restricted to the southernmost parts of the Antarctic margin, facilitated by a higher-than-modern Antarctic paleotopography (Paxman et al., 2019), while elsewhere the ice sheets were mostly terrestrial (e.g., Bijl et al., 2018; Sangiorgi et al., 2018), limiting the Antarctic glacial cooling effect on proximal SSTs (Singh et al., 2016). Or as a final hypothesis, a restricted width of critical Southern Ocean gateways (Tasmanian Gateway and Drake Passage) may have played a role in ocean heat redistribution (Hill et al., 2013). Closed ocean gateways, which can reduce meridional temperature gradients by enhancing ocean poleward heat transport or by increasing local radiative heating through albedo feedbacks or enhanced atmospheric moisture transport (England et al., 2017; Evangelinos et al., 2022) may thereby have sustained warm SSTs while simultaneously maintaining terrestrial ice sheets. Each of these factors (radiative forcing, ice sheet configuration and tectonic changes) would have had a unique spatial fingerprint of Southern Ocean SST changes relative to those at the Antarctic continental margin and unravelling the complexities is challenging. Atmospheric $p\text{CO}_2$ associated radiative forcing would be expected to cause globally synchronous temperature trends on both long- and orbital-time scales, although with a degree of polar amplification. Ice sheet growth increase poleward heat transport (Knorr and Lohmann, 2014), but at the same time induces local cooling at the Antarctic margin (Goldner et al., 2014). The different response to Antarctic glaciation in different model experiments (Supplementary Table 1) can be attributed to subtle changes in paleogeography and model set-up (Kennedy et al., 2015). In any case, ice volume change has the most effect close to the Antarctic continent, and is further evident in benthic foraminiferal $\delta^{18}\text{O}$ (Westerhold et al., 2020) and deep-sea cooling (Lear et al., 2004). Finally, opening of gateways would result in profound cooling of Antarctic proximal waters (Kennedy-Asser et al., 2019; Sauermilch et al., 2021) while leaving the rest of the world's sea water temperatures largely unaffected (Goldner et al., 2014; England et al., 2017). Thus, as opposed to ice volume changes, gateway opening cause a stepwise, unidirectional change in temperature: changes in SSTs could then be stratigraphically linked to phases of gateway opening (Sauermilch et al., 2021; van de Lagemaat et al., 2021). Currently, Oligocene SST records from the subtropics are lacking, which hinders establishing the latitudinal SST gradients needed to provide context for ice-proximal SST changes, and to evaluate the possible factors that drove the evolution of Oligocene Southern Ocean surface conditions.

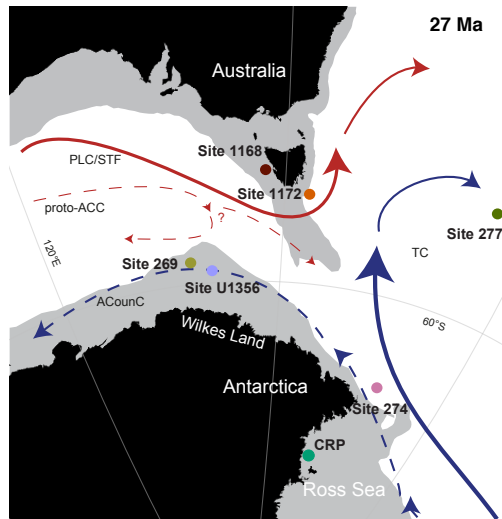


Figure 1. Paleogeographic map of the Oligocene locations of study sites and prevailing ocean currents. The approximate paleogeography at 27 Ma is reconstructed through G-plates (<http://www.gplates.org>), based on the global geodynamic rotation model from Müller, et al. (2018). Black represents the outline of modern coastlines. The grey outline corresponds to the modern 2000 m water depth contour. PLC=Proto-Leeuwin Current, STF=Subtropical front, TC=Tasman Current, proto-ACC=proto-Antarctic Circumpolar Current and ACounC=Antarctic counter current (after Houben et al., 2019).

Here, we present TEX_{86} based SST estimates from Late Eocene-Early Miocene ODP Site 1168 sediments (339-765 mbsf), west of Tasmania (red dot in Figure 1). To explore the evolution of the Oligocene SST gradient across the Tasmanian Gateway region, we compared our data with TEX_{86} based SSTs from east of Tasmania (ODP Site 1172; Bijl et al., 2021), west of the Campbell Plateau (DSDP Site 277; Liu et al., 2009), north of the Ross Sea (DSDP Site 274; Chapter 2), offshore Wilkes Land (IODP Site U1356; Hartman et al., 2018, and DSDP Site 269; Evangelinos et al., 2020) and inorganic chemical weathering indices recording terrestrial temperature from the Cape Roberts Project (CRP) in the Ross Sea (Passchier et al., 2013) (Figure 1). These SST records are compared to the temperature distribution in a coarse-resolution (3° horizontal), fully coupled general circulation model (GCM) following Kennedy-Asser, et al. (2019; HadCM3L – Hadley Centre Coupled Model), which simulates equilibrium temperature response to CO_2 forcing, and the role of ice volume and geographic boundary conditions of the Early- and Late Oligocene (33.9-28.1, 28.1-23 Ma). Details of ocean heat transport and consequences of local bathymetry are subsequently investigated comparing SST results to high horizontal resolution (0.25°) ocean-only model simulations (Sauerlich et al., 2021). Our results show an increase in the SST gradient across the Southern Ocean starting at 26 Ma, when Antarctic-proximal SSTs cooled. This is in contrast to a synchronous decrease in global benthic foraminiferal $\delta^{18}\text{O}$ indicating ice mass loss/deep sea warming. Considering the potential drivers of such cooling, we conclude that the Late Oligocene Antarctic-proximal SST cooling is not primarily driven by changes in $p\text{CO}_2$ and ice sheet configuration, but by paleogeographic configurations.

2 Methods

2.1 Site description, depositional setting and age model

We reconstruct the changes in sea surface temperature from the subtropical front region by studying marine sediments (766-339 mbsf) from Ocean Drilling Program (ODP) Site 1168 (42°38.40'S, 144°25.30'E; present water depth: 2463 m). The site is situated 70 km off the west Tasmanian coast, north of the oceanographic subtropical front, where relatively carbon rich siliciclastic sediments have filled the graben basin between two basement highs (mbsf25 km length) since the Late Eocene until Early Oligocene and continental slope sedimentation of calcium carbonate rich sediments thereafter (Exon, 2001; Chapter 3). A detailed description of the site location, depositional setting and oceanographic setting has been given in Chapter 3. For the age model, we updated ages of tie points interpolated (cf. Stickley et al., 2004; updated to GTS2012 ages (Gradstein et al., 2012) in Chapter 3) with the exemption of one last occurrence datum of foraminifera *Subbotina angiporoides*. We interpolated a loess smooth (span of 0.1) through age tie points to obtain the ages of our samples (Supplementary Figure 1).

2.2 TEX₈₆ paleothermometry

In order to reconstruct sea surface temperature (SST), we applied the TEX₈₆ (TetraEther indeX of 86 carbon atoms) proxy (Schouten et al., 2002), which is based on the temperature-dependent cyclisation of isoprenoidal glycerol dialkyl glycerol tetraethers (GDGTs) produced by thaumarchaeotal membrane lipids. A total of 123 samples spanning the period between 35 and 20 Ma (766-339 mbsf) were processed for analysis of GDGTs (Supplementary Methods; Supplementary Table 2). GDGTs were extracted from powdered and freeze-dried sediments using a Milestone Ethos X microwave or accelerated solvent extractor system. Lipid extracts were separated into an apolar, ketone and polar fraction by Silica gel column chromatography. GDGT standard was added to the polar fraction and filtered over a 0.45 µm polytetrafluoroethylene filter. The dissolved polar fractions were injected and analysed by high-performance liquid chromatography-mass spectrometry (HPLC-MS) at Utrecht University, using double-column separation (Hopmans et al., 2016). GDGT peaks in the HPLC chromatograms were integrated using ChemStation software. A more detailed description can be found in the Supplementary Methods.

TEX₈₆ was calculated as defined by Schouten et al. (2002):

$$\text{TEX}_{86} = (\text{GDGT-2} + \text{GDGT-3} + \text{Cren}') / (\text{GDGT-1} + \text{GDGT-2} + \text{GDGT-3} + \text{Cren}')$$

TEX₈₆ results were examined for non-thermal overprints (described in detail in Supplementary Methods) to verify the reliability of their SST signal (Supplementary Table 2; Supplementary Figure 2-6) and compared to an alkenone-derived (U^k₃₇) SST record from the same site (Gutián and Stoll, 2021; Supplementary Figure 7). For systematic calculation of GDGT ratios, data analysis, visualization, and evaluation of isoGDGT, brGDGT and/or brGMGT data, we utilized the R script of Bijl et al. (2021): <https://github.com/bijlpeter83/RGDGT.git>. We uploaded the measured peak areas (Supplementary Table 2) of GDGTs in the R script and calculated and plotted fractional abundances, overprinting indices and paleotemperature time series (Supplementary Figures 2-4).

In order to translate the TEX₈₆ values into SSTs, we used the regionally varying, Bayesian calibration; BAYSPAR SST (prior mean of 30°C, prior standard deviation of 20) of Tierney and Tingley (2015) (Supplementary Figure 5). The BAYSPAR method compares measured TEX₈₆ values with similar values in the modern SST observations, obtained from surface sediment samples, to

derive linear regression parameters: BAYSPAR propagates uncertainties in the surface sediment data into resulting temperature predictions (Tierney and Tingley, 2015). SST estimates obtained with the exponential transfer function BAYSPAR are very similar to the TEX_{86} -based SSTs produced by the exponential function from Kim et al. (2010) and linear function by O'Brien et al. (2017) (Supplementary Figure 6), varying, at most, by 2°C.

2.3 Temperature data compilation

We compiled existing Oligocene TEX_{86} data and applied the BAYSPAR SST calibration (Tierney and Tingley, 2015) for consistency, from east of Tasmania: ODP Site 1172 (Bijl et al., 2021), north of the Ross Sea: DSDP Site 274 (Chapter 2), offshore Wilkes Land: IODP Site U1356 (Hartman et al., 2018) and DSDP Site 269 (Evangelinos et al., 2020). The age model for the terrestrial temperature records from the Ross Sea: Cape Roberts Project (CRP) (Passchier et al., 2013) based on Lavelle (1998), McIntosh (1998), and Florindo et al. (2005), was converted to GTS2012 ages (Gradstein et al., 2012) for the purpose of this paper.

2.4 Fully coupled climate model

For model-data intercomparisons, we utilized a suite of general circulation model (GCM) HadCM3BL-M2.1aE model experiments, with full atmospheric coupling, compiled by the Bridge Consortium of the University of Bristol (found at <http://www.bridge.bris.ac.uk/resources/simulations>; Kennedy-Asser et al. 2019). Simulations that were selected for comparison (Figure 3b) were built using boundary conditions, developed by Getech Group plc, appropriate for Rupelian and Chattian-age paleogeographies with either a closed or open Drake Passage, using varying ice sheet constructions (either no ice sheet, East Antarctic Ice Sheet only, or full Antarctic Ice Sheet), and varying $p\text{CO}_2$ concentrations (either 560 or 1120 ppm) (Supplementary Table 3).

2.5 High resolution eddy resolving ocean model

The presented high-resolution ocean simulations (Figure 3C) are taken from Sauermilch, et al. (2021). It uses the Massachusetts Institute of Technology ocean general circulation model (MITgcm; Marshall et al., 1997) with a circum-Antarctic model domain (from 84°S to 25°S). The spatial resolution is 0.25° (3-25 km resolution) and vertical resolution contains 50 layers (ranging from 10 m at the sea surface to 368 m at the sea floor). Southern Ocean paleogeography is reconstructed to the Late Eocene (38 Ma) position using the plate tectonic model of Matthews et al. (2016) in a paleomagnetic reference frame (van Hinsbergen et al., 2015).

The model is ocean-only and atmospheric forcing are taken from a coupled atmosphere-ocean simulation (GFDL CM2.1) run with atmospheric $p\text{CO}_2$ concentration of 800 ppm (Hutchinson et al., 2018). A restoring time scale of 10 days is applied. Although not directly coupled to the atmosphere or ice sheet, the resolution of the ocean model is higher than most previous paleosimulations and permits the formation of ocean eddies which are responsible for the majority of the ocean heat transport (Viebahn et al., 2016). The high-resolution model is less diffusive, allowing accurate simulation of subsurface velocities and current structure. In addition, detailed paleobathymetry features such as the seafloor roughness, but also small depth changes in the critical gateway regions, Tasman Gateway and Drake Passage, can be accurately resolved. To accommodate this advantage, new high-resolution paleobathymetry grids are used (Hochmuth et al., 2020) which are able to reconstruct detailed seafloor roughness features, such as seamounts and fracture zones, that have a substantial impact on the large-scale ocean circulation (e.g., Lacasce et al., 2019). See

Sauermilch et al. (2021) for further details about the methodology of the high-resolution ocean model and paleobathymetry reconstruction.

3 Results

Our SST record is based on 123 samples from ODP Site 1168 which were processed for TEX_{86} paleothermometry. Twenty-one showed potential for non-thermal overprints, thereby considered unreliable, and discarded from the dataset (see Supplementary information). Results indicate Late Eocene-Early Miocene (35-20 Ma; red line Figure 2b; Supplementary Table 2) SSTs of 20-29°C ($\pm 4^\circ\text{C}$ standard error). The amplitude of SST variability was high (5-7°C) around 28 Ma and from 25 Ma onwards, and low ($\sim 3^\circ\text{C}$) between 32-29 Ma and 27-25 Ma. Our record indicates 4°C cooling (from 27 to 23°C) across the Eocene-Oligocene transition (ca. 34 Ma) and then a return to high temperatures, $\sim 29^\circ\text{C}$, at 33.2 Ma. Temperatures then gradually cooled until ~ 28 Ma. A transient warming of 6°C occurred from 27.8-24.3 Ma, followed by a gradual cooling from 24.3-22.2 Ma. The TEX_{86} -based SSTs are generally warm and in line with U^{k}_{37} -based SSTs of 19°C to 29°C derived from the same records for the 29.8-16.7 Ma interval (Gutián and Stoll, 2021) (Supplementary Figure 7). The U^{k}_{37} -based SST record shows a more prominent Late Oligocene warming, although U^{k}_{37} -based SSTs remains within the variability of the TEX_{86} -based SST record. Further support for the warm-temperate SSTs comes from dinoflagellate cyst (dinocyst) assemblages analyzed on the same samples, which suggest stable, open marine and warm-temperate conditions (Chapter 3).

4 Discussion

4.1 Temperature gradient across the Australian-Antarctic Gulf

We focus the discussion on the SST gradient across the Australian-Antarctic Gulf (AAG), between Sites 1168 and U1356 in the proxy data compilation (arrows, Figure 2), due to their high temporal resolution, while Sites 1172, 277, 274 and 269 will offer a broader regional context. We note a persistent SST gradient (5-10°C) between the Antarctic-proximal (Site U1356) and the subtropical (Site 1168) sites, albeit smaller than at present-day ($\sim 14^\circ\text{C}$) (Olbers et al., 2004). Still, this implies that (polar) frontal systems separated water masses latitudinally already in the Oligocene AAG. The Early Oligocene latitudinal separation of water masses is further corroborated by the strong latitudinal separation in dinocyst assemblages from ~ 30 Ma onwards between the relatively oligotrophic Australian Site 1172 (Houben et al., 2019) and Site 1168 (Chapter 3) and the eutrophic, upwelling proximal Antarctic Site U1356 (Bijl et al., 2018), Site 269 (Evangelinos et al., 2020) and 274 (Chapter 2) margins of the AAG.

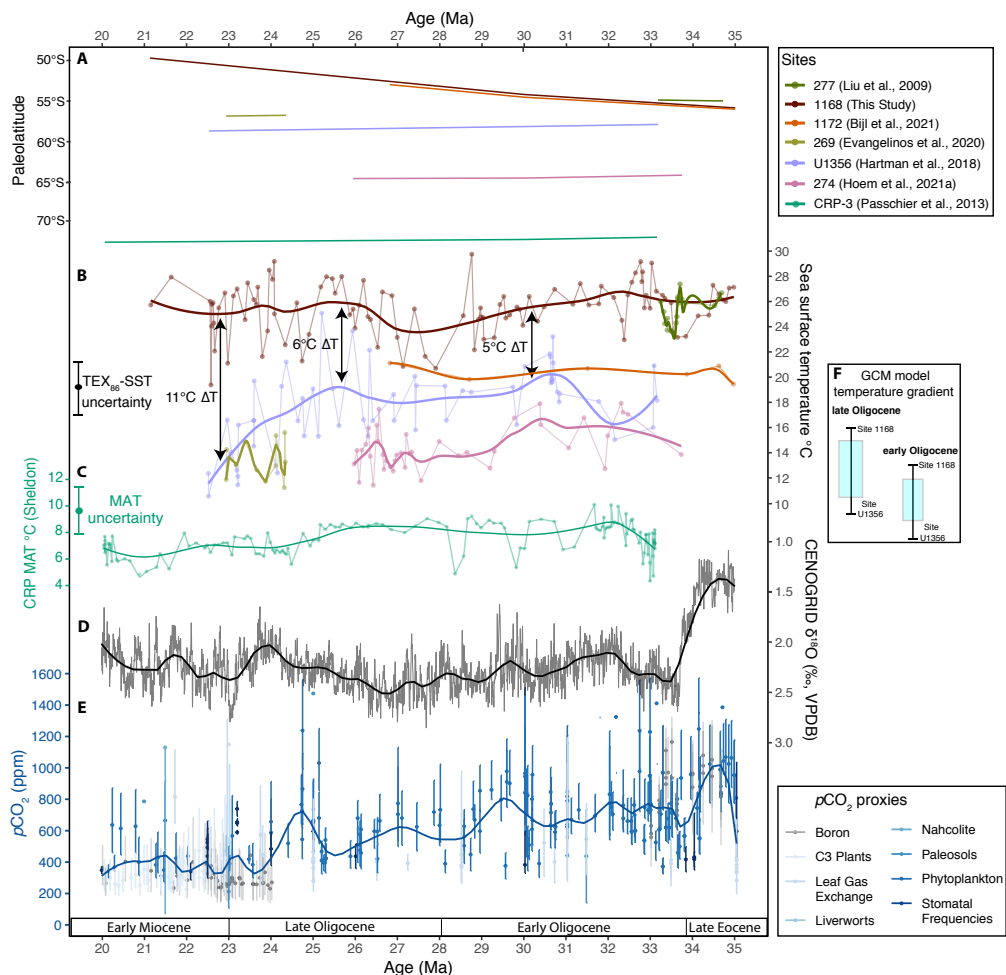


Figure 2. Late Eocene-Early Miocene Australian-Antarctic Gulf temperature records, with their paleolatitude, compared with global benthic $\delta^{18}\text{O}$ and $p\text{CO}_2$ records and GCM models. A) Paleolatitude evolution of sites (van Hinsbergen et al., 2015). Colors refer to sites in Figure 1. B) TEX₃₆-SST reconstructions. Thick lines represent smoothed long-term trends, with a local weighted polynomial regression (LOESS; span of 0.35). For the age model of Site 1168 see Supplementary Table 2. C) Mean annual air temperature (MAT) from Site CRP-3 (Passchier et al., 2013). All ages in A-C are converted to GTS2012 (Gradstein et al., 2012). D) Benthic foraminiferal $\delta^{18}\text{O}$, smoothed by a locally weighted function over 20 kyr (thin black curve; CENOGRID (Westerhold et al., 2020)). Thick black curve is the LOESS smoothed (span = 0.1). E) paleo-CO₂ compilation from <https://www.paleo-co2.org> (Hoenisch, 2021). Blue curve is the LOESS smoothed (span = 0.1). F) Shows the GCM model temperature gradient (corresponding to the scale in B) between Site 1168 and Site U1356 in the Early- and Late Oligocene.

The reconstructed SST gradient is in line with the output of two Oligocene GCM simulations (Figure 3), albeit absolute SSTs are in general lower throughout the region in the model simulations (10–20°C; Figure 2, Figure 3F) than in the TEX_{86} -based SST records (15–29°C). This could be the result of a warm bias in the TEX_{86} proxy (e.g., Hartman, et al., 2018), as suggested by the slightly cooler U^k_{37} -based SSTs (Gutián and Stoll, 2021; Supplementary Figure 7) and/or to too low climate sensitivity in the GCMs. The two different ice sheet sizes in the Early- and Late Oligocene simulations can be used to evaluate the effects of the glacial-interglacial variability in ice sheet size as well as the effect of long-term changes in geographic boundary conditions on the simulated latitudinal SST gradient. Interestingly, while the Site U1356 proxy data do show strong SST variability over glacial-interglacial cycles, two different ice sheet sizes in the Early- and Late Oligocene GCM simulations is of little ($\sim 1^\circ\text{C}$) impact to the simulated latitudinal SST gradient (Figure 3B). We also note that the difference in amplitude of glacial-interglacial SST change between offshore Australia and Antarctica is too large to be caused only by greenhouse gas induced radiative forcing with a factor of polar amplification. Therefore, we ascribe the high amplitude temperature signal to migrating ocean frontal systems. The small effect of the northward tectonic drift of Site 1168 on regional SSTs, indicates that the subtropical front (STF) likely migrated northward along with the Australian landmass, as has been suggested from microfossil data (Chapter 3). This effect is further muted at Site 1168, because Australia is hindering northward migration of the STF, which explains the smaller temperature swings offshore Australia on orbital timescales.

4.2 Late Oligocene paleogeographic, ocean temperature, atmospheric $p\text{CO}_2$ and ice volume changes.

In the Late Oligocene we note the substantially increasing temperature gradient across the AAG latitudinal transect from 6°C prior to 26 Ma to $>10^\circ\text{C}$ by 23 Ma (Figure 2). This is mostly due to unidirectional progressive cooling of the Antarctic-proximal SST record at Site U1356 and stepwise air temperature cooling at CRP (Passchier et al., 2013) starting at around 26 Ma, opposite to stable SSTs at Site 1168 and the benthic foraminiferal $\delta^{18}\text{O}$ record showing Late Oligocene warming and ice mass loss. The Antarctic-proximal cooling continues into the Miocene, where the $\delta^{18}\text{O}$ record also show deep ocean cooling. Meanwhile the subtropical SSTs at Site 1168 show a Late Oligocene warming coincident with trends in $\delta^{18}\text{O}$ record (Figure 2D). The slightly cooler Late Oligocene SSTs at Site 269, northeast of Site U1356, have been attributed to its proximal location to upwelling (Evangelinos et al., 2020), while the cooler SSTs at Site 274 is attributed to its higher latitude and proximity to the colder Ross Sea (Chapter 2), as also inferred from the air temperature record at CRP (Passchier et al., 2013) (Figure 2C). We break down the complex interplay of forcings and feedbacks that kept the Early Oligocene Southern Ocean warm and caused cooling of the Wilkes Land Antarctic Margin at 26 Ma – changes in atmospheric $p\text{CO}_2$ levels, ice volume or paleogeography (Table 1).

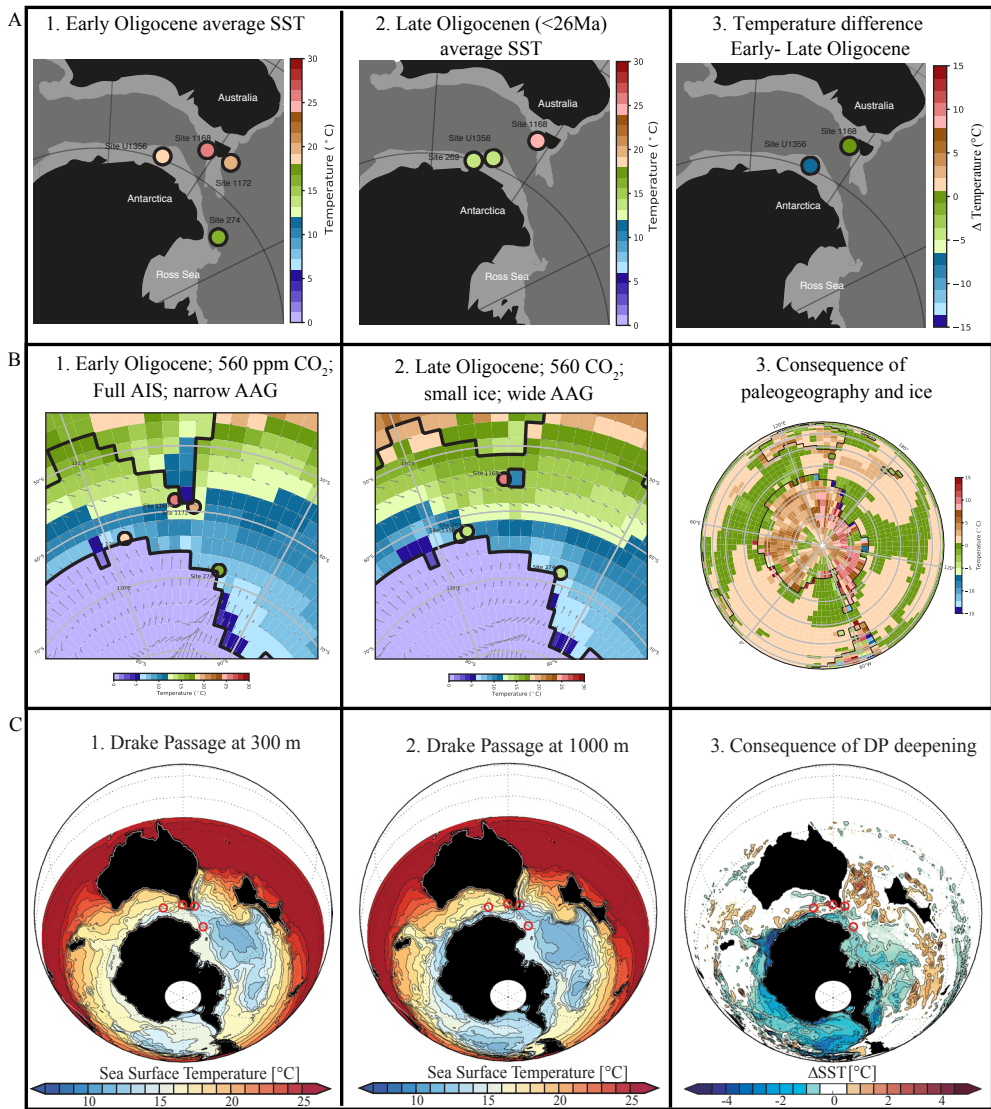


Figure 3. Data-model experiment comparisons. A. Paleogeographic map with SST data shown in colored dots from the respective drill sites. B. Fully coupled HadCM3L simulation of the Early-(33.9-28.4 Ma) and Late Oligocene (28.4-23.0 Ma) (Kennedy-Asser et al., 2019). C. High resolution ocean model (Sauermlch et al., 2021). The Southern Ocean paleogeography is reconstructed for Late Eocene (38 Ma), red circles indicate the studied sites.

Table 1. Scenarios to explain Late Oligocene trends in SST and deep sea $\delta^{18}\text{O}$

Scenario	Antarctic proximal SST	Subtropical SST	Deep ocean $\delta^{18}\text{O}$	Evaluation
<i>Late Oligocene proxy data results</i>	<i>Cooling</i>	<i>Stable</i>	<i>Decreasing</i>	<i>Target</i>
1. $p\text{CO}_2$ decrease	Cooling	Cooling	Increasing	Failure
2. Antarctic Ice Sheet expansion	Cooling	Stable/slight cooling	Increasing	Failure
3. Deepening of oceanic gateways and Antarctic ice loss	Cooling	Stable	Decreasing	Success

Indeed, Late Oligocene atmospheric $p\text{CO}_2$ does gradually decline (700-300 ppm (Hoenisch, 2021); Figure 2E). However, the contrasting paleotemperature trends, with Antarctic-proximal SSTs cooling, subtropics remaining warm and equatorial areas warming, question the role of $p\text{CO}_2$ as primary driver of Late Oligocene Southern Ocean temperature trends. In community earth system model simulations by Goldner, et al. (2014), the expansion of Antarctic ice sheets generates cooling of 6°C at the Antarctic margin, while in atmosphere-ocean GCM model simulations by Knorr and Lohmann (Knorr and Lohmann, 2014) an expanded ice sheet would cause regional warming at the Antarctic margin (Supplementary Table 1). Nonetheless, an expanding Late Oligocene ice volume is unlikely given the decreasing benthic $\delta^{18}\text{O}$ indicating loss of Antarctic ice volume with deep-sea warming (Lear et al., 2004; Westerhold et al., 2020), which has been ascribed to local tectonism on Antarctica (Singh et al., 2016; Paxman et al., 2019). Moreover, the Early- and Late Oligocene GCM model results showed little effect of ice volume changes on the Southern Ocean SST gradient (Figure 3B). The Late Oligocene breakdown of the relationship between SST, deep ocean temperature, atmospheric $p\text{CO}_2$ and ice volume (O'Brien et al., 2020) suggests that Antarctic proximal SST cooling was not limited to $p\text{CO}_2$ changes or glaciation-induced negative feedback (Goldner et al., 2014), but probably also affected by paleogeographic configurations.

4.3 Tectonic deepening of Drake Passage caused cooling along Antarctic Margin

Low resolution coupled climate models had suggested that opening of Southern Ocean gateways had little effect on poleward ocean heat transport and polar climate (Huber et al., 2004; Goldner et al., 2014). However, recently, the importance of high-resolution ocean model simulations in such experiments has been underlined (Kennedy et al., 2015; England et al., 2017). Eddy-permitting model simulations (Sauermlch et al., 2021) show that deepening of the second of two Southern Ocean gateways (Drake Passage and Tasmanian Gateway) below 300 m drives surface water cooling at the Antarctic margin (up to 5°C), while leaving the rest of the Southern Ocean with little relative temperature changes (Figure 3C). At 26 Ma, this is exactly what can be seen in the SST compilation: The SST at the STF remains relatively stable despite northward migration and the Antarctic proximal Site U1356 show profound cooling (Figure 2), while the benthic $\delta^{18}\text{O}$ records shows apparent global warming/ice loss. The gradual northward migration of Australia could have progressively invited a larger volume of east flowing STF water to follow the southward route around Australia (Hill et al., 2013), without changing the absolute temperature in the STF region. This southward route would also progressively line up better with the westerly wind belt, strengthening the proto-Antarctic Circumpolar Current (Scher et al., 2015; Nicholson and Stow, 2019). A strengthened proto-Antarctic Circumpolar Current would deflect the warm poleward extension of the subpolar gyres, including the proto-Leeuwin Current away from Antarctica, and reduce heat transport towards Wilkes Land Antarctic Margin, increasing polar isolation

(Sauermilch et al., 2021). Crucially, the timing of this observed gradient increase coincides with evidence from kinematic reconstructions of Drake Passage (van de Lagemaat et al., 2021) showing a first deep ocean connection around 26 Ma. Also, sediments from the South Pacific indicate the formation of the proto-Antarctic Circumpolar Current in the Late Oligocene (ca. 25-23 Ma; Lyle et al., 2007). Thus, we deduce that despite proximity to the Tasmanian Gateway, the deep opening of Drake Passage in the Late Oligocene induced strong increase in the Southern Ocean SST gradient and cooling of Antarctic surface waters, also in the Tasmanian Gateway area. Although radiative forcing (CO_2 , orbital variations) is (likely) the primary driver of the Cenozoic climatic evolution (e.g., Cramwinckel et al., 2018; Hutchinson et al., 2021), we here demonstrate the fundamental role paleogeography plays on Southern Ocean and Antarctic climate.

5 Conclusions

Our TEX_{86} -based SST record from the Oligocene Tasmanian Margin (ODP Site 1168), representing the SST evolution of the STF, in comparison with the benthic foraminiferal $\delta^{18}\text{O}$ compilation, $p\text{CO}_2$ estimates, regional SST records, and model simulations, show the following:

- The latitudinal SST gradient across the widening AAG was $\sim 6\text{-}8^\circ\text{C}$ in the Late Eocene-Early Oligocene, and increasing from 26 Ma, when Antarctic proximal cooling started.
- The latitudinal SST gradient is larger during glacial than interglacial intervals. This is a result of latitudinal migrations of ocean frontal systems, which are limited at the northern boundary of the Southern Ocean by the position of Australia.
- Long term trends in Antarctic ice volume and polar amplification due to decreasing $p\text{CO}_2$ cannot alone explain the Antarctic proximal cooling starting at 26 Ma. We correlate this cooling to the first deep opening of Drake Passage, which decreased the strength of subpolar ocean gyres and southward heat transport, enhancing Antarctic thermal isolation and circumpolar flow.

Acknowledgments

This work used archived samples and data provided and curated by the IODP and its predecessors. This work was financially supported by the NWO polar programme (ALW.2016.001). We thank José Guitián, Heather Stoll and Lena Thöle for providing the subset of samples from ETH Zürich and Mariska Hoorweg for technical support. IS and PB acknowledges funding through ERC starting grant 802835 “OceaNice”. MH acknowledges support from NSF OPP grant 1842059.

Supplementary Information Chapter 4

Lipid Extraction and GDGT Analysis

Sample processing involved extraction of 10 g freeze-dried and manually powdered sediments using a Milestone Ethos X microwave system and adding dichloromethane:methanol (DCM:MeOH) 9:1 v/v. The total lipid extract (TLE) were first filtered through a NaSO₄ column to discard potential remaining water and sediments. The N₂-dried TLE were then separated on an activated Al₂O₃ column into apolar, ketone and polar fractions, using hexane:dichloromethane (DCM) (9:1, v/v), DCM (1:1 v/v), and DCM: MeOH (1:1, v:v) as eluents, respectively. A subset of 26 samples was processed at the Swiss Federal Institute of Technology (ETH) in Zürich, Switzerland, where lipids were extracted from 30g of freeze-dried and manually powdered sediments by an accelerated solvent extractor (ASE 200, Dionex) with dichloromethane:methanol (DCM:MeOH) 9:1 (v/v). The TLE was saponified with ~2 ml of a 0.5M KOH in 95:5 MeOH:H₂O. The neutral fraction was obtained by adding 0.5 ml of hexane to the sample, shaking and pipetting out the saponified fraction three times. Silica gel column chromatography was thereafter applied by eluting 4 ml of Hexane, 4 ml of DCM and 4 ml of MeOH for separation of the neutral fraction into a hydrocarbon fraction, a ketone fraction and a polar fraction respectively. The polar fractions were sent to Utrecht University for further analysis. All polar fractions were dried under N₂. GDGT standard was added to the polar fraction, which was subsequently dissolved in hexane:isopropanol (99:1, v/v) to a concentration of ~2 mg ml⁻¹ and filtered through a 0.45 µm polytetrafluorethylene filter. After that, the dissolved polar fractions were injected and analyzed by ultra-high performance liquid chromatography/mass spectrometry (UHPLC/MS) according to the method described by Hopmans et al. (2016), using an Agilent 1260 Infinity UHPLC system coupled to an Agilent 6130 single quadrupole mass detector, at Utrecht University. Selected ion monitoring (SIM) was used to identify the GDGTs using their [M+H]⁺ ions and integrated using ChemStation software.

GDGT indices for non-thermal overprints on TEX₈₆

The use of TEX₈₆ as a proxy for SST relies upon the assumption that isoprenoidal GDGTs in marine sediments are principally derived from membrane lipids of marine pelagic Thaumarchaeota (Schouten et al., 2013). However, several non-thermal factors may alter the distribution of isoprenoidal GDGTs stored in the sediment and thus the temperature signal. We use the following GDGT-based ratios and indices to assess potential non-thermal effects on the GDGT distributions:

1. The relative contribution of soil organic matter to marine sediments can be reconstructed using the branched and isoprenoid tetraether (BIT) index (Hopmans et al., 2004), which evaluates the proportion of branched GDGTs, thought to be primarily produced by soil bacteria (Weijers et al., 2006) opposed to that of crenarchaeol, an isoprenoid GDGT that is solely produced by Thaumarchaeota (Sinninghe Damstè et al., 2002). Since isoprenoidal GDGT also occur in soils, large contributions of soil-derived isoGDGTs to marine sediments may alter the TEX₈₆ (Weijers et al., 2006).

$$\text{'BIT'} = (\text{IIIa} + \text{IIIa}' + \text{IIa} + \text{IIa}' + \text{Ia}) / (\text{Cren} + \text{IIIa} + \text{IIIa}' + \text{IIa} + \text{IIa}' + \text{Ia})$$

In the Site 1168 TEX₈₆ record, 27 samples have BIT index values >0.4, suggesting that they might be biased by soil- and river-derived GDGTs (Weijers et al., 2006; Bijl et al., 2013)(Supplementary

Figure 3b). However, we note that the validity of this index as a proxy for soil organic matter input has been questioned now that it has become evident that branched GDGTs are also produced in the marine realm (Peterse et al., 2009; Sinninghe Damsté, 2016). Additionally, the offshore depositional setting of the drill site (Chapter 3), makes a large contribution of terrestrial GDGTs to the site unlikely. Therefore, in line with other studies in similar palaeosettings (Leutert et al., 2020; Bijl et al., 2021) we do not use BIT index to exclude samples that show normal isoGDGT distributions. This retains 6 samples from the 27 that have high BIT index.

2. The f_{Cren} index evaluate variations in the relative abundance of the crenarchaeol regio-isomer.

$$f_{\text{Cren}} = (\% \text{Cren}') / (\% \text{Cren}' + \% \text{Cren})$$

The index is used to detect 'anomalous' versus 'warm' GDGT distributions, compared to values observed in the modern core-top dataset, which indicates non-thermal contributions, potentially water depth, of the crenarchaeol isomer (O'Brien et al., 2017). The index has a cutoff value at above 0.25, which only applied to one sample at Site 1168 (Supplementary Figure 3c).

3. The methane index (MI) detects isoprenoidal GDGT contributions from methanotrophic Euryarchaeota (Zhang et al., 2011).

$$\text{Methane Index (MI)} = (\text{GDGT-1} + \text{GDGT-2} + \text{GDGT-3}) / (\text{GDGT-1} + \text{GDGT-2} + \text{GDGT-3} + \text{Cren} + \text{Cren}')$$

MI values >0.3 conservatively reflect hydrate-impacted sediments and suggest that GDGT distribution might be affected by methanogenic archaea (Supplementary Figure 3d). In our record, 14 samples had MI values above 0.3.

4. Anaerobic oxidation of methane (AOM) is characterized by GDGT2/Cren ratio values above 0.2 (Weijers et al., 2011). AOM ratio values for Site 1168 sediments suggest an overprint from anaerobic methane oxidizers in 11 samples (Supplementary Figure 3e).
5. The GDGT-2/GDGT-3 ratio (Taylor et al., 2013) signals possible overprints by archaeal communities dwelling deeper in the water column. We use a conservative cut-off value of >5 , which was exceeded by 6 samples for which we assume that a deepwater contribution has altered the TEX_{86} (Supplementary Figure 3f).
6. The Methanogenesis index, measured by the GDGT-0/Crenarchaeol ratio (Blaga et al., 2009; Sinninghe Damsté et al., 2009; Taylor et al., 2013) is targeted to detect contributions of isoGDGTs (GDGT-0) from methanogens. Two samples with GDGT-0/Crenarchaeol ratio >2 were flagged as outliers for potential contribution by methanogenic archaea (Supplementary Figure 3g).

7. The Δ Ring Index (Δ RI) can detect deviations from a non-thermal character in the GDGT composition (Zhang et al., 2016).

$$\text{'RING'} = 0 \times [\text{GDGT} - 0] + 1 \times [\text{GDGT} - 1] + 2 \times [\text{GDGT} - 2] + 3 \times [\text{GDGT} - 3] + 4 \times [\text{cren}] + 4 \times [\text{cren}']$$

$$\text{'RITEX'} = (-0.77 \times \text{TEX}_{86}) + (3.32 \times \text{TEX}_{86}^2) + 1.59$$

$$\text{'\Delta RI'} = \text{RITEX} - \text{RING}$$

Δ RI values > 0.3 are thought to represent samples for which GDGT distributions diverge outside that of the modern TEX_{86} -RI relationship, based on the 95% confidence interval of the modern regression (Supplementary Figure 4). Higher values indicate that the sample distribution may reflect an archaeal community distinct from the modern production of GDGTs (Zhang et al., 2016). In total, 10 samples had a Δ RI higher than the cut off value of 0.3 (Supplementary Figure 3h, 95% confidence interval; Supplementary Figure 4) indicating a potential non-thermal overprint on the GDGT distribution.

Supplementary Figures

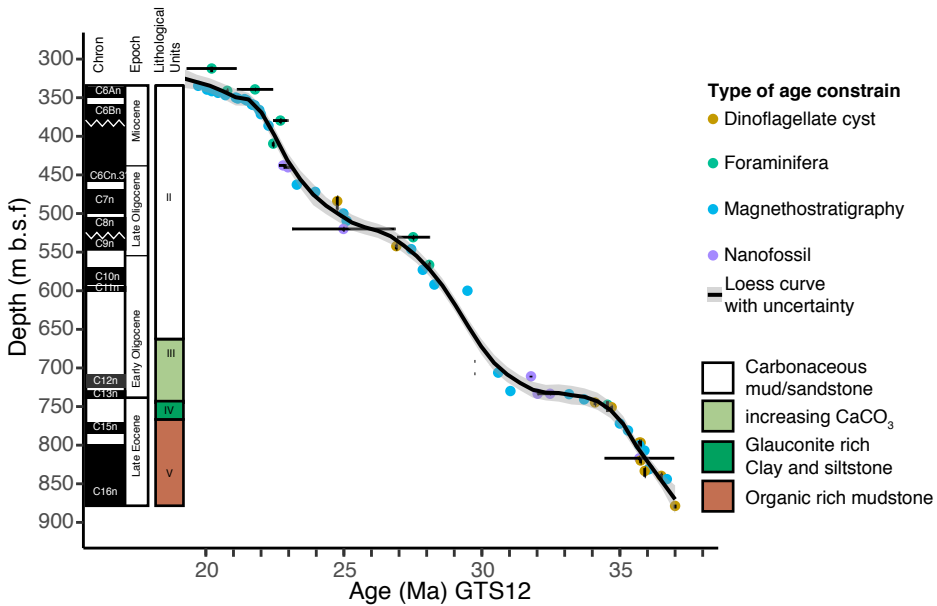
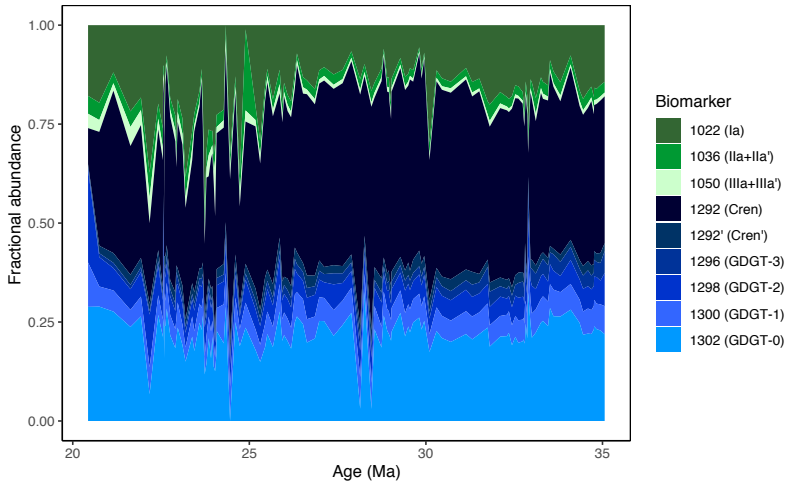
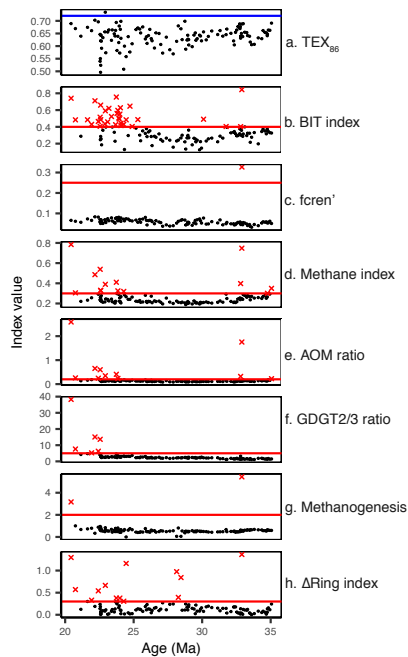


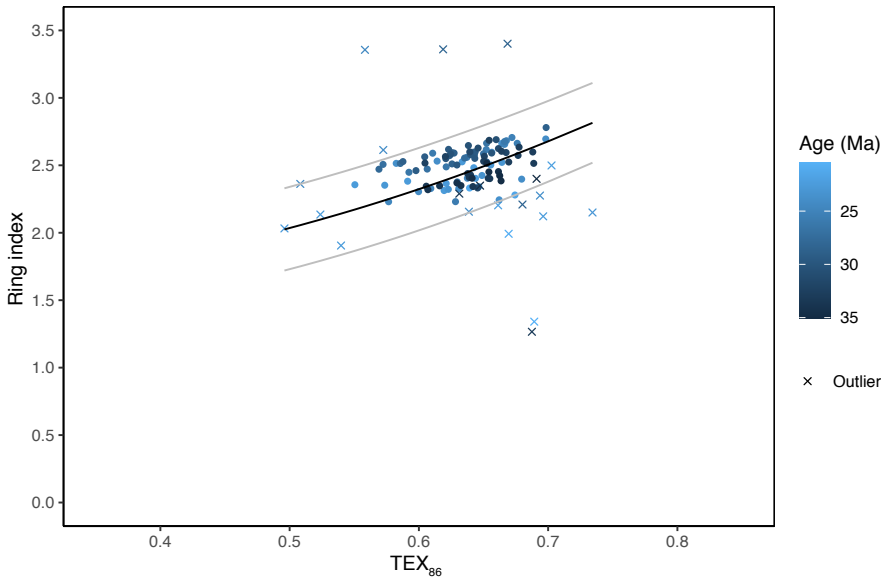
Figure 1 Age-depth model of ODP Site 1168. The age-model is based on magneto- and biostratigraphy (calcareous nanofossils, planktic foraminifera, diatoms and dinocysts) after Stickley et al. (2004b), recalibrated to GTS2012 of Gradstein et al. (2012), after Chapter 3. A smoothed line is drawn through the age constraints using the loess smoothing method with a span of 0.1. Lithological units are indicated to the right of the palaeomagnetic chrons and the indication of epochs (Exon et al., 2001b). The arrows indicate the sedimentation rate.



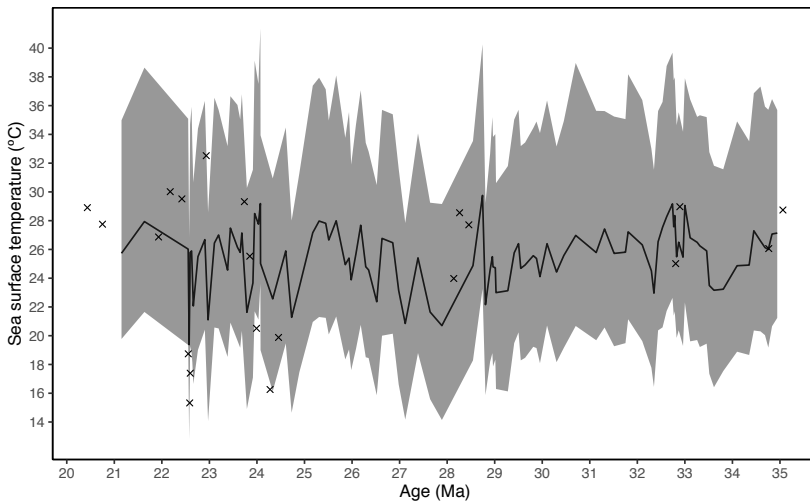
Supplementary Figure 2 The fractional Glycerol Dialkyl Glycerol Tetraether (GDGT) abundances. The stacked fractional abundance of individual isoprenoidal GDGTs in blue (GDGT-0, GDGT-1, GDGT-2, GDGT-3, Crenarchaeol (Cren) and the Crenarchaeol stereoisomer (Cren')) and branched GDGTs in green (GDGT-I, GDGT-II, GDGT-III).



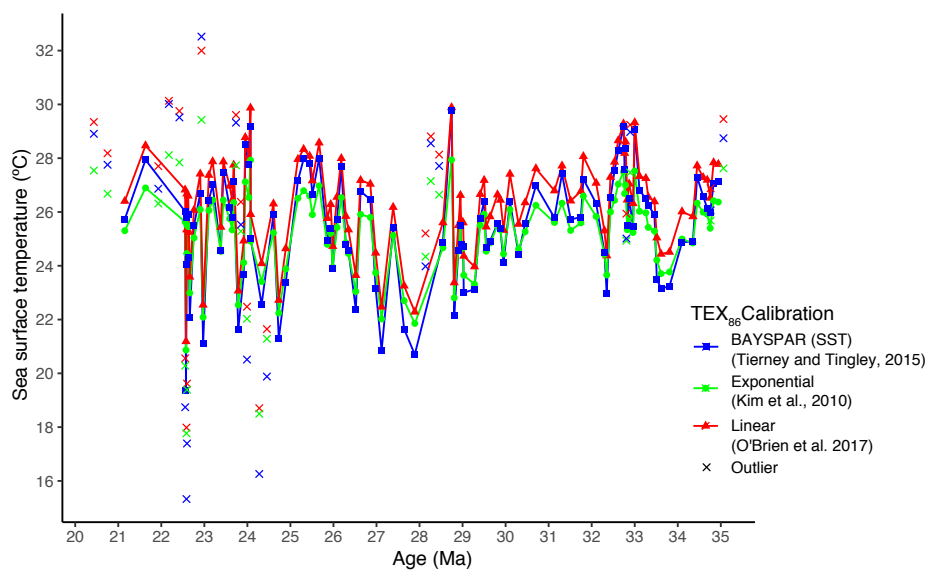
Supplementary Figure 3 TEX_{86} values and overprinting indices. Red lines indicate the cut-off values used for each of the indices, red crosses indicate samples marked with outlying values to the respective index. a. TEX_{86} (Schouten et al., 2002), with blue line indicating the maximum modern core-top value (~ 0.72). b. BIT index (Hopmans et al., 2004). c. $fcren'$ (O'Brien et al., 2017). d. Methane index (Zhang et al., 2011). e. AOM ratio (Weijers et al., 2011). f. GDGT-2/3 ratio (Taylor et al., 2013). g. Methanogenesis (Blaga et al., 2009), h. $\Delta Ring$ index (Zhang et al., 2016).



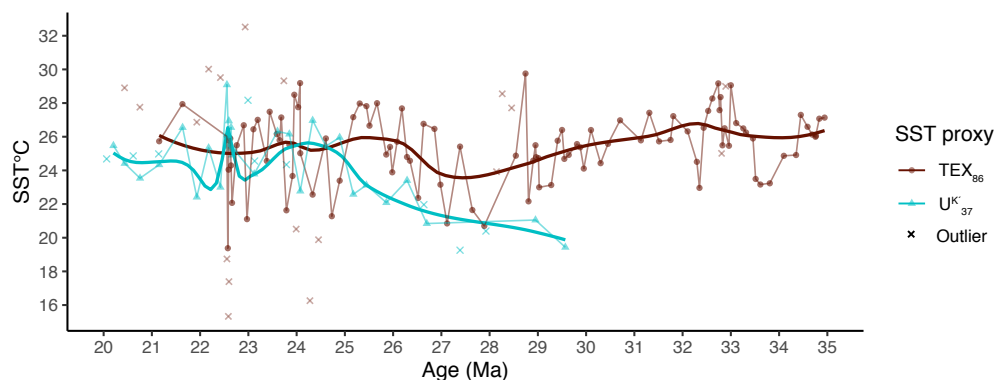
Supplementary Figure 4 Δ Ring Index are plotted relative to TEX₈₆. Black and grey lines represent the RI/TEX₈₆ relationship of modern core top samples, and the 95% confidence interval, respectively. Filled circles indicate RI/TEX₈₆ values for samples that are retained; crosses indicate samples that are discarded (Supplementary Figure 3). Color of all data points indicates age of the sample, from Late Eocene (dark blue) to Early Miocene (light blue).



Supplementary Figure 5 BAYSPAR calibrated SST. The Site 1168 SST record based on the BAYSPAR calibration (Tierney and Tingley, 2015) with 90% confidence interval in grey envelope. X=overprinted samples.



Supplementary Figure 6 Comparison of sea surface temperature calibrations. for the GDGT-based SST records for the different calibrations at ODP Site 1168: blue line = BAYSPAR SST (Tierney and Tingley, 2015), green line = exponential TEX_{86} calibration (Kim et al., 2010) and red line = linear TEX_{86} calibration (O'Brien et al. 2017). X = samples with overprinted GDGT distribution (see Supplementary Figure 3, Supplementary Figure 4).



Supplementary Figure 7 Comparison of sea surface temperature (SST) proxies from ODP Site 1168. Alkenone-derived (U^k_{37}) SST record in blue (Gutián and Stoll, 2021) and TEX_{86} -SST results (this study) in red. X = samples with overprinted GDGT distribution.

Supplementary Tables

Supplementary Table 1: Model comparison

Model simulation	Knorr and Lohmann, 2014	Goldner et al., 2014	Kennedy et al., 2015, Eocene	GCM model in this paper
Model type	Atmosphere-ocean GCM (AOGCM)	Community Earth System Modelling (CESM)	Fully coupled GCM (HadCM3L)	Fully coupled GCM (HadCM3L)
Ocean configuration	Three-dimensional ocean	Slab ocean		
Boundary conditions	Middle Miocene	EOT	Eocene	Oligocene
Oceanic gateway configuration	Open	Closed Tasmanian Gateway	Constricted Tasmanian Gateway	Open
CO ₂ (ppm)	400-500	1,120-560	280-560	560
Ice sheet expansion ocean reaction (SST Δ_{glac})	Warming (up to 6°C in the Atlantic-Indian sector)	Cooling (-6°C) (Matching our proxy SST data)	Warming in pacific, cooling in Indian: (More zonal ocean circulation owing to Antarctic glaciation and gateway opening causes increased heat transport)	Little SSST response (~1°C)

Supplementary Table 2: Glycerol Dialkyl Glycerol Tetraether (GDGT) peak areas at ODP Site 1168. The table also contains the calculated values of the TEX₈₆, BIT index, Methane Index and Δ Ring Index, and the converted SSTs from the BAYSPAR calibration (Tierney and Tingley, 2015), linear TEX₈₆ calibration (O'Brien et al., 2017), exponential TEX₈₆ calibration (Kim et al., 2010). *Too large for the print version. Available to download from preprint online:

<https://doi.org/10.21203/rs.3.rs-1516446/v1>



Supplementary Table 3: Rupelian and Chattian-aged model cases, built and simulated in HadC3ML by the Bridge Consortium (<http://www.bridge.bris.ac.uk/resources/simulations>). AIS – Antarctic Ice Sheet; EAIS – East Antarctic Ice Sheet.

Age (Ma)	Stage	pCO ₂ (ppm)	AIS state	Drake Passage	Simulation
28.1-23.0	Chattian	1,120	No ice	Open	TDLUY
28.1-23.0	Chattian	1,120	EAIS	Open	TDLUX
28.1-23.0	Chattian	1,120	Full AIS	Open	TDZSE
28.1-23.0	Chattian	560	No ice	Open	TDLUU
28.1-23.0	Chattian	560	EAIS	Open	TDLUQ
28.1-23.0	Chattian	560	Full AIS	Open	TDWQF
33.9-28.1	Rupelian	1,120	No ice	Open	TDLUV
33.9-28.1	Rupelian	1,120	Full AIS	Open	TDLUW
33.9-28.1	Rupelian	560	No ice	Open	TDLUT
33.9-28.1	Rupelian	560	EAIS	Open	TDWQE
33.9-28.1	Rupelian	560	Full AIS	Open	TDLUP

Chapter 5

Late Cenozoic Sea Surface Temperature evolution of the South Atlantic Ocean

Frida S. Hoem¹, Adrián López-Quirós², Suzanna van de Lagemaat¹, Johan Etourneau³, Henk Brinkhuis^{1,3}, Francien Peterse¹, Francesca Sangiorgi¹, Peter K. Bijl¹

1. Department of Earth Science, Utrecht University, Utrecht, the Netherlands

2. Department of Geoscience, Aarhus University, Aarhus C, Denmark

3. Département de Géologie et Océanographie, Université Bordeaux, Pessac, France

4. Department of Ocean Systems research OCS, Royal Netherlands Institute for Sea Research (NIOZ), Texel, the Netherlands

Abstract

At present, a strong latitudinal sea surface temperature (SST) gradient of $\sim 16^{\circ}\text{C}$ exists across the Southern Ocean, maintained by the Antarctic Circumpolar Current (ACC) and a set of complex frontal systems. Together with the Antarctic ice masses, this system formed and forms one of the most important global climate regulators. Yet, the timing of the onset of the ACC-system, its evolution towards modern-day strength, and the consequences for e.g., the SST development around the Southern Atlantic Ocean are still uncertain. Here we present new TEX_{86} -biomarker based SST records from two sites east of Drake Passage (southern Scotia Sea, South Atlantic) to assist in better understanding of two critical time intervals of prominent climate transitions during the Cenozoic, the Late Eocene-Early Oligocene (ODP Site 696) and Middle-Late Miocene (IODP Site U1536) transitions. Our results overall show rather temperate conditions ($20\text{--}11^{\circ}\text{C}$) during the Late Eocene to Early Miocene interval, with a weaker latitudinal temperature gradient across the Atlantic sector of the Southern Ocean compared to present day. We ascribe the regional similarity in SSTs across the Late Eocene-Early Oligocene South Atlantic to a persistent, strong Subpolar gyre circulation, connecting all sites, which can only exist in absence of a strong throughflow through Drake Passage. Surprisingly, the southern South Atlantic records show comparable SSTs ($\sim 12\text{--}14^{\circ}\text{C}$) during both the earliest Oligocene glacial maximum (~ 32 Ma) and the Miocene Climate Optimum (~ 16.5 Ma). Apparently, maximum Oligocene Antarctic ice volume could coexist with warm ice-proximal surface ocean conditions, while at similar ocean temperatures, the Middle Miocene Antarctic ice sheet was strongly reduced. Southern South Atlantic SSTs cooled to $\sim 5^{\circ}\text{C}$ at the onset of the Middle Miocene Climate Transition (MMCT, 14 Ma), making it the coldest oceanic region around Antarctica (from where we have records) and the likely location for deep water formation. The already cold southern South Atlantic conditions at MMCT meant it experienced little cooling during the latter part of the Miocene, which contrasts the profound cooling due to northward expansion of the Southern Ocean frontal systems in the lower latitudes and other sectors of the Southern Ocean.

1 Introduction

Today, Southern Ocean surface flow is dominated by the strongest ocean surface current on Earth, the Antarctic Circumpolar Current (ACC). This wind-driven, eastward flowing surface current is associated with strong ($\sim 16^{\circ}\text{C}$) zonal gradients in oceanographic conditions and temperature (Locarnini et al., 2018). Questions remain about the timing and nature of the development of the ACC and concomitant evolution the complex Southern Ocean frontal systems. A primary prerequisite for the existence of a strong ACC is an unobstructed latitudinal band of (deep ocean) water (Orsi et al., 1995; Barker and Thomas, 2004; Toggweiler et al., 2006), which is largely determined by the tectonic evolution and opening of the Tasmanian Gateway as well as the Drake Passage (Huber et al., 2004).

The tectonic evolution of the Tasmanian Gateway is relatively well constrained; early southern opening of the Tasmanian Gateway started around 49–50 Ma (Huber et al., 2004, Stickley et al., 2004, Bijl et al., 2013) with a change in course of tectonic drift of Australia from the Northeast to the North. Final breakup between Australia and Antarctica started around ~ 35.5 Ma, with ocean crust formation between southwestern Tasmania and Wilkes Land, Antarctica, and onset of bottom-water currents around 35.5–33.5 Ma (Stickley et al., 2004; Houben et al., 2019), although the relative and absolute strength and influence of this so-called ‘proto-ACC’ during the Oligocene remains debated (Hill et al., 2013; Scher et al., 2015; Sauermilch et al., 2021). New field data reconstructing sea surface temperatures (SST) and water properties (Bijl et al., 2018; Hartman et al., 2018; Sauermilch et al., 2021; Hou et al., in prep; Chapters 2–4) allows tracing of frontal systems’ migrations which may be reconducted to opening of gateways. Furthermore, our understanding of the effect of tectonic opening of the Southern Ocean gateways in the Australian–Antarctic Gulf oceanographic conditions has been improved through modelling exercises (England et al., 2017; Sauermilch et al., 2021). The recent TEX_{86} organic biomarker-based SST compilation from around the Tasmanian Gateway (Chapter 3) shows that the latitudinal gradient between the subtropical front and the Antarctic Margin progressively increased from ~ 26 Ma onwards, due to cooling at Antarctic-proximal sites. Since the Tasmanian Gateway was already open, wide and deep, and Australia had moved out of the way for ACC throughflow, this Antarctic cooling may have been related to the onset of deep ocean connections through Drake Passage (van de Lagemaat et al., 2021). The plate tectonic configuration of the Drake Passage region is complex, with various sub-continent, various rift basins that have uncertain interconnections and complex plate motions (Maldonado et al., 2006; Pérez et al., 2019). This complexity of the Drake Passage tectonics leaves the possibility that multiple cycles of opening and closing occurred, with consequences for the oceanography of the Southern Ocean. The timing and nature of the opening, widening, and deepening of the Drake Passage has also been much debated, broadly ranging from between 50 Ma to as young as 6 Ma (Barker et al., 2007; Livermore et al., 2007; Eagles and Jokat, 2014; Maldonado et al., 2014; van de Lagemaat et al., 2021). While some records suggest oceanographic rearrangements that were possibly linked to an early Drake Passage opening (Scher and Martin, 2006; López-Quirós et al., 2021), we lack knowledge of the long-term history of the evolution of SST gradients in the South Atlantic, which could be used to interpret phases of Antarctic cooling, strengthening of the ACC and shifts in the frontal systems that could be linked to the throughflow of surface and deep waters through the Drake Passage.



Figure 1. Present day map of the Southern Ocean showing the location of the drill sites included in this study. Grey areas represent present-day coastlines. The colors show average January SSTs from 1971–2000 (Reynolds et al., 2002). The white lines represent the smoothed, simplified position of circumpolar fronts interpreted by Orsi et al. (1995). From north to south: The Subtropical front (STF); the Subantarctic front (SAF); the Polar Front (PF); the southern ACC Front (sAACT); and the Southern Boundary (SBdy) front.

Recent drilling efforts in and around the Weddell Sea during IODP Expedition 382 (Weber et al., 2021), and a revisit of previously drilled ODP Leg 113 records increased the spatial coverage of sedimentary records across two prominent climate transitions, viz (1) The Eocene-Oligocene transition (EOT; 33.7 Ma) and (2) the Middle and Late Miocene cooling (LMC; ~14–5 Ma). Both are marked by increases in benthic foraminiferal $\delta^{18}\text{O}$, suggesting cooling and expansion of the Antarctic ice sheet (e.g., Miller et al., 1991; Zachos et al., 2001). Given the paucity of carbonaceous sediments in this region, typically employed for paleotemperature reconstructions, we here choose to generate organic geochemical (TetraEther index of tetraethers with 86 carbon atoms (TEX_{86})) proxy SST reconstructions from the South Scotia Sea at ODP Site 696 (Late Eocene–Early Oligocene) and IODP Site U1536 (mid–Late Miocene) (Figure 1). We compare our findings to available TEX_{86} , alkenone unsaturation index (U^k_{37}) and clumped isotope (Δ_{47}) derived SST records from the South Atlantic region (Figure 1) for a reconstruction of these climatic transitions in the South Atlantic Ocean.

2 Material

2.1 Sedimentary drill cores

2.1.1 Site 696 Lithology, age model and depositional setting

ODP Leg 113 Site 696 was drilled in the southern Scotia Sea (61° 50.959' S; 42° 55.996' W), on the South Orkney Microcontinent (SOM; Figure 1), located south of the Southern Boundary (SBdy) front. The site had a Late Eocene paleolatitude of ~67°S (paleolatitude.org Version 2.1; van Hinsbergen et al. (2015), using the paleomagnetic reference frame of Torsvik et al. (2012), and the geological reconstruction of Seton et al. (2012)).

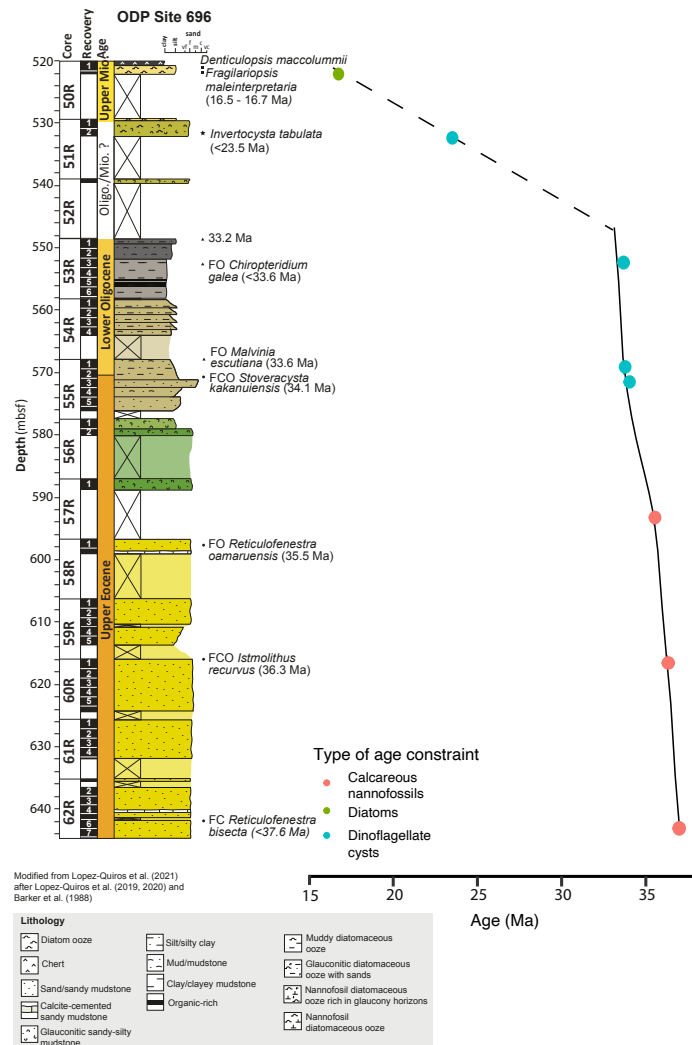


Figure 2. Age-depth model of ODP Site 696 (Supplementary Table 1) and lithological log as published in López-Quirós et al. (2021).

Lithological descriptions and age constraints are gathered from López-Quirós et al. (2021; Figure 2, Supplementary Table 1). The age model is based primarily on calcareous nannofossil biostratigraphy (Wei and Wise Jr, 1990; Villa et al., 2008), and updated age constraints from organic walled dinoflagellate cysts (dinocysts) published previously (Houben et al., 2013; 2019; López-Quirós et al., 2021) which places the studied section of 607.6-548.9 mbsf at 36.0 to 33.2 Ma (Houben et al., 2013). The sediments overlying the Lower Oligocene interval, 532-521 mbsf, have recently been dated through dinocyst biostratigraphy (first occurrence of *Invertocysta tabulata*, <23.5 Ma, at ~531.81 mbsf; López-Quirós et al., 2021) and diatom biostratigraphy (*Denticulopsis maccolummii* and *Actinocyclus ingens*, 521.49 mbsf; Carter et al., 2017; López-Quirós et al. in prep), inferring an age of 16.7-16.5 Ma (Figure 2).

The sediment package at Site 696, at 607.6-521.08 mbsf, consists of organic-rich sandy mudstone. The glauconitic packstone beds of latest Eocene age (~35.5-34.1 Ma) are attributed to a decline in terrigenous input to Site 696 and increased winnowing. The opening of the Powell Basin (at the tip of the Antarctic Peninsula) caused subsidence of South Orkney Microcontinent (SOM), thereby decreasing the delivery of terrigenous sediments to the site (López-Quirós et al., 2019). The Antarctic-proximal location makes the site prone to influx of terrigenous material transported by icebergs. Indeed, López-Quirós et al. (2021) show unequivocal evidence for the oldest iceberg rafted debris (IRD) deposited across the EOT (34.1-33.6 Ma, 576-568 mbsf) at Site 696. Across the EOT (~34.1-33.6 Ma) sediments reflect more distal and deeper environments while SOM continued to deepen. Dinocyst assemblages show eutrophic surface water conditions, indicative of productive and somewhat shallow-water and reduced-oxygen conditions (Houben et al., 2019; López-Quirós et al., 2019; 2021). The dominance of large sized heterotrophic protoperidiniacean dinocysts in the lowermost Oligocene is suggested to reflect seasonal sea-ice conditions (Houben et al., 2013). During the lowermost Oligocene (~33.6-33.2 Ma), the SOM shelf subsided further and biological production increased, partially driven by upwelling along the SOM shelf (López-Quirós et al., 2021). Deposition of moderately to intensely bioturbated silty-mudstones during the EOT (~34.1-33.6 Ma) is attributed to the continued subsidence-related deepening at Site 696 (López-Quirós et al., 2021). Above the claystone/clayey mudstones of the lowermost Oligocene (Core 53R, Figure 2) we find rhythmically interbedded sandy mudstones with glauconite-bearing sandstone beds, a result of reworked sediments, deposited under bottom current activity and possibly slumping. The nature of this sediment complicates dating of this material (López-Quirós et al., 2020). There is likely a break in the sedimentation (hiatus) around 529 mbsf (the top part of Core 51R), with a sharp contact from glauconitic-bearing sandstone to mud bearing diatom ooze 522-521 mbsf (Core 50R), dated to ~16.7-16.5 Ma (López-Quirós et al. in prep).

2.1.2 Site U1536: lithology, age model and depositional setting

Site U1536 is located in Dove Basin, in the southern Scotia Sea (59°26.4608'S, 41°3.6399'W, 3220 m water depth). The Site was drilled to study the Neogene flux of icebergs through "Iceberg Alley", the main pathway along which icebergs calved from the margin of the Antarctic ice sheet drift into the warmer waters of the ACC (Weber et al., 2021). Today, the site is located just south of the southern ACC Front (sACCf) and the SBdy front and is seasonally covered by sea ice (Figure 1). The rotary drilling at Hole U1536E penetrated down to 643 mbsf. Sediments have moderate to high core disturbance and biscuiting or brecciated core material due to the rough nature of rotary drilling and due to the compacted and gravel rich material. The lithology of the studied interval from Hole U1536E, 640-450 mbsf (Cores 13R-33R) consists of silty clays with interbedded diatom ooze (Figure

3), with an estimated average sedimentation rate of ~ 4.3 cm/kyr (3.9-6.4 cm/kyr) (Pérez et al., 2021). The shipboard bio- and magnetostratigraphic age model was used to date the sediments (Weber et al., 2021). Sediments between 480-450 mbsf (Cores 13R-16R) have an age of 6-5 Ma based on bio- and magnetostratigraphy. Diatom biostratigraphy between 548-535 mbsf (Cores 22R-24R) indicate ages of 7.7-6.4 Ma. The sediment directly overlying Reflector-c (Weber et al., 2021) at 617-570 mbsf (Cores 26R-30R) have an age of 8.4 Ma (Pérez et al., 2021). The sediments below Reflector-c, at 622 mbsf (Core 31R), is dated to ~ 14.2 Ma, and as the lithologic contact is not recovered, it means that Reflector-c could represent a prolonged time interval of slow sedimentation rates or non-deposition or erosion. The sparse brecciated lithology fragments in the lower cores below the Reflector-c (566 mbsf), consists of lithified mudstone and gravel-conglomerate-breccia (Weber et al., 2021; Perez et al., 2021).

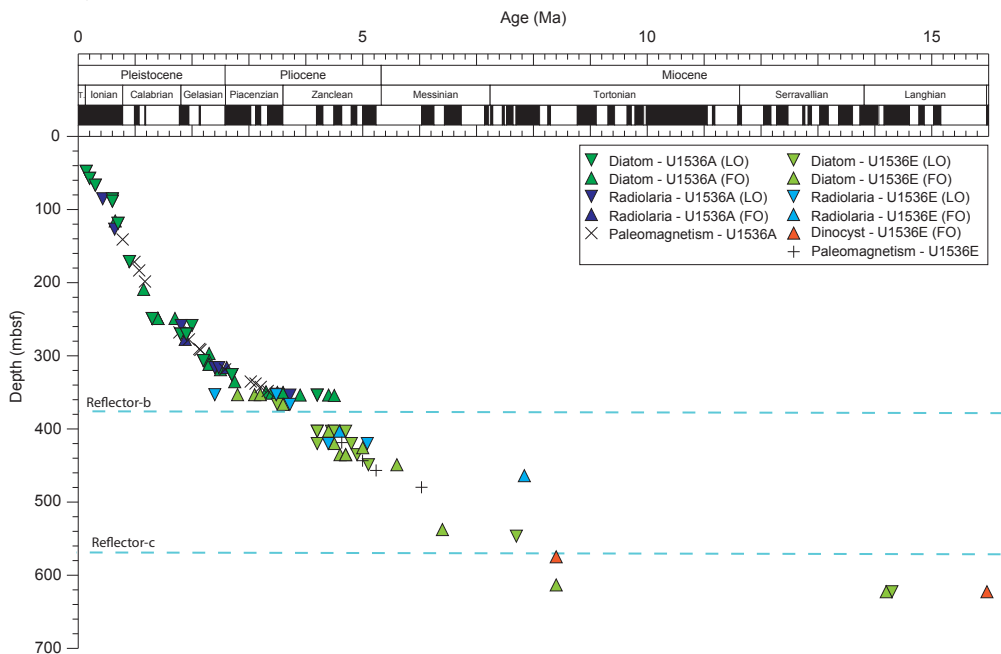


Figure 3. Site U1536 lithology and age model. The data is derived from the IODP Expedition 382 shipboard report (Weber et al., 2021). The depth and age of the stratigraphic discontinuities (seismic reflectors) are derived from Perez et al. (2021) (Supplementary Table 2, Perez et al., 2021). LO = Last occurrence, FO = First occurrence.

3 Methods

3.1 Lipid Extraction and GDGT Analysis

Lipid extraction of samples from Site 696 was performed at the Laboratoire d'Océanographie et du Climat, Expérimentations et Approches Numériques (LOCEAN-Université Pierre et Marie Curie, Paris, France). First, 70 sediment samples were freeze-dried and crushed to a fine powder. Total lipids were extracted from ~ 9.5 to 15 g of homogenized sediment using a solvent mixture

of 40 ml DCM:MeOH (3:1, v/v) to which an internal standard (5 α -cholestane) was added. The n-alkane fraction was separated from the polar lipids over a silica column using 3 ml hexane as eluent. The polar lipid fractions were sent to Utrecht University for further analysis. Samples from U1536E were processed for GDGT analysis by lipid extraction, at Utrecht University, from 10 g freeze-dried and manually powdered sediments using a Milestone Ethos X microwave system and adding dichloromethane:methanol (DCM:MeOH; 9:1, v/v). The total lipid extracts (TLE) were first filtered through a NaSO₄ column to remove potential remaining water and sediments. The TLE were then separated on an activated Al₂O₃ column into apolar, ketone and polar fractions, using hexane:dichloromethane (DCM) (9:1, v/v), hexane:DCM (1:1, v/v), and DCM: MeOH (1:1, v:v) as eluents, respectively. Silica gel column chromatography was thereafter applied by eluting 4 ml of hexane, 4 ml of DCM and 4 ml of MeOH for separation of the neutral fraction into a hydrocarbon fraction, a ketone fraction and a polar fraction respectively. All polar fractions were dried under N₂. A GDGT standard was added to the polar fraction, which was subsequently dissolved in hexane:isopropanol (99:1, v/v) to a concentration of ~2 mg ml⁻¹ and filtered through a 0.45 μ m polytetrafluorethylene filter. After that, the dissolved polar fractions were injected and analyzed by ultra-high performance liquid chromatography/mass spectrometry (UHPLC/MS) according to the method described by Hopmans et al. (2016), using an Agilent 1260 Infinity UHPLC system coupled to an Agilent 6130 single quadrupole mass detector, at Utrecht University. Selected ion monitoring (SIM) was used to identify the GDGTs using their [M+H]⁺ ions and integrated using ChemStation software. Samples with very low concentrations (i.e., peak area <3,000 mV/s and/or peak height <3 \times background signal) of any GDGT included in TEX₈₆ were excluded from analysis.

3.2 GDGT indices for non-thermal overprints on TEX₈₆

The TEX₈₆ SST proxy is based on the temperature dependence of the number of cyclopentane rings of GDGT membrane lipids produced by marine Thaumarchaeota (Schouten et al., 2002). The use of TEX₈₆ as a proxy for SST relies upon the assumption that isoprenoidal GDGTs in marine sediments are principally derived from membrane lipids of marine pelagic Thaumarchaeota (Schouten et al., 2013). TEX₈₆ was calculated as defined by Schouten et al. (2002):

$$a. \text{TEX}_{86} = ([\text{GDGT-2}] + [\text{GDGT-3}] + [\text{cren}']) / ([\text{GDGT-1}] + [\text{GDGT-2}] + [\text{GDGT-3}] + [\text{cren}']) \quad (1)$$

However, in some environments, non-thermal factors may alter the distribution of isoprenoidal GDGTs stored in the sediment and thus the temperature signal. We list the GDGT-based ratios and indices to assess potential non-thermal effects on the GDGT distributions. The letters correspond to Figure 4C (b-h) and Figure 5C (b-h) where the GDGT distributions from Site 696 and U1536, respectively, are displayed.

- b. The relative contribution of soil- and marine-derived organic matter in marine sediments can be reconstructed using the branched and isoprenoid tetraether (BIT) index (Hopmans et al., 2004). This index is taken as a proxy for the amount of terrestrial GDGT input, including allochthonous terrestrially-derived isoGDGTs (Weijers et al., 2006) into the marine sediments. BIT index values greater than 0.4, is the threshold above which elevated soil-derived GDGTs are suspected to significantly influence TEX₈₆-derived SST estimates (i.e., >2°C) (Weijers et al., 2006). However, this only applies when brGDGTs are sourced from land, as opposed to marine-sourced (see e.g., discussions in Bijl et al., 2021). We calculate the #rings_{tetra} in order to test this (Figure 5, 7). In effect no additional samples were discarded based on high BIT value alone.

- c. The fcren' index evaluates variations in the relative abundance of the crenarchaeol regio-isomer. The index is used to detect 'anomalous' versus 'warm' GDGT distributions, compared to values observed in the modern core-top dataset, which indicates non-thermal contributions, potentially water depth, of the crenarchaeol isomer (O'Brien et al., 2017). The index has a cutoff value at above 0.25.
- d. The methane index (MI) detects isoprenoidal GDGT contributions from methanotrophic Euryarchaeota (Zhang et al., 2011). MI values >0.3 conservatively reflect hydrate-impacted sediments and suggest that GDGT distribution might be affected by methanogenic archaea.
- e. Anaerobic oxidation of methane (AOM) is characterized by GDGT2/Cren ratio values above 0.2 (Weijers et al., 2011).
- f. The GDGT-2/GDGT-3 ratio (Taylor et al., 2013) signals possible overprints by archaeal communities dwelling deeper in the water column. We use a cut-off value of 7.
- g. The Methanogenesis index, measured by the GDGT-0/Crenarchaeol ratio (Blaga et al., 2009; Sinninghe Damsté et al., 2009; Taylor et al., 2013) is targeted to detect contributions of isoGDGTs (GDGT-0) from methanogens. Samples with GDGT-0/Crenarchaeol ratio >2 are flagged as outliers for potential contribution by methanogenic archaea.
- h. The Δ Ring Index (Δ RI) detects deviations from a normal pelagic GDGT composition (Zhang et al., 2016). Δ RI values > 0.3 are thought to represent samples for which GDGT distributions diverge outside that of the modern TEX_{86} -RI relationship, based on the 95% confidence interval of the modern regression.

3.3 TEX_{86} calibration

The empirical relationship between TEX_{86} values and SST is not always straightforward, as reflected by continued revisions of the approach of TEX_{86} – SST calibrations (Kim et al., 2010; Tierney and Tingley, 2015; O'Brien et al., 2017; Dunkley Jones et al., 2020). Particularly, the relationship between TEX_{86} and SST seems to become obscured in both extreme ends of the core-top calibration: at or above modern SSTs, and in cold polar regions. However, for the time intervals (Late Eocene-Early Oligocene and Middle-Late Miocene) and locations we are targeting, we expect SSTs, where commonly used calibrations yield similar results. In this study we used the regionally varying Bayesian BAYSPAR SST calibration of Tierney and Tingley (2015) to reconstruct SST from TEX_{86} index values ($\pm 4^\circ\text{C}$ standard calibration error). BAYSPAR compares measured TEX_{86} values to those in modern SST observations, obtained from surface sediment samples, to derive linear regression parameters: BAYSPAR propagates uncertainties in the surface sediment data into resulting temperature predictions (Tierney and Tingley, 2015). We also compare the SST estimates obtained through the exponential transfer function BAYSPAR in this study with the exponential function from Kim et al. (2010) and linear function by O'Brien et al. (2017). The BAYSPAR SSTs are similar and usually cooler to those produced by the exponential function from Kim et al. (2010) and linear function by O'Brien et al. (2017) (Supplementary Table 3, 4, Supplementary Figure 1, 2).

4 Results

4.1 Site 696

A total of 72 samples from ODP Site 696 were available for TEX_{86} palaeothermometry (Supplementary Table 3).

4.1.1 Site 696 GDGT distributions and indices for non-thermal overprints on TEX_{86}

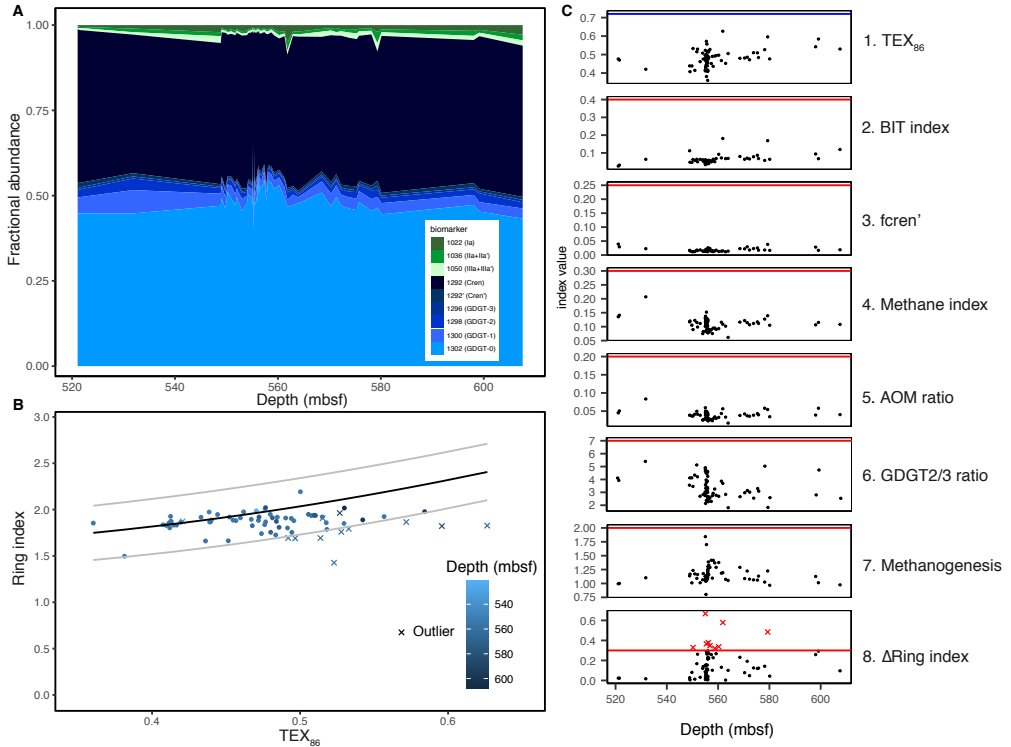


Figure 4. A. ODP Site 696 stacked relative GDGT distribution B. Δ Ring Index are plotted relative to TEX_{86} results of Site 696. Black and grey lines represent the RI/ TEX_{86} relationship of modern core top samples, and the 95% confidence interval, respectively. Filled circles indicate the RI/ TEX_{86} values for samples that are retained; crosses indicate samples that are discarded. Color of all data points indicates depth of the sample. C. Site 696 TEX_{86} values and overprinting indices. Red lines indicate the cut-off values used for each of the indices, red crosses indicate samples marked with outlying values to the respective index. 1. TEX_{86} (Schouten et al., 2002), with blue line indicating the maximum modern core-top value (~ 0.72). 2. BIT index (Hopmans et al., 2004). 3. f_{Cren} (O'Brien et al., 2017). 4. Methane index (Zhang et al., 2011). 5. AOM ratio (Weijers et al., 2011). 6. GDGT-2/3 ratio (Taylor et al., 2013). 7. Methanogenesis (Blaga et al., 2009), 8. Δ Ring index (Zhang et al., 2016).

The GDGTs consist of $90 \pm 5\%$ isoGDGTs and $10 \pm 5\%$ brGDGTs. The isoGDGT distributions indicate that GDGTs are primarily produced by surface ocean-dwelling Thaumarchaeota, with little influence of soil-derived GDGTs, as indicated by the low BIT index (< 0.2) throughout the record (Figure 4C; panel 2). Additionally, there are no elevated concentrations of specific isoGDGTs

pointing to enhanced GDGT contributions by methanotrophic or methanogenic microbes (Figure 4C; panel 4, 5, 6) (Weijers et al., 2006; Blaga et al., 2009; Zhang et al., 2011), nor non-thermal contributions of the crenarchaeol isomer (Figure 4C; panel 1) (O'Brien et al., 2017). No samples were flagged for the potential influence of deep ocean-dwelling archaea, with GDGT 2/3 ratio threshold of above 7 (Figure 4C; panel 7) (Taylor et al., 2013). In total, 9 samples had a ΔRI higher than the cut off value of 0.3 (Figure 4B, 4C; panel 8) indicating a potential non-thermal overprint on the GDGT distribution and are flagged as outliers. A total of 9 samples had overprinting values in the GDGT indices for non-thermal overprints (Figure 4) and were therefore considered as unreliable and marked as outliers in Figure 5 and excluded from SST analysis.

4.1.2 Trends and patterns in Site 696 TEX_{86} -SST

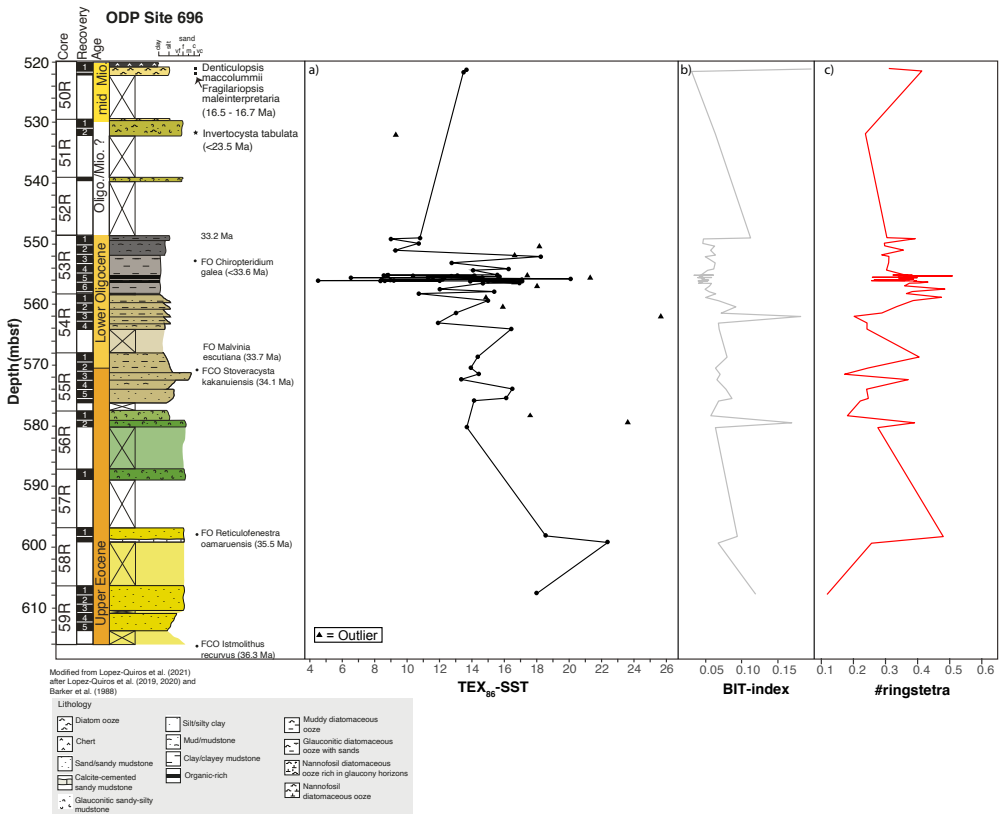


Figure 5. TEX_{86} -SST data (BAYSPAR calibration) and BIT-index values plotted next to the lithology and age constraints of Site 696 (López-Quirós et al., 2021).

The TEX_{86} -based SST record from Site 696 (607-521 mbsf, 36-33 Ma and ~16.5 Ma), consisting of 60 data points, shows values predominantly ranging between 12°C and 18°C, with an absolute temperature range between 4°C and 25°C ($\pm 4^\circ C$ standard error). There is a general cooling trend of ~8°C between the Upper Eocene and the Lower Oligocene (from 20°C to 12°C between 610-558 mbsf) interval, but with high sample-to-sample variability. This is followed by an average ~5°C increase in temperature between ~558 and ~552 mbsf. In the organic rich interval at ~555 mbsf

(Core 53R, section 5, 33.5–33.2 Ma), 35 samples were analyzed at high resolution (every 3 cm, ~15 kyr resolution). The TEX_{86} -SST record shows high-amplitude variability (total range; 4–21°C, with most samples falling within 8–17°C). At ~550 mbsf (Lower Oligocene) SSTs rapidly decreases to 10°C. In the Middle Miocene (~520 mbsf, 2 samples) SSTs values are ~14°C. We don't see a distinct trend between BIT and TEX_{86} -SST. The $\#rings_{tetra}$ is below 0.7 in the entire record.

4.2 Site U1536

A total of 40 samples from IODP Hole U1536E were processed for TEX_{86} palaeothermometry. 14 samples had insufficient GDGT concentrations, could not be integrated and were therefore excluded (Figure 7). Data of the remaining 26 samples are here presented (Supplementary Table 4).

4.1.1 Site U1536 GDGT Distributions and indices for non-thermal overprints on TEX_{86}

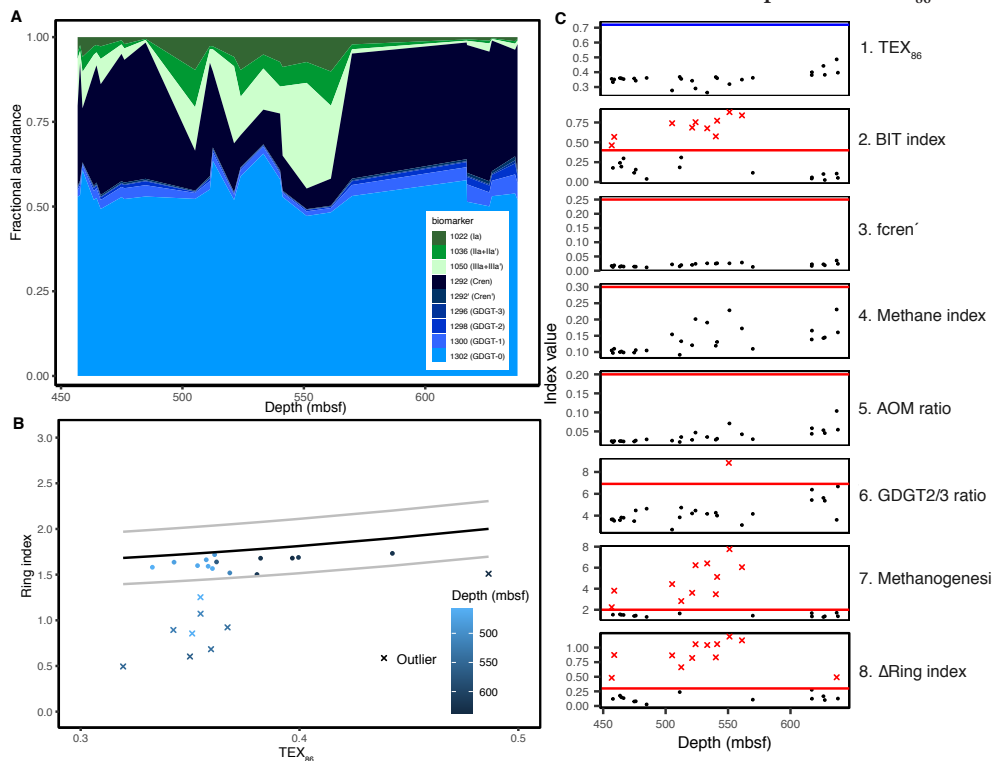


Figure 6. A. GDGT distributions Site U1536. B. Δ Ring Index versus TEX_{86} . Black and grey lines represent the RI/ TEX_{86} relationship of modern core top samples, and the 95% confidence interval, respectively. Filled circles indicate RI/ TEX_{86} values for samples that are retained; crosses indicate samples that are discarded. Color of all data points indicates depth of the sample. C. TEX_{86} values and overprinting indices. Red lines indicate the cut-off values used for each of the indices, red crosses indicate samples marked with outlying values to the respective index. 1. TEX_{86} (Schouten et al., 2002), with blue line indicating the maximum modern core-top value (~0.72). 2. BIT index (Hopmans et al., 2004). 3. $f_{cren'}$ (O'Brien et al., 2017). 4. Methane index (Zhang et al., 2011). 5. AOM ratio (Weijers et al., 2011). 6. GDGT-2/3 ratio (Taylor et al., 2013). 7. Methanogenesis (Blaga et al., 2009). 8. Δ Ring index (Zhang et al., 2016).

The measured isoGDGTs and brGDGTs vary throughout the record, with relatively high abundance of branched GDGTs in the middle (500-560 mbsf) and top parts of the record (440 mbsf) (Figure 6A). In total, 12 samples had a ΔRI higher than 0.3 (Figure 6B, 6C; panel 8) indicating a potential non-thermal overprint on the GDGT distribution and are flagged as outliers. Eleven of these have potential contribution by methanogenic archaea as depicted by the high Methanogenesis index. Furthermore, 10 of the same samples had high BIT values (0.4-0.8) (Figure 6C; panel 2) (Weijers et al., 2006) and were flagged as outliers with potential influence of soil-derived GDGTs. The #rings_{tetra} record (Figure 7c) does not show values that can be associated with marine in situ produced brGDGTs. There are no further high concentrations of specific isoGDGTs pointing to enhanced GDGT contributions by methanotrophic microbes (Figure 6C; panel 4, 5) (Blaga et al., 2009; Weijers et al., 2011), non-thermal contributions of the crenarchaeol isomer (Figure 6C; panel 3) (O'Brien et al., 2017), and one sample was flagged for potential influence of deep ocean-dwelling Archaea, with GDGT 2/3 ratio value above the threshold of 7 (Figure 6C; panel 7) (Taylor et al., 2013).

4.2.2 Trends and patterns in Site U1536 TEX₈₆-SST

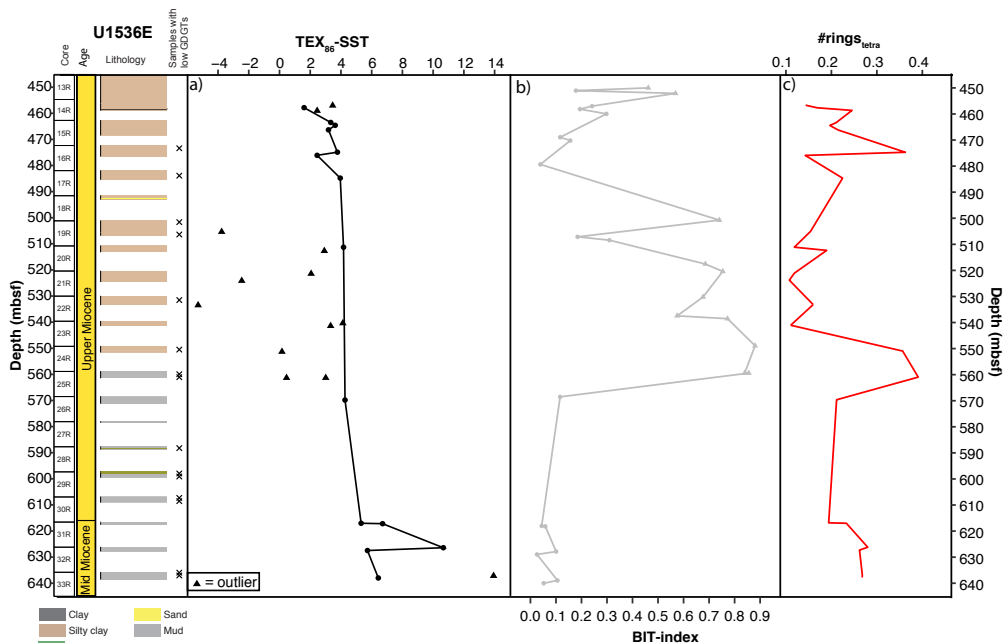


Figure 7. Biomarker indices from Site U1536. Left panel shows core recovery, estimated age and lithological composition (Weber et al., 2021). The crosses (X) indicated the samples which had too low GDGT concentrations to be integrated. A) TEX₈₆ data. B) BIT-index values. C) #rings_{tetra}.

The BAYSPAR-based TEX₈₆-SST record ($\pm 4^\circ\text{C}$ standard error) derives from the 14 samples with a clear pelagic isoGDGT signature (Figure 7). The record shows temperatures of 5-11°C in the Middle Miocene (619-640 mbsf) and 1.5-5°C in the Upper Miocene (570-450 mbsf). In the Upper Miocene

higher BIT seems to coincide to lower SSTs. The $\#rings_{tetra}$ values below 0.4 suggest marine in situ produced brGDGTs, rather than soil-derived GDGTs.

5 Discussion

5.1 Late Eocene-Early Oligocene South Atlantic SST conditions

Our SST record at Site 696 (yellow in Figure 8A) shows warm-temperate conditions (SST range between 22–14°C) during the latest Eocene (~36.5–33.6 Ma) and on average decreasing SSTs (~15–9°C) in the earliest Oligocene (33.6–33.2 Ma). Miospores at Site 696, believed to be of local origin from the South Orkney Microcontinent (SOM), changed concomitantly from southern beech, *Nothofagus*-dominated vegetation to an increase in gymnosperms and cryptogams, accompanied by a rapid rise in taxon diversity after the Earliest Oligocene Oxygen Isotope Step (EOIS, ~33.5 Ma, 568.82 mbsf) (Thompson et al., 2022). This shift in vegetation to a cooler and dryer climate occurred after the onset of earliest glacial expansions (~34.1 Ma), and corresponds to our SST drop below 12°C and the more common IRD in the sediment (see also López-Quirós et al., 2021). Sedimentological investigations by López-Quirós et al. (2021) for the same interval showed deepening of the SOM shelf and enhancement of biological production, possibly due to upwelling along the SOM shelf, leading to low oxygen conditions at the seafloor. The high-amplitude SST variability in our TEX_{86} -SST record would suggest that this upwelling regime was strongly variable. The strongly variable levels of upwelling could be induced by strong fluctuating ice sheet expansion and retreat and shifts in ocean frontal systems.

TEX_{86} - and U^{k}_{37} -based SST reconstructions from ODP Site 511 differ slightly in trends across the EOT, with U^{k}_{37} showing amplified cooling compared to TEX_{86} . U^{k}_{37} -temperature data reflect surface water temperature, while TEX_{86} can in some settings reflect subsurface temperatures (50–200 m water depth) (Schouten et al., 2013). Although U^{k}_{37} is calibrated to mean annual temperature (Müller et al., 1998), in some settings it reflects a seasonally-biased temperature (e.g., Ternois et al., 1997). In fact, modern high-latitude alkenone producing haptophyte communities primarily bloom in early spring (Herbert et al., 1998). Thus, at Site 511, the amplified cooling in U^{k}_{37} might reflect a shift towards early spring blooming, which could explain its amplified cooling trend across EOT, relative to that in TEX_{86} . As TEX_{86} is continuously warmer than U^{k}_{37} at this site, we argue TEX_{86} represents a warmer season than U^{k}_{37} and that it does seem to be reflecting a surface water signal rather than a subsurface signal.

The clumped isotope (Δ_{47})-based SST record from Seymour Island (34 Ma, purple square Figure 8) shows similar temperatures (13°C) to that from U^{k}_{37} and TEX_{86} proxies at the same site (Douglas et al., 2014). The correspondence of the biomarker-derived SSTs with those from Δ_{47} , three completely independent temperature proxies, adds reliability to both temperature proxies to accurately reflect SST. More importantly, the clumped isotope temperature at 34 Ma yield similar SSTs to those from Sites 696 and 511, even though there was a latitudinal difference of ~12° between Site 511 and Seymour Island. This suggests that all sites experienced similar paleoceanographic regimes. The subtropical Site 1090 is the warmest site (~19–27°C) in our compilation, which is expected given its lowest paleolatitude. Although a 2-step cooling across EOT can be interpreted from the U^{k}_{37} -based SST record at Site 1090, the magnitude of the cooling is smaller (4°C) than the cooling at Sites 511 and 696 (~6°C).

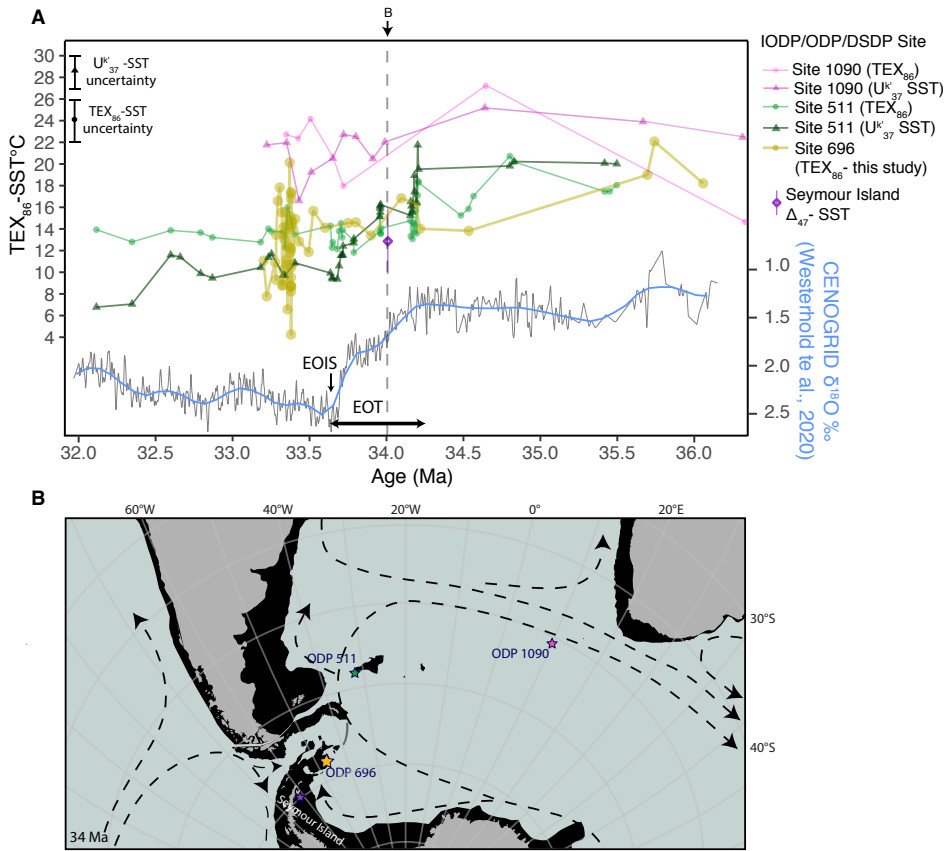


Figure 8. A. Biomarker-based SST trends from this study (Site 696) is compared with data from Site 1090 (Lie et al., 2009) and Site 511 (Houben et al., 2019) and clumped isotope SST from Seymour Island (Douglas et al., 2014). The benthic foraminiferal $\delta^{18}\text{O}$ compilation, smoothed by a locally weighted function over 20 kyr (black curve) (CENOGRID; Westerhold et al., 2020). The blue curve is the LOESS smoothed (span = 0.2). B. Reconstructed paleogeographic map at 34 Ma, based on the GPlates reconstruction of Van de Lagemaat et al. (2021) in the paleomagnetic reference frame of Torsvik et al. (2012). The ocean circulation derived from GCM circulation model by Goldner et al., 2014.

The absolute SSTs of Sites 696 and 511 are strikingly similar across the EOT, with Site 511 being only slightly warmer than Site 696 in the Late Eocene, and similar to Site 696 in the Early Oligocene (Figure 8A). The lack of an increase in SST gradient between these sites across EOT is surprising. Today, both sites are separated by the strong ACC with a SST gradient of $>7^{\circ}\text{C}$ (Locarnini et al., 2018). The lack of an increase in the SST gradient between the sites across EOT would suggest that both sites remained under the same oceanographic regime, and that the installation of the Antarctic ice sheet (terrestrial only and therefore less sensitive) did not cause an increase in SST gradient between these sites. It also implies that throughflow across Drake Passage did not change across the EOT, in contrast to what modelling results suggested earlier (Sauerlich et al., 2021).

Tectonic evidence suggests that the Drake Passage was narrow, with little deep-water connection from the Pacific to the Atlantic around EOT times (e.g., van de Lagemaat et al., 2021). Fully coupled

climate models from the EOT by Goldner et al. (2014) and Kennedy-Asser et al. (2015) show that with a restricted Drake Passage the Subpolar Gyre in the South Atlantic would expand further north in the absence of throughflow (Figure 8B). Moreover, recent model experiments (Hill et al., 2013; England et al., 2017) also showed that a closed Drake Passage could sustain warm currents to the Antarctic Margin. We propose that the small difference in SST between Sites 511 and 696 suggest a closed/restricted Drake Passage during the EOT – earliest Oligocene. A Southern Ocean without open gateways featured wind-driven clockwise gyres in the South Pacific and South Indian/Atlantic Ocean basins (Huber et al., 2004; Sauermlch et al., 2021) (Figure 8B) that would advect warm surface waters toward the Antarctic coast. Recent ocean model simulations show this would lead to SSTs reaching 19°C in the Australian-Antarctic Basin and 15–17°C in the subpolar Pacific and Atlantic (Sauermlch et al., 2021), which is similar to the temperatures we record.

Houben et al. (2019) found widespread glauconite-bearing facies in Southern Ocean sediment cores from about 35.7 Ma and attributed this to invigoration of the basin-wide bottom waters. This led to sediment winnowing, higher biological productivity and aided cooling of surface waters around Antarctica. This process could have been strengthened by concomitant Eocene Tasmanian Gateway widening and deepening (Kennedy-Asser et al., 2015; Sijp et al., 2014; 2016; Sauermlch et al., 2021) and/or invigorated atmospheric circulation induced by Late Eocene polar amplification of CO₂-forced cooling (Scher et al., 2014; Cramwinckel et al., 2018). Site 696 also contains glaucony-bearing facies of comparable age (~588.8 to 577.9 mbsf; López-Quirós et al., 2019), interpreted as the result of invigorating bottom currents. Stronger bottom currents were thought to be the result of the opening of the Powell Basin and the establishment of oceanic upwelling, which drove regional cooling and increased primary productivity. While this could be a plausible explanation, the tectonic opening of Powell Basin would apparently not have resulted in a increase in the SST gradient between Sites 696 and 511. Alternatively, both sites were similarly affected by the opening of the Powell Basin and the resulting atmospheric and/or oceanographic changes.

In summary, cooling of South Atlantic surface waters across EOT is in broad agreement with the average Southern Ocean-wide temperature drop (Kennedy-Asser et al., 2020), the increase in benthic foraminifer $\delta^{18}\text{O}$ values involving deep sea cooling and the growth of a continent-wide Antarctic ice sheet (Bohaty et al., 2012) and with a drop in atmospheric $p\text{CO}_2$ levels across the EOT (<https://www.paleo-co2.org>; Pearson et al., 2009; Steinhorsdottir et al., 2016; Hoenisch, 2021). Step-wise cooling across EOT (Hutchinson et al., 2021) is evident at Site 511 and the U^{k}_{37} record at Site 1090, and the first step around 34.1 Ma coincides with common IRDs at Site 696 suggesting glacial onset in the region (López-Quirós et al., 2021) and a second step across the Earliest Oligocene Oxygen Isotope Step (EOIS) (33.65 Ma)(Hutchinson et al., 2021). Yet, the lack of a strong SST gradient, and absence of a prominent increase thereof across EOT, suggest a persistent gyral circulation, that connected all sites (Sauermlch et al., 2021). Moreover, an invigoration of the Subpolar Gyre (Houben et al., 2019) did not induce stronger latitudinal temperature gradients between these sites either.

5.1.2 Middle to Late Miocene

To investigate the cooling step between the Middle to Late Miocene, the new Miocene SST records from the Antarctic-proximal southwest Atlantic Sites 696 and U1536 are compared to a record from Wilkes Land (Site U1356, Sangiorgi et al., 2018). However, the sedimentary record of Site U1536 has large age uncertainties (Weber et al., 2021; Perez et al., 2021). The TEX_{86} -derived SSTs are therefore presented as average temperatures within two broad time intervals, which represent the age uncertainties. Data are interpreted exclusively as general trends. We also compare SST trends

from the above mentioned sites to those from the subantarctic zone; ODP Site 1171, southwest Pacific Ocean (Leutert et al., 2020) and subtropical front; ODP Site 1088 (Herbert et al., 2018) in the Southeast Atlantic, and Site ODP 1168 west of Tasmania (Hou et al., in prep). Further, we compare our new SST record to clumped isotope bottom water temperatures (BWT) from South Indian Ocean ODP Site 747 (Leutert et al., 2021).

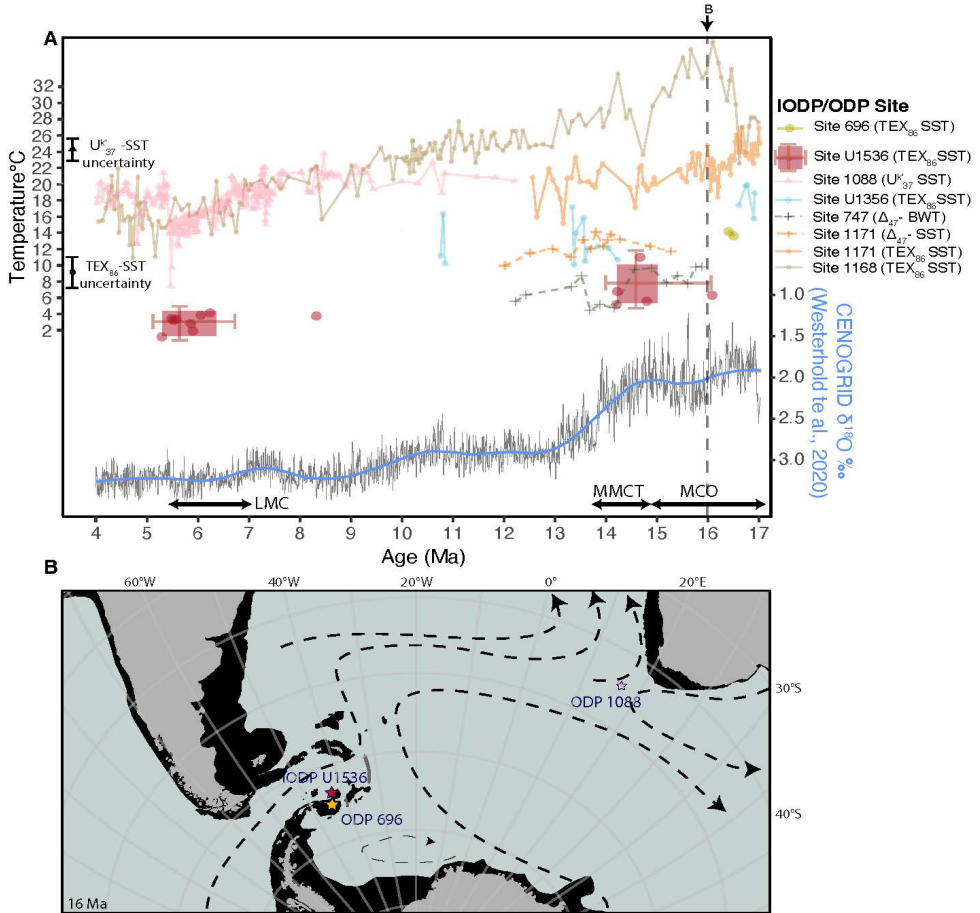


Figure 9. A. TEX₈₆-based SST data from Site 696 and U1536 (this study) compared to Southern Ocean wide SST and BWT records. Data of Site U1536 is displayed as two bar plots (red) showing the temperature ranges for the Middle Miocene (16-14 Ma) and late Miocene (7-5.3 Ma), individual data points are shown as red dots. We compare our data to SST records from Wilkes Land Site U1356 (Sangiorgi et al., 2018), Site 1168 (west of Tasmania; Hou et al., in prep), Site 1171 (southwest Pacific Ocean; (Leutert et al., 2020), U^k₃₇- SST data from Site 1088 (Herbert et al., 2016) and clumped isotope bottom water temperature (BWT) data from Leutert et al. (2021) (Site 747). The black line is the benthic foraminiferal $\delta^{18}O$ compilation, smoothed by a locally weighted function over 20 kyr (thin blue curve) (CENOGRID; Westerhold et al., 2020). Thick blue curve is the LOESS smoothed (span = 0.2). The stippled vertical line indicates the age for the paleogeographic map below. B. Paleogeographic reconstruction at 16 Ma, based on the GPlates reconstruction of van de Lagemaat et al. (2021) in the paleomagnetic reference frame of Torsvik et al. (2012). Dashed black line is the Miocene ocean currents derived from Herold et al. (2012). For the location of all sites in the data compilation in A see Figure 1.

The data compilation (Figure 9A) shows a 7°C SST decrease between Site 696 (yellow dots, ~14°C, ±4°C) during the Miocene Climate Optimum (MCO, ~16.5 Ma) and Site U1536 (red, ~7°C, ±4°C) in the Middle Miocene Climate Transition (MMCT, ~14.7-13.8 Ma). Both sites were at comparable paleolatitudes during the Miocene. SSTs at Wilkes Land Site U1356 were warmer (17°C around 17 Ma) than at Site 696 (~14°C), even though Site U1356 were situated at a higher latitude (59°S) than Sites 696 and U1536 (~65°S). Additionally, a less pronounced cooling (SST ~16-12°C) occurred across the MMCT at Site U1356 (Sangiorgi et al., 2018), than the on average ~7°C cooling our South Atlantic low-resolution dataset show. Thus, the South Atlantic was colder at the onset of MMCT than the Wilkes Land Antarctic margin. There was a ~6-10°C temperature difference between the South Atlantic Antarctic proximal Sites 696/U1536 and the subantarctic Site 1171 (southwest Pacific Ocean), with clumped isotope (Δ_{47}) SSTs of 14-12°C and TEX_{86} SSTs of 18-13°C during MMCT (Leutert et al., 2020). This suggests a relatively strong SST gradient between the coldest Antarctic-proximal regions and the subantarctic zone in the Middle Miocene, but the subantarctic zone was likely at lower paleolatitudes in the Australian-Antarctic Gulf than in the South Atlantic due to the more southerly position of Australia. The alkenone-based SST reconstructions at Site 1088 and TEX_{86} -based SST reconstructions at Site 1168, together representing Subtropical front conditions, show MCO temperatures between 32-27°C that progressively cooled during the MMCT (~24-14°C) (Hou et al., in prep) albeit less than at the Antarctic-proximal sites, which indicate an amplification of cooling at high latitudes. The clumped isotope (Δ_{47}) BWT record from Site 747 in the South Indian Ocean (Leutert et al., 2021) shows strikingly similar temperatures to the reconstructed SSTs at Site U1536, which suggests that the Weddell Gyre was an important region of deep water formation in the Miocene, like today (e.g., Orsi et al., 1999), and in line with what modelling studies suggest for the Miocene (e.g., Herold et al., 2012). The 7°C Antarctic-proximal cooling between the MCO and MMCT occurs in a time of declining $p\text{CO}_2$ (Foster et al., 2012; Greenop et al., 2014) (Figure 10D) and increasing benthic foraminiferal $\delta^{18}\text{O}$ (Figure 9A), reflecting increasingly colder climate with larger, more permanent and stable ice sheets (Lewis et al., 2008; Shevenell et al., 2008; Holbourn et al., 2018; Levy et al., 2019). In this time interval, the South Atlantic Antarctic-proximal records respond sensitively to the $p\text{CO}_2$ -induced cooling.

The 3-5°C SST decrease at IODP Site U1536 between the MMCT (~14 Ma) and the Late Miocene (~5 Ma) is perhaps surprisingly small, compared to the ~10°C cooling at the subtropical front sites in the same time. We surmise that this high-latitude cooling was subdued in this time interval because southern South Atlantic surface waters were already cold during MMCT. It is the rest of the Southern Ocean that experienced pronounced cooling in this time interval; the South Atlantic was possibly already the coldest region of the Southern Ocean since at least the Middle Miocene. However, there is a strong lack Antarctic proximal records (e.g., no records from the Ross sea; Levy et al., 2019) from the MMCT to Late Miocene (partly because of the glacial advances) to draw a full picture of circum- Antarctic cooling since the MMCT.

Both Site U1536 and 747 show a lack of latest-MMCT – Late Miocene cooling in SST and BWT, respectively (Leutert et al., 2021). Leutert et al. (2021) attributed the lack of cooling to the growing Antarctic ice sheet which could have led to increased stratification and shielding of deeper waters in the Southern Ocean. We here conclude that the South Atlantic Antarctic-proximal regions already reached cold conditions in the Middle Miocene and as a result could not cool much further given the global climate of the middle Miocene. The cooling in the subtropics is in the same interval much more pronounced because of northward expansion of the cold subantarctic waters (Leutert

et al., 2020) as the Antarctic ice sheet expanded in the Late Miocene. This process likely also further promoted cooling in other sectors of the Antarctic-proximal Southern Ocean.

5.3 South Atlantic SST gradient evolution

Combining the two time slices yields a unique insight into the long-term temperature trends in the South Atlantic Ocean. The SST records from the South Atlantic region show unidirectional temperature drops ($\sim 8^\circ\text{C}$) across the Eocene-Oligocene transition (EOT), with some degree of polar amplification between Antarctic-proximal and subtropical front records. Yet, the strong, large and persistent South Atlantic Subpolar Gyre reduces the latitudinal SST gradient in the southernmost part of the South Atlantic. Subtropical front SST records remain relatively stable from the earliest Oligocene (32 Ma) until the Late Miocene (Figure 10), with minimal cooling. The increasing temperature gradient across the South Atlantic in the Middle Miocene is thereby largely driven by high latitude cooling, but also that is subdued due to the already cool conditions at MMCT times.

The cooling phases across the EOT and from the MCO to the MMCT represent two climatic transitional phases, both characterized by declining atmospheric $p\text{CO}_2$ concentrations (Pearson et al., 2009; Foster et al., 2012; Greenop et al., 2014; Steinthorsdottir et al., 2016) and increasing benthic foraminiferal $\delta^{18}\text{O}$ values (Westerhold et al., 2020), indicating deep-sea cooling and/or ice sheet expansion (Flower and Kennett, 1993; Zachos et al., 1996). The EOT marks the first installation of a continent-wide Antarctic ice sheet (DeConto and Pollard, 2003; Coxall et al., 2005), with a volume between 60 and 130% of that of the present day ice sheet (Bohaty et al., 2012). The MCO is considered a global warm phase, with warm-temperate ice proximal conditions (Sangiorgi et al., 2018) and profoundly reduced Antarctic ice volumes (Shevenell et al., 2008; Foster et al., 2012), and the MMCT a strong, stepwise transition towards a larger Antarctic ice sheet. Surprisingly, southern South Atlantic records (Sites 696 and U1536) suggest similar Antarctic-proximal SSTs ($\sim 12\text{--}14^\circ\text{C}$) for the early Oligocene, when a modern-like ice sheet was installed, as for the MCO, when ice sheets were profoundly reduced. This puts both climate phases into perspective: apparently the Oligocene Antarctic ice sheet could coexist with warm ice-proximal surface ocean conditions, while the Middle Miocene Antarctic ice sheet could be strongly reduced despite a relatively cold ice-proximal South Atlantic Ocean.

Reconstructing the Late Eocene-Late Miocene SST trends in the South Atlantic still leaves us with questions about the evolution of the oceanographic regime, specifically the timing of southward retraction of the Subpolar Gyre into the small Weddell Gyre of today, and the onset of throughflow of the ACC at Drake Passage. In Chapter 6 we will discuss in more detail how the South Atlantic SST trends relate to oceanographic changes by looking into organic walled dinoflagellate cyst assemblages reconstructing the surface paleoenvironmental conditions and migrations of frontal systems.

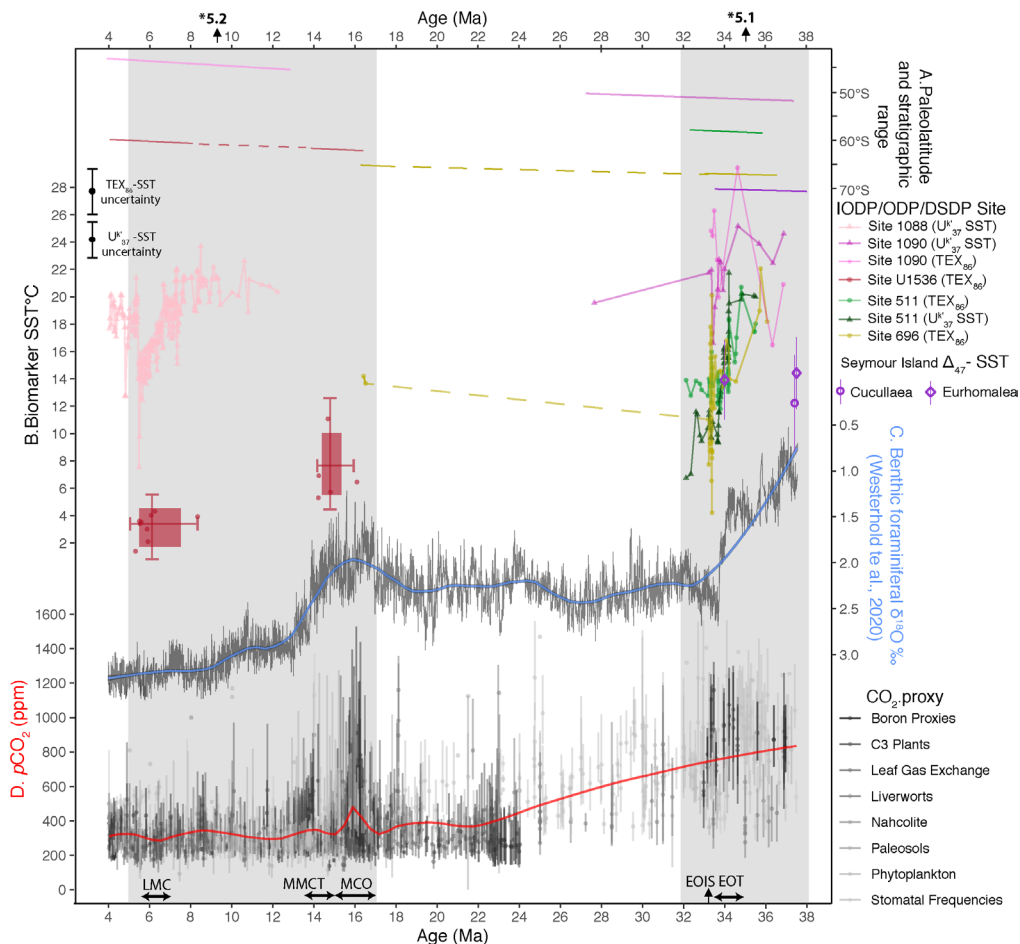


Figure 10. South Atlantic SST compilation. A. Paleolatitude evolution of sites presented in this study (see legend) (<http://www.paleolatitude.org>, version 2 by van Hinsbergen et al. (2015)). Stippled lines indicate hiatuses. B. The colored points and lines indicate the biomarker-based SST trends (see legend), excluding all samples with potential GDGT overprint (see section 3.2). TEX_{86} -SST data from Site 696 (yellow; this study). TEX_{86} -SST data from Site 1090 (dark pink; (Liu et al., 2009)). U^k_{37} -SST from Site 511 (blue; U^k_{37} , Houben et al., 2019). U^k_{37} -SST from 1088 (pink; Herbert et al. (2016)). The U^k_{37} index is converted to SST using the calibration of Müller et al. (1998), which has a standard error of $\sim 1.5^\circ C$ (Houben et al., 2019). TEX_{86} -SST from Site U1536 (red; this study). Clumped isotope (Δ_{47}) SST estimates from La Meseta Fm., Seymour Island (purple; (Douglas et al., 2014)). C. Benthic foraminiferal $\delta^{18}O$ compilation, with a locally weighted smooth over 20 kyr (black curve) (CENOGRID; Westerhold et al., 2020), and a LOESS smooth (blue; span = 0.2). D. Published paleo- CO_2 data (<https://www.paleo-co2.org>), with LOESS smooth (red; span = 0.2). LMC=Late Miocene Cooling, MCO=Miocene climatic optimum, EOIS=Early Oligocene oxygen isotope step, EOT=Eocene-Oligocene transition. The gray shaded areas indicate the time intervals we will discuss in sections 5.1 and 5.2. These sections are indicated at top of the figure.

6 Conclusions

Our records from IODP Site U1536 and ODP Site 696 have several profound implications for our understanding of the SST evolution of the South Atlantic Ocean, viz:

- The EOT in the South Atlantic is characterized by a comparatively small latitudinal SST gradient of ~5 degrees between the subtropical front and the western Weddell Sea.
- The SST decrease across the EOT was 4-6°C in the South Atlantic, with some polar amplification of cooling.
- We note the absence of a prominent increase in the SST gradient across the EOT, which we ascribe to the persistent gyral circulation, connecting all sites, and an absence of a strong throughflow through Drake Passage.
- South Atlantic Antarctic-proximal SSTs at the earliest Oligocene glaciation were similar to those of the warm MCO.
- The Weddell Sea experienced cold polar climates (SSTs of ~5°C) already at the onset of MMCT; This made it the coldest oceanic region around Antarctica and the likely region of deep water formation.
- Because the southern South Atlantic was already cold in the Middle Miocene, it experienced little cooling during the latter part of the Miocene. This is in contrast to lower latitudes and other sectors of the Southern Ocean, which experienced profound cooling due to northward expansion of the Southern Ocean frontal systems.

Supplementary Information Chapter 5

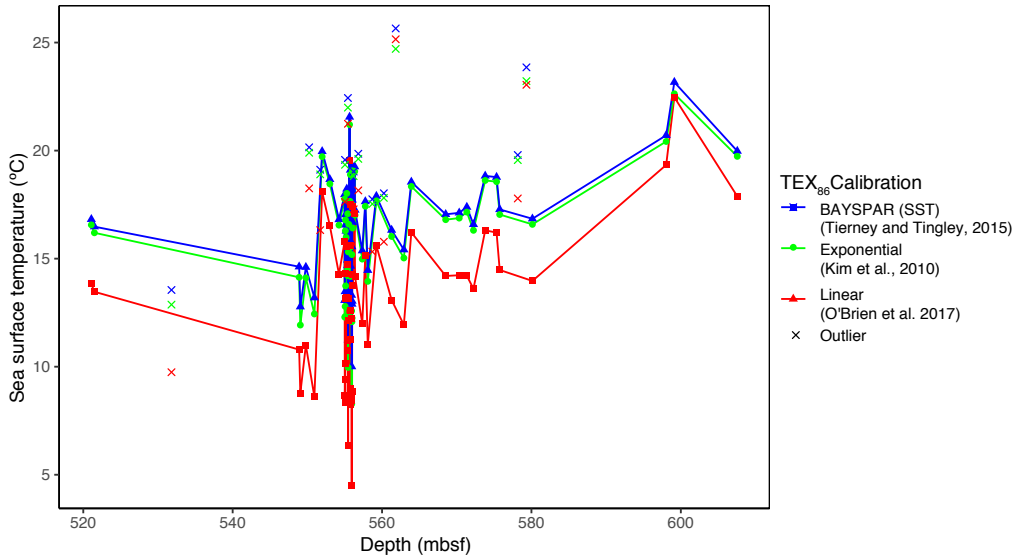
Supplementary Table 1. Site 696 age model as published in López-Quirós et al. (2021).

Event/ Characteristic	Kind	Lower level	Upper level	Mid- depth	Reference	Age (Ma)	Reference
<i>FAD Denticulopsis maccolummii</i> ;	Diatoms	50R-2W, 26-29	50R-1W, 88-92	52.49	*López- Quirós et al. (<i>in prep</i>)	16.5-16.7	Revised data by D. Harwood (base on <i>Denticulopsis maccolummii</i> and <i>Fragiliariopsis maleinterpretaria</i>), after Barker et al (1988); Gersonde and Burckle (1990)
<i>FAAD Actinocyclus ingens</i>	Diatoms	50R-2W, 26-29	50R-1W, 88-92	521.49	*López- Quirós et al. (<i>in prep</i>)	16.5-16.7	Revised data by D. Harwood, after Barker et al (1988); Gersonde and Burckle (1990)
<i>FO Invertocysta tabulata</i>	Dinocysts	51R-2W, 51-53	-	531.81	*López- Quirós et al. (<i>in prep</i>)	<23.5	Age from Frida Hoem (base on <i>Invertocysta tabulata</i>); Bijl et al. (2018)
<i>FO Chiropteridium Galea</i>	Dinocysts	53R-3W, 80	53R-2W, 130	552.20	Houben et al. 2012	<33.6	Pross et al. (2010)
<i>FO Malvinia escutiana</i>	Dinocysts	55R-1W, 117 cm	55R-1W, 62 cm	569.11	Houben et al. 2012; 2013	33.7	Houben et al. (2011)
<i>FO Stoveracysta kakanuiensis</i>	Dinocysts	55R-3W, 75 cm	55R-2W, 147 cm	571.55	Houben et al. 2012; 2013	34.1	Clowes (1985)
<i>FO Reticulofenestra oarnaruensis</i>	Calcareous nannofossils	58R-1W, 122 cm	57R-1W, 112 cm	593.57	Wei and Wise, 1990	~35.5	Villa et al. (2008)
<i>FCO Istmolithus recurvus</i>	Calcareous nannofossils	60R-1W, 36 cm	59R-CC	616.78	Wei and Wise, 1990	36.27	Villa et al. (2008)
<i>FO Reticulofenestra bisecta</i>	Calcareous nannofossils	62R-6W, 132 cm	-	643.62	Wei and Wise, 1990	<37.61	Villa et al. (2008)

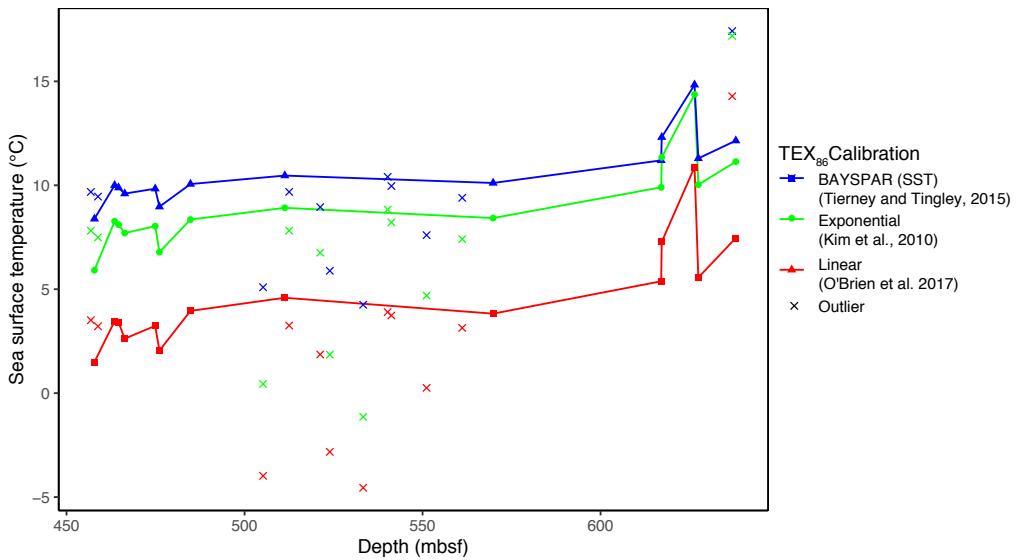
Supplementary Table 2. Biostratigraphic datums summarised for the depth of the stratigraphic discontinuities, with Sediment reflectors, see Pérez et al., 2021.

Supplementary Table 3. GDGT results Site 696 (available upon request)

Supplementary Table 4. GDGT results SiteU1536 (available upon request)



Supplementary Figure 1. Site 696 TEX₈₆ calibration comparison.



Supplementary Figure 2. Site U1536 TEX₈₆ calibration comparison.

Chapter 6

Late Cenozoic oceanographic evolution of the South Atlantic Ocean

Frida S. Hoem¹, Karlijn van den Broek¹, Adrián López-Quirós², Suzanna van de Lagemaat¹, Steven M. Bohaty³, Henk Brinkhuis^{1,4}, Francesca Sangiorgi¹, Peter K. Bijl¹

1. *Department of Earth Science, Utrecht University, Utrecht, the Netherlands*

2. *Department of Geoscience, Aarhus University, Aarhus C, Denmark*

3. *Institute of Earth Sciences, Heidelberg University, Heidelberg, Germany*

4. *Department of Ocean Systems research OCS, Royal Netherlands Institute for Sea Research (NIOZ), Texel, the Netherlands*

Abstract

From the Eocene (~50 Ma) to the present-day, the dominant mode of ocean circulation in the Southern Ocean transitioned from strong and large sub polar gyres to circumpolar circulation with a strong Antarctic Circumpolar Current (ACC) and complex ocean frontal systems. The removal of bathymetric and geographic obstructions allowing the birth of a cross-latitudinal band of open ocean water, and the cooling of polar climate with the onset of the Antarctic ice sheet, likely played a role in this transition. However, how the oceanographic evolution of the Southern Ocean developed is still largely unknown specifically because records of late Cenozoic South Atlantic Ocean are sparse. Our ability to reconstruct past Southern Ocean surface circulation and the varying latitudinal position of the frontal systems has increased over the past decade. Specifically, our increased understanding of the modern ecologic affinity of organic walled dinoflagellate cyst (dinocyst) assemblages from the Southern Ocean allowed us to improve the reconstruction of distinct oceanographic conditions (sea surface temperature, salinity, nutrients, sea ice) from downcore assemblages. Recent investigations in the South Indian and Pacific Ocean (Chapter 2-4) show warmer Oligocene conditions with weak frontal systems that started to strengthen and migrate northwards during the Late Oligocene. The Late Eocene-Late Miocene South Atlantic SST compilation (Chapter 5) showed the persistence of gyral circulation until the Early Oligocene and cooling high latitude conditions at the Middle Miocene Climatic Transition (MMCT). However, questions remain about the evolution of the frontal systems, presence of sea ice and the timing of southward retraction of the Subpolar Gyre into the small modern-like Weddell Gyre. To this end, we present new Late Eocene-Late Miocene dinocyst assemblage data from marine sediment drill cores in the southwestern South Atlantic (IODP Site U1536, ODP Site 696 and piston cores from Maurice Ewing Bank). We compare these to available Late Oligocene-Late Miocene southwestern South Atlantic dinocyst assemblage records and sea surface temperature (SST) reconstructions (Chapter 5). Late Oligocene-Late Miocene South Atlantic sees progressive retraction of the sub polar gyre and southward migration of the subtropical gyre, while the region progressively cools. Although the geographic coverage of data is sparse, the available data allows a first insight into the surface oceanographic evolution of the late Cenozoic South Atlantic Ocean.

1 Introduction

The Southern Ocean today is known for hosting the strongest surface current of the World, the mainly wind-driven, eastward flowing Antarctic Circumpolar Current (ACC, connecting the Pacific, Indian and Atlantic Oceans (Orsi et al., 1995). The system is further characterized by a strong Southern Ocean latitudinal temperature gradient, and associated changes in oceanographic conditions concentrated in a plexus of five frontal systems, viz the Subtropical Front (STF), the Subantarctic Front (SAF), the Polar Front (PF), the Southern ACC Front (sACCf), and the Southern Boundary (sBdy) Front (e.g., Orsi et al., 1995) (Figure 1). In the early Cenozoic, the ocean circulation was likely dominated by two large sub polar gyres (Huber et al., 2004; Bijl et al., 2011; Sijp et al., 2014; Sijp et al., 2016). Through the late Cenozoic the gyral circulation broke down as deep-water throughflow was made possible through open (and later deep) Southern Ocean gateways (Sauermlch et al., 2021) that eventually evolved into the vigorous ACC system of the present-day. While Stickley et al. (2004) showed that the Tasmanian Gateway opened to deep oceanic circulation between 35.5 and 33.5 Ma, and further widened between 33 and 30 Ma, questions remain to what extent the Australian continent formed a physical obstruction for strong circumpolar flow (Hill et al., 2013; Sauermlch et al., 2021). The evolution of the 'other' gateway, i.e. the timing and nature of opening, widening and deepening of Drake Passage is however still much debated, ranging from 41 Myrs (Scher and Martin, 2006) to 6 Myrs ago (Barker et al., 2007). A more recent, kinematic reconstruction of Drake Passage suggested a first deep ocean connection around 26 Ma (van de Lagemaat et al., 2021). A high-resolution ocean model by Sauermlch et al. (2021) demonstrated that as this second of two Southern Ocean gateways deepens to below 300 m water depth, high southern latitude surface waters would progressively cool, because throughflow of even a weak proto-ACC would break down the subtropical gyre circulation in the South Pacific and Indian-Atlantic oceans. Indeed, SSTs from the Wilkes Land Antarctic Margin started to cool in the Late Oligocene (~26 Ma) (Hartman et al., 2018), consistent with the onset of the deeper connection in Drake Passage (van de Lagemaat et al. 2021), and gyre circulation seems disrupted in the Southern Pacific with the widening of the Tasmanian Gateway (Houben et al., 2019) around the Eocene-Oligocene Transition (EOT). However, such a reconstruction of the oceanographic evolution of the South Atlantic subpolar gyre is thus far lacking.

In absence of calcareous, and often even siliceous, biotic remains, recent studies from the South Pacific and South Indian Ocean have successfully utilized the organic components preserved in the Southern Ocean sedimentary archives. Notably the remains of dinoflagellates (their organic cysts) and molecular organic geochemical analysis are employed to reconstruct the Oligocene-Miocene evolution of oceanic conditions, temperature gradients and positions of frontal systems in the Southern Ocean (Lyle et al., 2007; Houben et al., 2013; Scher et al., 2015; Bijl et al., 2018b; Hartman et al., 2018; Sangiorgi et al., 2018; Evangelinos et al., 2020; Chapter 2-3).

The Oligocene records of IODP Site U1356 offshore Wilkes Land (Bijl et al., 2018; Hartman et al., 2018;) and DSDP Site 274 offshore Ross Sea (Chapter 2) show surprisingly warm (10–21°C) SSTs and dinocyst assemblages of oligotrophic, open ocean and temperate conditions in the vicinity of the (East) Antarctic Ice Sheets. Across the Australian-Antarctic Gulf, Oligocene SST records show a small temperature gradient between the subtropical front (Site 1168) and the Antarctic Margin (Site U1356). This SST gradient increased from ~26 Ma onwards, due to cooling of the Antarctic-proximal SSTs (Chapter 4), while SSTs south of Australia remained warm. Early-to Middle Miocene warmth was followed by a gradual but profound 10°C cooling in the Middle to Late Miocene (Herbert et al., 2016; Hou et al., in prep). Yet, although a few records depicting

surface oceanographic conditions from the South Atlantic across the Eocene-Oligocene Transition (EOT) exist (Plancq et al., 2014; Houben et al., 2019), Oligocene and Miocene records from the South Atlantic are still lacking. In Chapter 5 we used organic biomarkers (TEX₈₆) to reconstruct the Late Eocene-Early Oligocene and Middle-Late Miocene SST gradient in the South Atlantic, but questions remain about the development and position of ocean frontal systems. Oceanic fronts are characterized by marked gradients in ocean conditions like temperature, nutrients and/or salinity (e.g., Orsi et al., 1995; Olbers et al., 2004). Studying dinocyst assemblages allows tracing of past positions of oceanic fronts and ocean dynamics. The reconstructions use established relationships between modern dinocysts from core-top sediments and environmental conditions in the upper surface waters like temperature, nutrients, upwelling intensity and sea ice (Prebble et al., 2013; Zonneveld et al., 2013; Thole et al., in prep). These studies have now started to show characteristic dinocyst assemblages for specific zones in the modern Southern Ocean. Many modern dinocysts have long lineages in the Southern Ocean (Bijl, 2022), dating back to the Oligocene. We assume that ecological affinities of modern and older species are the same or similar, although some species have shown variability in their ecological affinities (De Schepper et al., 2011). Dinocyst assemblages in the Southern Ocean have been successfully applied to reconstruct past ocean conditions, especially in the context of multi-proxy approaches (e.g., Bijl et al., 2018; Hartman et al., 2018; Salabarnada et al., 2018; Chapter 2-4).

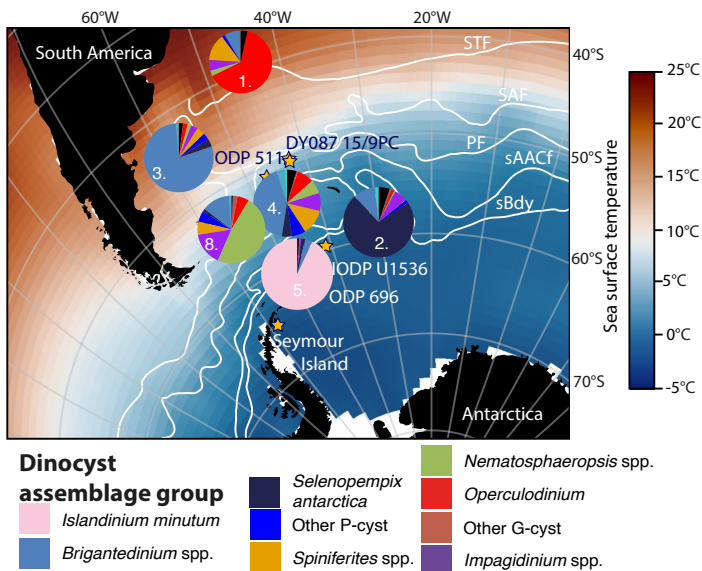


Figure 1. Modern distribution of dinocysts in surface sediments in the Southwest Atlantic. The map is generated through Gplates freeware (www.gplates.org; version 2; last access December 20th, 2021), based on the global plate geodynamic motion model from Müller et al. (2018). Black areas outline the coastlines. The colors in the map show the average January SSTs from 1971-2000 (Reynolds et al., 2002). The white lines are the smooth, continuous, circumpolar fronts interpreted by Orsi et al. (1995). The fronts are, north to south, the Subtropical front (STF); the Subantarctic front (SAF); the Polar Front (PF); the southern ACC Front (sACCf); and the Southern Boundary (SBdy) front. The pie charts show the present-day South Atlantic dinocyst assemblage distribution, derived from surface ocean data compiled by Lena Thöle. The numbers correspond to the present-day assemblage clusters as in Thole et al. (in review).

Here, to elucidate the late Cenozoic oceanographic evolution of the South Atlantic region we study the dinocyst assemblages in sediment cores from the Scotia Sea (ODP Site 696, IODP Site U1536) and piston cores obtained during a survey expedition in 2018 (DY087 15PC and 09PC) at Maurice Ewing Bank (stars in Figure 1). In conjunction with organic paleothermometry (TEX_{86}) for sea surface temperatures (see from Chapter 5), we aim to reconstruct the surface ocean properties including the lateral position of fronts and gyres, to identify the role of the deepening of the Drake Passage, the climatic cooling and the glacial expansions on the South Atlantic oceanography in the Late Eocene-Late Miocene.

2 Material

2.1 DY087 piston cores

We study sediments from two piston cores collected from the southeastern flank of Maurice Ewing Bank (MEB), Southwest Atlantic Ocean, recovered on the RRS Discovery cruise DY087 (January 2018); Site 09PC (3.36 m) at $50^{\circ}17.18'S$ $42^{\circ}27.32'W$, water depth of 1351 m, and Site 15PC, (2.39 m) at $50^{\circ}11.60'S$ $42^{\circ}32.72'W$ from a water depth of 1430 m. In the modern ocean, Circumpolar Deep Water sweeps across the shallower areas of the MEB (~ 500 - 3000 m) and northwards along the base of the eastern slope of MEB. Consequently, sea floor sediments of MEB are eroding, exposing Miocene and older strata. The seismic (Figure 2A) and piston coring data (Bohaty unpub. data) indicates that sediment deposition was influenced by bottom currents since the Oligocene, in the form of various packages of drift deposits that have non-conformable erosive bases.

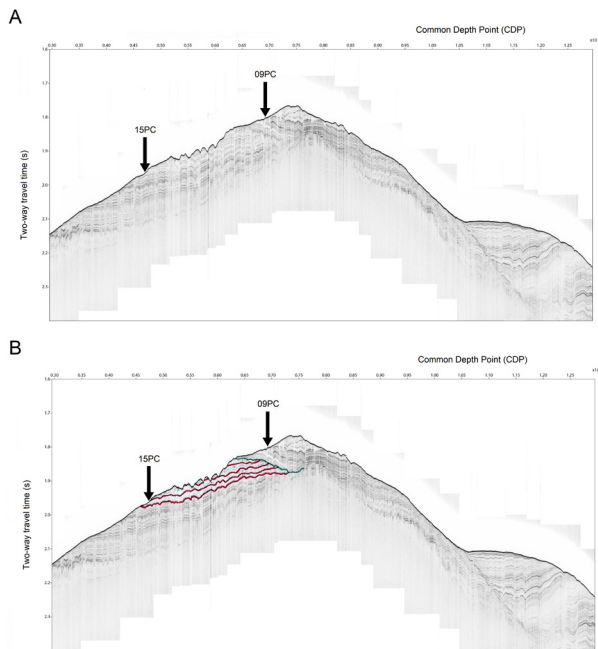


Figure 2. Cruise DY087 seismic reflection data line L20A. (A) original reflection data. (B) interpretation 15PC and 09PC, respectively (modified from Bohaty, unpub. data).

The various packages reflect changes in the mode of ocean currents in the region. The interpretation of these seismic lines is a subject of a parallel study and will not be further discussed here. The interpreted seismic reflection data of line L20A (Figure 2B) suggests the facies units at 15PC (red) do not continue onwards to 09PC but are non-conformably overlain by a younger facies unit (green). The initial age model of both piston cores, based on diatoms (Table 1), confirms an Early Miocene age for 09PC and Late Oligocene age for 15PC, with a veneer of younger material at the top (Bohaty unpub. data).

Table 1. Ages of piston cores DY087-09PC and -15PC.

09PC	15PC
Early Pleistocene 2.3-1.3 Ma (8 cm)	Pleistocene <2.3 Ma (27 cm)
Early Miocene 20.8-17.4 Ma (220 cm)	Late Pliocene to earliest Pleistocene 3.2-2.2 Ma (52 cm)
	Late Oligocene to earliest Miocene 26.4-22.7 Ma (64 cm, 113 cm, 122 cm)

For age model and core description for Site 696 and U1536 see Chapter 5, section 2.1.1 and section 2.1.2 respectively.

3 Methods

3.1 Palynological processing and analysis

Palynological processing follows standard procedures at GeoLab, Utrecht University, as described in Chapter 2. In short, processing involves digestion of 10-15 g dried sediment with added *Lycopodium clavatum* spores ($n = 9666 \pm 213$) using cold hydrochloric and hydrofluoric acid. The palynological residues are sieved through a 10 μm nylon mesh, aided by an ultrasonic bath and mounted glass slides using glycerine jelly, sealed with nail varnish and counted (under 400 \times magnification) using a transmitted light optical microscope. Dinocyst taxonomy follows Williams et al. (2017), Clowes et al. (2016) and informal species as presented in Bijl et al. (2018a).

3.2 Ecological affinities of dinocyst species

Dinocysts are increasingly and successfully used as a proxy for paleoceanographic reconstructions in the Southern Ocean (Houben et al., 2013; Guerstein et al., 2014; Clowes et al., 2016; Warny et al., 2016; Bijl et al., 2018b; Sangiorgi et al., 2018; Chapter 2-3). The pairing of assemblage studies in modern sediment samples to upper water conditions provides us this a wealth of information on the modern dinocyst ecology (e.g., Prebble et al., 2013; Zonneveld et al., 2013; Marret et al., 2020). Dinocyst distribution in the present ocean is controlled by various factors, mainly surface water temperature, but also nutrient availability, salinity, bottom water oxygen, sea ice and transport by surface to deep ocean currents (Dale, 1996; de Vernal et al., 1997; Prebble et al., 2013; Zonneveld et al., 2013). Most modern Antarctic dinocysts belong to either the gonyaulacoid (G) or the proteroperidinioid (P) dinoflagellates. P-cysts are today produced by heterotrophic dinoflagellates and are mostly found in and below nutrient-rich environments like river plumes, upwelling areas and sea ice zones (Zonneveld et al., 2013). They currently dominate the southern high latitude dinocyst assemblages south of the Subantarctic Front (Zonneveld et al., 2013), while the cysts produced by phototrophic and mixotrophic G-taxa dominate in temperate waters in a broad range of trophic

conditions, but are rare to absent in close proximity to the Antarctic ice sheet and where sea-ice is present throughout most of the year (Prebble et al., 2013). Today, a pronounced latitudinal separation of dinocyst assemblages exists across the Southern Atlantic (Esper and Zonneveld, 2002; Prebble et al., 2013; Marret et al., 2020; Thole et al., in prep.) (Figure 1). Dinocyst biogeographic distribution thus markedly changes across present-day oceanic fronts, making dinocysts promising tracers of past frontal systems movement. Surface samples from south of the Subantarctic Front (SAF), where mixing and upwelling of cold, nutrient-rich waters and strong seasonality in sea-ice cover occur, have assemblages overwhelmingly dominated by heterotrophic taxa producing P-cysts (Figure 1). Interestingly, surface samples around the Antarctic Peninsula in the South Atlantic are dominated by *Islandinium* spp., indicative of cold freshwater associated with iceberg discharge and melting (Cluster 5; Head et al., 2001; Thole et al., in prep.). In the south Scotia Sea, at the Southern Boundary (SBdy) front, assemblages are dominated by sea ice affiliated dinocyst *Selenopemphix antarctica* (Cluster 2; Zonneveld et al., 2013; Marret et al., 2020). South of the Polar Frontal (PF) assemblages contain abundant *Brigantedinium* spp., produced by heterotrophic taxa which indicates nutrient-rich waters due to mixing and upwelling (Cluster 4), but not necessarily influenced by sea ice, as well as common open ocean cosmopolitan species. *Nematosphaeropsis labyrinthus*, is typical for modern Subantarctic front zone conditions (Cluster 8), between SAF and Subtropical Front (STF). At the South American eastern margin, surface samples are dominated by *Brigantedinium* spp., indicating mixing and upwelling close and potentially high nutrient input from eastern South America (Cluster 3). In the open ocean, warmer water setting north of the STF are surface samples dominated by autotrophic cosmopolitan gonyaulacoid-derived species *Operculodinium* spp., accompanied by *Spiniferites* spp. (Cluster 1) and *Pyxidinosia* spp. Several *Impagidinium* species (*Impagidinium velorum*, *Impagidinium patulum*, and *Impagidinium aculeatum*) are also found in locations north of the STF. These species are the cysts of taxa thriving in open ocean, low productivity/oligotrophic environments and especially *Impagidinium aculeatum* reflects a warm-water species (Zonneveld et al., 2013).

With the assumption that the habitat affinities and feeding strategies of extant dinoflagellate species are similar in the past, we employ dinocyst assemblages as a paleoenvironmental proxy. Relative abundances of extinct dinocyst taxa have been compared against independent assessment of paleoecological conditions, using co-occurrence of extinct species with those for which the ecological information is still available, such as modern species (e.g., Schreck and Matthiessen, 2013), or in comparison to other palaeoceanographic proxies for temperature, runoff/freshwater input and nutrient conditions (Bijl et al., 2011; De Schepper et al., 2011; Frieling and Sluijs, 2018). A distinct group of dinocyst taxa, among which species of the now extinct P-cyst genera *Spinidinium* spp. and *Vozzhennikovia* spp. have an endemic Antarctic distribution in the Eocene (Bijl et al., 2011). These “Antarctic endemic taxa” track Antarctica-derived surface currents, while cosmopolitan dinocysts track currents sourced from low latitudes (Huber et al., 2004; Warnaar et al., 2009; Bijl et al., 2011; 2013). High abundances of extinct cosmopolitan species of *Phthanoperidinium* are usually associated with low-salinity, coastal and upwelling zones with high nutrient supply (Barke et al., 2011; Frieling and Sluijs, 2018). Remarkably the dominance of Antarctic endemic taxa in the Paleogene Southern Ocean became abruptly replaced by dinocyst assemblages similar to present-day in the earliest Oligocene (Houben et al., 2013; 2019).

4 Results

4.1 Age constraints

4.1.1 DY087

The two most important species for age constraints in sediments from Site 15PC (Figure 8) are *Invertocysta tabulata* and *Gelatia inflata*. The uppermost sample (100-105 cm) has a different palynological assemblage than the samples below. *Invertocysta tabulata* has only been identified in this sample, whereas *Gelatia inflata* has been identified in all samples except the uppermost sample. As *Gelatia inflata* has a biostratigraphic range of 33.7-23.8 Ma and *Invertocysta tabulata* a range of 23.6-16.5 Ma, the interval between these samples would have an age of ~23.7 Ma. Therefore, we refer to most of 15PC (120-234 cm) as having a Late Oligocene age, except one sample at 103 cm, which could have an earliest Miocene age (<23.03 Ma). The rest of the dinocyst assemblage is in support of that age.

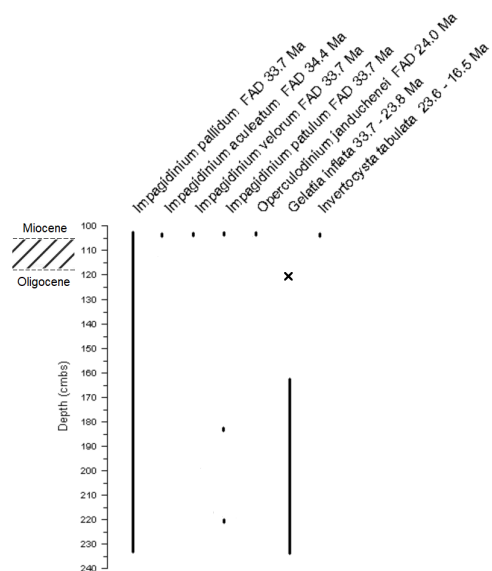


Figure 3. Stratigraphic range chart 15PC.

Dinocyst assemblages provided no additional age constraints to those provided from the diatoms at Site 09PC. The piston cores most likely represent short time intervals within the age constraints of the diatom ages (Table 1). Because of this we refer to Site 09PC (interval 63-310 cm) as Early Miocene (20.8-17.4 Ma).

4.2 Organic-walled dinoflagellate cyst assemblages

4.2.1 DY087-15PC

Dinocyst assemblages at DY087-15PC (Figure 4) are dominated by G-cysts; predominantly by *Operculodinium centrocarpum* (up to 91%) with minor contributions of *Gelatia inflata* and only rare *Nematosphaeropsis labyrinthus*. In the uppermost sample of the core (100-105 cm), the diversity is much higher, with relatively high abundances of *Nematosphaeropsis labyrinthus* (26.6%), *Impagidinium velorum* (17.9%) and *Impagidinium pallidum* (17.0%), together with minor contributions of *Operculodinium centrocarpum* and *Operculodinium janduchenei*. Due to the uncertain age of the single uppermost sample (<23 Ma), we exclude this sample from further interpretation.

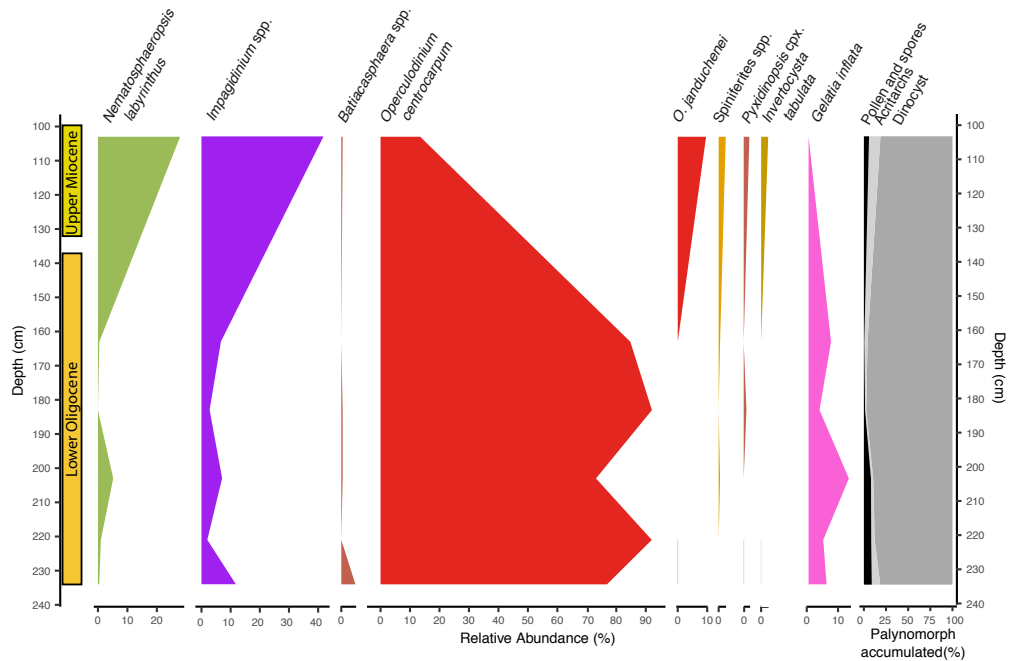


Figure 4. DY087-15PC: Relative abundances of dinocyst eco-groups (%), palynomorph relative abundance (acritarchs, dinocysts and terrestrial palynomorphs) (%).

4.2.2 DY087- 09PC

The dinocyst assemblages consist exclusively of G-cysts (Figure 5) and resemble those of the uppermost sample at DY087-15PC. The diversity is relatively high (14 species). *Nematosphaeropsis labyrinthus* is dominating the assemblages up to 68.9% with minor contributors from *Impagidinium pallidum*, *Impagidinium velorum*, *Operculodinium janduchenei* and *Operculodinium centrocarpum*.

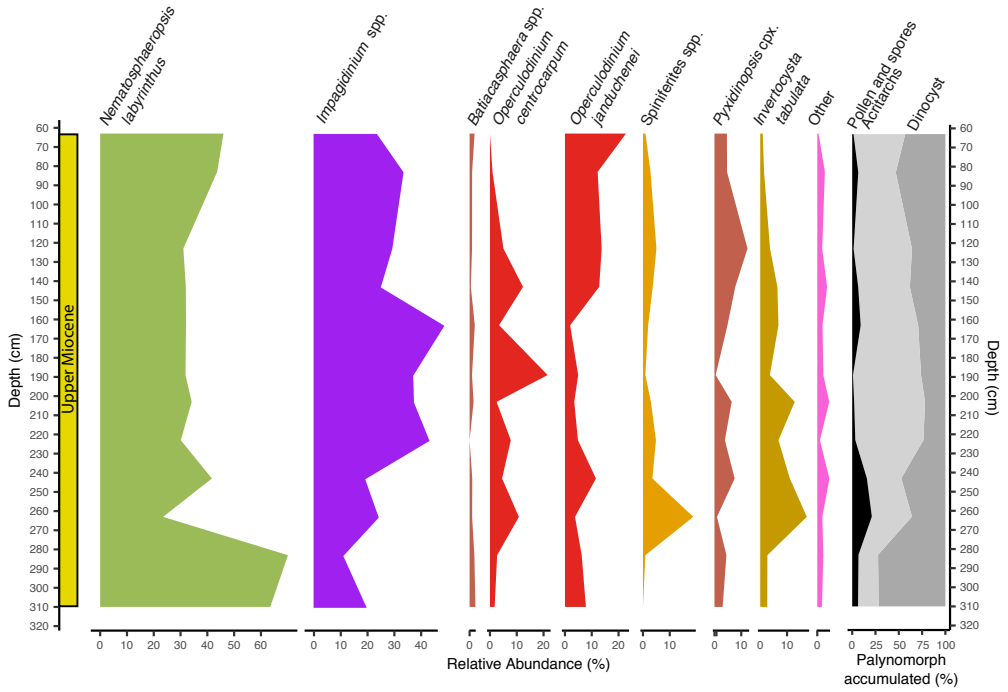


Figure 5. DY087-09PC: Relative abundances of dinocyst eco-groups (%) and palynomorph relative abundance (Pollen and spores, acritarchs and dinocysts) (%).

4.2.3 ODP Site 696

We processed 13 additional samples from 540-520 mbsf (Cores 52-50R) for palynological investigations, in order to extend the dinocyst record of Houben et al. (2019) further into the Oligocene. Three samples from 549-531 mbsf (Core 52 and 51R) contain but a few dinocysts. The preservation of organic matter is poor, and the few dinocysts encountered are mostly typical Eocene species, viz *Areosphaeridium diktyoplokum*, *Senegalinum* spp., and *Vozzhennikovia* spp., besides the ubiquitous long ranging *Brigantedinium* spp. Furthermore, given the presence of the rhythmically interbedded sandy mudstones with glauconite-bearing sandstone beds (López-Quirós et al., 2021) we assume this interval to likely contain reworked material. Therefore, we excluded these three samples from Core 50-52R from further interpretation (Figure 7). Five samples from 531-520 mbsf (Core 50R), estimated age of ~16.5 Ma (Diatom based, López-Quirós et al., in prep), contain abundant, well preserved, and diverse dinocysts. All samples are dominated by *Brigantedinium* spp., but in the topmost samples we note abundant G-cysts; *Nematosphaeropsis*, *Pyxidinoopsis* and *Operculodinium*. This new data extends the published record of Houben et al. (2019) into the Oligocene-Miocene.

4.2.4 IODP Site U1536

Quantitative analysis at Site U1536 was not achieved due to the low number of palynomorphs present. Therefore, we combine our limited observations with the shipboard analysis (Weber et al., 2021), and offer only a general overview of the dinocyst assemblages present for the Middle and Late Miocene interval (Supplementary Table 1). The palynomorphs detected in the interval (638-462 mbsf, mid-Late Miocene) predominantly consist of P-cysts; *Brigantedinium* spp., *Selenopemphix antarctica* and *Lejeunecysta* spp. This indicates that the low abundance of dinocysts is not due to lack of preservation in the sediment, as P-cysts are generally more sensitive to oxic bottom conditions than autotrophic dinoflagellates producing G-cysts (Zonneveld et al., 2010), but rather that the low presence of dinocysts is due to high sediment accumulation. There is an apparent change in the assemblages below 609 mbsf, with the disappearance of *Impagidinium* spp. and abundant *Lejeunecysta* spp.

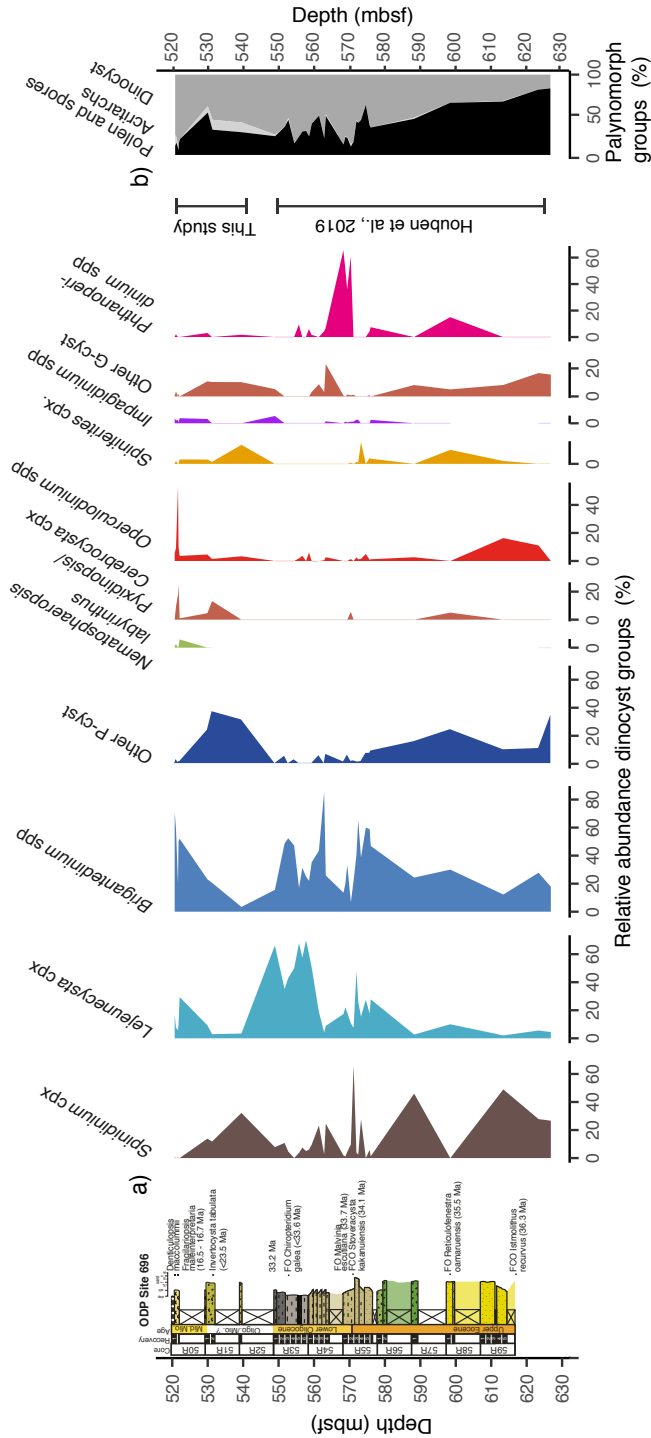


Figure 6. Polynormorphs at Site 696. a) relative abundance of dinocyst assemblage groups from Houben et al. (2019) and this study. The group named “Other P-cysts” consist of *Areosphaeridium* spp., *Senegalinium* spp., *Alterbidinium* spp. and *Achomosphaera*. b) stacked relative abundance of pollen and spores (Black), *Acritarchs* (light grey) and dinocysts (dark grey).

5 Discussion

5.1 Late Eocene-Late Miocene paleoceanographic changes

We compare our dinocyst assemblages from Sites 696, U1536 and DY087- 09/15PC, with existing dinocyst records from southern South Atlantic DSDP Site 511 and ODP Site 696 (Houben et al., 2019), Seymour Island (Douglas et al., 2014) and South American sites; Rio Los Palos (Bijl et al., 2021), Rio Turbio (Guerstein et al., 2014) and Monte León Formation (Parras et al., 2020), in order to develop a better picture of the South Atlantic based paleoceanographic evolution and migration of frontal systems.

During the latest Eocene (35-33.7 Ma), in the southernmost South Atlantic at Seymour Island dinocyst assemblages are dominated by freshwater- affiliated *Phthanoperidinium* spp., which indicate high rates of runoff (Douglas et al., 2014). Temperate SSTs (14-17°C) just northeast of the Antarctic Peninsula could sustain high precipitation rates in the hinterland, with drainage routes into the Weddell Sea region. At Site 696, Paleogene Antarctic endemic taxa such as *Vozzhennikovia* spp. and *Spinidinium* spp. are dominating the assemblage data together with high abundances of *Deflandrea antarctica*, *Senegalinium* spp., and P-cysts, suggesting high nutrients and fresh-water input (Houben et al., 2013). Similarly, at Site 511, Paleogene Antarctic endemic, predominantly peridinioid taxa are dominant (Houben et al., 2019). This similarity suggests that the subpolar gyre brought Antarctic-derived surface waters across both sites in the southwest Atlantic and extended relatively far north (Figure 7a). The abundant Paleogene Antarctic endemic dinocysts in the South American margin locations Rio Turbio (Guerstein et al., 2014) and Rio Los Palos (Bijl et al., 2021) also indicate that the ocean currents brought Antarctic derived surface waters northwards along the eastern South American margin. Our interpretation of a strong, persistent and large subpolar gyre is consistent with model simulations under closed (England et al., 2017), or shallow gateway configurations (Sauermilch et al., 2021), although some models already show an effect of high-latitude cooling under shallow open gateway configurations (e.g., Sijp and England, 2004; Toumoulin et al., 2020; Kennedy et al., 2015; Kennedy-Asser et al., 2019). Although such strong gyres must have prevented poleward transport of heat (Huber and Nof, 2006), the gyre itself is an effective transport mechanism bringing warm-temperate surface waters from the subtropical front to Antarctica. Indeed, a breakdown of such a gyre, e.g., invoked by the opening of Drake Passage, would cause profound cooling of the Antarctic Margin (Sauermilch et al., 2021; Chapter 4). The dinocyst assemblages of the Oligocene will indeed show whether the South Atlantic subpolar gyre broke down around EOT times.

However, the earliest Oligocene (33.7-32 Ma) dinocyst assemblages of the South Atlantic show a continuation of the subpolar gyre. In the Early Oligocene the Paleogene Antarctic endemic taxa were replaced by protoperidiniacean taxa at Site 696, showing increase in upwelling/mixing and higher nutrient availability in the surface waters. Following the EOT (33.7 Ma) there is an interval of high abundance of *Phthanoperidinium* spp. (Figure 6) suggesting significant freshwater input following the onset of Antarctic glaciation. The shift in dinocyst assemblage at DSDP Site 511, from relatively abundant Paleogene Antarctic endemic and protoperidiniacean taxa, to typically offshore cosmopolitan Gonyaulacoid taxa (Houben et al., 2019) suggests more oligotrophic conditions. There is a strong increase in the nutrient gradient between Site 696 and 511 across the EOT, and this suggests intensified deep ocean circulation (Houben et al., 2019), or latitudinal shifts in the region of upwelling. However, although cooling across the EOT is consistent with declining $p\text{CO}_2$ (Anagnostou et al., 2016), the difference in SSTs at both sites across EOT remains stable (Chapter 5). The lack of an increase in SST gradient across EOT suggests that both Sites 696 and 511 remained

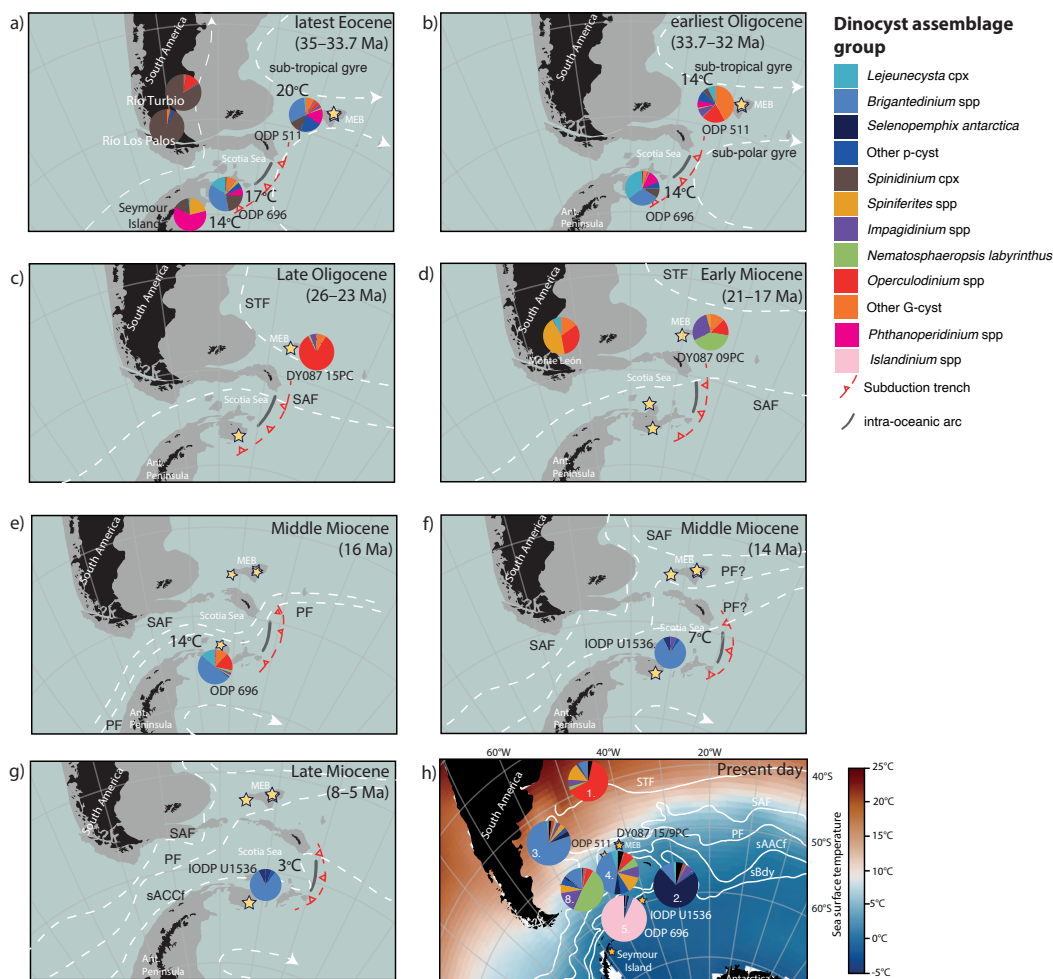


Figure 7. a-h) (Paleo)geographic maps for the southwest Atlantic (Gplates; version 2, www.gplates.org; last access December 20th, 2021), based on the global plate geodynamic motion model from Müller et al. (2018). The respective age of the maps is; 35, 32, 26, 19, 16, 14, 6 Ma and present day. Black outline represents present-day coastlines. Grey outline corresponds to present-day 2000 m water depth. The stars represent the paleogeographic location of the ocean drill sites discussed in the paper. The pie-charts in the Present-day chart present the average abundance of the different dinocyst assemblage groups listed in the legend. Dinocyst assemblage data comes from DSDP Site 511 and ODP 696 (Houben et al., 2019) (the Early Oligocene data from Site 696; this study), Seymour Island (Douglas et al., 2014), and South American sites; Rio Los Palos (Bijl et al., 2021), Rio Turbio (Guerstein et al., 2014), Monte León Formation (Parras et al., 2020), DY087-15/09PC and IODP Site U1536 (this study). The data can be found in Supplementary Table 1. The ocean circulation patterns (dashed white lines) is based on model simulations by (Sauermilch et al., 2021) (EOT) and Herold et al., 2012 (Miocene) in combination with interpretations from this study. e) same as Figure 1, added for reference to present day.

under the same oceanographic regime, and that the Antarctic ice sheet formation did not cause an increase in SST gradient between these sites. It also implies that throughflow across Drake Passage did not change across the EOT, in contrast to what modeling results and geologic data suggested earlier (Sauermilch et al., 2021). We therefore infer that the subpolar gyre was still persistent but positioned slightly more to the south in the earliest Oligocene (Figure 7b).

For the Late Oligocene (26.4–23 Ma), there are but a few suitable sites to employ for paleoceanographic reconstructions. However, the dominance of *Operculodinium* spp. at Maurice Ewing Bank (MEB) (DY087 15PC) (>80%), with a relatively minor presence of *Gelatia inflata* (named “other G-cysts” in Figure 7c), *Impagidinium* and *Nematosphaeropsis* suggests that the Subtropical Front (STF) was south of the site. Moreover, we lack dinocysts indicative of sea ice proximity that have been linked to the Subantarctic Front (SAF) and Polar Front (PF) (Prebble et al., 2013). Ocean models by Sauermilch et al. (2021) suggests that as the second Southern Ocean gateway deepens, even a weak proto-ACC penetrating through the deeper gateway would weaken the strength of the subpolar gyre. A weaker sub polar gyre would transport less water masses northward and thereby causing surface water cooling at the Antarctic margin. The tectonic reconstruction from van de Lagemaat et al. (2021) suggests that this happened around 26 Ma, with the first deep connections of the isolated ocean basins in the Scotia Sea. The single consequence of this tectonic change that we can infer from the dinocyst data is a southward shift of the STF, which may be associated to a weakening of the subpolar gyre as a result of Drake Passage throughflow. A better geographical spread of dinocyst records around the Scotia Sea is needed to confirm this.

Interestingly, by the Early Miocene (20.8–17.4 Ma), the dominance of *Nematosphaeropsis labyrinthus* at MEB suggests that the STF had migrated northwards. Unfortunately, we do not have any SST reconstructions from the Early Miocene to confirm our inferences from the dinocysts. In the paleogeographic reconstructions we see that the Scotia Sea banks are starting to break up (van de Lagemaat et al., 2021), which would allow for more throughflow of the ACC. We suggest this stronger throughflow across the Scotia Sea Basin would force a STF to migrate north of the MEB, as is reflected in the change in the dinocyst assemblages between the Late Oligocene and the Early Miocene.

In the Middle Miocene (~16 Ma), the high abundance of P-cysts suggests Site 696 was located south of the PF. However, the relatively high SSTs, and the common occurrence of temperate dinocysts *Operculodinium* spp. and *Nematosphaeropsis labyrinthus* and cosmopolitan species *Spiniferites* spp. suggest that the SAF was in the vicinity of the site in the Middle Miocene. The SAF was likely located south in the Scotia Sea until at least 16 Ma, based on the relatively large amount (35%) temperate G-cysts. The Miocene Climatic Optimum (MCO, ~17–14 Ma) represents a warming phase during which the Antarctic ice sheets partly melted (Shevenell et al., 2008; Foster et al., 2012). The high atmospheric $p\text{CO}_2$, intensification and poleward shift of the westerlies (Toggweiler, 2009) could potentially have moved frontal systems closer to Antarctica. Alternatively, the tectonic configuration of Drake Passage could have routed these fronts closer to Antarctica than today.

The temperate dinocysts present in the MCO sequences at Site U1536 were abundantly replaced by high-nutrient-loving *Brigantedinium* spp., and the sea-ice indicator *Selenopemphix antarctica* at ~14 Ma during the Middle Miocene climate transition (MMCT). The major change in dinocyst assemblages co-occurred with an average cooling from 14°C to 7–5°C in the TEX_{86} SST record (Chapter 5), indicating that SAF had migrated northwards. A similar shift in surface water fauna is recorded at Kerguelen plateau at 13.8 Ma from warm water to polar affiliated planktonic foraminiferal assemblages (Verducci et al., 2009), attributed to a northward migration of the PF

across the Kerguelen plateau. The loss of temperate dinocysts together with decreasing SSTs, is consistent with a drop in atmospheric $p\text{CO}_2$ (below 300 ppm; Badger et al., 2013) and coincident with a large 1.5‰ increase in benthic foraminifera $\delta^{18}\text{O}$ between ~13.9 and 13.8 Ma (Shevenell et al., 2008; Leutert et al., 2020), indicating global cooling conditions and/or increasing ice volume. Erosional disconformities dominated the Ross Sea (and continental shelf) drill core records through the MMCT (McKay et al., 2016; Levy et al., 2016, 2019) indicating there was a rapid glacial expansion to near-modern volume (Holbourn et al., 2005). Model experiments attribute the expanding Antarctic ice sheets to reduction of atmospheric CO_2 (Langebroek et al., 2009; DeConto and Pollard, 2016; Levy et al., 2016). We observe at ~14 Ma for the first time in our dinocyst records, the sea ice affiliated *Selenopemphix antarctica* (albeit in relatively low numbers) suggesting expansion of sea ice out of the Weddell Sea. The change to present day like dinocyst occurred earlier in the South Atlantic at Site U1536 than South Indian Ocean, Wilkes Land sector (Site U1356), which had abundant G-cysts until at least 11 Ma. This is also consistent with Chapter 5 which show cooling first occurred in the South Atlantic. However, unlike Wilkes Land Site U1356, we found no *Islandinium* in the south Scotia Sea. Today *Islandinium* is affiliated with freshwater input and is dominating in the south Scotia Sea (Thole et al., in prep.), which receives freshwater through calving icebergs (Stuart and Long, 2011). The absence of *Islandinium* might be due to potentially less iceberg discharge, or that they followed a different path or simply most of the melt occurred in a different location.

The complete disappearance of *Impagidinium* and more common *S. antarctica* in the Late Miocene (8-5 Ma) Site U1536 dinocyst record, and colder average SSTs (3°C) indicates further cooling of surface waters and a stronger sea ice influence. This must have further weakened the Weddell Gyre. With a deep water through flow through the northern end of the East Scotia Sea at ~10 Ma (Eagles and Jokat, 2014) and full Drake Passage opening by 6 Ma (e.g., Baker et al., 2007) we assume that modern-like frontal system configurations and ACC strength commenced at the earliest in the Late Miocene.

6 Conclusions

The South Atlantic dinocyst assemblages indicate persistent circulation of the subpolar gyre throughout the Eocene-Oligocene transition (EOT), consistent with the SST reconstructions from Chapter 5. The disappearance of Antarctic endemic and typical cold-water indicative dinocysts north of Drake Passage by the mid-Oligocene (between 32 and 26 Ma) suggests breakdown of the dominant gyral circulation and strengthening of frontal systems, separating the warm subtropics from the polar Antarctic margin. From the Middle Miocene climate optimum (MCO, 16 Ma) to the Middle Miocene climate transition (MMCT, 14 Ma), oligotrophic, warmer water indicative dinocysts are replaced by protoperidinioid dinocysts indicative of high nutrient, cold, sea-ice-influenced Antarctic-proximal surface water conditions, while TEX_{86} SSTs drop from 14°C to 7-5°C. Although many gaps in the sedimentary archives hamper a complete record of oceanographic change in the late Cenozoic Southern Atlantic, our compilation shows for the first time the stepwise breakdown of the large South Atlantic subpolar gyre into the modern-like oceanographic regime with strong frontal systems and latitudinal gradients.

References

- Anagnostou, E., John, E. H., Edgar, K. M., Foster, G. L., Ridgwell, A., Inglis, G. N., Pancost, R. D., Lunt, D. J., and Pearson, P. N.: Changing atmospheric CO₂ concentration was the primary driver of early Cenozoic climate, *Nature*, 533, 380-384, 2016.
- Askin, R. and Raine, J.: Oligocene and Early Miocene terrestrial palynology of the Cape Roberts Drillhole CRP-2/2A, Victoria Land Basin, Antarctica, *Terra Antarctica*, 7, 493-501, 2000.
- Auger, M., Morrow, R., Kestenare, E., Sallée, J.-B., and Cowley, R.: Southern Ocean in-situ temperature trends over 25 years emerge from interannual variability, *Nature Communications*, 12, 1-9, 2021.
- Baatsen, M., von der Heydt, A. S., Huber, M., Kliphuis, M. A., Bijl, P. K., Sluijs, A., and Dijkstra, H. A.: Equilibrium state and sensitivity of the simulated middle-to-late Eocene climate, *Clim Past Discuss*, 2018. 1-49, 2018.
- Barker, P. F., Filippelli, G. M., Florindo, F., Martin, E. E., and Scher, H. D.: Onset and role of the Antarctic Circumpolar Current, *Deep Sea Research Part II: Topical Studies in Oceanography*, 54, 2388-2398, 2007.
- Barrett, P. J.: Antarctic Cenozoic history from the CIROS-1 drillhole, McMurdo Sound, DSIR Pub., 1989.
- Becker, K., Austin, J. A., Exon, N., Humphris, S., Kastner, M., McKenzie, J. A., Miller, K. G., Suyehiro, K., and Taira, A.: 50 Years of Scientific Ocean Drilling, *Oceanography*, 32, 17-21, 2019.
- Bijl, P. K., Schouten, S., Sluijs, A., Reichert, G.-J., Zachos, J. C., and Brinkhuis, H.: Early Palaeogene temperature evolution of the southwest Pacific Ocean, *Nature*, 461, 776, 2009.
- Bijl, P. K., Pross, J., Warnaar, J., Stickley, C. E., Huber, M., Guerstein, R., Houben, A. J., Sluijs, A., Visscher, H., and Brinkhuis, H.: Environmental forcings of Paleogene Southern Ocean dinoflagellate biogeography, *Paleoceanography*, 26, 2011.
- Bijl, P. K., Sluijs, A., and Brinkhuis, H.: A magneto- and chemostratigraphically calibrated dinoflagellate cyst zonation of the early Palaeogene South Pacific Ocean, *Earth-Science Reviews*, 124, 1-31, 2013.
- Bijl, P. K., Bendle, J. A., Bohaty, S. M., Pross, J., Schouten, S., Tauxe, L., Stickley, C. E., McKay, R. M., Rohl, U., Olney, M., Sluijs, A., Escutia, C., Brinkhuis, H., and Expedition, S.: Eocene cooling linked to early flow across the Tasmanian Gateway, *Proc Natl Acad Sci U S A*, 110, 9645-9650, 2013.
- Bijl, P. K., Houben, A. J., Bruls, A., Pross, J., and Sangiorgi, F.: Stratigraphic calibration of Oligocene-Miocene organic-walled dinoflagellate cysts from offshore Wilkes Land, East Antarctica, and a zonation proposal, *Journal of Micropalaeontology*, 37, 105-138, 2018a.
- Bijl, P. K., Houben, A. J., Hartman, J. D., Pross, J., Salabarnada, A., Escutia, C., and Sangiorgi, F.: Paleoclimatology and ice sheet variability offshore Wilkes Land, Antarctica-Part 2: Insights from Oligocene-Miocene dinoflagellate cyst assemblages, *Climate of the Past*, 14, 1015-1033, 2018b.
- Bijl, P. K., Guerstein, G. R., Jaimes, E. A. S., Sluijs, A., Casadio, S., Valencia, V., Amenábar, C. R., and Encinas, A.: Campanian-Eocene dinoflagellate cyst biostratigraphy in the Southern Andean foreland basin: Implications for Drake Passage throughflow, *Andean Geology*, 48, 185-218, 2021.
- Bijl, P. K., Frieling, J., Cramwinckel, M. J., Boschman, C., Sluijs, A., and Peterse, F.: Maastrichtian-Rupelian paleoclimates in the southwest Pacific—a critical evaluation of biomarker paleothermometry and dinoflagellate cyst paleoecology at Ocean Drilling Program Site 1172, *Climate of the Past Discussions*, 2021. 1-82, 2021.
- Blaauw, M.: Methods and code for 'classical' age-modelling of radiocarbon sequences, *quaternary geochronology*, 5, 512-518, 2010.
- Blaga, C. I., Reichert, G.-J., Heiri, O., and Sinninghe Damsté, J. S.: Tetraether membrane lipid distributions in water-column particulate matter and sediments: a study of 47 European lakes along a north-south transect, *Journal of Paleolimnology*, 41, 523-540, 2009.
- Bohaty, S. M., Zachos, J. C., and Delaney, M. L.: Foraminiferal Mg/Ca evidence for southern ocean cooling across the eocene-oligocene transition, *Earth and Planetary Science Letters*, 317, 251-261, 2012.

- Boreham, C., Blevin, J., Duddy, I., Newman, J., Liu, K., Middleton, H., Macphail, M., and Cook, A.: Exploring the potential for oil generation, migration and accumulation in Cape Sorell–1, Sorell Basin, offshore West Tasmania, *The APPEA Journal*, 42, 405-435, 2002.
- Brinkhuis, H. and Biffi, U.: Dinoflagellate cyst stratigraphy of the Eocene/Oligocene transition in central Italy, *Marine Micropaleontology*, 22, 131-183, 1993.
- Brinkhuis, H.: Late Eocene to Early Oligocene dinoflagellate cysts from the Priabonian type-area (Northeast Italy): biostratigraphy and paleoenvironmental interpretation, *Palaeogeography, palaeoclimatology, palaeoecology*, 107, 121-163, 1994.
- Brinkhuis, H., Munsterman, D., Sengers, S., Sluijs, A., Warnaar, J., and Williams, G.: Late Eocene to Quaternary dinoflagellate cysts from ODP Site 1168, Off western Tasmania, *Proceedings of the Ocean Drilling Program. Scientific Results*, 189, 1-36, 2003.
- Burns, D. A.: Nannofossil biostratigraphy for Antarctic sediments, Leg 28, Deep Sea Drilling Project, 1975.
- Cande, S. C., Stock, J. M., Müller, R. D., and Ishihara, T.: Cenozoic motion between east and west Antarctica, *Nature*, 404, 145-150, 2000.
- Cande, S. C. and Stock, J. M.: Pacific—Antarctic—Australia motion and the formation of the Macquarie Plate, *Geophysical Journal International*, 157, 399-414, 2004.
- Carter, A., Riley, T. R., Hillenbrand, C.-D., and Rittner, M.: Widespread Antarctic glaciation during the late Eocene, *Earth and Planetary Science Letters*, 458, 49-57, 2017.
- Carter, R.: The mid-Oligocene Marshall Paraconformity, New Zealand: coincidence with global eustatic sea-level fall or rise?, *The Journal of Geology*, 93, 359-371, 1985.
- Church, M. J., DeLong, E. F., Ducklow, H. W., Karner, M. B., Preston, C. M., and Karl, D. M.: Abundance and distribution of planktonic Archaea and Bacteria in the waters west of the Antarctic Peninsula. *Limnology and Oceanography*, 48(5), 1893-1902, 2003.
- Clowes C. D., Stoveracysta, a new gonyaulacacean dinoflagellate genus from the upper Eocene and lower Oligocene of New Zealand. *Palynology* 9, 27, 1985.
- Clowes, C. D., Hannah, M. J., Wilson, G. J., and Wrenn, J. H.: Marine palynostratigraphy and new species from the Cape Roberts drill-holes, Victoria land basin, Antarctica, *Marine Micropaleontology*, 126, 65-84, 2016.
- Coxall, H. K., Wilson, P. A., Pälike, H., Lear, C. H., and Backman, J.: Rapid stepwise onset of Antarctic glaciation and deeper calcite compensation in the Pacific Ocean, *Nature*, 433, 53-57, 2005.
- Cramwinckel, M. J., Huber, M., Kocken, I. J., Agnini, C., Bijl, P. K., Bohaty, S. M., Frieling, J., Goldner, A., Hilgen, F. J., and Kip, E. L.: Synchronous tropical and polar temperature evolution in the Eocene, *Nature*, 559, 382-386, 2018.
- Cramwinckel, M. J., Woelders, L., Huurdeman, E. P., Peterse, F., Gallagher, S. J., Pross, J., Burgess, C. E., Reichert, G. J., Sluijs, A., and Bijl, P. K.: Surface-circulation change in the southwest Pacific Ocean across the Middle Eocene Climatic Optimum: inferences from dinoflagellate cysts and biomarker paleothermometry, *Clim. Past*, 16, 1667-1689, 2020.
- Crouch, E., Mildenhall, D., and Neil, H.: Distribution of organic-walled marine and terrestrial palynomorphs in surface sediments, offshore eastern New Zealand, *Marine Geology*, 270, 235-256, 2010.
- Crouch, E. M., Willumsen, P. S., Kulhanek, D. K., and Gibbs, S. J.: A revised Paleocene (Teurian) dinoflagellate cyst zonation from eastern New Zealand, *Review of Palaeobotany and Palynology*, 202, 47-79, 2014.
- Crouch, E., Shepherd, C., Morgans, H., Naafs, B., Dallanave, E., Phillips, A., Hollis, C., and Pancost, R.: Climatic and environmental changes across the early Eocene climatic optimum at mid-Waipara River, Canterbury Basin, New Zealand, *Earth-Science Reviews*, 200, 102961, 2020.
- Dale, B.: Dinoflagellate cyst ecology: modeling and geological applications, *Palynology: principles and applications*, AASP Found., College Station, Texas, USA, 1249-1275, 1996.
- De Santis, L., Anderson, J. B., Brancolini, G., and Zayatz, I.: Seismic record of late Oligocene through Miocene glaciation on the central and eastern continental shelf of the Ross Sea, in *Geology and Seismic Stratigraphy of*

- the Antarctic Margin, *Antarct. Res. Ser.*, vol. 68, edited by A. K. Cooper, P. F. Barker, and G. Brancolini, AGU, Washington, D. C, pp. 235–260, 1995.
- De Santis, L., Prato, S., Brancolini, G., Lovo, M., and Torelli, L.: The Eastern Ross Sea continental shelf during the Cenozoic: implications for the West Antarctic ice sheet development, *Global and Planetary Change*, 23, 173-196, 1999.
- De Schepper, S., Fischer, E. I., Groeneveld, J., Head, M. J., and Matthiessen, J.: Deciphering the palaeoecology of Late Pliocene and Early Pleistocene dinoflagellate cysts, *Palaeogeography, Palaeoclimatology, Palaeoecology*, 309, 17-32, 2011.
- De Schepper, S. and Head, M. J.: New late Cenozoic acritarchs: evolution, palaeoecology and correlation potential in high latitude oceans, *Journal of Systematic Palaeontology*, 12, 493-519, 2014.
- De Vernal, A., Rochon, A., Turon, J.-L., and Matthiessen, J.: Organic-walled dinoflagellate cysts: palynological tracers of sea-surface conditions in middle to high latitude marine environments, *Geobios*, 30, 905-920, 1997.
- De Vleeschouwer, D., Vahlenkamp, M., Crucifix, M., and Pälike, H.: Alternating Southern and Northern Hemisphere climate response to astronomical forcing during the past 35 my, *Geology*, 45, 375-378, 2017.
- DeConto, R. M. and Pollard, D.: Rapid Cenozoic glaciation of Antarctica induced by declining atmospheric CO₂, *Nature*, 421, 245-249, 2003.
- DeConto, R. M. and Pollard, D.: Contribution of Antarctica to past and future sea-level rise, *Nature*, 531, 591-597, 2016.
- DeConto, R. M., Pollard, D., Alley, R. B., Velicogna, I., Gasson, E., Gomez, N., Rogstad, S., Condron, A., Gilford, D. M., Ashe, E. L., & Kopp, R. E.: The Paris Climate Agreement and future sea level rise from Antarctica. *Nature*, 593(7857), 83-89, 2021.
- Deppeler, S. L. and Davidson, A. T.: Southern Ocean phytoplankton in a changing climate, *Frontiers in Marine Science*, 4, 40, 2017.
- Douglas, P. M., Affek, H. P., Ivany, L. C., Houben, A. J., Sijp, W. P., Sluijs, A., Schouten, S., and Pagani, M.: Pronounced zonal heterogeneity in Eocene southern high-latitude sea surface temperatures, *Proceedings of the National Academy of Sciences*, 111, 6582-6587, 2014.
- Duncan, B.: Cenozoic Antarctic climate evolution based on molecular and isotopic biomarker reconstructions from geological archives in the Ross Sea region (PhD Thesis), 2017.
- Dunkley Jones, T., Eley, Y. L., Thomson, W., Greene, S. E., Mandel, I., Edgar, K., and Bendle, J. A.: OPTiMAL: A new machine learning approach for GDGT-based palaeothermometry, *Climate of the Past*, 16, 2599-2617, 2020.
- Eagles, G. and Jokat, W.: Tectonic reconstructions for paleobathymetry in Drake Passage, *Tectonophysics*, 611, 28-50, 2014.
- Egger, L. M., Bahr, A., Friedrich, O., Wilson, P. A., Norris, R. D., Van Peer, T. E., Lippert, P. C., Liebrand, D., and Pross, J.: Sea-level and surface-water change in the western North Atlantic across the Oligocene–Miocene Transition: a palynological perspective from IODP Site U1406 (Newfoundland margin), *Marine Micropaleontology*, 139, 57-71, 2018.
- England, M. H., Hutchinson, D. K., Santoso, A., and Sijp, W. P.: Ice–atmosphere feedbacks dominate the response of the climate system to Drake Passage closure, *Journal of Climate*, 30, 5775-5790, 2017.
- Escutia, C., Brinkhuis, H., and Klaus, A.: IODP Expedition 318: From Greenhouse to Icehouse at the Wilkes Land Antarctic Margin, *Scientific Drilling*, 2011.
- Esper, O. and Zonneveld, K. A.: Distribution of organic-walled dinoflagellate cysts in surface sediments of the Southern Ocean (eastern Atlantic sector) between the Subtropical Front and the Weddell Gyre, *Marine Micropaleontology*, 46, 177-208, 2002.
- Evangelinou, D., Escutia, C., Etourneau, J., Hoem, F., Bijl, P., Boterblom, W., van de Flierdt, T., Valero, L., Flores, J.-A., Rodriguez-Tovar, F. J., Jimenez-Espejo, F. J., Salabarnada, A., and López-Quirós, A.: Late Oligocene-Miocene

- proto-Antarctic Circumpolar Current dynamics off the Wilkes Land margin, East Antarctica, *Global and Planetary Change*, 191, 103221, 2020.
- Evangelinos, D., Escutia, C., van de Fliedert, T., Valero, L., Flores, J.-A., Harwood, D. M., Hoem, F. S., Bijl, P., Etourneau, J., and Kreissig, K.: Absence of a strong, deep-reaching Antarctic Circumpolar Current zonal flow across the Tasmanian gateway during the Oligocene to early Miocene, *Global and Planetary Change*, 208, 103718, 2022.
- Evitt, W. R.: A discussion and proposals concerning fossil dinoflagellates, hystrichospheres, and acritarchs, I, *Proceedings of the National Academy of Sciences of the United States of America*, 49, 158, 1963.
- Exon, N. F., Kennett, J.P., Malone, M.J., et al.: Leg 189 summary, *Proceedings of the Ocean Drilling Program Initial Reports*, Ocean Drilling Program, College Station, TX., USA, 2001a.
- Exon, N. F., Kennett, J.P., Malone, M.J., et al.: Site 1168. , *Proceedings of the Ocean Drilling Program Initial Reports*, Ocean Drilling Program, College Station, TX., USA, 2001b.
- Exon, N. F., Kennett, J. P., and Malone, M. J.: Leg 189 synthesis: Cretaceous–Holocene history of the Tasmanian gateway, *Proceedings of the ocean drilling program, scientific results*, 189, 1-37, 2004.
- Fabry, V. J., McClintock, J. B., Mathis, J. T., and Grebmeier, J. M.: Ocean acidification at high latitudes: the bellwether, *Oceanography*, 22, 160-171, 2009.
- Feakins, S. J., Warny, S., and Lee, J.-E.: Hydrologic cycling over Antarctica during the middle Miocene warming, *Nature Geoscience*, 5, 557-560, 2012.
- Fensome, R. A.: A classification of living and fossil dinoflagellates, *Micropaleontology, special publication*, 7, 1-351, 1993.
- Fetterer, F., Knowles, K., Meier, W., Savoie, M., and Windnagel, A.: Updated daily. Sea ice index, version 3.[indicate subset used]. Boulder, Colorado USA. NSIDC: National Snow and Ice Data Center. 2020.
- Fielding, C. R., Naish, T., Woolfe, K., and Lavelle, M.: Facies analysis and sequence stratigraphy of CRP-2/2A, Victoria Land Basin, Antarctica, *Terra Antarctica*, 7, 323-338, 2000.
- Florindo, F., Wilson, G. S., Roberts, A. P., Sagnotti, L., and Verosub, K. L.: Magnetostratigraphic chronology of a late Eocene to early Miocene glacial marine succession from the Victoria Land Basin, Ross Sea, Antarctica, *Global and Planetary Change*, 45, 207-236, 2005.
- Flower, B. and Kennett, J.: Middle Miocene ocean-climate transition: High-resolution oxygen and carbon isotopic records from Deep Sea Drilling Project Site 588A, southwest Pacific, *Paleoceanography*, 8, 811-843, 1993.
- Foster, G. L., Lear, C. H., and Rae, J. W.: The evolution of pCO₂, ice volume and climate during the middle Miocene, *Earth and Planetary Science Letters*, 341, 243-254, 2012.
- Foster, G. L. and Rohling, E. J.: Relationship between sea level and climate forcing by CO₂ on geological timescales, *Proceedings of the National Academy of Sciences*, 110, 1209-1214, 2013.
- Fretwell, P., Pritchard, H. D., Vaughan, D. G., Bamber, J. L., Barrand, N. E., Bell, R., Bianchi, C., Bingham, R., Blankenship, D. D., and Casassa, G.: Bedmap2: improved ice bed, surface and thickness datasets for Antarctica, *The Cryosphere*, 7, 375-393, 2013.
- Frieling, J. and Sluijs, A.: Towards quantitative environmental reconstructions from ancient non-analogue microfossil assemblages: Ecological preferences of Paleocene – Eocene dinoflagellates, *Earth-Science Reviews*, 185, 956-973, 2018.
- Fulthorpe, C. S., Carter, R. M., Miller, K. G., and Wilson, J.: Marshall Paraconformity: a mid-Oligocene record of inception of the Antarctic circumpolar current and coeval glacio-eustatic lowstand?, *Marine and petroleum geology*, 13, 61-77, 1996.
- Galeotti, S., DeConto, R., Naish, T., Stocchi, P., Florindo, F., Pagani, M., Barrett, P., Bohaty, S. M., Lanci, L., and Pollard, D.: Antarctic Ice Sheet variability across the Eocene-Oligocene boundary climate transition, *Science*, 352, 76-80, 2016.
- Gallagher, S. J., Villa, G., Drysdale, R. N., Wade, B. S., Scher, H., Li, Q., Wallace, M. W., and Holdgate, G. R.: A near-field sea level record of East Antarctic Ice Sheet instability from 32 to 27 Myr, *Paleoceanography*, 28, 1-13, 2013.

- Gallagher, S. J., Wade, B., Qianyu, L., Holdgate, G. R., Bown, P., Korasidis, V. A., Scher, H., Houben, A. J., McGowran, B., and Allan, T.: Eocene to Oligocene high paleolatitude neritic record of Oi-1 glaciation in the Otway Basin southeast Australia, *Global and Planetary Change*, 191, 103218, 2020.
- Gasson, E., Lunt, D. J., DeConto, R., Goldner, A., Heinemann, M., Huber, M., LeGrande, A., Pollard, D., Sagoo, N., and Siddall, M.: Uncertainties in the modelled CO₂ threshold for Antarctic glaciation, *Climate of the Past*, 10, 451-466, 2014.
- Gasson, E. G. and Keisling, B. A.: The Antarctic ice sheet, *Oceanography*, 33, 90-100, 2020.
- Gersonde, R. and Burckle, L. H.: 43. NEOGENE DIATOM BIOSTRATIGRAPHY OF ODP LEG 113, WEDDELL SEA (ANTARCTIC OCEAN), 1990. 1990.
- Gillard, M., Autin, J., Manatschal, G., Sauter, D., Munsch, M., and Schaming, M.: Tectonomagmatic evolution of the final stages of rifting along the deep conjugate Australian-Antarctic magma-poor rifted margins: Constraints from seismic observations, *Tectonics*, 34, 753-783, 2015.
- Goldner, A., Herold, N., and Huber, M.: Antarctic glaciation caused ocean circulation changes at the Eocene-Oligocene transition, *Nature*, 511, 574-577, 2014.
- Gombos, A. M. and AM JR, G.: Paleogene and Neogene diatoms from the Falkland Plateau and Malvinas Outer Basin: Leg 36, Deep Sea Drilling Project, 1977.
- Gradstein, F. M., Ogg, J. G., Schmitz, M. D., and Ogg, G. M.: The geologic time scale 2012, Elsevier, 2012.
- Granot, R., Cande, S., Stock, J., Davey, F., and Clayton, R.: Postspreading rifting in the Adare Basin, Antarctica: regional tectonic consequences, *Geochemistry, Geophysics, Geosystems*, 11, 2010.
- Greenop, R., Foster, G. L., Wilson, P. A., and Lear, C. H.: Middle Miocene climate instability associated with high-amplitude CO₂ variability, *Paleoceanography*, 29, 845-853, 2014.
- Greenwood, D. R. and Wing, S. L.: Eocene continental climates and latitudinal temperature gradients, *Geology*, 23, 1044-1048, 1995.
- Guerstein, G. R., Estebenet, M. S. G., Alperin, M. I., Casadio, S. A., and Archangelsky, S.: Correlation and paleoenvironments of middle Paleogene marine beds based on dinoflagellate cysts in southwestern Patagonia, Argentina, *Journal of South American Earth Sciences*, 52, 166-178, 2014.
- Gutián, J. and Stoll, H. M.: Evolution of Sea Surface Temperature in the Southern Mid-latitudes from Late Oligocene through Early Miocene, *Paleoceanography and Paleoclimatology*, e2020PA004199, 2021.
- Hannah, M.: Climate controlled dinoflagellate distribution in late Eocene-earliest Oligocene strata from CIROS-1 Drillhole, McMurdo Sound, Antarctica, *Terra Antarctica*, 4, 73-78, 1997.
- Hannah, M., Wrenn, J., and Wilson, G.: Early Miocene and Quaternary marine palynomorphs from Cape Roberts Project CRP-1, McMurdo Sound, Antarctica, *Terra Antarctica*, 5, 527-538, 1998.
- Hannah, M., Wilson, G., and Wrenn, J.: Oligocene and miocene marine palynomorphs from CRP-2/2A, Victoria Land Basin, Antarctica, *Terra Antarctica*, 7, 503-511, 2000.
- Hannah, M. J.: The palynology of ODP site 1165, Prydz Bay, East Antarctica: a record of Miocene glacial advance and retreat, *Palaeogeography, Palaeoclimatology, Palaeoecology*, 231, 120-133, 2006.
- Harland, R. and Pudsey, C. J.: Dinoflagellate cysts from sediment traps deployed in the Bellingshausen, Weddell and Scotia seas, Antarctica, *Marine Micropaleontology*, 37, 77-99, 1999.
- Hartman, J. D., Bijl, P. K., and Sangiorgi, F.: A review of the ecological affinities of marine organic microfossils from a Holocene record offshore of Adélie Land (East Antarctica), *Journal of Micropaleontology*, 37, 445-497, 2018 (a).
- Hartman, J. D., Sangiorgi, F., Salabarnada, A., Peterse, F., Houben, A. J., Schouten, S., Brinkhuis, H., Escutia, C., and Bijl, P. K.: Paleooceanography and ice sheet variability offshore Wilkes Land, Antarctica-Part 3: Insights from Oligocene-Miocene TEX86-based sea surface temperature reconstructions, *Climate of the Past*, 14, 1275-1297, 2018.
- Harwood, D., Florindo, F., Talarico, F., and Levy, R.: Studies from the ANDRILL Southern McMurdo Sound Project, Antarctica, *Terra Antarctica*, 15, 1-235, 2008.

- Hayes, D. E., Frakes, L.A., Bar, P.J, Derek A Burns, Pei-hsin Chen, The Shipboard Scientific Party, et al., : 10. SITE 274 The Shipboard Scientific Party 1 SITE DATA, 28, 1975.
- Head, M.: Modern dinoflagellate cysts and their biological affinities, *Palynology: principles and applications*, 3, 1197-1248, 1996.
- Head, M. J., Harland, R., and Matthiessen, J.: Cold marine indicators of the late Quaternary: the new dinoflagellate cyst genus *Islandinium* and related morphotypes, *Journal of Quaternary Science: Published for the Quaternary Research Association*, 16, 621-636, 2001.
- Herbert, T., Schuffert, J., Thomas, D., Lange, C., Weinheimer, A., Peleo-Alampay, A., and Herguera, J. C.: Depth and seasonality of alkenone production along the California margin inferred from a core top transect, *Paleoceanography*, 13, 263-271, 1998.
- Herbert, T. D., Lawrence, K. T., Tzanova, A., Peterson, L. C., Caballero-Gill, R., and Kelly, C. S.: Late Miocene global cooling and the rise of modern ecosystems, *Nature Geoscience*, 9, 843-847, 2016.
- Herold, N., Huber, M., Müller, R., and Seton, M.: Modeling the Miocene climatic optimum: Ocean circulation, *Paleoceanography*, 27, 2012.
- Hill, P., Meixner, A., Moore, A., and Exon, N.: Structure and development of the west Tasmanian offshore sedimentary basins: results of recent marine and aeromagnetic surveys, *Australian Journal of Earth Sciences*, 44, 579-596, 1997.
- Hill, P. J. and Exon, N. F.: Tectonics and basin development of the offshore Tasmanian area incorporating results from deep ocean drilling, *Washington DC American Geophysical Union Geophysical Monograph Series*, 151, 19-42, 2004.
- Hill, D. J., Haywood, A. M., Valdes, P. J., Francis, J. E., Lunt, D. J., Wade, B. S., and Bowman, V. C.: Paleogeographic controls on the onset of the Antarctic circumpolar current, *Geophysical Research Letters*, 40, 5199-5204, 2013.
- Ho, S. L., Mollenhauer, G., Fietz, S., Martínez-García, A., Lamy, F., Rueda, G., Schipper, K., Méheust, M., Rosell-Melé, A., and Stein, R.: Appraisal of TEX86 and TEX86L thermometries in subpolar and polar regions, *Geochimica et Cosmochimica Acta*, 131, 213-226, 2014.
- Hochmuth, K., Gohl, K., Leitchenkov, G., Sauermilch, I., Whittaker, J. M., Uenzelmann-Neben, G., Davy, B., and De Santis, L.: The evolving paleobathymetry of the circum-Antarctic Southern Ocean since 34 Ma: A key to understanding past cryosphere-ocean developments, *Geochemistry, Geophysics, Geosystems*, 21, e2020GC009122, 2020.
- Hodel, F., Grespan, R., de Rafélis, M., Dera, G., Lezin, C., Nardin, E., Rouby, D., Aretz, M., Steinman, M., and Buatier, M.: Drake Passage gateway opening and Antarctic Circumpolar Current onset 31 Ma ago: The message of foraminifera and reconsideration of the Neodymium isotope record, *Chemical Geology*, 570, 120171, 2021.
- Hoem, F. S., Valero, L., Evangelinos, D., Escutia, C., Duncan, B., McKay, R. M., Brinkhuis, H., Sangiorgi, F., and Bijl, P. K.: Temperate Oligocene surface ocean conditions offshore of Cape Adare, Ross Sea, Antarctica, *Climate of the Past*, 17, 1423-1442, 2021a (Chapter 2).
- Hoem, F. S., Sauermilch, I., Hou, S., Brinkhuis, H., Sangiorgi, F., and Bijl, P. K.: Late Eocene–early Miocene evolution of the southern Australian subtropical front: a marine palynological approach, *Journal of Micropalaeontology*, 40, 175-193, 2021b (Chapter 3).
- Hoem, F., Sauermilch, I., Aleksinski, A., Huber, M., Peterse, F., Sangiorgi, F., and Bijl, P.: Strength and variability of the Oligocene Southern Ocean surface temperature gradient (Chapter 4), in review.
- Hoenisch, B., Paleo-CO2 data archive (Version 1) [Data set]. Zenodo. last access: 02.01.2022
- Holbourn, A., Kuhnt, W., Schulz, M., and Erlenkeuser, H.: Impacts of orbital forcing and atmospheric carbon dioxide on Miocene ice-sheet expansion, *Nature*, 438, 483-487, 2005.
- Holbourn, A. E., Kuhnt, W., Clemens, S. C., Kochhann, K. G., Jöhnck, J., Lübbers, J., and Andersen, N.: Late Miocene climate cooling and intensification of southeast Asian winter monsoon, *Nature communications*, 9, 1-13, 2018.

- Holdgate, G., Sluiter, I., and Taglieri, J.: Eocene-Oligocene coals of the Gipsland and Australo-Antarctic basins–Paleoclimatic and paleogeographic context and implications for the earliest Cenozoic glaciations, *Palaeogeography, Palaeoclimatology, Palaeoecology*, 472, 236-255, 2017.
- Hopmans, E. C., Weijers, J. W., Schefuß, E., Herfort, L., Damsté, J. S. S., and Schouten, S.: A novel proxy for terrestrial organic matter in sediments based on branched and isoprenoid tetraether lipids, *Earth and Planetary Science Letters*, 224, 107-116, 2004.
- Hopmans, E. C., Schouten, S., and Damsté, J. S. S.: The effect of improved chromatography on GDGT-based palaeoproxies, *Organic Geochemistry*, 93, 1-6, 2016.
- Houben, A. J., Bijl, P. K., Guerin, G. R., Sluijs, A., and Brinkhuis, H.: *Malvinia escutiana*, a new biostratigraphically important Oligocene dinoflagellate cyst from the Southern Ocean, *Review of Palaeobotany and Palynology*, 165, 175-182, 2011.
- Houben, A. J. P., Bijl, P. K., Pross, J., Bohaty, S. M., Passchier, S., Stickley, C. E., Rohl, U., Sugisaki, S., Tauxe, L., van de Flierdt, T., Olney, M., Sangiorgi, F., Sluijs, A., Escutia, C., Brinkhuis, H., Brinkhuis, H., Dotti, C. E., Klaus, A., Fehr, A., Williams, T., Bendle, J. A., Bijl, P. K., Bohaty, S. M., Carr, S. A., Dunbar, R. B., Flores, J. A., Gonzalez, J. J., Hayden, T. G., Iwai, M., Jimenez-Espejo, F. J., Katsuki, K., Kong, G. S., Mckay, R. M., Nakai, M., Olney, M. P., Passchier, S., Pekar, S. F., Pross, J., Riesselman, C., Rohl, U., Sakai, T., Salzmann, U., Shrivastava, P. K., Stickley, C. E., Sugisaki, S., Tauxe, L., Tuo, S., van de Flierdt, T., Welsh, K., Yamane, M., and Scientists, E.: Reorganization of Southern Ocean Plankton Ecosystem at the Onset of Antarctic Glaciation, *Science*, 340, 341-344, 2013.
- Houben, A. J., Bijl, P. K., Sluijs, A., Schouten, S., and Brinkhuis, H.: Late Eocene Southern Ocean cooling and invigoration of circulation preconditioned Antarctica for full-scale glaciation, *Geochemistry, Geophysics, Geosystems*, 2019.
- Huber, M., Brinkhuis, H., Stickley, C. E., Döös, K., Sluijs, A., Warnaar, J., Schellenberg, S. A., and Williams, G. L.: Eocene circulation of the Southern Ocean: Was Antarctica kept warm by subtropical waters?, *Paleoceanography*, 19, 2004.
- Huber, M., and Nof, D.: The ocean circulation in the southern hemisphere and its climatic impacts in the Eocene, *Palaeogeography, Palaeoclimatology, Palaeoecology*, 231, 9-28, 2006.
- Huber M, and Caballero R.: The early Eocene equable climate problem revisited. *Climate of the Past*, 2011.
- Huerta, A. D. and Harry, D. L.: The transition from diffuse to focused extension: Modeled evolution of the West Antarctic Rift system, *Earth and Planetary Science Letters*, 255, 133-147, 2007.
- Hutchinson, D. K., de Boer, A. M., Coxall, H. K., Caballero, R., Nilsson, J., and Baatsen, M.: Climate sensitivity and meridional overturning circulation in the late Eocene using GFDL CM2. 1, *Climate of the Past*, 14, 789-810, 2018.
- Hutchinson, D. K., Coxall, H. K., Lunt, D. J., Steinthorsdottir, M., De Boer, A. M., Baatsen, M., von der Heydt, A., Huber, M., Kennedy-Asser, A. T., and Kunzmann, L.: The Eocene–Oligocene transition: a review of marine and terrestrial proxy data, models and model–data comparisons, *Climate of the Past*, 17, 269-315, 2021.
- IPCC, H.-O. P. r., D.C. Roberts., V. Masson-Delmotte, P. Z., M. Tignor, E. Poloczanska, K. Mintenbeck, A. Alegria, M. Nicolai, A. Okem, J., and Petzold, B. R., N.M. Weyer (eds.): IPCC Special Report on the Ocean and Cryosphere in a Changing Climate, In press, 2019. 2019.
- Jovane, L., Florindo, F., Wilson, G., Leone, S. d. A. P. S., Hassan, M. B., Rodelli, D., and Cortese, G.: Magnetostratigraphic Chronology of a Cenozoic Sequence From DSDP Site 274, Ross Sea, Antarctica, Multi-Disciplinary Applications in Magnetic Chronostratigraphy, 8, 2020.
- Juggins, S.: C2: Software for ecological and palaeoecological data analysis and visualisation (user guide version 1.5), Newcastle upon Tyne: Newcastle University, 77, 2007.
- Kalanetra, K. M., Bano, N., and Hollibaugh, J. T.: Ammonia-oxidizing Archaea in the Arctic Ocean and Antarctic coastal waters. *Environmental Microbiology*, 11(9), 2434-2445, 2009.

- Kennedy, A. T., Farnsworth, A., Lunt, D., Lear, C. H., and Markwick, P.: Atmospheric and oceanic impacts of Antarctic glaciation across the Eocene–Oligocene transition, *Philosophical Transactions of the Royal Society A: Mathematical, Physical and Engineering Sciences*, 373, 20140419, 2015.
- Kennedy-Asser, A., Lunt, D. J., Farnsworth, A., and Valdes, P.: Assessing mechanisms and uncertainty in modeled climatic change at the Eocene–Oligocene transition, *Paleoceanography and Paleoclimatology*, 34, 16–34, 2019.
- Kennedy-Asser, A. T., Lunt, D. J., Valdes, P. J., Ladant, J.-B., Frieling, J., and Laetano, V.: Changes in the high-latitude Southern Hemisphere through the Eocene–Oligocene transition: a model–data comparison, *Climate of the Past*, 16, 555–573, 2020.
- Kennett, J. P.: Cenozoic evolution of Antarctic glaciation, the circum-Antarctic Ocean, and their impact on global paleoceanography, *Journal of geophysical research*, 82, 3843–3860, 1977.
- Kim, J.-H., Van der Meer, J., Schouten, S., Helmke, P., Willmott, V., Sangiorgi, F., Koç, N., Hopmans, E. C., and Damsté, J. S. S.: New indices and calibrations derived from the distribution of crenarchaeal isoprenoid tetraether lipids: Implications for past sea surface temperature reconstructions, *Geochimica et Cosmochimica Acta*, 74, 4639–4654, 2010.
- Kim, J. H., Crosta, X., Willmott, V., Renssen, H., Bonnin, J., Helmke, P., Schouten, S., and Sinninghe Damsté, J. S.: Holocene subsurface temperature variability in the eastern Antarctic continental margin, *Geophysical Research Letters*, 39, 2012.
- Knorr, G. and Lohmann, G.: Climate warming during Antarctic ice sheet expansion at the Middle Miocene transition, *Nature Geoscience*, 7, 376–381, 2014.
- Kominz, M. A., Browning, J., Miller, K., Sugarman, P., Mizintseva, S., and Scotese, C.: Late Cretaceous to Miocene sea-level estimates from the New Jersey and Delaware coastal plain coreholes: An error analysis, *Basin Research*, 20, 211–226, 2008.
- Kulhanek, D. K., Levy, R. H., Clowes, C. D., Prebble, J. G., Rodelli, D., Jovane, L., Morgans, H. E., Kraus, C., Zwingmann, H., and Griffith, E. M.: Revised chronostratigraphy of DSDP Site 270 and late Oligocene to early Miocene paleoecology of the Ross Sea sector of Antarctica, *Global and Planetary Change*, 178, 46–64, 2019.
- Lacasse, J. H., Escartin, J., Chassignet, E. P., and Xu, X.: Jet instability over smooth, corrugated, and realistic bathymetry, *Journal of Physical Oceanography*, 49, 585–605, 2019.
- Lamy, F., Kilian, R., Arz, H. W., Francois, J.-P., Kaiser, J., Prange, M., and Steinke, T.: Holocene changes in the position and intensity of the southern westerly wind belt, *Nature Geoscience*, 3, 695–699, 2010.
- Langebroek, P. M., Paul, A., and Schulz, M.: Antarctic ice-sheet response to atmospheric CO₂ and insolation in the Middle Miocene, *Climate of the Past*, 5, 633–646, 2009.
- Lavelle, M.: Strontium isotope stratigraphy of the CRP-1 drillhole, Ross Sea, Antarctica, *Terra Antarctica*, 5, 691–696, 1998.
- Lawver, L. A., Gahagan, L. M., and Coffin, M. F.: The development of paleoseaways around Antarctica, *Antarctic research series*, 56, 7–30, 1992.
- Lear, C. H., Elderfield, H., and Wilson, P. A.: Cenozoic deep-sea temperatures and global ice volumes from Mg/Ca in benthic foraminiferal calcite, *science*, 287, 269–272, 2000.
- Lear, C. H., Rosenthal, Y., Coxall, H. K., and Wilson, P.: Late Eocene to early Miocene ice sheet dynamics and the global carbon cycle, *Paleoceanography*, 19, 2004.
- Leutert, T. J., Auderset, A., Martínez-García, A., Modestou, S., and Meckler, A. N.: Coupled Southern Ocean cooling and Antarctic ice sheet expansion during the middle Miocene, *Nature Geoscience*, 13, 634–639, 2020.
- Leutert, T. J., Modestou, S., Bernasconi, S. M., and Meckler, A. N.: Southern Ocean bottom-water cooling and ice sheet expansion during the middle Miocene climate transition, *Climate of the Past*, 17, 2255–2271, 2021.
- Levy, R. H. and Harwood, D. M.: Tertiary marine palynomorphs from the McMurdo Sound erratics, Antarctica, *Paleobiology and Paleoenvironments of Eocene Rocks: McMurdo Sound, East Antarctica*, 76, 183–242, 2000.

- Levy, R., Harwood, D., Florindo, F., Sangiorgi, F., Tripati, R., Von Eynatten, H., Gasson, E., Kuhn, G., Tripati, A., and DeConto, R.: Antarctic ice sheet sensitivity to atmospheric CO₂ variations in the early to mid-Miocene, *Proceedings of the National Academy of Sciences*, 113, 3453-3458, 2016.
- Levy, R. H., Meyers, S. R., Naish, T. R., Golledge, N. R., McKay, R. M., Crampton, J. S., DeConto, R. M., De Santis, L., Florindo, F., Gasson, E. G. W., Harwood, D. M., Luyendyk, B. P., Powell, R. D., Clowes, C., and Kulhanek, D. K.: Antarctic ice-sheet sensitivity to obliquity forcing enhanced through ocean connections, *Nature Geoscience*, 12, 132-137, 2019.
- Lewis, A. R., Marchant, D. R., Ashworth, A. C., Hedenäs, L., Hemming, S. R., Johnson, J. V., Leng, M. J., Machlus, M. L., Newton, A. E., and Raine, J. I.: Mid-Miocene cooling and the extinction of tundra in continental Antarctica, *Proceedings of the National Academy of Sciences*, 105, 10676-10680, 2008.
- Liebrand, D., de Bakker, A. T., Beddow, H. M., Wilson, P. A., Bohaty, S. M., Ruessink, G., Palike, H., Batenburg, S. J., Hilgen, F. J., Hodell, D. A., Huck, C. E., Kroon, D., Raffi, I., Saes, M. J., van Dijk, A. E., and Lourens, L. J.: Evolution of the early Antarctic ice ages, *Proc Natl Acad Sci U S A*, 114, 3867-3872, 2017.
- Liu, Z., Pagani, M., Zinniker, D., Deconto, R., Huber, M., Brinkhuis, H., Shah, S. R., Leckie, R. M., and Pearson, A.: Global cooling during the eocene-oligocene climate transition, *Science*, 323, 1187-1190, 2009.
- Livermore, R., Hillenbrand, C. D., Meredith, M., and Eagles, G.: Drake Passage and Cenozoic climate: an open and shut case?, *Geochemistry, Geophysics, Geosystems*, 8, 2007.
- Locarnini, M., Mishonov, A., Baranova, O., Boyer, T., Zweng, M., Garcia, H., Seidov, D., Weathers, K., Paver, C., and Smolyar, I.: World ocean atlas 2018, volume 1: Temperature, 2018. 2018.
- López-Quiros, A., Escutia, C., Sánchez-Navas, A., Nieto, F., Garcia-Casco, A., Martín-Algarra, A., Evangelinos, D., and Salabarnada, A.: Glaucony authigenesis, maturity and alteration in the Weddell Sea: An indicator of paleoenvironmental conditions before the onset of Antarctic glaciation, *Scientific reports*, 9, 1-12, 2019.
- López-Quiros, A., Sánchez-Navas, A., Nieto, F., and Escutia, C.: New insights into the nature of glauconite, *American Mineralogist: Journal of Earth and Planetary Materials*, 105, 674-686, 2020.
- López-Quiros, A., Escutia, C., Etourneau, J., Rodríguez-Tovar, F. J., Roignant, S., Lobo, F. J., Thompson, N., Bijl, P. K., Bohoyo, F., and Salzmann, U.: Eocene-Oligocene paleoenvironmental changes in the South Orkney Microcontinent (Antarctica) linked to the opening of Powell Basin, *Global and Planetary Change*, 204, 103581, 2021.
- Louwye, S., Foubert, A., Mertens, K., and Van Rooij, D.: Integrated stratigraphy and palaeoecology of the Lower and Middle Miocene of the Porcupine Basin, *Geological magazine*, 145, 321-344, 2008.
- Lyle, M., Gibbs, S., Moore, T. C., and Rea, D. K.: Late Oligocene initiation of the Antarctic Circumpolar Current: Evidence from the South Pacific, *Geology*, 35, 691-694, 2007.
- Macphail, M.: The Sabrina Microfloras of East Antarctica: Late Cretaceous Paleogene or reworked?, *Palynology*, 2021. 1-12, 2021.
- Maldonado, A., Bohoyo, F., Galindo-Zaldívar, J., Hernández-Molina, J., Jabaloy, A., Lobo, F., Rodríguez-Fernández, J., Suriñach, E., and Vázquez, J.: Ocean basins near the Scotia–Antarctic plate boundary: influence of tectonics and paleoceanography on the Cenozoic deposits, *Marine Geophysical Researches*, 27, 83-107, 2006.
- Maldonado, A., Bohoyo, F., Galindo-Zaldívar, J., Hernández-Molina, F. J., Lobo, F. J., Lodolo, E., Martos, Y. M., Pérez, L. F., Schreider, A. A., and Somoza, L.: A model of oceanic development by ridge jumping: opening of the Scotia Sea, *Global and Planetary Change*, 123, 152-173, 2014.
- Marret, F., Bradley, L., de Vernal, A., Hardy, W., Kim, S.-Y., Mudie, P., Penaud, A., Pospelova, V., Price, A. M., Radi, T., and Rochon, A.: From bi-polar to regional distribution of modern dinoflagellate cysts, an overview of their biogeography, *Marine Micropaleontology*, 159, 101753, 2020.
- Marshall, J., Adcroft, A., Hill, C., Perelman, L., and Heisey, C.: A finite-volume, incompressible Navier Stokes model for studies of the ocean on parallel computers, *Journal of Geophysical Research: Oceans*, 102, 5753-5766, 1997.

- Massana, R., Taylor, L. T., Murray, A. E., Wu, K. Y., Jeffrey, W. H., and DeLong, E. F.: Vertical distribution and temporal variation of marine planktonic archaea in the Gerlache Strait, Antarctica, during early spring. *Limnology and Oceanography*, 43(4), 607-617, 1998.
- Masson-Delmotte, V., Zhai, P., Pirani, A., Connors, S. L., Péan, C., Berger, S., Caud, N., Chen, Y., Goldfarb, L., and Gomis, M. I.: *Climate Change 2021: The Physical Science Basis. Contribution of Working Group I to the Sixth Assessment Report of the Intergovernmental Panel on Climate Change*, IPCC: Geneva, Switzerland, 2021. 2021.
- Matthews, K. J., Maloney, K. T., Zahirovic, S., Williams, S. E., Seton, M., and Mueller, R. D.: Global plate boundary evolution and kinematics since the late Paleozoic, *Global and Planetary Change*, 146, 226-250, 2016.
- McCarthy, A., Falloon, T., Sauermilch, I., Whittaker, J., Niida, K., and Green, D.: Revisiting the Australian-Antarctic ocean-continent transition zone using petrological and geophysical characterization of exhumed subcontinental mantle, *Geochemistry, Geophysics, Geosystems*, 21, e2020GC009040, 2020.
- McIntosh, W.: ⁴⁰Ar/³⁹Ar geochronology of volcanic clasts and pumice in CRP-1 core, Cape Roberts, Antarctica, *Terra Antarctica*, 5, 683-690, 1998.
- McKay, R., Barrett, P., Levy, R., Naish, T., Golledge, N., and Pyne, A.: Antarctic Cenozoic climate history from sedimentary records: ANDRILL and beyond, *Philosophical Transactions of the Royal Society A: Mathematical, Physical and Engineering Sciences*, 374, 20140301, 2016.
- Mertens, K. N., Verhoeven, K., Verleye, T., Louwye, S., Amorim, A., Ribeiro, S., Deaf, A. S., Harding, I. C., De Schepper, S., and González, C.: Determining the absolute abundance of dinoflagellate cysts in recent marine sediments: the Lycopodium marker-grain method put to the test, *Review of Palaeobotany and Palynology*, 157, 238-252, 2009.
- Miller, K. G., Wright, J. D., and Fairbanks, R. G.: Unlocking the ice house: Oligocene-Miocene oxygen isotopes, eustasy, and margin erosion, *Journal of Geophysical Research: Solid Earth*, 96, 6829-6848, 1991.
- Miller, J. M., Norvick, M. S., and Wilson, C. J.: Basement controls on rifting and the associated formation of ocean transform faults—Cretaceous continental extension of the southern margin of Australia, *Tectonophysics*, 359, 131-155, 2002.
- Miller, K. G., Wright, J. D., Katz, M. E., Wade, B. S., Browning, J. V., Cramer, B. S., and Rosenthal, Y.: Climate threshold at the Eocene-Oligocene transition: Antarctic ice sheet influence on ocean circulation, *The Late Eocene Earth: Hothouse, Icehouse, and Impacts*, 452, 169, 2009.
- Miller, K. G., Browning, J. V., Schmelz, W. J., Kopp, R. E., Mountain, G. S., and Wright, J. D.: Cenozoic sea-level and cryospheric evolution from deep-sea geochemical and continental margin records, *Science advances*, 6, eaaz1346, 2020.
- Mudie, P.: Neogene and quaternary dinoflagellate cysts and acritarchs, *American Association of Stratigraphic Palynologists, Dallas, USA1992*, 347-390, 1992.
- Mudie, P. J., Marret, F., Gurdebeke, P. R., Hartman, J. D., and Reid, P. C.: Marine dinocysts, acritarchs and less well-known NPP: tintinnids, ostracod and foraminiferal linings, copepod and worm remains, *Geological Society, London, Special Publications*, 511, 2021.
- Müller, P. J., Kirst, G., Ruhland, G., Von Storch, I., and Rosell-Melé, A.: Calibration of the alkenone paleotemperature index U37K- based on core-tops from the eastern South Atlantic and the global ocean (60 N-60 S), *Geochimica et Cosmochimica Acta*, 62, 1757-1772, 1998.
- Müller, R. D., Cannon, J., Qin, X., Watson, R. J., Gurnis, M., Williams, S., Pfaffelmoser, T., Seton, M., Russell, S. H., and Zahirovic, S.: GPlates: building a virtual Earth through deep time, *Geochemistry, Geophysics, Geosystems*, 19, 2243-2261, 2018.
- Müntener, O., Manatschal, G., Desmurs, L., and Pettke, T.: Plagioclase peridotites in ocean-continent transitions: refertilized mantle domains generated by melt stagnation in the shallow mantle lithosphere, *Journal of Petrology*, 51, 255-294, 2010.

- Naish, T. R., Woolfe, K. J., Barrett, P. J., Wilson, G. S., Atkins, C., Bohaty, S. M., Bücker, C. J., Claps, M., Davey, F. J., and Dunbar, G. B.: Orbitally induced oscillations in the East Antarctic ice sheet at the Oligocene/Miocene boundary, *Nature*, 413, 719-723, 2001.
- Nelson, C. S. and Cooke, P. J.: History of oceanic front development in the New Zealand sector of the Southern Ocean during the Cenozoic—a synthesis, *New Zealand Journal of geology and geophysics*, 44, 535-553, 2001.
- Nicholson, U. and Stow, D.: Erosion and deposition beneath the Subantarctic Front since the Early Oligocene, *Scientific reports*, 9, 1-9, 2019.
- O'Brien, C. L., Robinson, S. A., Pancost, R. D., Damsté, J. S. S., Schouten, S., Lunt, D. J., Alsenz, H., Bornemann, A., Bottini, C., and Brassell, S. C.: Cretaceous sea-surface temperature evolution: Constraints from TEX86 and planktonic foraminiferal oxygen isotopes, *Earth-Science Reviews*, 172, 224-247, 2017.
- O'Brien, C. L., Huber, M., Thomas, E., Pagani, M., Super, J. R., Elder, L. E., and Hull, P. M.: The enigma of Oligocene climate and global surface temperature evolution, *Proceedings of the National Academy of Sciences*, 117, 25302-25309, 2020.
- Olbers, D., Borowski, D., Völker, C., and WOeLFF, J.-O.: The dynamical balance, transport and circulation of the Antarctic Circumpolar Current, *Antarctic science*, 16, 439-470, 2004.
- Orsi, A. H., Whitworth, T., and Nowlin, W. D.: On the meridional extent and fronts of the Antarctic Circumpolar Current, *Deep Sea Research Part I: Oceanographic Research Papers*, 42, 641-673, 1995.
- Orsi, A. H. and Wiederwohl, C. L.: A recount of Ross Sea waters, *Deep Sea Research Part II: Topical Studies in Oceanography*, 56, 778-795, 2009.
- Pälike, H., Norris, R. D., Herrle, J. O., Wilson, P. A., Coxall, H. K., Lear, C. H., Shackleton, N. J., Tripathi, A. K., and Wade, B. S.: The heartbeat of the Oligocene climate system, *science*, 314, 1894-1898, 2006.
- Park, E., Hefter, J., Fischer, G., Iversen, M. H., Ramondenc, S., Nöthig, E.-M., and Mollenhauer, G.: Seasonality of archaeal lipid flux and GDGT-based thermometry in sinking particles of high-latitude oceans: Fram Strait (79 N) and Antarctic Polar Front (50 S), *Biogeosciences*, 16, 2247-2268, 2019.
- Parke, M., Boalch, G., Jowett, R., and Harbour, D.: The genus *Pterosperma* (Prasinophyceae): species with a single equatorial ala, *Journal of the Marine Biological Association of the United Kingdom*, 58, 239-276, 1978.
- Pascher, K. M., Hollis, C. J., Bohaty, S. M., Cortese, G., McKay, R. M., Seebeck, H., Suzuki, N., and Chiba, K.: Expansion and diversification of high-latitude radiolarian assemblages in the late Eocene linked to a cooling event in the southwest Pacific, *Climate of the Past*, 11, 1599-1620, 2015.
- Passchier, S., Bohaty, S. M., Jiménez-Espejo, F., Pross, J., Röhl, U., van de Flierdt, T., Escutia, C., and Brinkhuis, H.: Early Eocene to middle Miocene cooling and aridification of East Antarctica, *Geochemistry, Geophysics, Geosystems*, 14, 1399-1410, 2013.
- Passchier, S., Ciarletta, D. J., Henao, V., and Sekkas, V.: Sedimentary processes and facies on a high-latitude passive continental margin, Wilkes Land, East Antarctica, *Geological Society, London, Special Publications*, 475, 181-201, 2019.
- Parras, A., Guerin, G. R., Panera, J. P. P., Griffin, M., Nández, C., Cusminsky, G., and Quiroga, A.: Integrated stratigraphy and paleontology of the lower Miocene Monte León Formation, southeastern Patagonia, Argentina: Unraveling paleoenvironmental changes and factors controlling sedimentation, *Palaeogeography, Palaeoclimatology, Palaeoecology*, 556, 109701, 2020.
- Paxman, G. J., Jamieson, S. S., Hochmuth, K., Gohl, K., Bentley, M. J., Leitchenkov, G., and Ferraccioli, F.: Reconstructions of Antarctic topography since the Eocene–Oligocene boundary, *Palaeogeography, palaeoclimatology, palaeoecology*, 535, 109346, 2019.
- Pearson, A., Huang, Z., Ingalls, A., Romanek, C., Wiegel, J., Freeman, K. H., Smittenberg, R., and Zhang, C.: Nonmarine crenarchaeol in Nevada hot springs, *Appl. Environ. Microbiol.*, 70, 5229-5237, 2004.
- Pearson, P. N., Foster, G. L., and Wade, B. S.: Atmospheric carbon dioxide through the Eocene–Oligocene climate transition, *Nature*, 461, 1110-1113, 2009.

- Pekar, S. F., Christie-Blick, N., Kominz, M. A., and Miller, K. G.: Calibration between eustatic estimates from backstripping and oxygen isotopic records for the Oligocene, *Geology*, 30, 903-906, 2002.
- Pekar, S. F., DeConto, R. M., and Harwood, D. M.: Resolving a late Oligocene conundrum: Deep-sea warming and Antarctic glaciation, *Palaeogeography, Palaeoclimatology, Palaeoecology*, 231, 29-40, 2006.
- Pekar, S. F. and DeConto, R. M.: High-resolution ice-volume estimates for the early Miocene: Evidence for a dynamic ice sheet in Antarctica, *Palaeogeography, Palaeoclimatology, Palaeoecology*, 231, 101-109, 2006.
- Pérez, L. F., Hernández-Molina, F. J., Lodolo, E., Bohoyo, F., Galindo-Zaldívar, J., and Maldonado, A.: Oceanographic and climatic consequences of the tectonic evolution of the southern scotia sea basins, Antarctica, *Earth-Science Reviews*, 198, 102922, 2019.
- Pérez, L. F., De Santis, L., McKay, R. M., Larter, R. D., Ash, J., Bart, P. J., Böhm, G., Brancatelli, G., Browne, I., and Colleoni, F.: Early and middle Miocene ice sheet dynamics in the Ross Sea: Results from integrated core-log-seismic interpretation, *GSA Bulletin*, 2021.
- Pérez, L. F., Martos, Y. M., García, M., Weber, M. E., Raymo, M. E., Williams, T., Bohoyo, F., Armbricht, L., Bailey, I., and Brachfeld, S.: Miocene to present oceanographic variability in the Scotia Sea and Antarctic ice sheets dynamics: Insight from revised seismic-stratigraphy following IODP Expedition 382, *Earth and Planetary Science Letters*, 553, 116657, 2021.
- Peterse, F., van Der Meer, M., Schouten, S., Jia, G., Ossebaar, J., Blokker, J., and Sinninghe Damsté, J.: Assessment of soil n-alkane δD and branched tetraether membrane lipid distributions as tools for paleoelevation reconstruction, *Biogeosciences*, 6, 2799-2807, 2009.
- Pfuhl, H. A. and McCave, I. N.: Integrated age models for the early Oligocene-early Miocene, sites 1168 and 1170-1172, *Proc. ODP, Sci. Results*, 189, 1-21, 2003.
- Pierce, E. L., van de Flierdt, T., Williams, T., Hemming, S. R., Cook, C. P., and Passchier, S.: Evidence for a dynamic East Antarctic ice sheet during the mid-Miocene climate transition, *Earth and Planetary Science Letters*, 478, 1-13, 2017.
- Plancq, J., Mattioli, E., Pittet, B., Simon, L., and Grossi, V.: Productivity and sea-surface temperature changes recorded during the late Eocene-early Oligocene at DSDP Site 511 (South Atlantic), *Palaeogeography, Palaeoclimatology, Palaeoecology*, 407, 34-44, 2014.
- Prebble, J., Hannah, M., and Barrett, P.: Changing Oligocene climate recorded by palynomorphs from two glacio-eustatic sedimentary cycles, Cape Roberts Project, Victoria Land Basin, Antarctica, *Palaeogeography, Palaeoclimatology, Palaeoecology*, 231, 58-70, 2006.
- Prebble, J., Raine, J., Barrett, P., and Hannah, M.: Vegetation and climate from two Oligocene glacioeustatic sedimentary cycles (31 and 24 Ma) cored by the Cape Roberts Project, Victoria Land Basin, Antarctica, *Palaeogeography, Palaeoclimatology, Palaeoecology*, 231, 41-57, 2006.
- Prebble, J., Crouch, E., Carter, L., Cortese, G., Bostock, H., and Neil, H.: An expanded modern dinoflagellate cyst dataset for the Southwest Pacific and Southern Hemisphere with environmental associations, *Marine Micropaleontology*, 101, 33-48, 2013a.
- Prebble, J., Crouch, E., Carter, L., Cortese, G., and Nodder, S.: Dinoflagellate cysts from two sediment traps east of New Zealand, *Marine Micropaleontology*, 104, 25-37, 2013b.
- Pritchard, H., Ligtenberg, S. R., Fricker, H. A., Vaughan, D. G., van den Broeke, M. R., and Padman, L.: Antarctic ice-sheet loss driven by basal melting of ice shelves, *Nature*, 484, 502-505, 2012.
- Pross, J. and Brinkhuis, H.: Organic-walled dinoflagellate cysts as paleoenvironmental indicators in the Paleogene; a synopsis of concepts, *Paläontologische Zeitschrift*, 79, 53-59, 2005.
- Pross, J., Houben, A. J., van Simaey, S., Williams, G. L., Kotthoff, U., Coccioni, R., Wilpshaar, M., Brinkhuis, H.: Umbria-Marche revisited: a refined magnetostratigraphic calibration of dinoflagellate cyst events for the Oligocene of the Western Tethys. *Review of Palaeobotany and Palynology*, 158, 213-35, 2010.

- Pross, J., Contreras, L., Bijl, P. K., Greenwood, D. R., Bohaty, S. M., Schouten, S., Bendle, J. A., Röhl, U., Tauxe, L., and Raine, J. I.: Persistent near-tropical warmth on the Antarctic continent during the early Eocene epoch, *Nature*, 488, 73-77, 2012.
- Reynolds, R. W., Rayner, N. A., Smith, T. M., Stokes, D. C., and Wang, W.: An improved in situ and satellite SST analysis for climate, *Journal of climate*, 15, 1609-1625, 2002.
- Richey, J. N. and Tierney, J. E.: GDGT and alkenone flux in the northern Gulf of Mexico: Implications for the TEX86 and UK'37 paleothermometers, *Paleoceanography*, 31, 1547-1561, 2016.
- Ridgway, K. and Condie, S.: The 5500-km-long boundary flow off western and southern Australia, *Journal of Geophysical Research: Oceans*, 109, 2004.
- Rintoul, S. R., Chown, S. L., DeConto, R. M., England, M. H., Fricker, H. A., Masson-Delmotte, V., Naish, T. R., Siebert, M. J., and Xavier, J. C.: Choosing the future of Antarctica, *Nature*, 558, 233-241, 2018.
- Röhl, U., Brinkhuis, H., Sluijs, A., and Fuller, M.: On the search for the Paleocene/Eocene boundary in the Southern Ocean: exploring ODP Leg 189 Holes 1171D and 1172D, Tasman Sea, The Cenozoic Southern Ocean: Tectonics, Sedimentation, and Climate Change Between Australia and Antarctica. *Geophysical Monograph Series*, 151, 113-125, 2004.
- Salabarnada, A., Escutia, C., Röhl, U., Nelson, C. H., McKay, R., Jiménez-Espejo, F., Bijl, P., Hartman, J., Strother, S., and Salzmann, U.: Paleoceanography and ice sheet variability offshore Wilkes Land, Antarctica—Part 1: Insights from late Oligocene astronomically paced contourite sedimentation, *Climate of the Past*, 14, 991-1014, 2018.
- Sallée, J.-B.: Southern ocean warming, *Oceanography*, 31, 52-62, 2018.
- Sangiorgi, F., Bijl, P. K., Passchier, S., Salzmann, U., Schouten, S., McKay, R., Cody, R. D., Pross, J., van de Flierdt, T., Bohaty, S. M., Levy, R., Williams, T., Escutia, C., and Brinkhuis, H.: Southern Ocean warming and Wilkes Land ice sheet retreat during the mid-Miocene, *Nat Commun*, 9, 317, 2018.
- Sarkar, S., Basak, C., Frank, M., Berndt, C., Huuse, M., Badhani, S., and Bialas, J.: Late Eocene onset of the proto-Antarctic circumpolar current, *Scientific reports*, 9, 1-10, 2019.
- Sauermilch, I., Whittaker, J. M., Klocker, A., Munday, D. R., Hochmuth, K., LaCasce, J. H., and Bijl, P.: Gateway-driven Southern Ocean cooling – The crucial role of ocean gyres., *Nature Communications*, 2021, 2021.
- Sauermilch, I., Whittaker, J. M., Bijl, P. K., Totterdell, J., and Jokat, W.: Tectonic, oceanographic, and climatic controls on the Cretaceous-Cenozoic sedimentary record of the Australian-Antarctic Basin, *Journal of Geophysical Research: Solid Earth*, 124, 7699-7724, 2019a.
- Sauermilch, I., Mateo, Z. R. P., and Boaga, J.: A comparative analysis of time–depth relationships derived from scientific ocean drilling expeditions, *Marine Geophysical Research*, 40, 635-641, 2019b.
- Scher, H. D. and Martin, E. E.: Timing and climatic consequences of the opening of Drake Passage, *science*, 312, 428-430, 2006.
- Scher HD, Bohaty SM, Zachos JC, Delaney ML. Two-stepping into the icehouse: East Antarctic weathering during progressive ice-sheet expansion at the Eocene–Oligocene transition. *Geology*. 39(4), 383-386, 2011.
- Scher, H. D., Bohaty, S. M., Smith, B. W., and Munn, G. H.: Isotopic interrogation of a suspected late Eocene glaciation, *Paleoceanography*, 29, 628-644, 2014.
- Scher, H. D., Whittaker, J. M., Williams, S. E., Latimer, J. C., Kordesch, W. E. C., and Delaney, M. L.: Onset of Antarctic Circumpolar Current 30 million years ago as Tasmanian Gateway aligned with westerlies, *Nature*, 523, 580, 2015.
- Schmidtko, S., Heywood, K. J., Thompson, A. F., and Aoki, S.: Multidecadal warming of Antarctic waters, *Science*, 346, 1227-1231, 2014.
- Schoof, C.: Ice sheet grounding line dynamics: Steady states, stability, and hysteresis, *Journal of Geophysical Research: Earth Surface*, 112, 2007.
- Schouten, S., Hopmans, E. C., Rosell-Melé, A., Pearson, A., Adam, P., Bauersachs, T., Bard, E., Bernasconi, S. M., Bianchi, T. S., and Brocks, J. J.: An interlaboratory study of TEX86 and BIT analysis of sediments, extracts, and standard mixtures, *Geochemistry, Geophysics, Geosystems*, 14, 5263-5285, 2013.

- Schouten, S., Hopmans, E. C., and Damsté, J. S. S.: The organic geochemistry of glycerol dialkyl glycerol tetraether lipids: A review, *Organic geochemistry*, 54, 19-61, 2013.
- Schouten, S., Hopmans, E. C., Schefuß, E., and Damsté, J. S. S.: Distributional variations in marine crenarchaeotal membrane lipids: a new tool for reconstructing ancient sea water temperatures?, *Earth and Planetary Science Letters*, 204, 265-274, 2002.
- Schreck, M. and Matthiessen, J.: Batiacasphaera micropapillata: Palaeobiogeographic distribution and palaeoecological implications of a critical Neogene species complex, *Biological and Geological Perspectives of Dinoflagellates. The Micropalaeontological Society, Special Publications. Geological Society, London*, 5, 301-314, 2013.
- Seton, M., Müller, R. D., Zahirovic, S., Gaina, C., Torsvik, T., Shephard, G., Talsma, A., Gurnis, M., Turner, M., Maus, S., and Chandler, M.: Global continental and ocean basin reconstructions since 200Ma, *Earth-Science Reviews*, 113, 212-270, 2012.
- Shen, Q., Wang, H., Shum, C., Jiang, L., Hsu, H. T., and Dong, J.: Recent high-resolution Antarctic ice velocity maps reveal increased mass loss in Wilkes Land, East Antarctica, *Scientific reports*, 8, 4477, 2018.
- Shevenell, A. E., Kennett, J. P., and Lea, D. W.: Middle Miocene ice sheet dynamics, deep-sea temperatures, and carbon cycling: A Southern Ocean perspective, *Geochemistry, Geophysics, Geosystems*, 9, 2008.
- Sijp, W. P. and England, M. H.: Effect of the Drake Passage throughflow on global climate, *Journal of Physical Oceanography*, 34, 1254-1266, 2004.
- Sijp, W. P., Anna, S., Dijkstra, H. A., Flögel, S., Douglas, P. M., and Bijl, P. K.: The role of ocean gateways on cooling climate on long time scales, *Global and Planetary Change*, 119, 1-22, 2014.
- Sijp, W. P., von der Heydt, A. S., and Bijl, P. K.: Model simulations of early westward flow across the Tasman Gateway during the early Eocene, *Climate of the Past*, 12, 807-817, 2016.
- Singh, H. K., Bitz, C. M., and Frierson, D. M.: The global climate response to lowering surface orography of Antarctica and the importance of atmosphere–ocean coupling, *Journal of Climate*, 29, 4137-4153, 2016.
- Sinninghe Damsté, J. S., Schouten, S., Hopmans, E. C., Van Duin, A. C., and Geenevasen, J. A.: Crenarchaeol: the characteristic core glycerol dibiphytanyl glycerol tetraether membrane lipid of cosmopolitan pelagic crenarchaeota, *Journal of lipid research*, 43, 1641-1651, 2002.
- Sinninghe Damsté, J. S., Ossebaar, J., Abbas, B., Schouten, S., and Verschuren, D.: Fluxes and distribution of tetraether lipids in an equatorial African lake: constraints on the application of the TEX86 palaeothermometer and BIT index in lacustrine settings, *Geochimica et Cosmochimica Acta*, 73, 4232-4249, 2009.
- Sinninghe Damsté, J. S.: Spatial heterogeneity of sources of branched tetraethers in shelf systems: The geochemistry of tetraethers in the Berau River delta (Kalimantan, Indonesia), *Geochimica et Cosmochimica Acta*, 186, 13-31, 2016.
- Sluijs, A., Brinkhuis, H., Stickley, C., Warnaar, J., Williams, G., and Fuller, M.: Dinoflagellate cysts from the Eocene/Oligocene transition in the Southern Ocean; results from ODP Leg 189, *Proceedings of the Ocean Drilling Program. Scientific Results*, doi: <https://doi.org/10.2973/odp.proc.sr.189.104.2003>, 2003.
- Sluijs, A., Pross, J., and Brinkhuis, H.: From greenhouse to icehouse; organic-walled dinoflagellate cysts as paleoenvironmental indicators in the Paleogene, *Earth-Science Reviews*, 68, 281-315, 2005.
- Sluijs, A., Röhl, U., Schouten, S., Brumsack, H. J., Sangiorgi, F., Damsté, J. S. S., and Brinkhuis, H.: Arctic late Paleocene–early Eocene paleoenvironments with special emphasis on the Paleocene-Eocene thermal maximum (Lomonosov Ridge, Integrated Ocean Drilling Program Expedition 302), *Paleoceanography*, 23, 2008.
- Sluijs, A. and Brinkhuis, H.: A dynamic climate and ecosystem state during the Paleocene-Eocene Thermal Maximum: inferences from dinoflagellate cyst assemblages on the New Jersey Shelf, *Biogeosciences*, 6, 1755-1781, 2009.
- Speelman, E. N., Sewall, J. O., Noone, D., Huber, M., von der Heydt, A., Damsté, J. S., and Reichert, G.-J.: Modeling the influence of a reduced equator-to-pole sea surface temperature gradient on the distribution of water isotopes in the Early/Middle Eocene, *Earth and Planetary Science Letters*, 298, 57-65, 2010.

- Stap, L. B., Van De Wal, R. S., Boer, B. d., Bintanja, R., and Lourens, L. J.: The influence of ice sheets on temperature during the past 38 million years inferred from a one-dimensional ice sheet–climate model, *Climate of the Past*, 13, 1243-1257, 2017.
- Steinthsordottir, M., Coxall, H., De Boer, A., Huber, M., Barbolini, N., Bradshaw, C., Burls, N., Feakins, S., Gasson, E., and Henderiks, J.: The Miocene: The future of the past, *Paleoceanography and Paleoclimatology*, 36, e2020PA004037, 2021.
- Stickley, C. E., Brinkhuis, H., Schellenberg, S. A., Sluijs, A., Röhl, U., Fuller, M., Grauert, M., Huber, M., Warnaar, J., and Williams, G. L.: Timing and nature of the deepening of the Tasmanian Gateway, *Paleoceanography*, 19, 2004a.
- Stickley, C., Brinkhuis, H., McGonigal, K., Chaproniere, G., Fuller, M., Kelly, D., Nürnberg, D., Pfuhl, H., Schellenberg, S., and Schönfeld, J.: Late Cretaceous–Quaternary biomagnetostratigraphy of ODP Sites 1168, 1170, 1171, and 1172, Tasmanian Gateway, *Proceedings of the Ocean Drilling Program, Scientific Results*, 189, 1-57, 2004b.
- Stocchi, P., Escutia, C., Houben, A. J., Vermeersen, B. L., Bijl, P. K., Brinkhuis, H., DeConto, R. M., Galeotti, S., Passchier, S., and Pollard, D.: Relative sea-level rise around East Antarctica during Oligocene glaciation, *Nature Geoscience*, 6, 380, 2013.
- Stover, L., Brinkhuis, H., Damassa, S., De Verteuil, L., Helby, R., Monteil, E., Partridge, A., Powell, A., Riding, J., and Smelror, M.: Mesozoic-Tertiary dinoflagellates, acritarchs and prasinophytes, *Palynology: principles and applications*, 2, 641-750, 1996.
- Stuart, K. and Long, D.: Tracking large tabular icebergs using the SeaWinds Ku-band microwave scatterometer, *Deep Sea Research Part II: Topical Studies in Oceanography*, 58, 1285-1300, 2011.
- Taylor, K. W., Huber, M., Hollis, C. J., Hernandez-Sanchez, M. T., and Pancost, R. D.: Re-evaluating modern and Palaeogene GDGT distributions: Implications for SST reconstructions, *Global and Planetary Change*, 108, 158-174, 2013.
- Terhaar, J., Frölicher, T. L., and Joos, F.: Southern Ocean anthropogenic carbon sink constrained by sea surface salinity, *Science Advances*, 7, eabd5964, 2021.
- Ternois, Y., Sicre, M.-A., Boireau, A., and Conte, M.: Evaluation of long-chain alkenones as paleo-temperature indicators in the Mediterranean Sea, *Deep Sea Research Part I: Oceanographic Research Papers*, 44, 271-286, 1997.
- Thompson, N., Salzmann, U., López-Quirós, A., Bijl, P. K., Hoem, F. S., Etourneau, J., Sicre, M.-A., Roignant, S., Hocking, E., and Amoo, M.: Vegetation change across the Drake Passage region linked to late Eocene cooling and glacial disturbance after the Eocene–Oligocene Transition, *Climate of the Past*, 18, 209-232, 2022.
- Tierney, J. E. and Tingley, M. P.: A Bayesian, spatially-varying calibration model for the TEX86 proxy, *Geochimica et Cosmochimica Acta*, 127, 83-106, 2014.
- Tierney, J. E. and Tingley, M. P.: A TEX 86 surface sediment database and extended Bayesian calibration, *Scientific data*, 2, 1-10, 2015.
- Toggweiler, J. R., Russell, J. L., and Carson, S. R.: Midlatitude westerlies, atmospheric CO₂, and climate change during the ice ages, *Paleoceanography*, 21, 2006.
- Toggweiler, J.: Shifting westerlies, *Science*, 323, 1434-1435, 2009.
- Torsvik, T. H., Van der Voo, R., Preeden, U., Mac Niocail, C., Steinberger, B., Doubrovine, P. V., van Hinsbergen, D. J. J., Domeier, M., Gaina, C., Tohver, E., Meert, J. G., McCausland, P. J. A., and Cocks, L. R. M.: Phanerozoic polar wander, palaeogeography and dynamics, *Earth-Science Reviews*, 114, 325-368, 2012.
- Toumoulin, A., Donnadieu, Y., Ladant, J. B., Batenburg, S., Poblete, F., and Dupont-Nivet, G.: Quantifying the effect of the Drake Passage opening on the Eocene Ocean, *Paleoceanography and Paleoclimatology*, 35, e2020PA003889, 2020.
- Van Cappellen, P. and Qiu, L.: Biogenic silica dissolution in sediments of the Southern Ocean. II. Kinetics, *Deep Sea Research Part II: Topical Studies in Oceanography*, 44, 1129-1149, 1997.

- van de Lagemaat, S. H., Swart, M. L., Vaes, B., Kusters, M. E., Boschman, L. M., Burton-Johnson, A., Bijl, P. K., Spakman, W., and van Hinsbergen, D. J.: Subduction initiation in the Scotia Sea region and opening of the Drake Passage: When and why?, *Earth-Science Reviews*, 2021. 103551, 2021.
- van Hinsbergen, D. J., de Groot, L. V., van Schaik, S. J., Spakman, W., Bijl, P. K., Sluijs, A., Langereis, C. G., and Brinkhuis, H.: A Paleolatitude Calculator for Paleoclimate Studies, *PLoS One*, 10, e0126946, 2015.
- van Simaey, S., Brinkhuis, H., Pross, J. r., Williams, G. L., and Zachos, J. C.: Arctic dinoflagellate migrations mark the strongest Oligocene glaciations, *Geology*, 33, 709-712, 2005.
- Verducci, M., Foresi, L., Scott, G., Sprovieri, M., Lirer, F., and Pelosi, N.: The Middle Miocene climatic transition in the Southern Ocean: evidence of paleoclimatic and hydrographic changes at Kerguelen plateau from planktonic foraminifers and stable isotopes, *Palaeogeography, Palaeoclimatology, Palaeoecology*, 280, 371-386, 2009.
- Viebahn, J. P., von der Heydt, A. S., Le Bars, D., and Dijkstra, H. A.: Effects of Drake Passage on a strongly eddying global ocean, *Paleoceanography*, 31, 564-581, 2016.
- Villa, G., Fioroni, C., Pea, L., Bohaty, S., and Persico, D.: Middle Eocene–late Oligocene climate variability: calcareous nannofossil response at Kerguelen Plateau, Site 748, *Marine Micropaleontology*, 69, 173-192, 2008.
- Von Schuckmann, K., Cheng, L., Palmer, M. D., Hansen, J., Tassone, C., Aich, V., Adusumilli, S., Beltrami, H., Boyer, T., and Cuesta-Valero, F. J.: Heat stored in the Earth system: where does the energy go?, *Earth System Science Data*, 12, 2013-2041, 2020.
- Wall, D. and Dale, B.: “Living fossils” in western Atlantic plankton *Nature*, 211, 1025-1026, 1966.
- Wall, D., Dale, B., Lohmann, G., and Smith, W. K.: The environmental and climatic distribution of dinoflagellate cysts in modern marine sediments from regions in the North and South Atlantic Oceans and adjacent seas, *Marine micropaleontology*, 2, 121-200, 1977.
- Warny, S., Wrenn, J. H., Bart, P. J., and Askin, R.: Palynology of the NBP03–01A transect in the Northern Basin, western Ross Sea, Antarctica: A late Pliocene record, *Palynology*, 30, 151-182, 2006.
- Warny, S., Kymes, C. M., Askin, R. A., Krajewski, K. P., and Bart, P. J.: Remnants of Antarctic vegetation on King George Island during the early Miocene Melville glaciation, *Palynology*, 40, 66-82, 2016.
- Weatherall, P., Marks, K. M., Jakobsson, M., Schmitt, T., Tani, S., Arndt, J. E., Rovere, M., Chayes, D., Ferrini, V., and Wigley, R.: A new digital bathymetric model of the world's oceans, *Earth and Space Science*, 2, 331-345, 2015.
- Weber, M., Raymo, M., Peck, V., Williams, T., Armbrecht, L., Bailey, I., Brachfeld, S., Cardillo, F., Du, Z., and Fauth, G.: Expedition 382 summary. IODP Publications, 2021.
- Wei, W. and Wise Jr, S. W.: Biogeographic gradients of middle Eocene-Oligocene calcareous nannoplankton in the South Atlantic Ocean, *Palaeogeography, Palaeoclimatology, Palaeoecology*, 79, 29-61, 1990.
- Weijers, J. W., Schouten, S., Spaargaren, O. C., and Damsté, J. S. S.: Occurrence and distribution of tetraether membrane lipids in soils: Implications for the use of the TEX86 proxy and the BIT index, *Organic Geochemistry*, 37, 1680-1693, 2006.
- Weijers, J. W., Lim, K. L., Aquilina, A., Sinninghe Damsté, J. S., and Pancost, R. D.: Biogeochemical controls on glycerol dialkyl glycerol tetraether lipid distributions in sediments characterized by diffusive methane flux, *Geochemistry, Geophysics, Geosystems*, 12, 2011.
- Westerhold, T., Marwan, N., Drury, A. J., Liebrand, D., Agnini, C., Anagnostou, E., Barnet, J. S. K., Bohaty, S. M., De Vleeschouwer, D., Florindo, F., Frederichs, T., Hodell, D. A., Holbourn, A. E., Kroon, D., Lauretano, V., Littler, K., Lourens, L. J., Lyle, M., Palike, H., Rohl, U., Tian, J., Wilkens, R. H., Wilson, P. A., and Zachos, J. C.: An astronomically dated record of Earth's climate and its predictability over the last 66 million years, *Science*, 369, 1383-1387, 2020.
- Whittaker, J. M., Williams, S. E., and Müller, R. D.: Revised tectonic evolution of the Eastern Indian Ocean, *Geochemistry, Geophysics, Geosystems*, 14, 1891-1909, 2013.

- Williams, G., Fensome, R., and MacRae, R.: The Lentin and Williams index of fossil dinoflagellates, 2017 Edition, American Association of Stratigraphic Palynologists Foundation (AASP) Contributions Series Number 48., Dallas, Texas, USA, 2017.
- Williams, S. E., Whittaker, J. M., Halpin, J. A., and Müller, R. D.: Australian-Antarctic breakup and seafloor spreading: Balancing geological and geophysical constraints, *Earth-Science Reviews*, 188, 41-58, 2019.
- Wilson, D. S., Pollard, D., DeConto, R. M., Jamieson, S. S., and Luyendyk, B. P.: Initiation of the West Antarctic Ice Sheet and estimates of total Antarctic ice volume in the earliest Oligocene, *Geophysical Research Letters*, 40, 4305-4309, 2013.
- Woodruff, S. D., Worley, S. J., Lubker, S. J., Ji, Z., Eric Freeman, J., Berry, D. I., Brohan, P., Kent, E. C., Reynolds, R. W., and Smith, S. R.: ICOADS Release 2.5: extensions and enhancements to the surface marine meteorological archive, *International journal of climatology*, 31, 951-967, 2011.
- Wouters, B., Martín-Español, A., Helm, V., Flament, T., van Wessem, J. M., Ligtenberg, S. R., Van den Broeke, M. R., and Bamber, J. L.: Dynamic thinning of glaciers on the Southern Antarctic Peninsula, *Science*, 348, 899-903, 2015.
- Wrenn, J. H. and Beckman, S. W.: Maceral, total organic carbon, and palynological analyses of ross ice shelf project site j9 cores, *Science*, 216, 187-189, 1982.
- Wu, S., Lembke-Jene, L., Lamy, F., Arz, H. W., Nowaczyk, N., Xiao, W., Zhang, X., Hass, H. C., Titschack, J., and Zheng, X.: Orbital-and millennial-scale Antarctic Circumpolar Current variability in Drake Passage over the past 140,000 years, *Nature Communications*, 12, 1-9, 2021.
- Zachos, J. C., Stott, L. D., and Lohmann, K. C.: Evolution of early Cenozoic marine temperatures, *Paleoceanography*, 9, 353-387, 1994.
- Zachos, J. C., Quinn, T. M., and Salamy, K. A.: High-resolution (104 years) deep-sea foraminiferal stable isotope records of the Eocene-Oligocene climate transition, *Paleoceanography*, 11, 251-266, 1996.
- Zachos, J., Pagani, M., Sloan, L., Thomas, E., and Billups, K.: Trends, rhythms, and aberrations in global climate 65 Ma to present, *science*, 292, 686-693, 2001.
- Zachos, J. C., Dickens, G. R., and Zeebe, R. E.: An early Cenozoic perspective on greenhouse warming and carbon-cycle dynamics, *nature*, 451, 279-283, 2008.
- Zhang, Y. G., Zhang, C. L., Liu, X.-L., Li, L., Hinrichs, K.-U., and Noakes, J. E.: Methane Index: A tetraether archaeal lipid biomarker indicator for detecting the instability of marine gas hydrates, *Earth and Planetary Science Letters*, 307, 525-534, 2011.
- Zhang, Y. G., Pagani, M., Liu, Z., Bohaty, S. M., and DeConto, R.: A 40-million-year history of atmospheric CO₂, *Philosophical Transactions of the Royal Society A: Mathematical, Physical and Engineering Sciences*, 371, 20130096, 2013.
- Zhang, Y. G., Pagani, M., and Wang, Z.: Ring Index: A new strategy to evaluate the integrity of TEX₈₆ paleothermometry, *Paleoceanography*, 31, 220-232, 2016.
- Zhong-Shi, Z., Qing, Y., and Hui-Jun, W.: Has the Drake Passage played an essential role in the Cenozoic cooling?, *Atmospheric and Oceanic Science Letters*, 3, 288-292, 2010.
- Zonneveld, K. A. F., Versteegh, G. J. M., Kasten, S., Eglinton, T. I., Emeis, K. C., Huguët, C., Koch, B. P., de Lange, G. J., de Leeuw, J. W., Middelburg, J. J., Mollenhauer, G., Prah, F. G., Rethemeyer, J., and Wakeham, S. G.: Selective preservation of organic matter in marine environments; processes and impact on the sedimentary record, *Biogeosciences*, 7, 483-511, 2010.
- Zonneveld, K. A., Marret, F., Versteegh, G. J., Bogus, K., Bonnet, S., Bouimtarhan, I., Crouch, E., de Vernal, A., Elshaniawany, R., and Edwards, L.: Atlas of modern dinoflagellate cyst distribution based on 2405 data points, *Review of Palaeobotany and Palynology*, 191, 1-197, 2013.

Samenvatting in het Nederlands

De verbranding van fossiele brandstoffen heeft sinds het industriële tijdperk geleid tot een verhoogde hoeveelheid broeikasgassen in de atmosfeer en de daaropvolgende opwarming van de aarde. De Zuidelijke Oceaan rond Antarctica is in staat om veel van deze overtollige warmte in de atmosfeer op te nemen en vertraagt zo de opwarming van de aarde. Warmere zeemassa's kunnen leiden tot het smelten en afkalven van ijsplaten die de daarachterliggende gletsjers tegenhouden. Binnen enkele eeuwen kan dit leiden tot enkele meters zeespiegelstijging wereldwijd. De huidige observaties zijn te kort om nauwkeurige toekomstvoorspellingen hierover te maken. Ijskapmodellen die deze doorberekeningen doen moeten worden getest op hun betrouwbaarheid. Om dit te doen is kennis over de geologische geschiedenis cruciaal, omdat de Antarctische ijskap in het geologische verleden ook warme periodes met veel CO₂ heeft gekend. Het is daarom belangrijk om de dynamiek van de Zuidelijke Oceaan en haar rol in de (de)stabilisatie van de Antarctische ijskap in vroegere geologische tijdperken met hogere CO₂-concentraties en warmere klimaten beter te begrijpen.

In dit proefschrift reconstrueer ik, samen met collega's, de oceanografische omstandigheden in het Oligoceen-Mioceen (~34-5 miljoen jaar geleden (Ma)). We beschrijven variaties in zeevatertemperatuur, zee-ijs, voedingsstoffen en zeefrontsystemen in de zeegebieden rond de Tasman Straat, op de grens tussen de Indische Oceaan en de Stille Oceaan (Hoofdstukken 2-4) en in de Zuid-Atlantische Oceaan, ten oosten van de Drake Passage (Hoofdstukken 5-6). Dit doen we door de organische membraanstructuur van eencellige organismen (Archea) te bestuderen met behulp van de TEX₈₆-methode, en de kwantificering van verschillende algenpopulaties (cysten van Dinoflagellaten) in sedimenten die zijn afgezet op de zeebodem in de Zuidelijke Oceaan.

Onze resultaten wijzen op warme oppervlaktewatertemperaturen vroeg in het Oligoceen, dicht bij de ijskap en een klein temperatuurverschil (zgn. temperatuurgradiënt) van zuid naar noord in de Zuidelijke Oceaan. Dit suggereert zwakkere frontale oceaanstroom en een zwakke Zuidelijke Oceaanstroom. De nauwere zeestraten van Tasman en Drake in het vroege Oligoceen leidde waarschijnlijk tot actieve gyre-circulatie die warme oceaanstromingen naar hogere breedtegraden bracht. Aan het einde van het Oligoceen (26 Ma) begonnen de gebieden in de nabijheid van Wilkes Land, Antarctica, af te koelen, terwijl de lagere breedtegraden in de Zuidelijke Oceaan warm bleven. Aangezien dit niet overeenkomt met een verandering in atmosferische CO₂ of toegenomen ijsvolume, suggereren we dat tektonische verdieping van de Drake Passage leidde tot een sterkere stroming van de Zuidelijke Oceaanstroom, waardoor de thermische isolatie van Antarctica toenam. De verdwijning van Antarctische endemische en typische koudwater-indicatieve dinoflagellaatcysten ten noorden van de Drake Passage aan het einde van het Oligoceen suggereert ook de ineenstorting van de gyre-circulatie en de versterking van frontale systemen. Na een periode van opwarming van de aarde die bekend staat als het *Mid-Mioceen Climate Optimum* rond 16 Ma, tonen de resultaten van dinoflagellaatcysten een verschuiving van een voedselarm en warm Antarctische proximale zeewater naar voedselrijke, koude en zee-ijs beïnvloede zee. Tegelijkertijd daalde de temperatuur van het oppervlaktewater van 14°C naar 7-5°C. Dit komt overeen met een daling van de atmosferische CO₂, mondiale afkoeling en een toenemend ijsvolume.

Er zijn nog veel hiaten in de reconstructies van de oceanografische veranderingen in de Zuidelijke Oceaan. Dit proefschrift toont voor het eerst een stapsgewijze afbraak van de gyre-circulaties en de ontwikkeling van een modern oceanografisch regime, gekenmerkt door sterke frontale systemen en grote temperatuurverschillen tussen breedtegraden in de Zuidelijke Oceaan.

Sammendrag av doktorgrad på norsk

Siden begynnelsen av den industrielle æra har brensel av fossile brennstoffer ført til en økt mengde drivhusgasser i atmosfæren og påfølgende global oppvarming. Sørishavet rundt Antarktis har evnen til å ta opp mye av denne overskuddsvarmen i atmosfæren og bremser dermed den globale oppvarmingen. Varmere havmasser kan medføre til smelting og kalving av ishyller som holder tilbake Antarktisen som ligger bak, noe som kan forårsake flere meter med global havnivåstigning på få århundre. Moderne observasjoner er for korte til å nøyaktig kunne spå fremtidige endringer. Klimamodeller som gjør disse beregningene må testes for pålitelighet. Den geologiske historien er avgjørende der, for det Antarktiske isdekket har også kjent varmeperioder med mye CO₂ i geologisk fortid. Det er derfor primært å få en bedre forståelse av dynamikken til Sørishavet og dens rolle i (de)stabiliseringen av Antarktis isdekket i tidligere geologiske tidsepoker med høyere CO₂ konsentrasjoner og varmere klima.

I denne doktorgradsavhandlingen rekonstruerer jeg, sammen med kollegaer, de oseanografiske forholdene i Oligocene-Miocene (~34-5 Millioner år siden (Ma)). Vi beskriver variasjoner i havoverflatetemperatur, sjøis utbredelse, næringsstoffer og havfrontsystemer i havområdene rundt Tasmanstredet, ved grensen mellom det Indiske hav og Stillehavet (Kapittel 2-4) og i Sør-Atlanteren, øst for Drakestredet (Kapittel 5-6). Dette gjør vi ved å studere den organiske membranstrukturen av encellede organismer (Arker) gjennom bruken av TEX₈₆ metoden, og kvantifiseringen av ulike algebestander (cyster av Dinoflagellater) i sedimenter avsatt på havbunnen i Sørishavet.

Våre resultater indikerer at det var en mye mer temperert havoverflate tidlig i Oligocene nært isdekket og en lavere temperatur forskjell (temperaturgradient) fra sør til nord i Sørishavet enn i dag. Dette tyder på svakere havfrontsystemer og svak Sørishavstrøm. De smalere Tasman- og Drakestredene i tidlig Oligocene førte trolig til aktiv gyresirkulasjon som førte varme havstrømmer til høyere breddegrader. I slutten av Oligocene (26 Ma) begynte områder nært Antarktis, utenfor Wilkes Land, å kjøles ned, mens lavere breddegrader i Sørishavet forble tempererte. Siden dette ikke samsvarer med en endring i atmosfærisk CO₂ eller økt is volum, foreslår vi at tektonisk fordypning av Drakestredet førte til sterkere gjennomstrømning av Sørishavstrømmen som økte den termiske isolasjonen av Antarktis. Forsvinningen av Antarktiske endemiske og typiske kaldtvannsendikerende dinoflagellate cyster nord for Drakestredet ved slutten av Oligocene indikerer også et sammenbrudd av gyresirkulasjon og styrking av frontale systemer. Etter en periode med global oppvarming kjent som Mid-Miocene Climate Optimum rundt 16 Ma, viser resultater fra dinoflagellate cyster et skifte fra næringsfattig, varmt hav til næringsrike, kalde, sjø-is-påvirket Antarktiske-proksimale forhold. Samtidig sank overflatevanntemperaturen fra 14°C til 7-5°C. Dette samsvarer med et fall i atmosfærisk CO₂ og global nedkjøling og økende isvolum.

Det er fortsatt mange hull i rekonstruksjonene av de oseanografiske endringene i Sørishavet. Denne doktorgradsavhandlingen viser for første gang et trinnav sammenbrudd av gyresirkulasjonene og utviklingen av moderne-lignende oseanografiske regime, karakterisert av sterke frontale systemer og store temperatur forskjeller mellom breddegradene i Sørishavet. Informasjonen om Sørishavets havoverflatetemperatur og økologi/miljø gitt i denne avhandlingen kan brukes som grunnleggende grensebetingelser for å forbedre og teste modeller som simulerer tidligere og fremtidige oseanografiske forhold.

Acknowledgments

While reflecting over my PhD and writing these acknowledgements in early September of 2022 I'm ill with covid for the second time, looking out on a yellow, dry lawn after one of the warmest and driest summers on record and checking for news on the latest development in the war in Ukraine. Writing a PhD about past climates and ocean circulation has at times felt pretty meaningless and motivation has not always been high. Therefore, having a strong network of friends, family and colleagues around me to support, entertain and motivate me has been crucial. In the end, gaining and sharing knowledge, unlocking some of the mysteries of our planet, giving context to current climatic developments and trying to better predict the future by adding some new puzzles of data to the big puzzle has felt purposeful. I hereby attempt to show my deep gratitude to the individuals making this PhD happen in the first place, but also making it an enjoyable and educational process.

First and foremost, I would like to thank my daily supervisors Peter and Francesca for tirelessly devoting so much of your time mentoring, supporting and helping me. You've not had an easy job with me who'd never seen a dinocyst in her life, with only a basic chemistry background and some dyslectic struggles. I've also been very lucky with my legendary promotor Henk who has been there keeping a close eye from NIOZ or his mill, always offering speedy support, critically revising and well-timed upbuilding words. You have all helped me get over the finish line. This has been a huge team effort! I'm very happy that I get to continue to work with you as a post-doc, and hoping we will continue collaborating in the future.

A significant amount of lab work has been conducted in this thesis which would not have been possible without the help and support of Mariska, Giovanni, Natasha, Desmond and Klaas. Also a big thank you to the bachelor and master students contributing with data results and discussion in this thesis: Pelle Adema, Cecile Hilgen and Karlijn van den Broek.

I have had a lot of collaborators who happily shared their knowledge, data, and samples as well as included me in their work. The Granada Armada: Dimitris Evangelinos, Adrián López-Quirós, Carlota Escutia, Luis Valero and Johan Etourneau for sedimentary reconstructions, samples and age model improvements. The Northumbria pollen group: Ulrich Salzmann, Michael Amoo and Nick Thompson. Matt Huber and Adam Aleksinski for contributing climate model simulations. Suzanna van de Lagemaat for figures and discussions about tectonic reconstructions. New Zealanders Rob McKay and Bella Duncan for the Ross Sea input and Joe Prebble for the dinocyst discussions. Last but not least the great OceaNice team; Mariska, Lena, Isabel, Suning, Martin and Peter. As a OceaNice sidekick, now team member, I've greatly enjoyed the helpfulness, open and constructive collaboration and discussions as well as the dinners.

A big thank you to journal editors and reviewers for taking the time for constructive and critical reviews of our submitted papers. Especially, thank you to the reading and dissertation committee for reading and reviewing this PhD thesis and being oponents at the defence. I'm looking forward to further discussions.

Ulysses and Kikki, my inspirational masters supervisors in Bergen talked highly of going on science cruises, saying all I needed to do was start a PhD and apply. They planted a seed that grew to reality with starting this PhD and sailing on IODP Expedition 382 to Iceberg Alley. This expedition with exciting science, kilometres of sediment cores, icebergs, whales, penguins and already several publications has set an unrealistically high standard for any future expeditions/fieldwork to come. Thanks for believing in me Trevor, Mike and Mo, and thank you particularly to Anna, Marlo and Michelle for making it the best cruise and staying in touch after. Marlo Gransworthy you are so talented and goodhearted, thank you for creating the coolest cover art one could wish for.

Moving to a new country and university can be intimidating, but gratefully the collaborative, supportive, fun and social group of colleagues (MPP/PE/OG/PPGU++) made it go smoothly. Our tradition of biweekly or so drinks in the office, followed by beers at Jan Primus and stumbling loudly into the Pizza places next door never gets old. Starting my PhD as the first non-Dutchie hired for a while and following me a hiatus of new PhDs, I could've easily fallen between two stools. But luckily, I clung to both groups. I even forced some of you to hang out with me outside of work functions. First the Unnik/asbest crew of Margot, Carolien, Ilja, Joost, Robin, Tjerk, Tom, Niels, Emily, Margriet, Fabian, Julian, Matthias and Nina set me up for a great start in Utrecht. Then later in the new VMA building a wave of new PhDs and post-docs came onboard; Evi, Domi, Suning, Mei, Chris, Remco, Christopher, Yord, Tobias, Anne, Signe, Melanie, Alice, Addison, Madalina, Olga, Olivier, Martin, Isabel and Lena ++. You run a tight ship Appy, Peter, Francesca, Francien, Timme, Caroline, Frits, Jack, Luc, Martin, Bas, Henk and more, with the help from Tjitsk and Annuska. Thank you for all support, advice, discussions as well as for getting the funds and having great taste in people you hire.

Through this PhD, I've been so lucky to go combine my passions for science and travel with some amazing trips around the world (at least pre-pandemic). E.g. getting sediment samples and tacos in Texas, teaching fieldwork in Spain and Belgium, learning about dinocysts in the Nottingham (UK) and paleoclimate in Urbino (Italy), hiking in Patagonia pre-cruise and diving in Australia post-conference. Particularly Urbino summerschool 2018 set me up for success with great lectures, discussions and lots of PhD friends I meet regularly at conferences.

Lots of fun has been had outside of work the last 5 years. The Bouldering crew; Carolien, Alice, Ilja, Jaap, Guido, Niels, Aaron, Jeroen, Hannah and Line. I'm sorry bouldering didn't work out for me... Although the immobility scooter was a lot of fun, I'm not doing that again. I will still always be there for the cake, drinks, trips, hikes, swims and way too deep and inappropriate conversations. BaTiJuNa++; 10 very kind, unique, intellectual, individuals whom I highly appreciate and don't mind discussing/arguing with into the late hours or deep forests. SACT and cocktails group aka. corona cohort; Eline, Tamar, Saskia, James and Estee. Bah where to begin. You've incorporated me into your lives, and let me tag along to your fun adventures, making the years in Utrecht the best possible. The fact that I'm not immediately moving back to the fjords, mountains and higher salary in Norway after this PhD is a big compliment to you all (as well as the city of Utrecht, you beauty).

Familie og venner i Norge jeg har ikke glemt dere enda. Jeg savner dere hele tiden, og bruker derfor minst 90% av feriedager på å dra tilbake til Norge med glede. Det har vært utrolig gøy å ha dere på besøk i Utrecht i løpet av disse åra (Ida, Kristine, Anne-Mari og Liva spesielt) og utrolig stas at så mange av dere tar turen for å feire doktorgraden. Mamma, Pappa, Åsa og Liva, vi har ikke sett

hverander så mye som vi har ønsket de siste årene, men likevell har dere fortsatt å være mitt viktigste støtteapparat og heiaklubb. Vi gleder oss til å flytte hjem til Norge om ikke lenge.

De Seliers en de Sluisjes, jullie hebben me snel in de familie opgenomen als een van jullie en sinds het begin geduld gehad met mijn slechte nederlands. Mijn taal is nu veel beter dankzij jullie. Bedankt ook voor het tonen van oprechte interesse in mij en wat ik doe en voor jullie volledige steun.

Two specially selected paranymphs are standing at my side as I defend this PhD; Signe Haukelidsæter and Dr. Eline Huiberts. First of all thank you both for the Dutch and Norwegian proofreading and help in getting the celebration together. Signe, all of a sudden sharing an office with another Norwegian, whom I already knew from studies in Bergen, have added another dimension to life I didn't know I missed. Its been really nice seeing you get settled in the Netherlands and PhD life meanwhile creating a little person, hat off to you. How a facebook message can change the course in life is pretty fascinating, but moving in with Eline in Tolsteegplantsoen has been defining for where and with whom I spend my days. Its been such an adventure raising a cat, Pai Mei, together and creating or own "friends" sit-com with adjacent apartments and friends with keys running down our doors, more days then not a week telling their wild stories. Thank you to Pai Mei for the emotional support, cuddles and hide and seek fun.

Finally, I would like to share my love and appreciation for Tim. Meeting you only one month into my PhD, you've been supporting me through it all. Being your kind, generous self you did not even complain when you had to move and fix up our new apartment alone for 10 weeks when I was cruising in the Southern Ocean. Thank you for your endless patience with me. Building a campervan with you and going on a 3-month long holiday after submitting the PhD has been the best celebration.

Thank you,
Frida Snilstveit Hoem
Utrecht, 5 September 2022

Curriculum Vitae

Frida Snilstveit Hoem was born on the 9th of January 1992 in Oslo, but raised in Kristiansund, Norway. In 2011 she started her studies in Earth Science (BSc) and Marine Geology and Geophysics (MSc) at the University of Bergen, with exchange periods at Utrecht University (2015) and the University Center in Svalbard (2016). She obtained her Master of Science degree in 2017 with the project “Centennial-millennial scale variations in West Antarctic Ice Sheet discharge and their relationship to climate and ocean changes during the late Holocene” under the supervision of Ulysses Ninnemann, Nil Irvani and Kikki Kleiven. By the end of 2017 she moved to The Netherlands and started working on an NWO (polar programme) funded PhD project at Utrecht University, at the Department of Earth Sciences, in the group of Marine Palynology and Paleoceanography, subject of this thesis. Supervised by Henk Brinkhuis, Peter Bijl and Francesca Sangiorgi she investigated the Oligocene – Miocene Southern Ocean in relation to Antarctic ice-sheet variability, atmospheric CO₂ variations and changing paleogeography by reconstructing sea-ice paleoceanographic conditions and sea surface temperatures using dinoflagellate cysts and organic biomarkers. Frida sailed as the shipboard palynologist on the *Joides Resolution* IODP Expedition 382 to Iceberg Alley, Southern Ocean, March-May 2019. Frida expresses her passion for climate and scientific outreach by volunteering as an editor for KlimaatHelpdesk, a website providing peer-reviewed answers by scientists/experts to climate-related questions from the public. Her PhD thesis was approved on 5th of July 2022 and will be defended on October 7th 2022. Frida is continuing as a postdoctoral researcher at Utrecht University until February 2023.



Publications in peer-reviewed journals

- Evangelinos, D., Escutia, C., Etourneau, J., **Hoem, F.**, Bijl, P., Boterblom, W., van de Flierdt, T., Valero, L., Flores, J. A., Rodriguez-Tovar, F. J., Jimenez-Espejo, F. J., Salabarnada, A., and Lopez-Quiros, A.: Late Oligocene-Miocene proto-Antarctic Circumpolar Current dynamics off the Wilkes Land margin, East Antarctica, *Global and Planetary Change*, 191, 103221, ARTN 103221. 10.1016/j.gloplacha.2020.103221, 2020.
- Hoem, F. S.**, Sauermlch, I., Hou, S. N., Brinkhuis, H., Sangiorgi, F., and Bijl, P. K.: Late Eocene-early Miocene evolution of the southern Australian subtropical front: a marine palynological approach, *Journal of Micropalaeontology*, 40, 175-193, 10.5194/jm-40-175-2021, 2021a.
- Hoem, F. S.**, Valero, L., Evangelinos, D., Escutia, C., Duncan, B., McKay, R. M., Brinkhuis, H., Sangiorgi, F., and Bijl, P. K.: Temperate Oligocene surface ocean conditions offshore of Cape Adare, Ross Sea, Antarctica, *Climate of the Past*, 17, 1423-1442, 10.5194/cp-17-1423-2021, 2021b.
- López-Quiros, A., Escutia, C., Etourneau, J., Rodríguez-Tovar, F. J., Roignant, S., Lobo, F. J., Thompson, N., Bijl, P. K., Bohoyo, F., Salzmann, U., Evangelinos, D., Salabarnada, A., **Hoem, F. S.**, and Sicre, M.-A.: Eocene-Oligocene paleoenvironmental changes in the South Orkney Microcontinent (Antarctica) linked to the opening of Powell Basin, *Global and Planetary Change*, 204, 103581, 2021.
- Pérez, L. F., Martos, Y. M., García, M., Weber, M. E., Raymo, M. E., Williams, T., Bohoyo, F., Armbrecht, L., Bailey, I., Brachfeld, S., Cardillo, F., Du, Z., Fauth, G., Garcia, M., Garnsworthy, M., Gluder, A., Guitard, M., Gutjahr, M., Hernandez-Almeida, I., **Hoem, F. S.**, Hwang, J. H., Iizuka, M., Kato, Y., Kenlee, B., S. O. C., Perez, L. F., Seki, O., Stevens, L., Tauxe, L., Tripathi, S., Warnock, J., and Zheng, X.: Miocene to present oceanographic variability in the Scotia Sea and Antarctic ice sheets dynamics: Insight from revised seismic-stratigraphy following IODP Expedition 382, *Earth and Planetary Science Letters*, 553, 116657, 2021.
- Reilly, B. T., Tauxe, L., Brachfeld, S., Raymo, M., Bailey, I., Hemming, S., Weber, M. E., Williams, T., Garcia, M., Guitard, M., Hernandez-Almeida, I., **Hoem, F. S.**, Hwang, J. H., Iizuka, M., Kato, Y., Kenlee, B., S. O. C., Perez, L. F., Seki, O., Stevens, L., Tauxe, L., Tripathi, S., Warnock, J., and Zheng, X.: New magnetostratigraphic insights from Iceberg Alley on the rhythms of Antarctic climate during the Plio-Pleistocene, *Paleoceanography and Paleoclimatology*, 36, e2020PA003994, 2021.
- Weber, M., Raymo, M., Peck, V., Williams, T., Armbrecht, L., Bailey, I., Brachfeld, S., Cardillo, F., Du, Z., Fauth, G., Fogwill, C. J., Garcia, M., Garnsworthy, M., Gluder, A., Guitard, M., Gutjahr, M., Hernandez-Almeida, I., **Hoem, F. S.**, Hwang, J. H., Iizuka, M., Kato, Y., Kenlee, B., S. O. C., Perez, L. F., Seki, O., Stevens, L., Tauxe, L., Tripathi, S., Warnock, J., and Zheng, X.: Expedition 382 summary, *Proceedings of the International Ocean Discovery Program*, 2021.
- Evangelinos, D., Escutia, C., van de Flierdt, T., Valero, L., Flores, J.-A., Harwood, D. M., **Hoem, F. S.**, Bijl, P., Etourneau, J., and Kreissig, K.: Absence of a strong, deep-reaching Antarctic Circumpolar Current zonal flow across the Tasmanian gateway during the Oligocene to early Miocene, *Global and Planetary Change*, 208, 103718, 2022.
- Weber, M. E., Bailey, I., Hemming, S. R., Martos, Y. M., Reilly, B. T., Ronge, T. A., Brachfeld, S., Williams, T., Raymo, M., Belt, S. T., Smik, L., Vogel, H., Peck, V. L., Armbrecht, L., Cage, A., Cardillo, F. G., Du, Z., Fauth, G., Fogwill, C. J., Garcia, M., Garnsworthy, M., Gluder, A., Guitard, M., Gutjahr, M., Hernandez-Almeida, I., **Hoem, F. S.**, Hwang, J. H., Iizuka, M., Kato, Y., Kenlee, B., S. O. C., Perez, L. F., Seki, O., Stevens, L., Tauxe, L., Tripathi, S., Warnock, J., and Zheng, X.: Antiphased dust deposition and productivity in the Antarctic Zone over 1.5 million years, *Nature Communications*, 13, 2044, 10.1038/s41467-022-29642-5, 2022.

- Thompson, N., Salzmann, U., Lopez-Quiros, A., Bijl, P. K., **Hoem, F. S.**, Etourneau, J., Sicre, M. A., Roignant, S., Hocking, E., Amoo, M., and Escutia, C.: Vegetation change across the Drake Passage region linked to late Eocene cooling and glacial disturbance after the Eocene-Oligocene transition, *Climate of the Past*, 18, 209-232, 10.5194/cp-18-209-2022, 2022.
- Bailey, I., Hemming, S., Reilly, B. T., Rollinson, G., Williams, T., Weber, M. E., Raymo, M. E., Peck, V. L., Ronge, T. A., Brachfeld, S., L., Armbrrecht, L., Cage, F., Cardillo, F., Du, Z., Fauth, G., Fogwill, C. J., Garcia, M., Garnsworthy, M., Gluder, A., Guitard, M., Gutjahr, M., Hernandez-Almeida, I., **Hoem, F. S.**, Hwang, J. H., Iizuka, M., Kato, Y., Kenlee, B., S. O. C., Perez, L. F., Seki, O., Stevens, L., Tauxe, L., Tripathi, S., Warnock, J., and Zheng, X.: Episodes of early Pleistocene West Antarctic Ice Sheet retreat recorded by Iceberg Alley sediments, *Paleoceanography and Paleoclimatology*, 37, e2022PA004433, 2022.
- Warnock, J., Reilly, B., Raymo, M., Weber, M., Peck, V., Williams, T., Armbrrecht, L., Bailey, I., Brachfeld, S., Du, Z., Fauth, G., Fogwill, C. J., Garcia, M., Garnsworthy, M., Gluder, A., Guitard, M., Gutjahr, M., Hernandez-Almeida, I., **Hoem, F. S.**, Hwang, J. H., Iizuka, M., Kato, Y., Kenlee, B., S. O. C., Perez, L. F., Seki, O., Stevens, L., Tauxe, L., Tripathi, S., Warnock, J., and Zheng, X.: Latitudinal variance in the drivers and pacing of warmth during mid-Pleistocene MIS 31 in the Antarctic Zone of the Southern Ocean, *Paleoceanography and Paleoclimatology*, 2022.
- Duncan, B., McKay, R., Levy, R., Naish, T., Prebble, J., Sangiorgi, F., Krishnan, S., **Hoem, F.**, Clowes, C., Dunkley Jones, T., Gasson, E., Kraus, C., Kulhanek, D. K., Meyers, S., Moossen, H., Warren, C., Willmott, V., Ventura, G.T. & Bendle, J.: Climatic and tectonic drivers of late Oligocene Antarctic ice volume, *Nature Geoscience*, <https://www.nature.com/articles/s41561-022-01025-x>, 2022.

In review/accepted:

- Hoem, F.**, Sauerlich, I., Aleksinski, A., Huber, M., Peterse, F., Sangiorgi, F., and Bijl, P.: Strength and variability of the Oligocene Southern Ocean surface temperature gradient, *Nature Communications Earth and Environment*, in review.
- Armbrrecht et al., Oldest (~600 ka) marine eukaryote sedaDNA reveals diatom transition in Antarctica (IODP Exp. 382) *Nature communications*, accepted, in print.
- Michael Amoo, Ulrich Salzmann, Matthew J. Pound, **Frida S. Hoem**, Nick Thompson and Peter K. Bijl.: Terrestrial climate and vegetation change in the western Tasmanian region from the late Eocene to late Oligocene, *Palaeogeography, Palaeoclimatology, Palaeoecology*, in review.

Utrecht University
Faculty of Geosciences
Department of Earth Sciences



ISSN 2211-4335